Analyzing energy-saving options in greenhouse cultivation using a simulation model

H.F. de Zwart

Analyzing energy-saving options in greenhouse cultivation using a simulation model

Promotoren: **Dr. Ir. G.P.A. Bot**
Hoogleraar in de Technische Natuurkunde

Dr. Ir. L. Speelman
Hooglereaar in de Landbouwmechanisatie en
Bedrijfsuitrusting

Analyzing energy-saving options in greenhouse cultivation using a simulation model

H.F. de Zwart

Proefschrift

Cover illustration:
C.P. de Bruijne

Stellingen

1. Bij de berekening van de warmtebehoefte van kassen na toepassing van kasomhullingsmaterialen met een hoge isolatiewaarde moet terdege rekening worden gehouden met de vochthuishouding.
   dit proefschrift

2. Realisatie van de doelstelling voor de energie-efficiëntie, zoals geformuleerd in de meerjarenafspraak-energie, zal bij de huidige trend van het toenemend areaal onder glas en het stijgend gemiddeld verbruik per m^2 ertoe leiden dat de CO_2-doelstelling zoals geformuleerd in het NMP-plus niet wordt gehaald.
   dit proefschrift

3. Het 'multi-node' model voor een gestratificeerde warmte-opslagtank is niet te parametriseren naar fysisch meetbare grootheden.
   dit proefschrift

4. Window-functions zoals gebruikt voor de beschrijving van het ventilatie-debiet door raam-openingen in kassen moeten worden opgevat als complexe overdrachtsfuncties.
   T. de Jong, 1990, Natural ventilation of large multi-span greenhouses. Proefschrift Landbouwuniversiteit Wageningen

5. De huidige wijze van normeren van het jaarlijks gasverbruik met behulp van het aantal graaddagen resulteert in een te grote correctiefactor.
   N.J.A. van der Velden et. al., 1996, Energie in de glastuinbouw van Nederland; ontwikkelingen in de sector en op de bedrijven t/m 1994

6. Het eco-keurmerk is op chemisch gebied zeer stringent maar hanteert op fysisch gebied een vergaand laissez-faire beleid.
   J.G. Bokhorst, 1995, Biologische kasgroenteteelt Louis Bolk Instituut, Driebergen

7. De 'Caps Lock' toets van de PC wordt door alle gangbare programmatuur geïnterpreteerd als 'Case Inverse' en heeft daarmee een overbodige, meestal zelfs lastige functie toegekend gekregen.

8. In verband met papierbesparing zouden kopieermachines default op 'tweezijdig afdrukken' moeten staan

9. Omdat het uitrijden van een ambulance in de regel voorbode is van een moeilijke periode in het leven van het slachtoffer en diens verwanten zou de sirene beter gebruik kunnen maken van een mineur toonladder dan van de nu toegepaste majeur toonladder.

10. Een Let-systeem (Local Exchange and Trading System) is een sympathiek besloten zwart geld circuit.
De Volkskrant, 15 maart 1996

11. Het noemen van de garantie dat de Interliner niet vóór de aangegeven tijd vertrekt als één van de plus-punten van deze vorm van openbaar vervoer zegt veel over de kwaliteit van ander busvervoer.
Brochure Interliner, november 1995

Stellingen behorende bij het proefschrift 'Analyzing energy-saving options in greenhouse cultivation using a simulation model',
H.F. de Zwart, Wageningen, 19 april 1996

ABSTRACT

Hendrik Feije de Zwart, 1996, Analyzing energy-saving potentials in greenhouse cultivation using a simulation model. Ph.D. Dissertation, Landbouwuniversiteit, Wageningen. Also available as a publication of the DLO Institute of Agricultural and Environmental Engineering (IMAG-DLO), Wageningen, The Netherlands

Greenhouse Horticulture in the Netherlands has set itself the task of having halved its primary energy consumption per unit of production at the end of the century, compared to 1980. As a result, a large number of energy-saving measures have been suggested to meet this target.

In this book a simulation model is presented that can be used as a tool to judge the measures proposed. The model describes the dynamics of the greenhouse climate, the components of the heating system and the greenhouse climate controller with a time resolution of up to 1 minute. Also, the photosynthetic activity of the canopy is described. Consequently the model takes account for the complicated horticultural practice.

The simulation model is constructed from sub-models. Each of these sub-models is discussed in detail. The sub-models for the heating circuit, the condenser and the short-term heat storage facility were newly developed. Therefore, these parts of the model are discussed extensively. The greenhouse climate controller and the greenhouse climate simulation are described integrally, however briefly, because these parts of the model are a reflection of the current state-of-the-art.

To proof the quality of the simulation model, computations are compared to measurements on a rose crop in a research facility. These comparisons are made both with a high resolution on a small time scale (10 minutes) and with aggregated values on a large time scale (year round daily results).

To analyze the prospects of energy-saving measures in greenhouse cultivation, the simulation model was applied to nine energy-saving options. The results of the model on these options with respect to energy consumption and biomass production are compared with a reference situation. The reference situation comprised a customary greenhouse growing tomatoes in the Netherlands. From the options evaluated, the application of combined heat and power and alternative cladding materials appeared to yield the largest decrement of specific energy consumption (the energy consumption corrected for production effects).

Key words: Energy saving, greenhouse climate simulation, heat storage, climate control, heating systems

CONTENTS

1. INTRODUCTION AND ORGANIZATION OF THE THESIS

During recent decades, the quantity per unit of growth area and quality of green-house vegetable and flower production in the Netherlands has increased considerably Comparing statistical information on horticulture from 1977 with data from 1991 shows an increase in the number of cut roses (*Motrea*) from 200 to 320 per m^2 per year and an increase in tomato production from 23 to 46 kg per m^2 per year (Vademecum voor de Glastuinbouw, 1978; Kwantitatieve informatie, 1992). These high production figures can be attributed to the intensive and well thought-out conditioning of the canopy's growing environment, comprising temperature, humidity, radiation, CO_2-supply and nutrient solution. Other important factors are the increased level of education amongst growers and improvements in the genetic properties of the plants. Also the mean length of the growth season has been increased.

Parallel to increments in production levels, the primary energy consumption (the consumption of gas and oil) has also increased. Currently, horticultural boilers account for about 5% of the fossil fuel consumption in the Netherlands (Novem, 1994). Chapter 2 presents a brief outline of these recent developments.

Due to growing public and governmental concern about the effect of increasing carbon dioxide concentrations in the atmosphere, effort is being made in many sectors of economy to reduce the consumption of fossil fuels. In 1992, in an official agreement with the government, glasshouse horticulture in the Netherlands set itself the task of halving its energy consumption per unit of production by the end of the millennium, compared to 1980. To reach this target, a strategy has been formulated that includes extension work, education on energy saving techniques and research. As a result, researchers and companies have offered a large number of suggestions to this end.

For most of these suggestions the energy-saving effects of the techniques in isolated, well-defined situations can be determined accurately. However, the performance of these techniques in the practical horticultural situation is much more difficult to estimate. This is because the overall effects of improvements on details of the greenhouse system are related to the duration and intensity of application. Moreover, in general the application of a combination of energy-saving techniques will result in less saving than a simple multiplication of the individual effects. For both reasons, the effects of strategies on energy saving can only be judged in the context of horticultural practice.

Horticultural practice can be taken into account by studying the effects of energy-saving techniques in a number of operational greenhouses where some do apply the considered techniques and others do not. However, these full-scale experiments are expensive and difficult to perform, mainly because it is hard to formulate an experimental set-up in which the subject of research can be considered as the only

independent variable. Small-scale research in specialist facilities, which is another way of conducting such a survey, can overcome most of these problems, but it appears to be difficult to generalize the results to horticultural practice. Moreover, an important problem for full-scale as well as small-scale experiments is the year round time span during which the effects must be studied. In addition, locational and yearly variation of the weather to which a greenhouse is exposed confuses the observation of empirical research objects.

Because of these difficulties there is a need for a method to judge energy-saving techniques in the context of complicated horticultural practice in an unambiguous and reconstructible way. Therefore, this work presents a simulation model intending to meet this need. With this model a large number of energy-saving options is analyzed.

With respect to energy saving, attention has been focused on the heating of greenhouses, since heating is responsible for 95% of the horticultural energy demand (Novem, 1994). The energy-saving options can be divided into three categories, namely the efficient production and handling of heat, methods to reduce the heat demand of greenhouses and measures to enhance production capacity.

The efficient production of heat involves the application of a condenser, the use of waste heat from public electricity production plants and the application of on-site combined heat and power units. Handling of heat involves the heating system lay-out and the application of short-term heat storage. Developments to decrease the heat demand of greenhouses include improvements in the insulation of greenhouses, such as the application of alternative cladding materials and the use of thermal screens. Another important contribution to reducing the heat demand of a greenhouse is the formulation of a greenhouse climate which combines a high production level with a low energy demand (Bakker, 1994; Rijsdijk, 1993). Here, the development of new climate control strategies is of major importance (Henten, 1995).

The simulation model used tool to study energy-saving options is described in Chapter 3, 4 and 5. In Chapter 3 the functional demands on the model are defined and the modelling technique is selected. It is shown that the energy consumption of a greenhouse is the product of the interaction between the greenhouse climate controller, the heating system and the greenhouse climate in conjunction with environmental conditions and horticultural requirements.

Of the three components of the model, the greenhouse heating system has not yet been a subject of detailed study. Therefore, the formulation and application of sub-models for heating system devices is a substantial element in this work and is presented in Chapter 4. After discussing the individual elements, an integration of the sub-models into a coherent heating system model is presented. Finally, the heating system simulation is coupled to the greenhouse climate simulation by means of the greenhouse climate controller. Despite the recent scientific develop-

ments in greenhouse climate controllers (Hashimoto e.a., 1993), in the present work (the essence of) a commercially available controller is applied. This has been done to stay close to the current practical situation. The functional description of this climate controller is presented in Chapter 4.

The components of the model describing the greenhouse climate are discussed briefly but integrally in Chapter 5. The discussion is brief because this part of the model has a state-of-the-art character.

Obviously, a model can only be an approach to reality. Therefore, prior to the application of the model for the analysis of the various energy-saving options, the quality of the model is studied by comparing of the results of the model computations with measurements taken in an actual greenhouse. This part of the results of this work is presented in Section 6.2.

After the quality of the simulation model has been proved, a large number of energy-saving options are evaluated in relation to a reference situation (Section 6.3). The reference situation was an average greenhouse growing tomatoes in the Netherlands.

Finally, the conclusions of the study are presented and discussed in Chapter 7.

2. ENERGY-SAVING OPTIONS FOR HORTICULTURE IN THE NETHERLANDS

Glasshouse horticulture makes an important contribution to economy in the Netherlands. Production accounts for about 5% of gross domestic product (CBS, 1994b). About 76% of production is exported. In 1992 this represented a value of NLG $16.3 \cdot 10^9$, which was about 6.6% of total export value.

On the other hand, modern glasshouse horticulture is an energy-intensive economic activity. In 1992, about 10% of the domestic gas-consumption (equivalent to 5% of domestic primary energy consumption) was used in horticultural boilers. Because of wide public concern about the global effects of the combustion of fossil fuels, the government aims to stimulate all sectors in economy to reduce their fossil fuel use. In this context, the government of the Netherlands has made an agreement with representatives of horticulture to make an effort in the direction of energy conservation. The target formulated in the agreement, henceforth referred to by the MJA (Meerjarenafspraak), is to cut the economically normalized specific energy consumption (ENSEC) measured by 1980 standards by half by the end of the millennium (Meerjarenafspraak, 1992). In the MJA a number of measures to achieve this target are proposed.

The MJA also contains a definition of ENSEC. Basically the ENSEC is a dimensionless figure representing the outcome of the division of an annual primary energy consumption by an economic value of the production that it generated, as a percentage to the outcome of the same expression with data holding for 1980. The energy consumption is corrected for deviating weather conditions and the production is corrected for inflation. In a formula:

$$\text{ENSEC} = 100 \ \frac{E_{\text{prim,act}}}{\text{production}_{\text{act}}} \ \frac{\text{production}_{1980}}{E_{\text{prim,1980}}} \qquad \text{[-] (2.1)}$$

By expressing the production using the economic value of the produce, the quantity can be computed for every mix of horticultural products. In Section 2.1 the target of the MJA is explained and discussed within the context of the developments of energy consumption and production in the period 1980 to 1993.

From the definition of ENSEC we can see that its value can be decreased both by a decrement of primary energy consumption and by an increment of the production. However, the majority of the measures mentioned in the MJA concern energy-saving techniques, rather than techniques that enhance production. Therefore, this study concentrates on technical improvements only. In Section 2.2 the options mentioned in the MJA are discussed briefly. From these options, a number have been selected and evaluated in this study.

5

2.1 ENERGY CONSUMPTION AND PRODUCTION IN HORTICULTURE

The DLO Agricultural Economics Research Institute (LEI-DLO) periodically publishes a report on the developments of the horticultural sector with special reference to energy consumption (Velden, 1993; Velden, 1995). The results of these reports are based on questionnaires distributed amongst 300 nurseries, of which a 100 produce vegetables, 100 produce flowers and 100 produce pot-plants. The companies are selected unbiased and are considered to be representative for the sector. All data mentioned and displayed graphically in this section are derived from these periodic reports.

From the data presented by LEI-DLO, the course of the ENSEC for three sub-sectors and the aggregated mean value could be deduced. These results are presented in Figure 2.1, together with the objective formulated in the MJA.
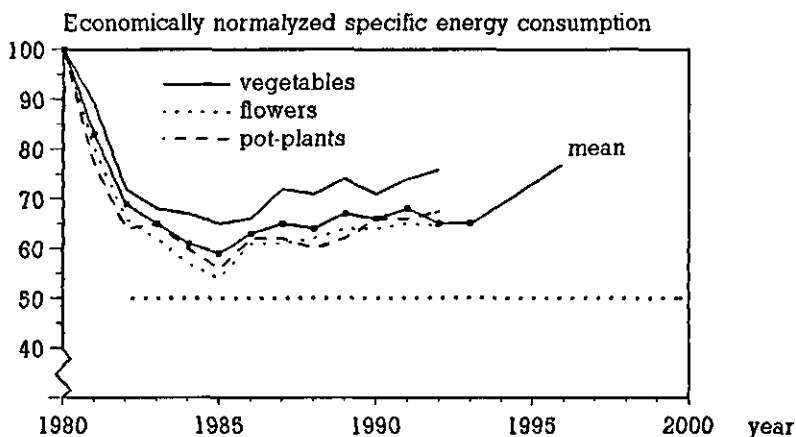
Figure 2.1 Course of the ENSEC during the period 1980 up to 1993. The dotted straight line shows the objective to have been reached by the end of the millennium.

In Figure 2.1 it is remarkable that, in recent years, the mean value of the ENSEC is very close to the curve for flowers and pot-plants and seems hardly to be affected by the higher values for vegetables. This is a result of the weighing of the contribution of each of the horticultural sub-sectors in the final figure according to their relative production value. Thus, the course of the partial ENSEC for flowers and pot-plants, having high economic values, despite the comparable growth area (see Fig. 2.2), has a larger impact on the mean ENSEC than the course of the partial ENSEC for vegetables. The fact that in 1992 all partial ENSEC's are larger or equal to the mean ENSEC is assumed to be caused by a

low partial ENSEC of plant breederies, for which no detailed data were published. Figure 2.1 shows that in the early 1980[s] a vast decrease in ENSEC has been achieved. After, say 1986, this tendency changes into a slight increment. Together with the ever increasing area (see Fig. 2.2), horticulture in the Netherlands shows a gradual increment in primary energy consumption towards 139 PJ in 1993 (see Fig. 2.3).

Glass covered area [10^3 ha]
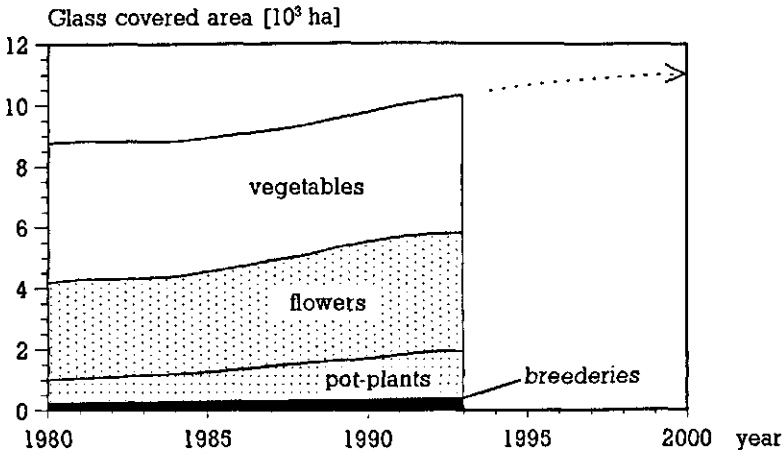
Figure 2.2 Glass covered area

With respect to the absolute energy consumption of horticulture in the Netherlands, the MJA cites the general governmental objective to reduce the CO_2-exhaust of each economic sector to 96% of the CO_2-exhaust of that sector in 1990 by the end of the millennium. Because the CO_2-exhaust is practically linearly dependent on primary energy consumption, the CO_2-exhaust objective can be translated into a target for the absolute energy consumption in the year 2000. This target (111 PJ) is indicated with an arrow in Figure 2.3.

As said, a decrement of ENSEC can be achieved by a decrement in primary energy consumption (the nominator) or an increment of production value (the denominator). In Figure 2.4, the course of the value of horticultural products per unit of area, indexed to 1980, is shown. The figure shows a steady increment of production value, although the slope seems to have flatten somewhat in recent years. Part of the increment of production can be attributed to developments in glasshouse equipment such as the application of a rockwool rooting medium and the gradual replacement of old, relatively dark greenhouses, by new buildings with a higher transparency for solar radiation.

Primairy energy consumption [PJ year⁻¹]
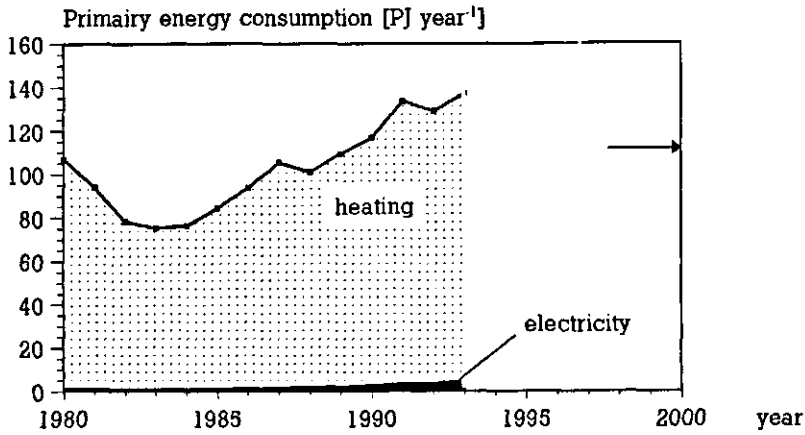
Figure 2.3 Primary energy consumption of horticulture in the Netherlands

Production [NLGm⁻²year⁻¹]
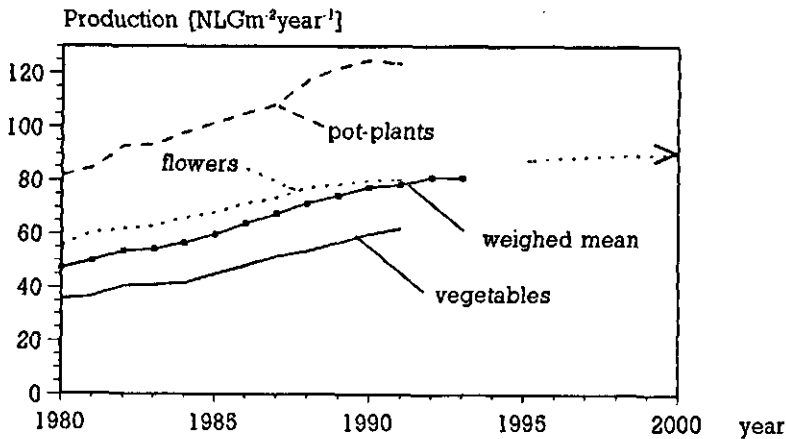
Figure 2.4 Course of horticultural production per m² greenhouse in 1980 guilders. Courses of individual products are weighed according to their contribution to the total economic value of horticultural products.

However, after observing Figure 2.1, it must be concluded that most production enhancement must be related to energy consuming modifications, such as CO_2 supply with exhaust gases and artificial illumination. Indeed, Figure 2.5 shows that, in the period 1988 - 1993 the mean primary energy consumption per unit of greenhouse surface tends to increase by 0.05 $GJm^{-2}year^{-1}$ per year.

Extrapolating the production value per m^2 (Fig. 2.4) and the primary energy consumption per m^2 (Fig. 2.5) to the values marked with an arrow, the ENSEC will be 72 at the end of the millennium. Obviously, in order to reach the target of the MJA, a serious change in current trends must be realized. Against the background of the flattening curve in Figure 2.4 and the causal relation that seems to exist between increment of production and increment of primary energy consumption, it is more likely that the necessary decrement of ENSEC can be achieved by changing the trend of Figure 2.5 than changing the production value per unit of greenhouse surface.

Assuming that the decrement of energy consumption per m^2 greenhouse can be achieved by technical measures that do not affect production, an ENSEC of 50 can be achieved when the mean primary energy consumption per m^2 greenhouse is decreased to 1.15 GJm^{2}year^{-1}. A possible path to that value is shown by the dashed line in Figure 2.5.
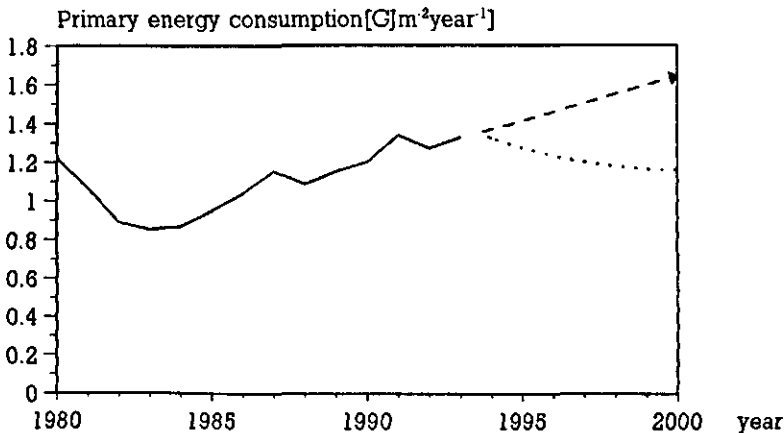
Figure 2.5 Mean primary energy consumption per m^2 greenhouse. The dotted line follows the trend of recent years. The dashed line is a possible curve that brings the ENSEC to 50 in the year 2000 if the production value were to develop according to the dashed line shown in Figure 2.4.

When the glass covered area in the year 2000 has grown to 11·10^3 ha in the year 2000 (the dotted line in Figure 2.2), and assuming a mean primary energy consumption of 1.15 GJm^{2}year^{-1} (the dotted line in Figure 2.5), the absolute yearly energy consumption in horticulture will be 126 PJ. This is more than the target cited in the MJA (111 PJ). If the ENSEC is brought back to the agreed value by means of enhancing the production value (increasing the denominator instead of decreasing the nominator in Eqn. 2.1) the violation of the objective with respect

9

to the absolute level of the energy consumption in horticulture would become even more severe. Therefore, the measures proposed in the MJA to decrease ENSEC aim at the decrement of energy consumption rather than the increment of production. In Section 2.2 these measures are presented in more detail.

2.2 OPTIONS THAT CONTRIBUTE TO ENERGY SAVING

Having read Section 2.1, it is obvious that, in order to reach the target of the MJA, there is a great need necessity to decrease energy consumption in glasshouse production. In the MJA a strategy has been formulated to achieve this decrement. The strategy is based on extension work, education on energy-saving techniques and research. The document presents a large number of energy-saving measures, which are subdivided into six clusters. The first five clusters are arranged in a sequential level of applicability. The sixth cluster consists of measures in which organizational and management problems dominate the technical issue. The suggestions are listed in Table 2.1

Table 2.1 Measures proposed by the MJA (Meerjarenafspraak) to save primary energy.

Cluster	Proposed measurements
1.	a. Condenser
	b. Boiler insulation
	c. Attachment of the expansion tank
	d. Location of the heating pipes
	e. Decrement of leakage
	f. Insulation of transport pipes
	g. Boiler control
	h. Climate controller
2.	a. Overhead screens
	b. Screens along gables
3.	a. Heat storage
	b. CO_2 supply with pure CO_2
	c. Distribution circuit volume
4.	a. Heat pump
	b. Alternative cladding materials
5.	a. Geothermal energy
	b. Long-term heat storage
	c. Wind turbines
	d. Application of Biogas
	e. Low energy demanding greenhouses
	f. (Semi)closed greenhouses
	g. CO_2-storage
6.	a. Waste heat at low temperature level (about 60 °C)
	b. Reject heat at high temperature level (about 90 °C)
	c. Combined heat and power

In all activities in the field of extension work and education on energy-saving techniques, the energy-saving prospects and the costs associated with implementation are the two central points of interest. Such information, combined with economic constraints, enables growers and extension workers to select appropriate measures. As far as economic quantities are concerned, a vast amount of information is readily available (Kwantitatieve Informatie, 1994). However, gathering data on the energy conserving prospects of the proposed options is much more difficult.

The major problem with energy-saving techniques that saving potentials are dependent on the horticultural context in which the measures are applied. This difficulty is explained in more detail in Chapter 3. To overcome this problem, the present study uses a simulation model that serves as a tool to estimate energy-saving measures in the context of today's horticulture. To illustrate the results that can be obtained using this tool, nine of the options mentioned in Table 2.1 are evaluated. The evaluated options are grouped according to three items. The results of the evaluations are presented in Chapter 6.

The first item concerns relatively simple improvements to the engineering of the greenhouse heating system. The second item concerns improvements to the greenhouse building and the third item involves the application of energy-saving heating devices. These three items are discussed briefly below.

2.2.1 Improvements of heating system engineering

In Table 2.1 five measures are proposed that deal with the engineering of the heating system (Option 1b, 1c, 1d, 1f, 3c). Most of these measures are stated in the first cluster, meaning that they are readily available. Decrement of the volume of the distribution circuit (Option 3c), which improves the controllability of the heating system, means the replacement of all heat distribution loops in a heating circuit and, therefore, it is a major operation (heat distribution loops in a one hectare greenhouse have a total length of some 12 km). Thus the application of small volume heating pipes is only an option in nurseries that have yet to be built. The effect of the volume of heating pipes has not been considered in this study in order to limit the number of options to be discussed.

Of the four remaining options, three options will be evaluated in Chapter 6, namely the insulation of the boiler, the insulation of transport pipes and the attachment of the expansion system. Insulation of the boiler and transport pipes is a relatively simple operation. The attachment of the expansion system to the heating system is expected to affect energy consumption because it affects the mean temperature of the expansion vessel (and therefore its energy loss).

Computations on energy-savings from the alteration of the location of heating pipes are not performed because the present work does not provide sufficient entries to study this effect.

2.2.2 Improvements of the greenhouse building

With respect to measures concerning the greenhouse building six options have been identified in Table 2.1 (Option 1e, 2a, 2b, 4b, 5e and 5f). In Chapter 6 Option 1e, 2a, 4b and 5e will be evaluated.

The decrement of leakage involves the careful tuning of the ventilation equipment to ensure that all windows are closed when they are meant to be closed. Overhead screens are considered to be an important method in decreasing heat loss from the greenhouse cover. Screens in gables (Option 2b) have been left out of this discussion because of the one-dimensional character of the simulation model (see Chapter 3).

With respect to alternative cladding materials the energy saving property of a number of options to increase insulation will be studied. This will be done along the line of yet available techniques.

Option 5e is treated in the context of the improvement of greenhouse cladding, since the heat loss can be considered to be concentrated around the covering structure.

Option 5f is not studied because the thrust of this option is strongly dependent on new technologies for cooling and dehumidification, which lay far beyond the scope of this work.

Contrary to the measures discussed in Section 2.2.1, improved insulation of the greenhouse may have implications for biomass production because the amount of solar radiation entering the greenhouse can be diminished by additional absorbtion by the covering structure. Therefore, the effect of measures in this item are expressed in terms of specific energy consumption, defined as the amount of primary energy consumption per unit of photosynthesis.

2.2.3 Energy conserving heating devices

In Chapter 6 three options concerning the application of energy-saving heating devices are discussed, namely the condenser (Option 1a), the short-term heat storage facility (Option 3a) and the combined heat and power engine (Option 6c). All these options can be readily applied in nowadays horticulture.

The hardware and software that will be assumed to be used with the condenser and the combined heat and power engine will have a negligible effect on the greenhouse climate. Therefore, these devices will not have an effect on biomass

production. However, this is not the case as far as a heat storage tank is concerned because the CO_2 supply regime and, with it the indoor CO_2 concentration is linked to a heat storage tank. Thus, just as in Section 2.2.2 the energy savings from heat storage are judged on its effect on specific energy consumption.

Again, the implementation of measures from the fifth cluster, such as Option 5a, 5c and 5d are left out of discussion because of their experimental character. Heat pumps and the application of reject and waste heat are not discussed either because these heating devices require a thorough revision of the heating system in the present generation of greenhouses.

3. A SIMULATION MODEL AS A TOOL TO ANALYZE ENERGY-CONSERVING TECHNIQUES

3.1 INTRODUCTION

The most simple concept of a modern greenhouse with respect to energy consumption is a building that gains heat from the sun and from combustion of fossil fuels and looses energy to its environment through sensible and latent heat release. Of these energy inputs, only the consumption of primary fuels (oil, natural gas etc.) are generally considered as energy consumption. Therefore, energy conservation is judged on its impact on fossil fuel input only. Energy-saving techniques affect the energy household by enlarging the contribution of solar radiation in the energy input, improving the conversion efficiency between primary fuels and usable heat or by achieving a decrement of energy losses.

The absolute, and often even the relative effect of measures to save fossil fuels are related to the level of energy demand. This energy demand is a highly dynamic quantity due to the diurnal variations in weather conditions outside the glasshouse and, to a lesser extent, variations in the required indoor climate. Therefore, to study the impact of energy-conserving techniques, the dynamic characteristics of energy demand on which these techniques act must be available. Generally, these characteristics involve more than one factor. A condenser, for example, increases the conversion efficiency of a boiler as a function of two variables, namely the current heating power of the boiler and the temperature of the water fed to the condenser. Another example is the application of thermal screens, which save significantly more in a greenhouse with a young crop than in a greenhouse with a mature crop, because in the latter the screen is quite often opened to some extent to carry off moisture.

Especially the last example demonstrates that the potentials of energy saving techniques must be studied within the context of a greenhouse. In this work, this context is created artificially by means of a simulation model. The model describes primary energy demand, as a function of the required indoor climate and outside weather conditions. To realize the required indoor climate the model includes a greenhouse climate controller. Its characteristics and that of the building, the canopy and the heating and ventilation systems are taken into account.

The application of a simulation model enables a fast and reproducible analysis of the effect of various energy-saving strategies on a year round base. In this chapter the requirements on the model are formulated. Moreover, the approach chosen to build such a model is presented.

3.2 MODEL REQUIREMENTS

The consumption of primary energy in greenhouses takes place in the heating devices that comprise the heating system. The heating devices considered in this work are a boiler, a heat storage tank, a condenser and a combined heat and power engine (CHP engine). The boiler and the CHP engine are assumed to apply natural gas as the primary energy source. The heat storage tank delays the application of heat produced earlier by the boiler or the CHP engine and the condenser produces heat from exhaust gases. Thus a heat storage tank and a condenser do not consume primary energy. Therefore they have an indirect effect on energy consumption only. The performance of the heating devices, especially the condenser the heat storage tank, depends on operating conditions, such as the required heating power, the required supply temperature and the temperature of the water returning from the heating circuits.

The required heating power and supply temperature are determined by the greenhouse climate controller. Therefore, the formulation of the demands on the simulation model begins with the requirements of the climate controller.

Climate controller actions are based on a comparison between the desired conditions of the greenhouse air (temperature, humidity and CO_2 concentration) and actual values. Thus the actual values of the greenhouse air conditions have to be described by the simulation model. The desired conditions are defined by controller setpoints. Because the greenhouse climate controller is part of a closed-loop process (except illumination control), the simulation model has to describe the impact of controller actions such as heating power and carbon dioxide supply on its feed-back quantities. Feed-back quantities for customary greenhouse climate controllers are the greenhouse air temperature, humidity and CO_2 concentration and the temperatures of the upper and lower heating circuit. When a storage tank is available, the temperatures at the top and bottom of the tank are two additional important quantities. Consequently, all these quantities have to be described by the state variables of the model.

In line with the decision to begin the description of the demands on the model with the climate controller, the state variables that serve as an input variable for the climate controller are referred to as primary state variables. The course of the primary state variables is not determined by controller actions only, but are also a result of interactions with the environment of the physical objects they represent. The environment includes other objects, represented by other state variables (defined as secondary state variables) and the outside weather conditions. The course of secondary state variables affect the greenhouse climate controller's actions only indirectly.

Among the secondary state variables in the greenhouse, the canopy temperature is the most important because it has a considerable impact on transpiration and photosynthesis (Stanghellini, 1987; Gijzen, 1992). Photosynthesis affects the CO_2

concentration, and transpiration has an important impact on humidity and the heat demand of the greenhouse.

The temperatures of the greenhouse cover, floor and soil are the next important secondary state variables. The cover temperature determines the extent of convective and radiative losses at the roof. Moreover, in case its temperature is below the dewpoint, condensation occurs, resulting in a dehumidification of the greenhouse air. The soil temperature has a considerable influence on the greenhouse climate on days with large fluctuations in temperature and solar radiation level because it can accumulate and release large amounts of heat. To be able to describe a temperature gradient, the soil has to be split into a number of layers (Bot, 1983; Houter, 1989; Takakura, 1990). The top layer of the soil is referred to as the floor.

The energy losses at the roof are significantly diminished by the application of a thermal screen. Because the closed screen acts as a shield to thermal radiation, the temperature of the screen is an important quantity. Moreover, a closed screen separates the greenhouse air into two compartments. Therefore, by the definition of three state variables for the air above the screen, the temperature, humidity and CO_2 concentration of the air above the closed screen is distinguished from the temperature, humidity and CO_2 concentration of the air below the screen.

If the greenhouse is equipped with a heat storage tank another set of secondary state variables has to be distinguished, namely the temperature of the water strata between the top and bottom of the storage tank. During charge and discharge of the tank these strata shift downward and upward respectively.

In Figure 3.1, all state variables are depicted in closed frames. The open frames refer to the exogenous state variables (see below). The primary state variables are accentuated by bold frames. The frame of the state variable representing the thermal screen's temperature is extended to improve readability of the picture. The notational conventions with respect to the naming of variables are presented in Sections 5.2.1, 5.2.4 and 5.2.5.

Besides by actions of the greenhouse controller, conditions in the greenhouse are severely affected by the exogenous state variables representing the outside air and sky temperature and the outside humidity and CO_2 concentration. The air and sky temperature affect the convective and radiative heat losses at the greenhouse cover. The sky temperature is defined as the black body temperature of the sky vault, representing the thermal radiation from the atmosphere according to Stefan Boltzman (see appendix E). Outside air temperature, humidity and CO_2 concentration have implications for the indoor climate conditions by air exchange through opened windows and cracks.

Solar radiation is an important exogenous flux variable since the sun is the most important heat source of a greenhouse. Moreover, the sun is essential for photosynthesis and important with respect to canopy transpiration. Because greenhouse

transmissivity and photosynthetic activity differ significantly for direct and diffuse radiation, the solar radiation data have to describe both quantities. The third meteorological quantity required for the simulation model is wind speed because of its impact on ventilation and heat losses from the cover.
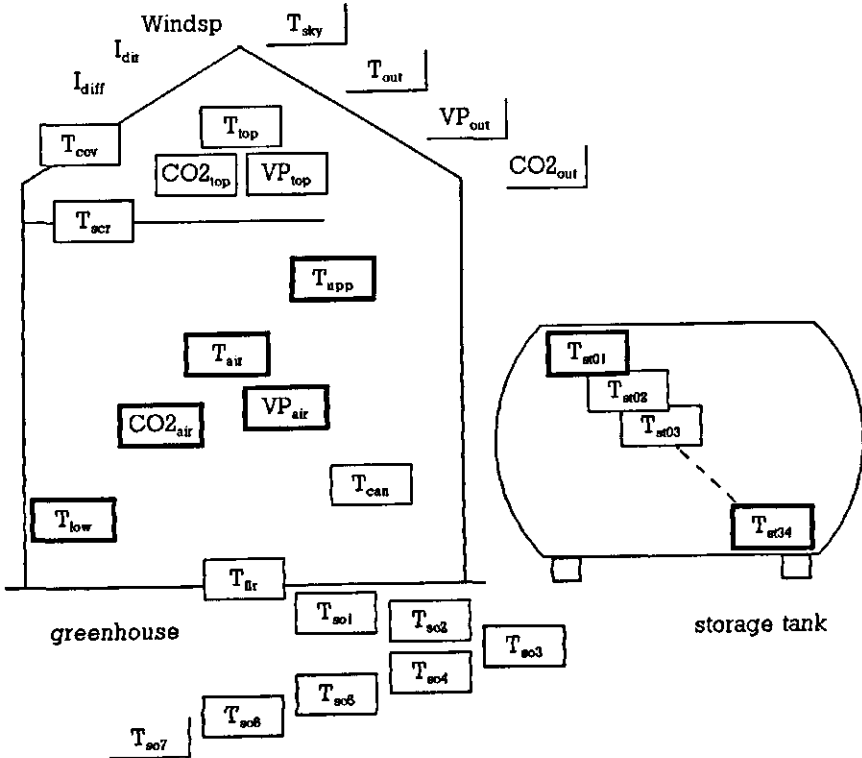
Figure 3.1 Graphic representation of the state variables in the model.

During the night, the variations of outside weather conditions and the indoor climate are relatively small. Thus the controller output and performance of the heating devices is quite constant, which allows a simulation model that generates data on greenhouse conditions with hourly intervals or even larger. However, some time before sunrise, and during the daytime, greenhouse climate conditions can change quickly due to setpoint changes, opening of the thermal screen, variations in solar radiation and ventilation. As a result the controller output also changes frequently. Thus, to keep up with the dynamics of real greenhouse climate controllers, the interval for simulated data on greenhouse air conditions must be in the order of minutes.

Since many weather data sets are presented in hourly averages, the model samples the weather data with at one hourly intervals, However, to prevent large stepwise

changes from one hour to the next, the meteorological data between the hourly means are approximated by linear interpolation.

Finally, because alterations to the greenhouse building, its heating devices and its control may have implications for canopy growth, the model requires the description of biomass production.

3.3 MODEL BUILDING

The development of simulation models can be considered two follow one of two routes (Palm, 1986). One route is to find a relation between the input and output of a system solely by observing the input and output data. This is called system identification and the model generated is often referred to as a black-box model. This technique is employed successfully in control engineering applications. In greenhouse climate modelling the black-box approach was adopted by Udink ten Cate (1983) for instance. In general, the parameters in this type of model have a limited physical interpretation and have to be determined in an experimental set-up.

The second route is to split up the system to be modelled into a number of smaller subsystems whose properties are well known from previous experience, and to follow this with an appropriate interconnection (Ljung, 1987). This modelling approach is based on the computation of the level of a state variable in a part of the system from the net flux to the considered part. The energy content of such a part is governed by an energy balance according to

$$\frac{dE}{dt} = \phi_{net,E} \qquad \qquad [Js^{-1}] \; (3.1)$$

If the state variable concerns a mass content, its rate of change is governed by a mass balance reading:

$$\frac{dm}{dt} = \phi_{net,m} \qquad \qquad [kgs^{-1}] \; (3.2)$$

In general terms a net flux is defined by:

$$\phi_{net} = \sum \phi_{in} - \sum \phi_{out} + \sum \text{production} \qquad [a.u.s^{-1}] \; (3.3)$$

The production term, which is generally important in models for chemical reactions, is zero in all net flux computations stated in this work. The fluxes ϕ_{in} and ϕ_{out} are either forced fluxes (e.g. an electric heater) or fluxes that result from a potential difference between the considered part of the system and its environment (e.g. a temperature difference between a heating pipe and air). By definition, forced fluxes have an imposed magnitude. Fluxes that result from a potential difference are determined by a flux equation.

For heat transport ϕ_{net} is expressed in W. The flux equation between two discrete physical entities reads:

$$\phi_E = G \, (T_a - T_b) \qquad \text{[W] (3.4)}$$

with G a conductivity (WK^{-1}) and T_a-T_b (K) the temperature difference that serves as a potential difference. The conductivity can be a function of the temperature difference. When T_a refers to the physical entity of interest and T_b to a temperature of an entity of its environment Eqn. 3.4 describes an outward flux (otherwise Eqn. 3.4 describes an inward flux). T_a can be either a boundary variable or the temperature of other modelled entities.

The net heat flux to a physical entity induces a temperature change rate according to

$$\frac{dT}{dt} = \frac{1}{V \rho \, c_p} \; (\sum_{i=1}^{n} G_i(T-T_i)+ \; \sum \text{ production}) \qquad \text{[Ks}^{-1}\text{] (3.5)}$$

with V the volume (m^3), ρ the density (kgm^{-3}) and c_p the specific thermal capacity $(Jkg^{-1}K^{-1})$ of the entity. n is the number of distinguished fluxes from other entities. The notation of Eqn. 3.5 with T at the right hand side of the equation and dT/dt at the left hand side stresses that the differential equation can be solved by forward integration. The denominator of the right hand side of Eqn. 3.5 is referred to as the capacity of the state variable.

For mass transport ϕ_{net} is expressed in kgs^{-1}. The flux equation for mass transport relates the flux to a concentration difference. In general terms it reads:

$$\phi_m = k \, (c_a - c_b) \qquad \text{[kgs}^{-1}\text{] (3.6)}$$

with k a mass transfer coefficient (m^3s^{-1}) and c_a-c_b (K) the concentration difference. The net mass flux to a distinguished volume induces a concentration change rate according to

$$\frac{dc}{dt} = \frac{1}{V} \; (\sum_{i=1}^{n} k_i(c-c_i) + \; \sum \text{ production}) \qquad \text{[kgm}^{-3}\text{s}^{-1}\text{] (3.7)}$$

with V the volume (m^3) of the entity. As in Eqn. 3.5, n is the number of distinguished fluxes from other entities. In the present model, state variables that are governed by mass balances are expressed as a partial pressure. However, a concentration can be expressed as a partial pressure quite easily by application of the ideal gas law. Doing so, Eqn. 3.7 turns into:

$$\frac{dP}{dt} = \frac{R \, T}{M \, V} \; (\sum_{i=1}^{n} k_i^*(P-P_i) + \; \sum \text{ production}) \qquad \text{[Pas}^{-1}\text{] (3.8)}$$

with R the universal gas constant $(8314 \; Jkmol^{-1}K^{-1})$ and T the temperature of the volume (K), M the molar mass of the constituent of interest $(kgkmol^{-1})$ and V the dimension of the volume (m^3). k^* is an exchange coefficient that relates a mass

flux to partial pressure difference.

The integrals of Eqns. 3.5 and 3.7 or 3.8 describe the course of the state variables over time. For simple systems, when the fluxes depend linearly on the values of the state variables, the integral can be solved analytically. However, when models become a bit more complex, as is certainly the case with the model discussed in this work, the equations are solved with a numerical integration scheme (e.g. Euler-integration).

The major advantage of the construction of models by combining previous experience over the black-box model, is the physical meaning of the variables and intermediate results in a model developed along the second route. Because these quantities (fluxes, temperatures and pressures) can be interpreted physically, adaptions of the greenhouse system in order to decrease its energy consumption can be studied by modifying small parts to the model.

The second route of model building was employed by Bot & van Dixhoorn (1978) in order to build a detailed and validated greenhouse climate simulation model. From general theory on heat and mass transport, they assembled a model that described the course of temperature and humidity in a greenhouse as a function of pipe-temperature, solar radiation, ventilation and outside weather. An important part of the simulation model presented in this work is an elaboration on their model.

Since the late seventies, scientific progress in the field of greenhouse climate models has been achieved by improving the description of the heat exchange processes in the greenhouse. Goudriaan (1977) developed impressive tools to compute the absorbtion of both long-wave and short-wave radiation within a canopy stand. Bot (1983) was the first to present a complete greenhouse climate simulation model that could readily be implemented on a computer. He extensively described the ventilation process, light transmission and convective heat exchange at the greenhouse cladding and convective heat exchange processes between the greenhouse air, the heating pipes, the canopy and the soil. In addition he made a first start to the computation of the transpiration of a canopy. Stanghellini (1987) provided a sounder base for the description of canopy transpiration, in particular for a tomato stand. Balemans (1989) described heat and mass exchange at and through thermal screens. De Jong (1991) contributed considerably to the description and computation of the ventilation process through windows.

Many others have constructed greenhouse climate simulation models by compositions, and mostly small modifications or simplifications, of the work as compared to the previously mentioned authors (Takakura, 1992; Houter, 1989; Jolliet and Bailey, 1991).

With the theories presented in literature, the greenhouse climate part of the simulation model could be assembled. The description of the state-of-the-art greenhouse climate simulation model that emerged is presented in Chapter 5.

Contrary to the massive attention in the literature on the modelling of greenhouse climate, little attention has been given to the dynamics of the heating system and the description of the interaction between devices in that system. Therefore an important part of this study is devoted to the definition of models for elements in the heating system. Attention is also paid to the connection between these elements as they form an integrated system. The heating system model is presented in Chapter 4.

4. THE GREENHOUSE HEATING SYSTEM

4.1 INTRODUCTION

A greenhouse heating system consists of devices for heat production and heat dissipation. The devices for dissipation of heat, like pipes filled with hot water or hot air blowers, serve to create a favourable micro-climate around the canopy. When heat is dissipated from hot water pipes, the water is heated by one or more heat production devices. Hot air blowers combine dissipation and heat production. However, because of the relatively small importance of these devices in today horticulture, hot air blowers are not discussed here.

In Chapter 3 it was argued that the relation between the primary energy consumption of heat production devices and the heat produced depends on the duration and the conditions in which the devices are operated. Both factors are affected by the greenhouse climate controller and the greenhouse climate produced. In turn, the heating devices affect the greenhouse climate.

To structure this chain of processes, the greenhouse climate controller is considered to be the initiator of heating system performance. The interactions of the greenhouse climate controller with the heating system and the greenhouse climate is schematized in Figure 4.1
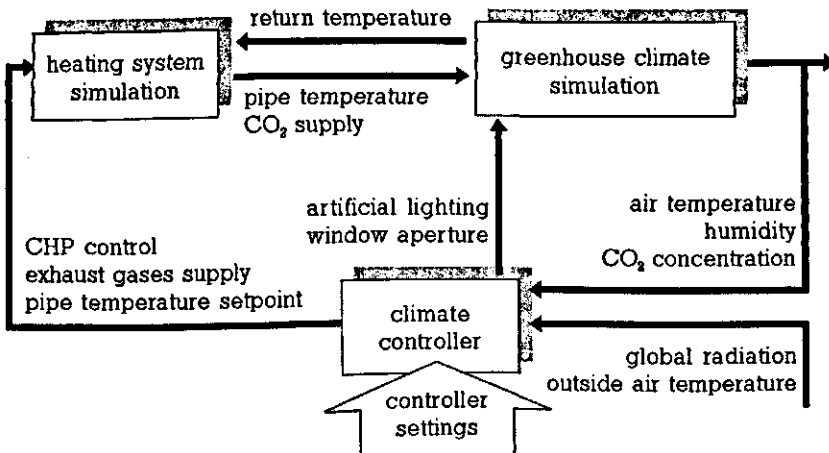
Figure 4.1 A schematic representation of the greenhouse climate controller initiating control actions on the heating system and the greenhouse. The greenhouse climate controller reacts to greenhouse air conditions.

Because of the central role assigned to the greenhouse climate controller, this chapter begins with a description of its functionality. The control actions imply the heating system, the control of ventilators, artificial illumination, carbon dioxide supply and thermal screens. Temperature, humidity and CO_2 concentration control require feed-back quantities to be compared to setpoints. The feed-back quantities are to be obtained from the greenhouse climate, which links the climate controller to the greenhouse climate simulation model. The greenhouse climate simulation model is discussed in Chapter 5.

The relation between control actions on the heating system and primary energy consumption is determined by the characteristics of individual devices in the heating system in conjunction with each other. Therefore, after discussing the greenhouse climate controller, the structure of a modern greenhouse heating system is displayed. This is followed by a presentation of models that describe the behaviour of the constituting devices.

4.2 A CUSTOMARY GREENHOUSE CLIMATE CONTROLLER

One of the reasons for the important improvements that have taken place in horticultural production during the last decades is the widespread introduction of integrated greenhouse climate controllers. A greenhouse climate controller attempts to realize a requested set of greenhouse air conditions by means of adjusting heating, ventilation and CO_2 supply. Also, it is quite common that the climate controller affects the amount of short-wave radiation in the greenhouse with shading screens (to decrease the amount of light) and artificial lighting (to increase radiation levels). In this work, shading screens are not discussed because principally they are not related to energy consumption, although the shading screen can be used as a thermal screen with very poor energy saving characteristics.

The determination of actual values for temperature, humidity and CO_2 setpoints can be situated at the top of the functional hierarchy of a climate controller. In general these setpoints are a result of settings obtained from the user interface, in combination with the time of day and the measurement of meteorological quantities. For example, the setpoint for the greenhouse air temperature is parametrized by a day and night temperature setpoint, a slope to increase the setpoint from the night value to the day value, a slope to bring the setpoint back from the day to the night value and a 'light dependent temperature setpoint increment'. The light dependent temperature setpoint increment constitutes a linear relation between the temperature setpoint and solar radiation. It is parametrized by the tangent of the relation, a threshold on which to start the increment and a maximum increment. Humidity setpoints are commonly defined by a daytime and a nighttime value only. The climate controller of the present model takes account for all parametrizations mentioned above.

To control the carbon dioxide concentration, a climate controller supplies CO_2 by means of a strategy related to the maximal supply rate, rather than by realizing a CO_2 setpoint. In fact the parametrization concerns a maximal CO_2 concentration and a maximal supply rate. In modern controllers, the supply rate is governed by algorithms that take account of the presence of a heat storage facility. However, the greenhouse climate controller in the present model confines with the first mentioned, simple CO_2 supply strategy.

The on-off control of artificial illumination is based on the comparison of the actual intensity of global radiation with a setpoint. Besides the control based on outside radiation, for a preset period during the night, illumination is switched off. Moreover, illumination is commonly not applied between May and August.

The second level of functionality comprises the computation of requested window apertures and the determination of pipe temperature setpoints. Windows in a greenhouse can be opened either for dehumidification or to cool the greenhouse. Thus, in fact the window aperture is determined by two controllers. In the present model, both are implemented by proportional controllers. The controller for temperature opens the window only when the temperature exceeds the setpoint by a certain extent (e.g. 1 °C). A temperature excess above this dead zone implies an opening according to a particular proportional band. The humidity controller opens the window at an angle proportional to the relative excess compared to a humidity setpoint. The final window aperture is the maximum of the apertures requested by the controllers.

The window controller first opens the leeside ventilators. When the computed window aperture exceeds a particular deflection (e.g. 30°), the controller on the leeside windows becomes saturated. Then the windward side windows are opened as well. In fact, in the model, the control of the windward side windows is similar to the control of leeside windows but with a dead zone of 7 °C.

The heating pipe controller computes a requested pipe temperature excess on the greenhouse air temperature setpoint with a (digital) PI-controller. In the first instance, the controller output is assigned to the primary heating circuit. However, when this temperature exceeds a threshold, which is defined in the user interface, the secondary heating circuit starts to accompany the primary heating circuit. The excess of the requested temperature on this threshold is assigned partly to the primary and partly to the secondary circuit.

Apart from the temperature controller, a preset minimum pipe temperature affects the requested pipe temperature. A minimum pipe temperature is defined in the user interface and is commonly set at some 40 to 50 °C. In general the requested minimum pipe temperature during the night differs from the minimum pipe temperature setpoint for the day. Moreover, during the day, when the intensity of outside global radiation exceeds a threshold (e.g. 100 Wm^{-2}) the setpoint for the minimum pipe temperature is decreased linear on the excess. In the present model

the rate of decrease is such that the minimum pipe temperature equals the air temperature setpoint when the solar radiation is 300 Wm^{-2}. The pipe temperature to be realized is the maximum of the minimum pipe temperature and the tempearture computed by greenhouse air temperature controller.

The third level of hierarchy in a greenhouse climate controller is constituted by mixing valve controllers. The mixing valve controllers adjust the valve position when the temperature of the water deviates from the setpoint passed from the heating pipe controller. Commonly the temperature of the water after mixing is measured just behind the valve.

4.3 BASIC STRUCTURE OF A MODERN GREENHOUSE HEATING SYSTEM

In this study, the term heating system refers to a set of devices for the production, transport and dissipation of heat. The simplest heating system consists of a boiler, transport pipes and one or more heating circuits. In Figure 4.2 a sketch of such a heating system is presented. To strain different agglomerates in the heating system the boiler is drawn in a boiler house, which is connected to the greenhouse by a transport pipe. The heating circuits are located in the greenhouse, which is the other agglomerate.
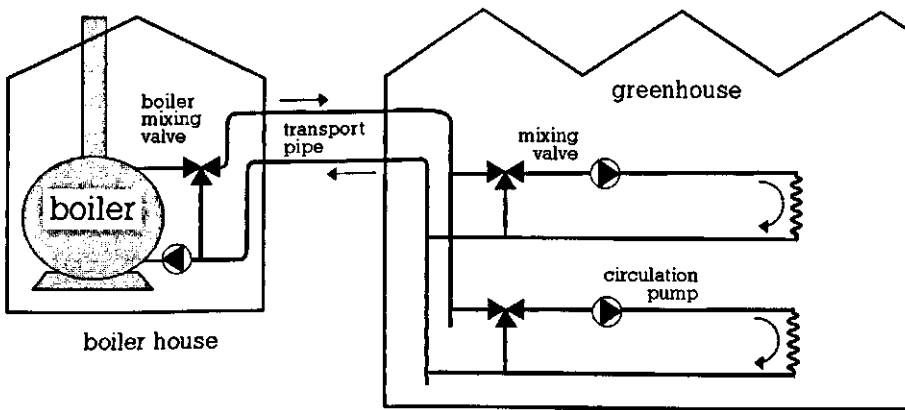
Figure 4.2 A simple greenhouse heating system.

By controlling the boiler mixing valve, the temperature in the transport pipe can be kept a few degrees higher than the highest temperature requested in the heating circuits. The temperature of the water in the heating circuits is controlled by a mixing valve on each circuit.

In recent years, the simple concept shown in Figure 4.2 has evolved into a much more complicated system, which includes a condenser, a heat storage tank and a combined heat and power engine (CHP engine). The condenser was introduced after the first energy crisis in the early seventies. The introduction of heat storage tanks was coupled to the application of CO_2 from exhaust gases from the boiler and began in the mid-eighties (Vermeulen, 1987). Such a storage tank accumulates heat surpluses when the boiler combusts gas in order to produce CO_2 during periods when there is no (or limited) heat demand. Accumulated heat can be withdrawn during periods of heavy heat demand. The application of CHP engines began in the late eighties. First these engines appear on nurseries that applied artificial illumination in order to produce their own electricity. Nowadays the majority of CHP engines in horticulture produce electricity for the public grid (CBS, 1994a).

The addition of these components to the heating system implied serious adaptions of the boiler house. Both the boiler and CHP engine have to be connected to the heat storage tank and the condenser requires a second transport pipe from the boiler house to the greenhouse. This second transport pipe brings the return water from the coldest heating circuit to the condenser. When this second transport pipe is omitted the condenser is fed from the return side of the transport pipe, at a temperature close to the return temperature of the hottest heating circuit. Such a high temperature affects the efficiency of the condenser negatively.

An example of a heating system made up of the devices mentioned above is presented in Figure 4.3
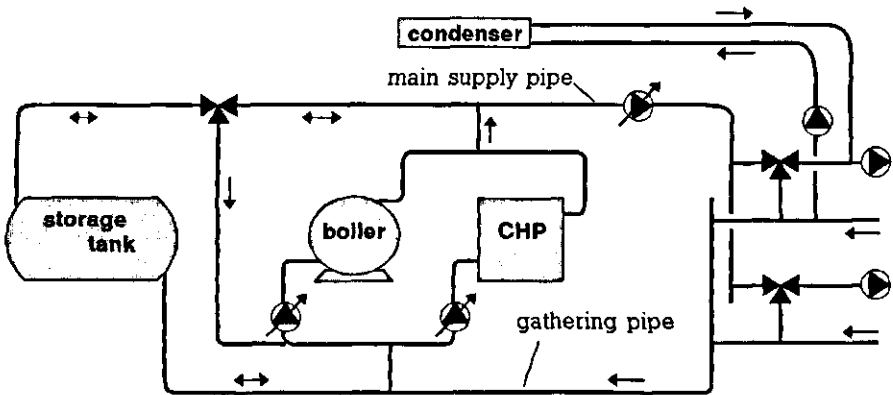
Figure 4.3 A heating system with a boiler, a condenser, combined heat and power and a short-term heat storage facility.

Figure 4.3 makes clear that the CHP engine is treated in the same way as the boiler. The heating circuit connected to the condenser also has a connection with the transport pipe from the boiler (and CHP and heat storage tank). This facility enables a supply of additional power to this heating circuit if the heating power of the condenser is insufficient.

Each of the devices in the heating system as shown in Figure 4.3 has it's own peculiarities. In the next section, models for the various elements are proposed.

4.4 MODELS FOR HEATING SYSTEM DEVICES

4.4.1 The heating circuit

A greenhouse heating circuit consists of a main supply and return pipe, to which a large number of parallel heat distribution loops are connected. A sketch of such a heating circuit is presented in Figure 4.4.

The valve determines the mixing ratio between hot water supplied to the circuit and cooled water returning from the distribution loops. Thus the mixing valve enables the climate controller to realize a pipe temperature in the heating circuit, lower than the temperature of the water fed to the valve. The valve is able to realize any mixing ratio, although in general the relation between the valve position and mixing ratio is non-linear, especially near the extreme positions.

The circulation pump ensures a (more or less) constant flow through the heating circuitry, irrespective of the position of the mixing valve. Commonly the capacity of the circulation pump is such that the velocity in the distribution loops is about 0.08 ms^{-1}.
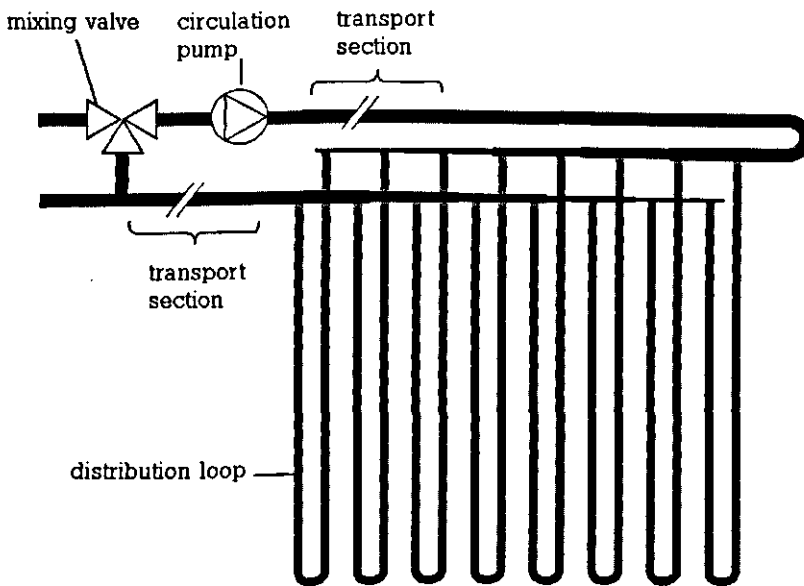
Figure 4.4 A greenhouse heating circuit with circulation pump and mixing valve.

A heating circuit contains a substantial amount of water (about $2.5 \cdot 10^{-3} \text{ m}^3$ per m^2 greenhouse) and, therefore, has a large heat capacity. Moreover, due to the structure of the heating circuit, and the capacity of the circulation pump, the time-lag between a temperature change at the main supply pipe and a new stationary situation at the main return pipe is in the order of twenty minutes. Because the

temperature of a heating circuit has to rise and fall frequently, the capacity and time lag of the heating circuitry has been taken into account in the present model. Most of the piping network is designed to serve both as a heat transport duct and a heating surface. Part of the piping is insulated and has a transport function only. In this section, a model is described that determines the temperature distribution along the heating circuit as a function of the temperature at the supply side of the circuit, taking into account the dynamics of the system. The model description is followed by a comparison of the model with measurements.

4.4.1.1 Model description

The starting point of the model description is the concept of a piece of heating pipe, filled with moving water. On the outer side, the pipe releases heat to its environment and on the inner side the pipe is heated by the water flowing through the pipe. This conceptualization is depicted in Figure 4.5.
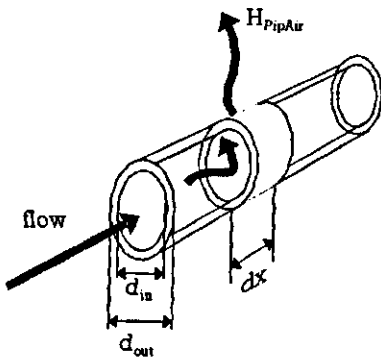
Figure 4.5 A section of a heat distribution loop loosing heat to the environment and gaining heat form water flowing through the pipe.

If the velocity of the water in the pipe is about 0.08 ms^{-1} and assuming an internal diameter of 0.047 m, the Reynolds number is about $6 \cdot 10^3$. Therefore it is allowed to neglect a radial temperature gradient. Moreover, because the resistance to heat transport from the outer pipe surface to the air is far greater than the resistance to heat transport from the inner to the outer surface of the piping material (a factor 100) it is allowed to state that the temperature of the pipe surface equals the water temperature. With the assumptions stated above the general differential equation that describes the temperature of an infinitesimal length dx reads:

$$\frac{\delta T_{pip}}{\delta t} = \frac{1}{cap} \ (-\alpha_{pip} \, P_{pip} \, dx (T_{pip} - T_{air}) + v\rho c_p \, A_{wet} \frac{\delta T}{\delta x}) \qquad [Ks^{-1}] \ (4.1)$$

The first term between the brackets of Eqn. 4.1 takes account of the heat exchange between the pipe and the environment. The thermal capacity of the pipe slice *cap* is computed from the lumped capacity of water and piping material. α_{pip} is a combined heat exchange coefficient of convective heat exchange between pipe and air and radiative heat exchange between the pipe and the opaque bodies around the pipe. p_{pip} is the perimeter of the pipe.

The second term in Eqn. 4.1 contributes for the net inflow of energy into the infinitesimal pipe slice. This term includes the velocity of the water v (ms^{-1}), the volumetric heat capacity of water ρc_p (Jm^{-3}K^{-1}), the wet surface of the pipe slice A_{wet} and the axial temperature gradient $\delta T/\delta x$.

In the present model, all differential equations are solved numerically. Therefore, both the axial gradient and the infinitesimal time step dt must be assigned to a finite length and time respectively. By making the length of a pipe segment such that the volume of the segment equals the volume of the water displaced through the pipe within the finite step in time both discretizations are parametrized by the discrete time step only. With the time step denoted by t_s the length of a discrete pipe segment is defined by:

$$l_{seg} = \frac{v \, t_s}{A_{wet}} \qquad \text{[m] (4.2)}$$

Denoting the temperature of a particular pipe segment $T_{pip,i}$ and the temperature of the adjacent pipe segment upstream $T_{pip,i-1}$, the discretization of Eqn. 4.1 yields:

$$\frac{dT_{pip,i}}{dt} = \frac{v\rho c_p A_{wet}(T_{pip,i-1}-T_{pip,i}) - \alpha_{pip}l_{seg}p_{pip}(T_{pip,i}-T_{air})}{Cap_{seg}} \qquad \text{[Ks}^{-1}\text{] (4.3)}$$

The thermal capacity of a pipe segment is computed by:

$$Cap_{seg} = \tfrac{1}{4}\pi \, l_{seg} \, (d_{in}^2 \, 4.18{\cdot}10^6 + 3.63{\cdot}10^6 \, (d_{out}^2 - d_{in}^2)) \qquad \text{[JK}^{-1}\text{] (4.4)}$$

where $4.18{\cdot}10^6$ and $3.63{\cdot}10^6$ are the volumetric thermal capacities of water and steel respectively (JK^{-1}m^{-3}).

Numerical integration of Eqn. 4.3 yields the course of the temperature of a pipe-segment in time. Application of the Euler-algorithm with the previously mentioned time step t_s yields:

$$T_{pip,i}(t+t_s) = T_{pip,i}(t) + t_s \frac{dT_{pip,i}(t)}{dt} \qquad \text{[K] (4.5)}$$

In case the heat loss of a pipe segment is negligible and the heat capacity of the piping material is small compared to the heat capacity of the water in the pipe, as is the case with the wide insulated main supply and return pipes in greenhouses it can be shown that Eqn 4.5 turns into a simple shift-register algorithm of the form $T_{pip,i}(t+t_s) = T_{pip,i-1}(t)$.

4.4.1.2 Results with the model

To test the model, measurements were carried out on the overhead heating circuit of a small greenhouse research accommodation of 200 m² (see also Section 6.2.1). A sketch of the heating circuit of this research facility is depicted in Fig. 4.6. The dimensions of the sketch are not to scale.
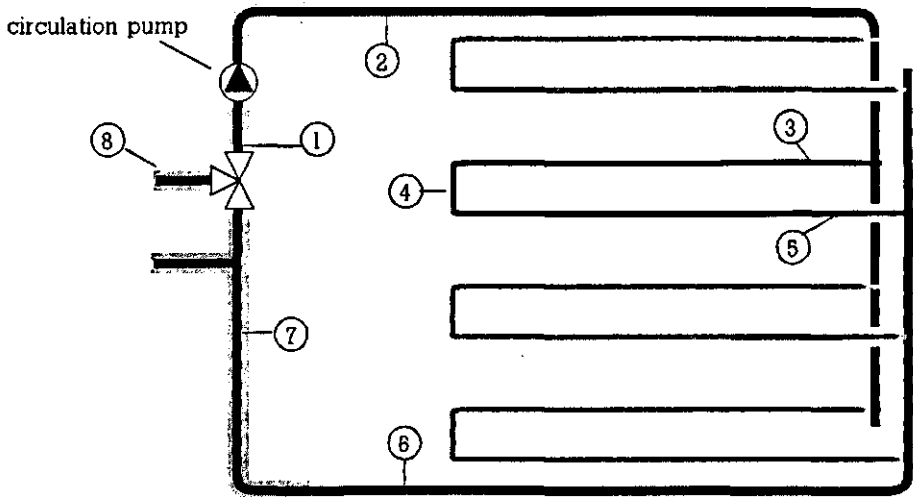
Figure 4.6 A sketch of the heat distribution circuit applied to test the heating circuit model. The location of the temperature sensors is indicated.

In the experiment eight temperature sensors (thermocouple, K-type) were attached on the pipe and wrapped with insulating material. The sensors were scanned every ten seconds by a datataker 500 data-acquisition device.

The first part of the heating system, which ran from the first sensor to the second, is a 12 meter steel pipe with an inner diameter of 41 mm and an outer diameter of 45 mm. With a capacity of the circulation pump being $3.3 \cdot 10^{-4}$ m³s⁻¹ the time lag of this part of the distribution system is 52 seconds. Thus, with a 10 seconds integration step (chosen to be equal to the sample interval of the measurements) five segments were used to represent the first part. The remaining two seconds were neglected. Since most of this section in the distribution system is insulated, the heat loss component was applied to the last segment only. The temperature at the first sensor is modelled by the temperature of the first segment.

The second section of the distributing system is a 28.5 meter pipe with a 47 mm inner diameter and a 51 mm outer diameter. This pipe section spans from the second sensor up to the attachment of the heat distribution loop. The time-lag in

this part of the system is 178 seconds, resulting in 18 model segments. The temperature at the second sensor is represented by the first segment of this part of the model.

The third section is formed by the heat distribution loop, which is 44 meter long. As can be seen in Fig. 4.6 the heat distribution loop with the sensors is the second of four loops. The pipe has an inner diameter of 25 mm, and when it is assumed that the water is divided equally over the heat distribution loops the time-lag in the third section is 282 seconds (28 segments). The temperature at the 3rd, 4th and 5th sensor is described by the 2nd, 14th and 27th segment of this section of the model respectively.

The fourth section, built from the same piping material as the second, spanned 31.5 meters. This section was modelled by 20 segments. The last segment of this model-section represents the temperature at the sixth sensor.

The final section, which ran from the sixth sensor to the mixing valve, is 17 meter long and is assembled from the same pipes as the first section. Thus it is described by a 7 segments model-section. Because the major part of this pipe is insulated, only the first two sections contribute to a heat loss component.

In the experiment, both the dynamic effects of a sudden opening of the valve and the cooling down process after the mixing valve is closed have been observed. The observation of the first effect was carried out after the valve has been closed for a long period of time to ensure that all water in the distribution circuit had the same temperature. The results of the measurements and the simulated temperatures are depicted in Figure 4.7.

Due to the specific characteristics of the heating system of the experimental greenhouse the supply water at the mixing valve (measured with sensor 8 and depicted with the dashed curve) took about 2 minutes to reach a temperature close to its final value. Moreover, during the time span of the rest of the experiment it showed a slow further increase. Because the supply water temperature at the mixing valve did not rise stepwise, in the simulation the measured supply water temperature was treated as an input variable. Figure 4.7 shows that the measured and simulated temperatures for Sensor 1 were very close to the dashed line. Indeed this must be expected because practically all return water from the distribution circuit is refreshed when the mixing valve is opened.

Besides the supply water temperature, the heat exchange coefficient α_{pip} is another input factor in the simulation model. From convective and radiative heat exchange theory, presented in Appendix A and Appendix E, an overall heat exchange coefficient was fitted as a function of temperature difference between pipe and air temperature, assuming that the radiative environment of the heating pipe concerns black elements at a temperature T_{air}. The best fit for the overall heat exchange coefficient for temperature differences in a range between 1 and 60 °C for the three types of heating pipes appeared to be:

$$\alpha = 6.8(T_{pip}-T_{air})^{0.18} \quad \text{1st and 5th section (45 mm)} \quad [Wm^{-2}K^{-1}] \text{ (4.6a)}$$
$$\alpha = 6.7(T_{pip}-T_{air})^{0.18} \quad \text{2nd and 4th section (51 mm)} \quad [Wm^{-2}K^{-1}] \text{ (4.6b)}$$
$$\alpha = 7.2(T_{pip}-T_{air})^{0.18} \quad \text{3rd section (28 mm)} \quad [Wm^{-2}K^{-1}] \text{ (4.6c)}$$

In these equations T_{pip} refers to the mean pipe temperature of a section. The exponent for the combined radiative and convective heat exchange coefficient is somewhat lower than the 0.25 that holds for a convective heat exchange coefficient solely because, for small temperature differences, the exchange coefficient of the radiative part in the heat exchange process is fairly constant (exponent zero).

In order to improve the match, for the comparisons between measurements and simulation the constant 6.7 in Eqn. 4.6b was incremented to 7.5 and the constant 7.2 in Eqn. 4.6c was enlarged to 8.0. An explanation for these higher values is that a number of assemblies were attached to these pipe sections (taps, chains to hang it in the greenhouse).
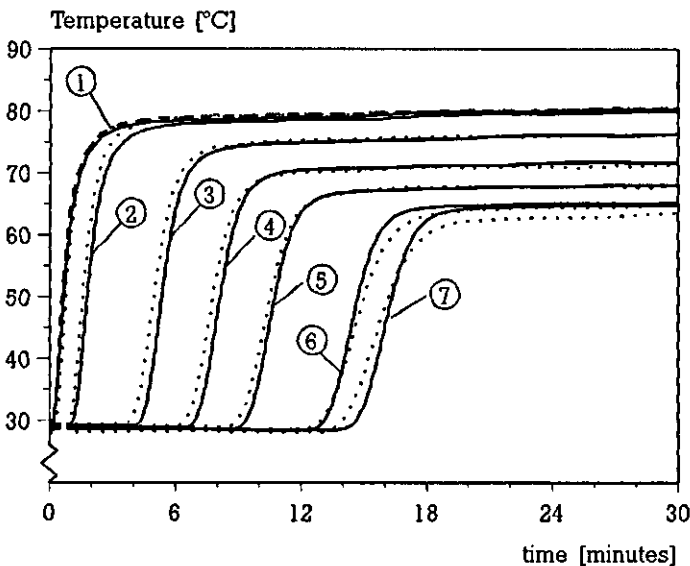
Figure 4.7 Temperatures at seven points in a distribution circuit half an hour after a stepwise opening of the mixing valve of the circuit. The numbers refer to Fig. 4.6. (··· = measured, —— = simulated, – – – = temperature of supply water, measured with sensor number 8).

In general Fig. 4.7 shows a good similarity between measurements and simulation, except for the seventh sensor. However, the considerable final temperature difference between the measured temperatures at Sensor 6 and 7 give rise to doubts about the signal of the seventh sensor. It is very unlikely that 17 meter pipe,

which is insulated for a large part, gives a temperature decrement comparable to the decrement of a more than thirty meters non-insulated and wider pipe in the fourth section of the distribution circuit. Therefore in the following no value is attributed to the level of the seventh sensor, but only to its dynamics.

The major difference between measurement and model occurs in the dynamics of the temperature at the 6th and 7th sensor. Contrary to the measurements the slope of the simulated temperatures at the 6th and 7th is similar to the slope of the other curves. The slope of the measured temperature curves for these last two sensors is significantly less than the slope of the other curves. A plausible reason for this discrepancy is the model assumption that the time for a water sample to travel through the circuit is equal irrespective of the distribution loop through which it travels, whereas in a real circuit slightly different hydraulic resistances cause small velocity differences in the distribution loops. Since the main return pipe mixes the water from four distribution loops the differences in travelling times induce a less steep temperature rise.

Measurement and simulation of the cooling down of the heating circuit are shown in Figures 4.8 and 4.9.
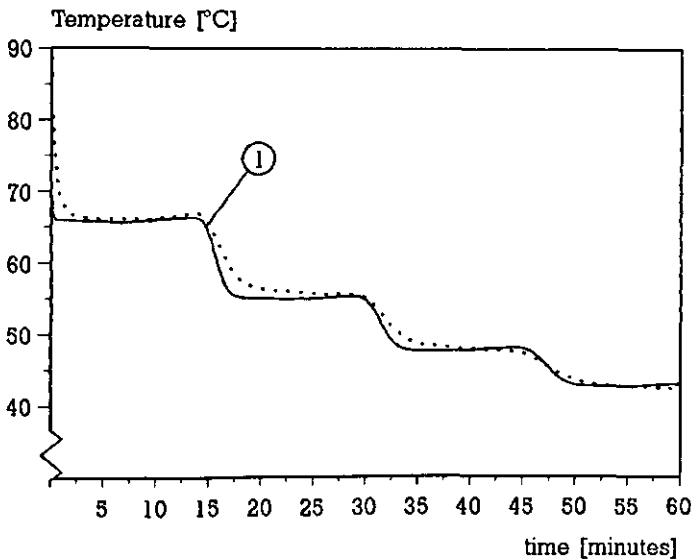
Figure 4.8 Measured (· · ·) and simulated (———) temperature at the first sensor after closing the mixing valve.
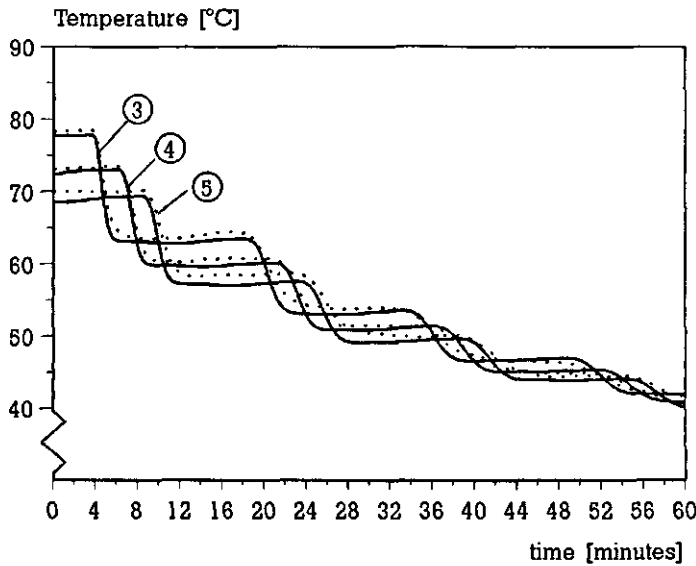
Temperature [°C]

Figure 4.9 Temperatures at the third, fourth and fifth sensor after closing the mixing valve (· · · = measured, ⎯⎯⎯ = simulated).

Again, the simulation is in fair agreement with the measurements. However, in Fig. 4.8 it can be seen that the simulated temperature drops are slightly steeper than the measured curve. The slow decrease of the measured temperature at the first sensor, just at the beginning of the process is probably caused by some capacitive effects of the attachment of the sensor to the pipe.

The other less steep slopes of measured temperature decrements than the simulated curves can be contributed to the same effect that caused the slower temperature rise at the 6th and 7th sensor as discussed above. The fact that in this graph the measured and simulated temperatures at the first sensor show a good match after a few minutes, gives further reason for doubting the measured temperatures at the 7th sensor (see discussion on Fig. 4.7). because, after closing the valve, the temperatures at the seventh and first sensor are in fact about equal (apart from a small time-lag).

In Figure 4.9 it can be clearly seen that it takes about 4 minutes before the effects of changes at the mixing valve occur at the beginning of the heat distribution loop.

4.4.1.3 Conclusions

From a comparison of the results of simulation and measurement, as discussed in the previous section, it can be concluded that the proposed model indeed describes the dynamics of the type of heat distribution systems commonly applied nowadays in horticulture. Moreover the results show that the cooling down curve of a distribution circuit does not yield a smoothly decreasing return temperature but a series of rather fast temperature decrements succeeded by rather long periods of constant temperature. However, in a commercial greenhouse, where normally more than some 50 distribution loops are attached to a single main supply and return pipe this effect will be much less pronounced because quite important differences in travelling times through the distribution loops will are likely.

4.4.1.4 Connection between the heating circuit model and the greenhouse climate simulation model

As stated in Chapter 3, the greenhouse climate simulation model takes account of a single state variable for both the upper and lower heating pipe, whereas the heating circuit model applies some 50 state variables per heating circuit. To connect both approaches, the pipe temperature applied for a heating pipe in the greenhouse climate simulation model is the mean of the pipe segment temperatures in the distribution loop section of the heating circuit model.

Another complication is the heat exchange coefficient at the distribution loops (α_{pip}), which has to be a lumped convective and radiative heat exchange coefficient in the present model, whereas, as will appear in Chapter 5, the greenhouse climate simulation model separates the heat release in a convective and several radiative heat transfer processes. This problem is solved by the computation of a heat exchange coefficient at each simulation step from the sum of all heat losses from the heating pipe, as computed by the greenhouse climate simulation model, and the actual temperature difference between the mean pipe temperature and the air temperature. As a formula this approach reads:

$$\alpha_{pip} = \frac{H_{loss}}{(mean(T_{pip}) - T_{air}) \, l_{pip} \, P_{pip}} \qquad [\text{Wm}^{-2}\text{K}^{-1}] \ (4.7)$$

where the operator *mean* refers to a function computing the mean value of the temperatures of the pipe segments.

4.4.2 Main supply pipe and gathering pipe

The main supply pipe (see Fig. 4.3) collects hot water from the devices that produce heat and transports this water to the mixing valves of the heating circuits. The gathering pipe brings the water back from the heating circuits to the heat producing devices. In this study, in order to be in line with the tendency in present day horticulture, the flow through the main supply pipe, and consequently through the gathering pipe as well, is assumed to be variable.

The volume-perimeter ratio of transport pipes is comparable to, or even larger then, that of the main supply and return pipes, discussed in the former section. Moreover the pipes are commonly insulated. Thus, if the pipes are long, the time lag induced can be described by a simple shift register (see Section 4.4.1.1).

However, in most greenhouses the mixing valves of the heating circuits are concentrated in the boiler house. Consequently, the model presented in this work omits a time-lag in the distributing pipes.

4.4.3 Boiler

Boilers applied in horticulture are devices with a heating capacity that ranges up to about 7.5 MW. Typically the installed heating capacity is 250 Wm^{-2} greenhouse. The boilers are constructed from a horizontal cylindric vessel filled with water in which a large combustion chamber and a number of tubes conducting hot combustion gases are situated (see Fig. 4.10).
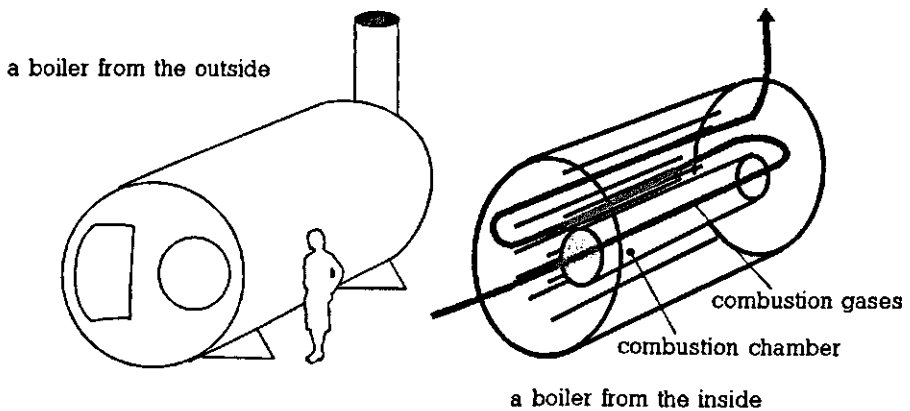
Figure 4.10 Sketch of a horticultural boiler.

The combustion gases flow from the combustion chamber to the rear side of the boiler. Then the gases make their way to the front of the boiler through some 10 to 20 pipes. At the front, the direction of flow is again reversed. The flue gases flow backward through another set of pipes. Finally the gases leave the boiler to the chimney or, if present, to the condenser.

Due to the heavy construction and large amount of water in the boiler (in the order of 10 m^3 for a boiler in a one hectare nursery) the boiler represents a massive heat capacity. However, since the temperature of the water in the boiler is kept (about) constant (90 °C), with respect to the p[resent model the capacity of the boiler is of little interest.

Commonly, a single loop controller on the temperature of the water in the boiler adjusts the power of the heater in the boiler. By adjusting the flow from the boiler to the transport pipe, the device can produce any heating power requested. For a short time the boiler can even supply more power than the maximal power of the heater.

Apart from the production of heat, the boiler can be used to generate CO_2 to enrich the greenhouse air with carbon dioxide. To ensure the production of CO_2 when there is a need for CO_2 supply, the heating power of the boiler can be bounded to a minimal value.

To limit the heat losses at the surface of the boiler, the boiler is insulated with rockwool and covered with thin PVC or aluminum plates. With insulation, the total resistance to heat transport of the boiler wall is a series of two resistances, namely the thermal resistance of the rockwool and the surface resistance to heat transport of the boiler covering. Thus, the overall heat exchange coefficient for heat loss from the boiler surface, being the reciprocal of the total resistance, is defined by:

$$\alpha_{boiler} = (\ 1/\alpha_{insu} + 1/\alpha_{surf})^{-1} \qquad\qquad [Wm^{-2}K^{-1}]\ (4.8)$$

In Eqn. 4.8 the resistances of the insulation material and the boiler surface are expressed by the reciprocal of the heat exchange coefficients.

For the insulation material, the heat exchange coefficient can be found in handbooks. For rockwool a value $\alpha_{insu} = 0.04/d_{insu}$ was found (polytechnisch zakboekje 1987), with d_{insu} the thickness of the insulation (m).

The heat loss at the surface results from the sum of radiative and convective heat exchange. Both these exchange mechanisms are a non-linear function of temperature difference between surface and environment (see Appendices A and E). Since the surface temperature depends on the thermal resistance of the boiler wall, the heat loss at the surface has to be determined by an iterative procedure. The result of this procedure for the heat exchange coefficient of a boiler with water at 90 °C to an environment at 20 °C as a function of insulation thickness is shown in Figure 4.11. The diameter of the boiler (the characteristic dimension for the com-

putation of the convective heat loss) was assumed to be 2.3 m and the emission coefficient of the aluminum covering was assumed to be 0.3.

To illustrate that the overall heat exchange coefficient above a certain insulation thickness is governed by the insulation, the heat exchange coefficient of rockwool is shown as a dashed line. Obviously, when the insulation thickness exceeds 5 cm, the overall heat exchange coefficient is governed completely by the thermal resistance of the insulation material.

Heat exchange coefficient [$Wm^{-2}K^{-1}$]
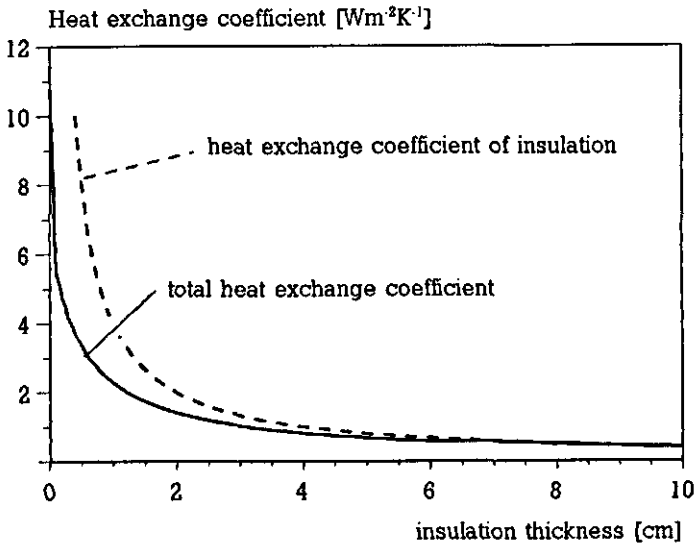
Figure 4.11 Heat exchange coefficient of a boiler with water at 90 °C to an environment at 20 °C as a function of insulation thickness (full curve). The dashed curve shows the heat exchange coefficient of the rockwool insulation solely.

4.4.4 Condenser

A condenser exploits the latent heat present in the exhaust gases of a boiler or a combined heat and power engine. Thus, the heating power of a condenser is primarily governed by the amount and composition of exhaust gases. However, since a condenser is a heat exchanger, the second determining factor for the heating power is the temperature of the water entering the condenser. This is because condensation occurs only when the temperature of the heat exchanging surface is below the dewpoint of the exhaust gases. This dewpoint is some 60 °C (Meijndert, 1983).

In horticultural practice a distinction is made between a 'single condenser' and a 'combi condenser'. A single condenser has only one heat exchanging circuit and a combi condenser has two. In a combi condenser the heat extraction from the exhaust gases is performed in two stages. The first stage is meant to cool the gases to a temperature of about 80 °C, whereas in the second stage the gases are cooled to temperatures below the dewpoint. In a single condenser the entire cooling process is performed in the one heat exchanger.

The major reason for using a combi condenser rather than a single condenser is that the first enables to connect the first stage of the device to the gathering pipe (see Fig. 4.3). For this type of condenser, only the second stage of the device has to be connected to a low temerature heating circuit. Thus, part of the heat gathered by the condenser becomes available at a widely applicable, relatively high temperature. Consequently, the heat release capacity of the heating circuit applied to carry off the latent heat of the exhaust gases (gathered in the second stage) can be smaller. In fact, the typical characteristics of a condenser are concentrated on the second section of the combi condenser only. Because the high temperature character of the heat gathered in the first section, from modelling point of view, this section can be considered a part of the boiler. Thus, the second section of a combi condenser can be treated as a single condenser which cools exhaust gases from a boiler with an enhanced conversion efficiency.

The reasoning above leads to the conclusion that, from the modelling perspective, the same approach can be taken to a single and a combi condenser, providing that the conversion efficiency of the boiler is treated as a variable. Such a model is presented in the next section. In Section 4.4.4.2 some results obtained with the model are shown.

4.4.4.1 Model description

The first factor that affects condenser performance is the constitution of the combustion gases. From the literature (Gasunie, 1980) it can be calculated that the combustion of 1 m³ natural gas (Slochteren quality, at 0 °C and standard pressure

of 101 kPa) requires 2.52 kg O_2 and produces 1.35 kg water. Since the combustion of gas is performed by the addition of outside air which contains about 20.7% oxygen, it can be computed that stoichiometric combustion[a] of natural gas requires 11.0 kg of outside air.

With the density of natural gas, being 0.834 kgm^{-3} and λ the air factor[b], the total mass flow of the exhaust gases is expressed by:

$$\mu_{exh} = 0.83 + 11.0\,\lambda \qquad\qquad\qquad \text{[kgm}^{-3} \text{ combusted gas] (4.9)}$$

The major components in the exhaust gases are N_2 and O_2, which originate from the outside air, and H_2O and CO_2, which are combustion products. Only a small fraction of the exhaust gases is made up of other gases (Argon, NO_x etc).

The specific heat capacity of the exhaust gas can be computed from the specific heat of the components, weighed according to their mass ratio in the mixture.

$$c_{p,exh} = \frac{(2.0\ \mu_{H2O} + 1.07\ \mu_{N2} + 0.82\ \mu_{CO2} + 0.92\ \mu_{O2})\ 10^3}{(\mu_{H2O} + \mu_{N2} + \mu_{CO2} + \mu_{O2})} \qquad \text{[Jm}^{-3}\text{K}^{-1}\text{] (4.10)}$$

with μ_{H2O}, μ_{N2}, μ_{CO2} and μ_{O2} the mass of the major elements in the exhaust gases after combusting a m^3 natural gas and $2.0 \cdot 10^3$, $1.07 \cdot 10^3$, $0.82 \cdot 10^3$ and $0.92 \cdot 10^3$ the specific heat capacities of vapour, nitrogen, carbon dioxide and oxygen respectively. The mass of the major elements is stated by:

$$\mu_{H2O} = 1.35 + 0.08\,\lambda \qquad\qquad \text{[kgm}^{-3} \text{ combusted gas] (4.11a)}$$
$$\mu_{N2} = 8.20\,\lambda \qquad\qquad\qquad\ \text{[kgm}^{-3} \text{ combusted gas] (4.11b)}$$
$$\mu_{CO2} = 1.76 \qquad\qquad\qquad\quad\ \text{[kgm}^{-3} \text{ combusted gas] (4.11c)}$$
$$\mu_{O2} = (\lambda - 1)\ 2.50 \qquad\qquad\ \text{[kgm}^{-3} \text{ combusted gas] (4.11d)}$$

The term $0.08\,\lambda$ contributes to the vapour content of air led in to the combustion chamber. The value 0.08 is based on a humidity content of 7 gkg^{-1}, which holds for air of 15 °C and 70% RH. Of course weather conditions will affect the term, but as the term $0.08\,\lambda$ is already small compared to 1.35, the differences due to outside weather conditions have been neglected. The CO_2 content of outside air has also been neglected since, for a common value (340 ppm), this constitutes no more than about $0.56 \cdot 10^{-3}$ kgkg^{-1}.

The temperature at which the exhaust gases enter the condenser is dependent on the conversion efficiency of the boiler. To elucidate the heat fluxes, Figure 4.12 presents a schematic overview of the heat fluxes per m^3 combusted gas and temperatures in a boiler-condenser combination.

Referring to the boiler efficiency with a variable η_{boiler}, the heat content of the

---

[a]Combustion with exactly the required amount of oxygen

[b]The relative excess of oxygen compared to the amount required for stoichiometric combustion

exhaust gases at the entrance of the condenser is defined by:

$$Q_{exh} = (1 - \eta_{boiler})\, 35.16 \cdot 10^6 \qquad \text{[Jm}^{-3}\text{ combusted gas] (4.12)}$$

with $35.16 \cdot 10^6$ the upper heating value of natural gas [Jm^3]. Following the reasoning set out in the introduction to this section, in the case of a single condenser η_{boiler} is in the order of 0.85 (Handboek Verwarming Glastuinbouw, 1995), whereas the application of a combi condenser can be modelled by increasing η_{boiler} (to some figure between 0.87, and 0.89, depending on the size of the first stage) followed by a neglection of the first section of the combi condenser.
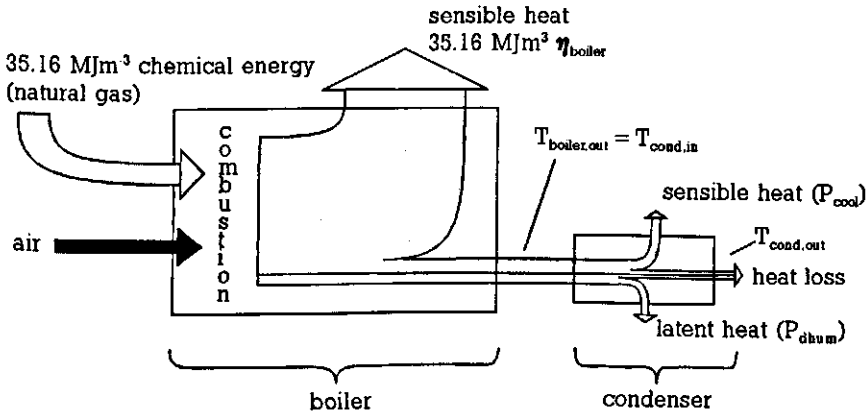
Figure 4.12 Heat fluxes per m^3 combusted gas and temperatures in a boiler-condenser combination.

A substantial fraction of the heat content consists of latent heat. The amount of latent heat can be determined easily from the amount of vapour produced by the combustion process.

$$Q_{latent} = \Delta H\, \mu_{H2O} \qquad \text{[Jm}^{-3}\text{ combusted gas] (4.13)}$$

with ΔH the heat of evaporation of water ($2.45 \cdot 10^6$ Jkg^{-1}). After computation of Q_{exh} and Q_{latent} the temperature of the exhaust gases at the outlet of the boiler is defined by:

$$T_{boiler,out} = T_{boiler,in} + \frac{Q_{exh} - Q_{latent}}{c_{p,exh}} \qquad \text{[K] (4.14)}$$

Air for combustion is normally extracted from the air of the boiler house. For convenience, the temperature of this air ($T_{boiler,in}$) is treated as a constant of 20 °C, which is a reasonable temperature for a boiler house.

After they have left the boiler, the condenser cools the gases to a temperature

which is some degrees higher than the water led to the condenser. The temperature difference between the gases leaving the condenser and the water fed to the condenser depends on the engineering characteristics of the device, and the magnitude of the exhaust gas flow. Within the context of this work there was no detailed information available on these characteristics. Product information on condensers shows that, at maximal exhaust gas flow, 12 °C is a reasonable value for the temperature difference between the gases leaving and the temperature of the water fed to the condenser (van Dijk Heating, 1995). At minimum exhaust gas flow (10% of full capacity), the temperature difference drops to 3 °C. As a first approach the relation between the temperature difference and exhaust gas flow is assumed to be linear dependent to the gas flow. Thus, since the exhaust gas flow depends linearly on the heating power of the boiler, the temperature of the gases leaving the condenser is described by:

$$T_{cond,out} = T_{water,in} + 2 + P_{boiler}/P_{boiler,max} \qquad [°C] (4.15)$$

The value P_{boiler} is the actual heating power of the boiler.

In case $T_{cond,out}$ is lower than the dew-point of the exhaust gases, the condenser withdraws latent heat by condensation. The amount of condensate can be computed easily by subtracting the moisture content of saturated exhaust air at a temperature $T_{cond,out}$ from the moisture content of the gases that leave the boiler. The saturated moisture content of the gases leaving the condenser can be determined by a fitted curve. A good approximation of the saturated moisture content of air in the temperature range between 30 and 60 °C was found to be:

$$x(t) = 1.882 \cdot 10^{-3} t^3 - 0.1412 t^2 + 5.018 t - 46.57 \qquad [gkg^{-1}] (4.16)$$

The moisture content of the gases that leave the boiler (and enter the condenser) is determined by:

$$x_{boiler,out} = \frac{\mu_{H2O}}{\mu_{exh} - \mu_{H2O}} 1 \cdot 10^3 \qquad [gkg^{-1}] (4.17)$$

The power added to the heating system by cooling (P_{cool}) and dehumidification (P_{dhum}) of the exhaust gases can now be expressed as:

$$P_{cool} = \Phi \, \mu_{exh} \, c_{p,exh}(T_{boiler,out} - T_{cond,out}) \qquad [W] (4.18a)$$

$$P_{dhum} = \Phi \, \mu_{exh} \, (1-x_{boiler,out}) \, 2.45 \cdot 10^3 (x(T_{cond,out}) - x_{boiler,out}) \qquad [W] (4.18b)$$

with Φ the gas combustion rate (m³natural gas per second). The term $(1-x_{boiler,out})$ is added because the moisture content is expressed as kg vapour per kg dry air, whereas μ_{exh} refers to the mass of humid air. The sum of Eqn. 4.18a and Eqn. 4.18b yields the heating power of the condenser.

$$P_{condenser} = P_{cool} + max\{0, P_{dhum}\} \qquad [W] (4.19)$$

The '*max*'-operator provides that P_{dhum} is zero when the temperature of the gases leaving the condenser is still above the dewpoint of the boiler exhaust.

4.4.4.2 Results

The calculation scheme described above was applied to determine the efficiency of a condenser as a function of the temperature fed to the condenser for two air factors (1.2 and 1.4) and for two relative exhaust gas flows (a value 0.2 and a value 0.8 times the maximal capacity). The results are shown in Figure 4.13. In the figure, an efficiency 1 means that all heat present in the exhaust gases (sensible and latent) is gained. In the computations the boiler is assumed to have an efficiency of 0.85 with respect to the upper heating value of natural gas.
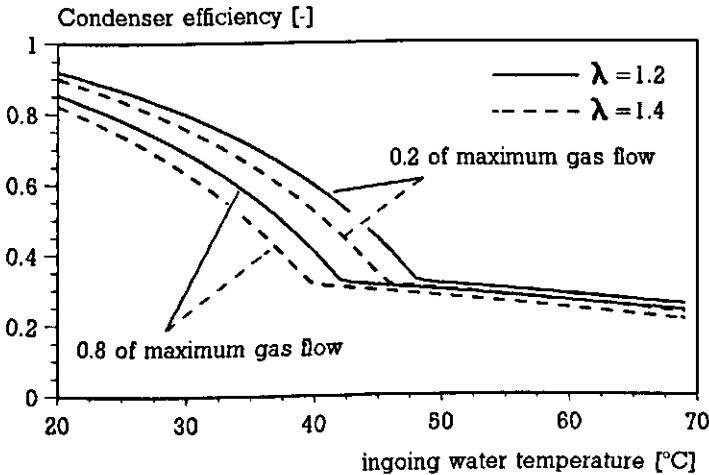
Figure 4.13 Efficiency of a condenser as a function of water temperature fed to the device, the air ratio and the relative exhaust gas flow.

The figure shows clearly that the condenser efficiency drops rapidly when the temperature of the water fed to the device increases. However, when the exhaust gases leave the condenser at a temperature above the dewpoint, the efficiency decreases slowly.

Figure 4.13 also shows that an increasing air factor reduces the efficiency of the condenser. This is caused by a decreasing dewpoint of the exhaust gases for higher values of the air factor, which can be seen from a combination of Eqn. 4.9 and Eqn. 4.17.

4.4.5 Combined Heat and Power

Combined heat and power engines (CHP engines) are designed to utilize the waste heat inherent in the conversion of fossil fuels to mechanical energy. Recent horticulture in the Netherlands shows a rapid increase in the application of these devices. By the end of 1993 CHP engines could be found on 12% of the nurseries (Velden et.al., 1995). The electricity produced by these engines is used on the nursery itself, but more and more of it is being fed to the public grid. Combinations of private use and supply to the public grid are also customary.

An on-site combined heat and power device used in horticulture is based on a piston engine that runs on natural gas. Nowadays, the typical thermal power output is about 400 kW per hectare. The typical accompanying electric power is about 250 kW. Figure 4.14 shows the frequency distribution of the installed thermal power of CHP engines in a recent survey on CHP-performance in 28 enterprises (Verhoeven et.al. 1995).
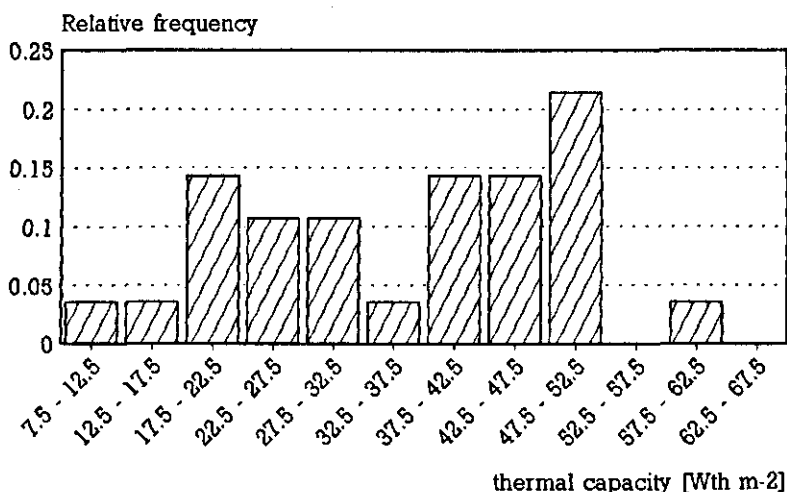
Figure 4.14 Frequency distribution of thermal capacity of CHP engines in a representative set of greenhouses with CHP in the Netherlands.

In general the larger engines were installed more recently than the smaller ones. Although the heating power output can usually be adjusted, a combined heat and power engine is operated at 100% capacity as much as possible. This is because the electric efficiency of the engine drops quickly when the shaft power of the engine decreases. Klimstra (1991) mentions a decrement of electricity production to 60% when the heat output is decreased to 70% of its full- load value. Parallel, the conversion efficiency of gas to electricity drops form 35% to 30%. When the

heat output is turned down to half the full-load capacity, the electricity production even drops to only 25% of its maximal value. Then the conversion efficiency of gas to electricity is only 17%. To prevent having to temper the heating output of the engine, in practice either a small heating power is chosen (<40 $W_{th}m^{-2}$), or the engine is coupled to a short-term heat storage tank.

As a consequence of the preference for operating a CHP engine at full-load, this work limits itself to treating the CHP engine as an on/off heat source. This simple approach tends to yield a large number of engine starts. However, because in all the simulations where CHP is applied a short term heat storage facility is also present, the number of starts and stops remains limited.

Since, due to the application of a storage tank the number of starts and stops is small (once or twice a day) and the heat capacity of the engine normalized per m^2 greenhouse is small (about 40 $JK^{-1}m^{-2}$ greenhouse[a]) in the present model the dynamic behaviour of the engine is neglected. Thus, when switched on, the combined heat and power engine is modelled to generate heat instantaneously at a level defined by its thermal heating power.

4.4.6 Short term heat storage facility

The short-term heat storage tanks used in horticulture are commonly horizontal oriented cylindrical vessels with a large diameter and filled with water. The water in the storage tank can be exchanged with the water in the heating system without passing heat exchangers. The vessels are well insulated. About 10 cm of rockwool is customary. The dimension of these tanks varies between some 50 m^3 to 150 m^3. Figure 4.15 gives an impression of such a facility and shows a cross section of the tank.

During heat accumulation, hot water flows into the tank at the upper side, and the replaces colder water which is sucked from the bottom of the tank. During discharge the process is reversed. By means of a careful design of in- and outstream pipes at the top and bottom of the storage tank the mixing of warm water in the upper part of the tank with cold water in the lower part is prevented as much as possible.

On a time scale of the order of some hours, the temperature of the water at the outlet of the storage tank has no relation with the charge or discharge power of the tank. This means that the instantaneous power that can be withdrawn from the storage tank is very large. Only when the temperature difference between inlet and

---

[a]Assuming a temperature difference of 60 °C between the on and off status of a CHP engine, the heat associated with its thermal capacity is less than 1 ‰ of the daily heat demand.

outlet is small, the power absorption or supply is seriously limited by the maximal flow to or from the tank.

In the following a model is presented, describing the dynamics of horticultural heat storage tanks.

cross-section detail

distributing pipe
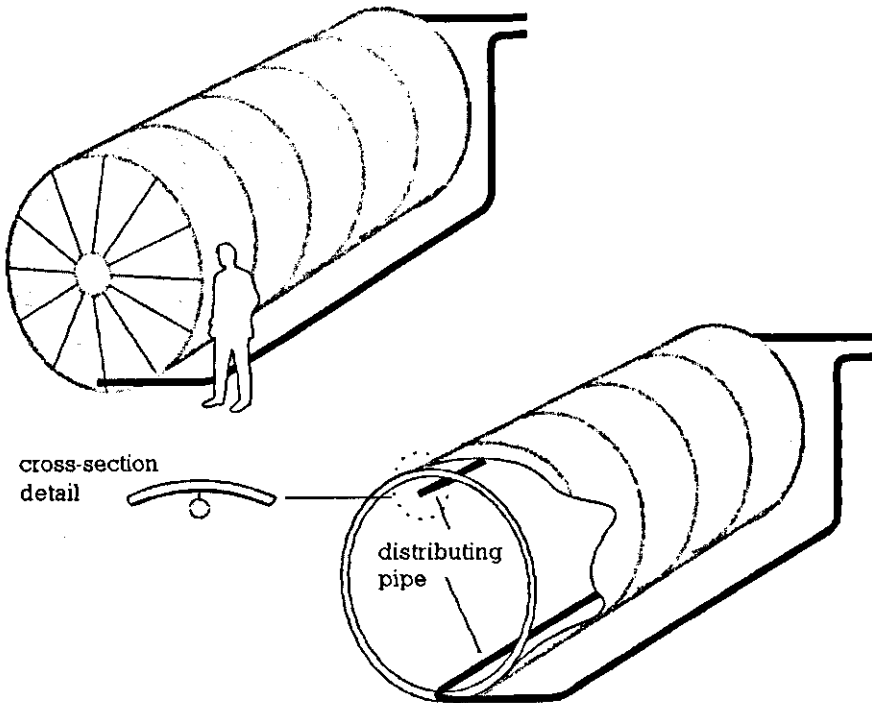
Figure 4.15 A horticultural heat storage tank.

4.4.6.1 Model description

Modelling and characterizing heat storage tanks is an important aspect of the theoretical and experimental work being done in relation to domestic solar heat collectors. Therefore, a large amount of literature on storage vessel modelling can be found in this field.

A central theme in both domestic heat storage vessels and the large storage tanks applied in horticulture is the stratification within the vessel. This is because in general a small amount of hot water is more favourable than a larger amount of warm water, providing the heat content is the same.

Since the density of water decreases with rising temperatures (temperatures above

4 °C), hot water tends to float on colder water. However, apart from the convective charging flow that moves the hot water strata through the vessel, buoyancy flows and conduction induce heat transport from the warm to the cold region. The relevance of conduction compared to displacement due to the forced charging flow is expressed by the Peclet number (Pe) (Yoo and Pak, 1993) as defined by:

$$\text{Pe} = \frac{v\,h}{a} \qquad\qquad \text{[-] (4.20)}$$

where v is the bulk flow velocity (ms^{-1}), h the height of the tank (m) and a the thermal diffusivity ($1.8 \cdot 10^{-7}$ m^{2}s^{-1} for water at 55 °C). In a heat storage process characterized by a small Peclet number (e.g. 100) diffusion plays an important role and the temperature changes from hot to cold over a large region. Therefore, the temperature of the cold water at the outlet of the tank already begins to increase when only 60% of the volume of the tank has been replaced by hot water. A large Peclet number (e.g. 800) means a steep change from hot to cold. In this way it is not un till the tank has been filled to about 90% that a temperature rise in the water coming out of the tank can be noticed.

During the operation of a heat storage tank in horticultural applications the Peclet number is commonly high, although not a constant. It not a constant because the charge and discharge flows vary in time. Moreover, even if the flow were be constant, the velocity of displacement of the boundary between hot and cold water would vary with the location of the interface due to the changing width of the (horizontal) cylinder. To get an indication of the Peclet number the bulk flow velocity of an 80 m^3 storage tank with a diameter of 2.8 m and a length of 13.0 m is determined where the charging flow is 10 m^3 per hour (taken as a practical figure). When the interface between the warm and cold water is located halfway up the tank the Pe number is at its minimum. From the figures above it can be calculated that the minimal Pe number equals $1.2 \cdot 10^3$.

Kleinbach, Beckman and Klein (1993) presented several types of numerical models to describe the dynamics of heat storage vessels. The first type, termed a multinode model, is simple, but neglects the specific property of a stratified storage tank, where hot water floats on colder water. This omission is not important when the Peclet number is small (e.g. 50). However, where the Pe number is large, the multinode model requires a very large amount (about 100) of 'nodes' (state variables) to yield steep temperature changes. Because, this is not the case in horticultural practice, as demonstrated above, the multinode model is less suitable. Therefore, in this study, the second model type, termed the plug-flow model is applied.

In the plug-flow model, hot packages of water shift upwards or downwards in a conceptual stack, according to a discharge or a charge flow respectively. In fact, the storage tank can be seen as a shift register which is able to shift in two direc-

tions. Sooner or later stored packages are extracted from the upper or lower side of the stack.

Contrary to the shift registers for the main supply and return pipe, applied in the heating circuit model described in Section 4.4.1, the speed with which water is displaced through the storage tank is not constant. As suggested, but not described, by Kleinbach et.al. (1993), the connection between the shifting process through the storage tank model and the other parts of the heating system can be performed by the definition of an accumulator at the head and tail of the shift register representing the storage tank. During charging, the top-accumulator shifts downwards into the first element of the shift register, but not before it has accumulated the continuous flow up to the volume of a shift register volume. During filling of the top-accumulator, the bottom-accumulator empties simultaneously. Because the actual volume of both accumulators together equals the volume of an element in the shift register, the moment the content of the top-accumulator is emptied in the first element of the shift register the content of the last element can be pushed into the bottom-accumulator which is empty at the same moment the top-accumulator is full. When the storage tank is being discharged, the process is reversed.

A visual presentation of the accumulator functionality is depicted in Figure 4.15.
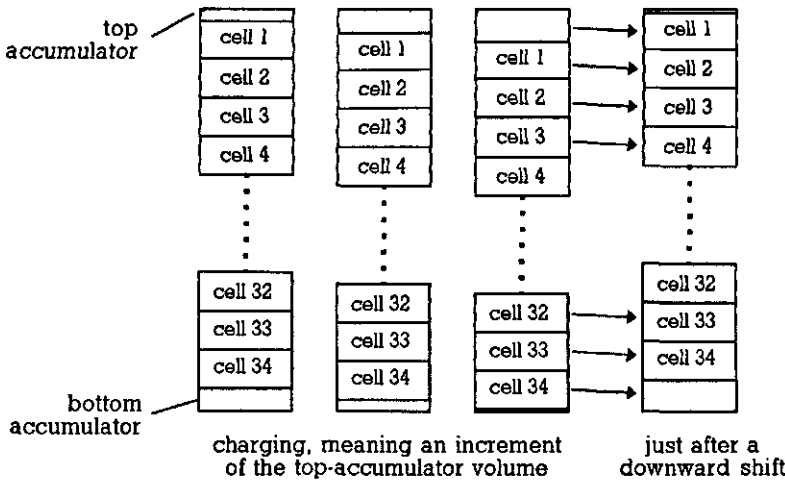
Figure 4.16 The shift register representing the storage tank with its top- and bottom-accumulator.

The temperature of the top-accumulator is equal to the temperature of the first element in the shift register. The temperature of the bottom-accumulator equals the temperature of the last element in the shift register.

During the filling of an accumulator, it is assumed that the in-flowing water is

perfectly mixed with the water already in the accumulator (which has the temperature of the adjacent compartment. This is acceptable since it is likely that there will be an intensive mixture of water near the inlet.

Besides temperature changes due to upward or downward shifting packages of water, temperature changes are induced by convective and conductive heat fluxes between water strata. Moreover, the storage tank looses heat through the wall to the outside air. Especially buoyancy flows, which occur at temperature inversions, induce a fast heat exchange between water strata. Kleinbach et.al. (1993) suggest taking account of buoyancy flows by averaging the temperature of adjacent compartments where the upper one has a lower temperature than the one beneath.

To describe these heat exchange processes, besides as elements of a shift register, the cells in the stack are considered as state variables capable to exchange heat with each other and through the wall to the outside air. The conductive heat exchange between compartments is determined by the discrete formulation for heat transfer through continuous media (see Section 5.5.2.2). If the distance between the centres of the first and second compartment is denoted d_i and the heat exchanging surface is called A_i (see figure 4.17), then the conductive heat loss from an element i to an element i+1 ($H_{StiSti+1}$) is described by:

$$H_{StiSti+1} = \frac{\lambda A_i (T_{sti} - T_{sti+1})}{d_i} \qquad [W] \; (4.21)$$

where λ denotes the thermal conductivity of water (0.6 Wm^{-1}K^{-1}). The variable A_i can be computed for the elements in a horizontal cylinder from the angle ω_i by $A_i = 2 l r \sin(\omega_i)$ (m^2), with l the length of the storage tank and r the radius of the tank (m). ω_i is solved from the equation:

$$\omega_i - \sin(\omega_i)\cos(\omega_i) = \pi \frac{V_{accu,top} + i \, V_{comp}}{V_{buffer}} \qquad [-] \; (4.22)$$

with $V_{accu,top}$ the actual volume of the top-accumulator. The variable d_i is determined by $d_i = r(\cos(\omega_{i-1})-\cos(\omega_{i+1}))/2$ (m). An example of the variables mentioned above for a storage tank represented by a shift register of 8 cells (N=8) is presented in Figure 4.17.

Obviously, when the volume of the top-accumulator changes, the angles ω_i change. For the first and last compartment the changes of ω have large effects, for the others the effect is very small. However, in the present model these changes of ω_i are neglected.

The heat losses to the environment are modelled with a simple coefficient of conductance referred to as G_{tank} (Wm^{-2}K^{-1}). Denoting the heat exchanging surface S_i, where the index i indicates the compartment number, the expression for the heat losses to the environment becomes

$$H_{StiOut} = G_{tank} \, S_i \, (T_{sti} - T_{out}) \qquad [W] \; (4.23)$$

where T_{out} denotes the temperature of the environment of the tank. Obviously the conductance of the insulation of the tank is taken to be constant. This is allowed since the (constant) thermal resistance of the insulation material fairly prevails over the resistance due to the varying outside convective heat exchange.

The variable S_i can be computed from $S_i = 2\,(l\,r\,(\omega_{i+1} - \omega_i) + \pi\,r\,V_{comp}/V_{buffer})\ (m^2)$. After computation of the heat fluxes, the temperature of the compartments a time-step ahead can be determined from:

$$T_{Sti}(t+t_s) = T_{Sti}(t) + \frac{t_s(H_{Sti-1Sti} - H_{StiSti+1} - H_{StiOut})}{\rho\,c_p\,V_{comp}} \qquad [°C]\ (4.24)$$

In Eqn. 4.24 t_s denotes the step-size. V_{comp} is $V_{buffer}/(N+1)$ for the second up to the last compartment but one. The volume of the first and last compartment is the same as the others, but incremented with the volume of the top- and bottom-accumulator respectively.
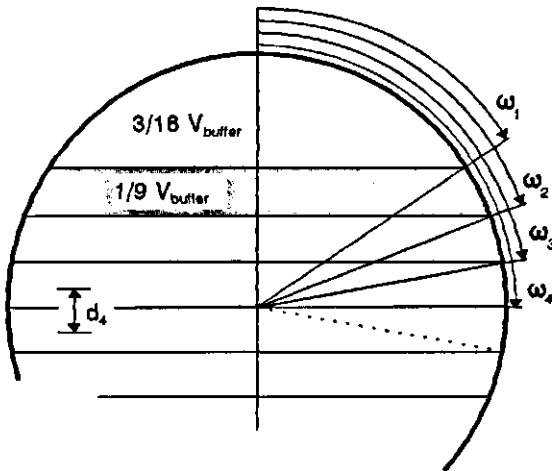
Figure 4.17 Examples of the angles ω_i, the distances d_i the volumes V_{comp} and the surfaces A_i for a heat storage simulation with eight compartments. The top-accumulator (and thus the bottom-accumulator) is filled for 50%.

Compared to the multi-node model, the steepness of temperature changes at the outlet is much less affected by the number of state variables. Where in a multi-node model an increment of the number of cells implies an increasingly steep temperature gradient, an increment of the number of state variables in the plug-flow model only affects the resolution of the temperature gradient (both in time and temperature level). This is because the output of the tank simulation has a zero-order hold character due to the discontinuous shifting process.

In this study the number of compartments is set at 34 (meaning that each cell in

the shift register represents $1/35^{th}$ of the storage tank volume.

In the theory described above a uniform velocity profile on the interface between warm and cold water was assumed. However, it is likely that the velocity at some parts of the interface is larger than at other parts. To include this in the plug-flow model, the emptying of the accumulator can be somewhat advanced. This means that an accumulator can be emptied into the shift register when its volume has grown to 90% of the register cell volume for example. In this case a fraction of the volume remains in each cell of the shift register (in this case 10%) and the rest shifts into the next cell. This modification yields a model comparable to the heating circuit model, where the piping material represents a thermal capacity that does not displace (see Section 4.4.1).

4.4.6.2 Results

To check the modelling approach, a heat storage tank in one of the IMAG-DLO research facilities was charged and discharged. Unlike the storage tanks used in actual horticulture, this tank was standing upright. However, the physical phenomena to be checked do not depend on the type of storage tank. Figure 4.18 shows a cross-section of the storage tank used. The volume of the tank was 4 m³ and it was insulated with 10 cm of rockwool, covered with aluminum plates.
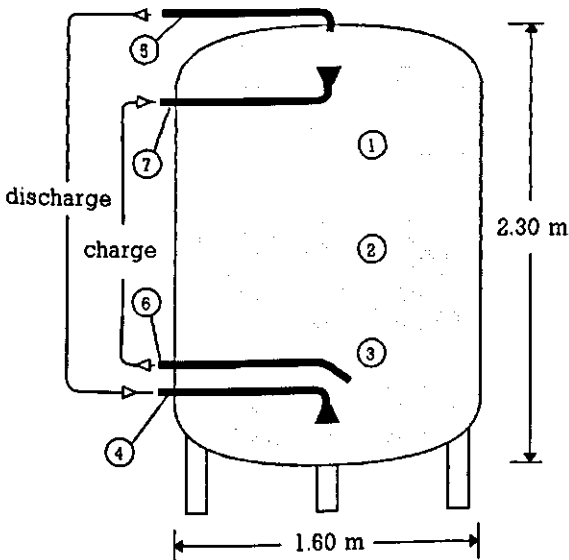
Figure 4.18 Cross-section of the heat storage facility applied to test the simulation model. The numbers refer to temperature sensors.

During discharge, the outlet at the upper side of the tank was supplied to the upper heating circuit of the research facility. The characteristics of this circuit are described in Section 4.4.1.2. When charging, as can be seen in the figure, another set of pipes is used than when discharge is taking place. This is another difference in the particular tank used here, compared to commonly tanks used in horticulture. In the simulations, 20% of the water in the model compartments is not displaced in order to account for the velocity differences at the interface between cold and hot water. This means that the accumulator is emptied when it reaches 80% of the volume of a compartment in the shift register.

The comparison of the model computations with measurements for a discharging tank which previously has been charged to a temperature of 67 °C is shown in Figure 4.19.
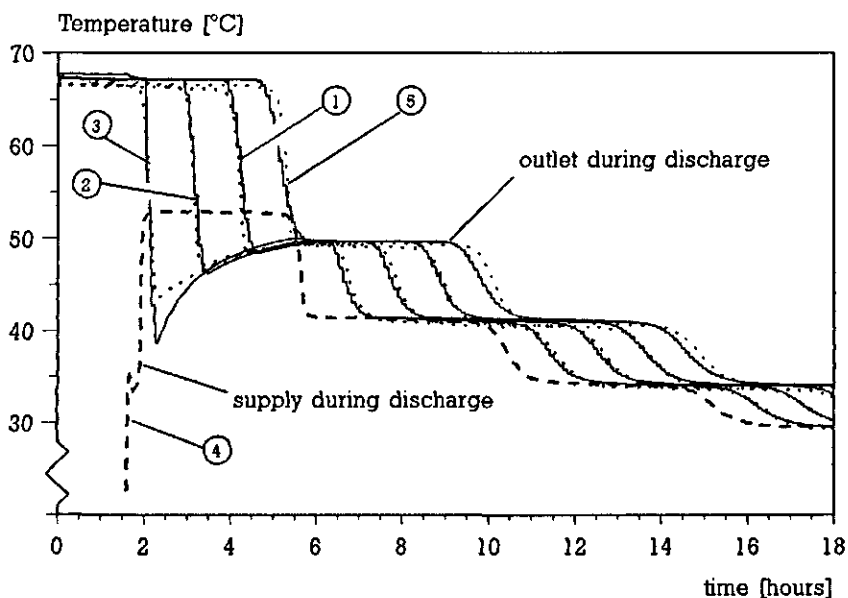
Figure 4.19 Comparison of model-output with measurement for the discharge of a heat storage tank. The numbers refer to figure 4.18 ($\cdots$ = measured, —— = simulated, – – – = temperature of supply water).

Except for the first hour for Sensor 3, the model and the simulation agree very well. The discharge process starts at t=1.6 hours. This point is marked by a steep increment in the dashed curve from 23 °C to about 34 °C. This 34 °C is the initial temperature of the water returning from the heating circuit that, the moment the discharge begins, flows along temperature Sensor 4 (see Figure 4.18). During the first hours of the discharge process, the heating circuit is fed with water at a temperature of 68 °C (Sensor Number 5). The circulation pump drives the dis-

charge with a flow that fluctuates between 0.90 and 0.92 m³ per hour (the flow was measured and passed to the model). After about 20 minutes, the return temperature of the heating circuit starts to rise towards 53 °C. This time lag of 20 minutes is larger than the 16 minutes that appear in Figure 4.8 because, during discharge of the storage tank, the pumping capacity is a factor 0.8 compared to the experiment subject to Section 4.4.1.2. This decreased flow is caused by an increased hydraulic resistance when the pump does not only transports the water through the heating circuit, but also through the storage tank (and its pipes and valves).

With a mean flow of 0.91 m³ per hour, the bending point in the flank of the outlet temperature drop is expected to occur 4.4 hours after the start of the discharge process. However, in the picture it appears that this point was reached half an hour earlier. This means that there is quite a lot of so called 'dead space' in the tank. The model has been tuned for this dead spaces by emptying the bottom accumulator in the 33nd cell instead of the 34th. This adaption was performed because the nozzle on the outlet of the pipe that brings the water into the tank is situated at about 20 cm above the bottom of the tank. The other reason of the advancement of the bending point is the fraction of 0.2 of the compartment volume that is modelled not to shift.

The fact that the output of the storage tank from t=6 hours up till t=9 hours was measured (and simulated) to be 49 °C and not the 53 °C that was supplied to the tank during the first hours of the discharge process is surprising. An explanation for this, and which has been included in the model, is that during charging, the storage tank was not completely heated to 67 °C, but that the bottom 50 cm remains relatively cold. This assumption is based on the location of the pipe that sucks the water from the tank during the charging process (see Figure 4.18). This will be discussed in more detail in the comments on the results of the charging process. Apparently the cold bottom stratum mixes with the supply water during the discharge. However, because this is a special peculiarity of this particular storage tank, no further comments are made on this subject.

The results of the comparison between model and measurements for the charge process are shown in Figure 4.20. The agreement of measurements and simulation for the charging process appears to be good. The course of the outlet temperature matches particularly well. Note that in the figure, the zero-order hold character of the model output can be seen very clearly.

The first part of the figure shows the end of a discharge process. During discharge the water is supplied to the bottom of the tank. The picture shows that the course of the temperature of the water that is sucked from the tank after the charging process has started (the curve labelled 6, starting at t=5 hours) is mirrored compared to the course of the temperature of the water pushed into the tank in the hours prior to t=5 hours (the curve labelled 4). However, a part of curve 4 cannot

be found in curve 6. This is because the pipe that sucks the water from the tank during charge is positioned higher in the tank than the pipe that pushes the water into the tank during discharge. The water below this pipe remains relatively cold, which leads to the peculiarity discussed in the comments in Fig. 4.19. The position of this pipe is also the reason for the relatively small time span between the rise of the temperature at Sensor 3 and the rise of the outlet temperature during the charging process (Sensor 6).
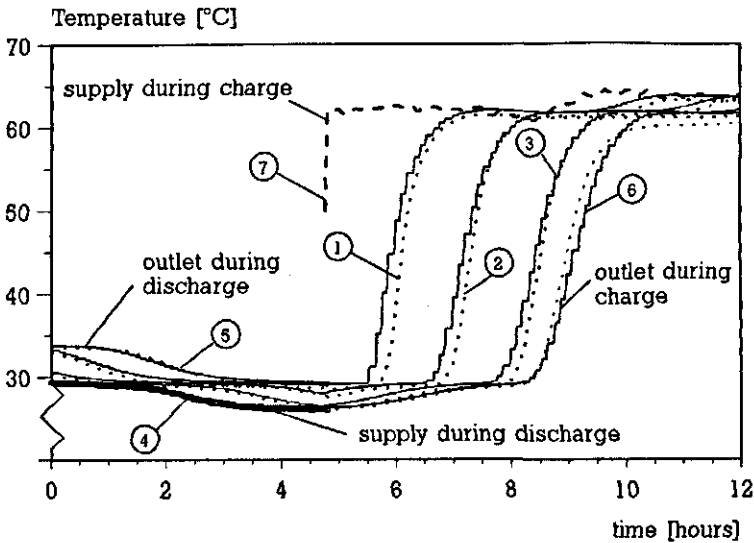
Figure 4.20 Comparison of model-output with measurement for the charge of a heat storage tank. The numbers refer to figure 4.18 (· · · · = measured, ——— = simulated, – – – = temperature of supply water).

4.4.6.3 Conclusions

The model proposed to describe the storage and extraction of heat from a storage tank compares satisfactorily with measurements on a storage tank at one of the research facilities in IMAG-DLO. By applying the plug-flow model only one modelling parameter, namely the fraction of the volume of a compartment that resists in a cell of the shift register, has to be estimated. All other parameters of the model are simply geometrical data.

4.4.7 Expansion system

The expansion system takes account of the varying volume of the heating system caused by the varying temperatures. The tank is attached somewhere to the heating system. The pressure in the tank is controlled by a compressor, which switches on when the pressure drops beneath a particular threshold (some 1.2 bar) and a valve that flushes air when the pressure exceeds an upper threshold (some 1.6 bar). Fig. 4.21 shows a sketch of an expansion system.

supply and return
pipe connected to
the heating system
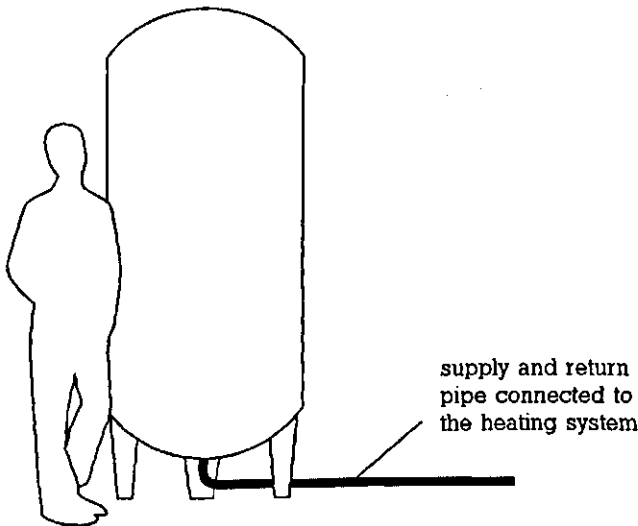
Figure 4.21 Expansion vessel.

When the mean temperature of the heating system increases, water flows into the expansion vessel. In this study it is assumed that this fresh water mixes completely with the water already in the vessel, which is likely since the fresh hot water enters the vessel at the bottom. Thus, the temperature of the water in the vessel after a certain amount of fresh water has entered can be computed by a weighed mean of temperatures. The weighing factors are the water volume in the expansion tank before the entrance of the fresh water and the volume that entered the expansion vessel The inflow of water is computed from the cubic expansion coefficient of water $(0.21 \cdot 10^{-3} \ K^{-1})$ and the temperature change in the different components in the heating system, each rated according to their volume.

When the water in the expansion vessel has a temperature that is higher than the temperature of its surrounding, the vessel looses energy through its uninsulated wall. Insulation of the vessel in order to decrease its heat loss is discouraged by

installers because it appears that current expansion vessels do not withstand continuously high temperatures.

To compute the energy loss, the tank is divided into two sections. The lower part of the tank is assumed to have the temperature of the water inside the tank. The temperature of the upper part is computed from a weighed mean of the water temperature and the temperature of the surroundings. The temperature of the water is weighed according to the surface of the interface between the lower and upper part of the vessel (the cross section of the vessel) and the surrounding temperature is weighed according to the surface of the upper side of the vessel.

The height of the lower side is computed from the current water volume in the tank and the area of the cross section of the tank.

The convective heat exchange coefficient of the vessel is computed from a Nu-Gr relation reading $Nu = 0.11 \, Gr^{0.33}$. This yielded a convective heat exchange coefficient of $1.44 \, \Delta T^{0.33} \, Wm^{-2}K^{-1}$. To this convective heat exchange coefficient a radiative heat exchange coefficient was added, assuming an emission coefficient of 0.8.

4.5 ASSEMBLING THE HEATING DEVICE MODELS

In the heating system all heating devices, apart from the condenser, are connected to each other by means of the main supply pipe (see Figure 4.3). The condenser is connected to the upper heating circuit. However, during periods of high heat demand, hot water from the main supply pipe can be added to the upper heating circuit. Obviously, on these occasions the efficiency of the condenser will be decimated. This practice, therefore, is a compromise between a high condenser efficiency throughout the year and an extra heating circuit.

In contrast to the situation in a working greenhouse, which as a rule is divided into a number of growth-compartments, each having their own heating circuits, the simulation model considered in this study limits itself to a description of one set of greenhouse air conditions only. Thus, the heating system comprises only two heating circuits. However, the theory presented below does not exclude an extension in the number of heating circuits fed by the heat producing devices.

4.5.1 Model assumptions

The contribution of each of the heating devices to the production or consumption of heat in a real greenhouse heating system is commonly controlled by the position of mixing valves. The valves are actuators in single loop controllers that attempt to realize a temperature setpoint of the water directly behind the valve. By passing a suitable set of setpoints, the heating system controller manages the

opening, closing and mixing ratio of the appropriate valves.

The customary time span necessary to bring a mixing valve from the one extreme position to the other is about two minutes. However, during normal operation the requested mixing ratios do not change very quickly (see the discussion on Figure 4.24). Therefore, a simplification of the mixing valve dynamics by assuming that required mixing ratios are instantaneously realized is allowed.

The greenhouse climate controller generates setpoints for the heating circuits and control signals to the boiler, in order to produce CO_2, and to start or stop the combined heat and power engine.

In a well-engineered heating system in a greenhouse, the valve positions of the heating circuits (V_{upp} and V_{low}) do not affect flows through these circuits. Thus, these flows are assumed to be constant. The other flows in the heating system are assumed to be controllable by means of a frequency controlled pump or a bypass configuration. These variable flows can be controlled by single loop controllers that maintain appropriate pressure differences in the heating system.

4.5.2 Computations

Figure 4.22 serves as a guide throughout this section. This figure is a copy of Figure 4.3, but has been extended with references to particular valves, flows and temperatures.
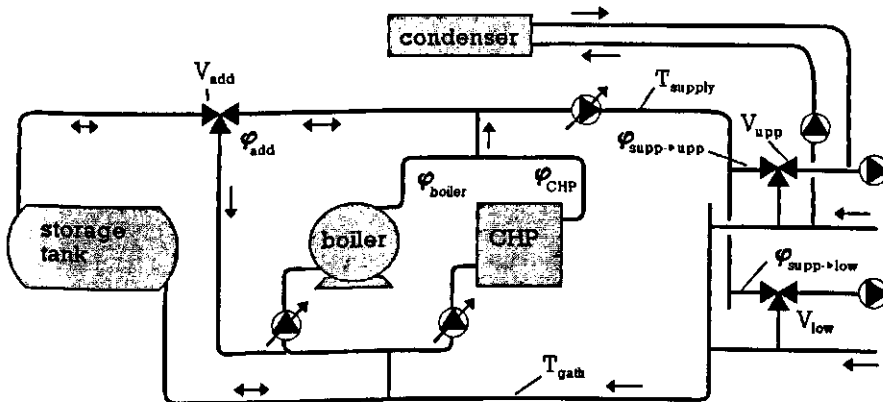
Figure 4.22 Flows and temperatures in the heating system.

A heating system with a storage tank, as is the case in the greenhouse considered in this study, has two operating modes: charging and discharging. The situation in which a storage tank neither fills nor empties is covered by the charging mode,

but with a charging flow zero.

The computations start with the formulation of general equations for the requested flow to the upper and lower heating circuit and the temperature of the water in the gathering pipe, all as a function of the temperature of the main supply pipe. Then, the computation of the charging flow to the storage tank will be presented for the situation where the heat produced exceeds the heat being demanded. Thereafter the discharge flow and, if necessary, the additional heating power will be computed.

4.5.2.1 Flows to the heating circuits and the gathering pipe temperature

The supply side temperature in the upper heating circuit, T_{SupUpp} is controlled by the mixing valve V_{upp}. In order to satisfy the setpoint for the upper heating circuit (Setp$_{upp}$) the mass flow resulting from the mixing ratio of V_{upp} is expressed by:

$$\varphi_{supp \to upp} = max \left\{ 0, \varphi_{upp} \frac{SetpT_{upp} - T_{RetUpp}}{T_{supply} - T_{RetUpp}} \right\} \qquad [kgm^{-2}s^{-1}] \ (4.25)$$

with φ_{upp} the mass flow through the upper heating circuit (determined by its circulation pump), T_{RetUpp} the return temperature of the heating circuit and T_{supply} the temperature of the main supply pipe. The *max* operator prohibits negative results. Without this operator the computed mass flow would be negative when the distribution circuit cools down.

Analogue to V_{upp}, V_{low} controls the mixing ratio of hot supply water with return water from the lower heating circuit.

$$\varphi_{supp \to low} = max \left\{ 0, \varphi_{low} \frac{Setp_{low} - T_{RetLow}}{T_{supply} - T_{RetLow}} \right\} \qquad [kgm^{-2}s^{-1}] \ (4.26)$$

where the meaning of the variables is analogue to the Eqn. 4.25.

The mass flows from the return sides of the distribution circuits to the gathering pipe are equal to the mass flows $\varphi_{supp \to upp}$ and $\varphi_{supp \to low}$. Thus, providing the absence of a shortcut between the main supply and gathering pipe the temperature of the gathering-pipe is expressed by:

$$T_{gath} = \frac{\varphi_{supp \to upp} T_{RetUpp} + \varphi_{supp \to low} T_{RetLow}}{\varphi_{supp \to upp} + \varphi_{supp \to low}} \qquad [°C] \ (4.27)$$

If there is a shortcut between main supply and gathering pipe, Eqn. 4.27 would have to be extended with an extra term in both the nominator and denominator. The mass flow through the gathering pipe (φ_{gath}) is the sum of $\varphi_{supp \to upp}$ and $\varphi_{supp \to low}$.

4.5.2.2 Charging flow to the storage tank

The fact whether the storage tank is charging or discharging can be determined by comparing the sum of the required power of the distributing pipes with the currently produced reject heat from combined power and CO_2-addition. The current power demand P_D of the greenhouse is determined by:

$$P_D = c_p (\varphi_{upp} (Setp_{upp} - T_{RetUpp}) + \varphi_{low} (Setp_{low} - T_{RetLow})) \quad [Wm^{-2}] \ (4.28)$$

with c_p the thermal capacity of water $(Jkg^{-1}K^{-1})$. The current power supply from CHP (P_{CHP}) and CO_2-addition (P_{CO2}) is given by the status (on or off) and the thermal heating power associated with the on-status. In case $(P_{CHP} + P_{CO2}) \geq P_D$ the heating system is in charging mode, otherwise the heating system is in discharging mode.

When the storage tank is being charged, the temperature of the main supply pipe (T_{supply}) is equal to the charging temperature of the storage tank (T_{charge}). In the present work T_{charge} is set to 90 °C. The mass flow to the storage tank $(\varphi_{supp \to sto})$ has such a level that the power surplus is absorbed. This flow can be computed easily by:

$$\varphi_{supp \to sto} = \frac{P_{CHP} + P_{CO2} - P_D}{(T_{supply} - T_{sto,bot}) \, c_p} \qquad [kgm^{-2}s^{-1}] \ (4.29)$$

$T_{sto,bot}$ is the temperature at the bottom of the storage tank. In case the storage tank is almost completely filled, $\varphi_{supp \to sto}$ grows to infinity. When this occurs, the simulation model pushes the heat extent into the lower heating circuit to be carried off.

4.5.2.3 Discharging the storage tank

The heating system switches to discharge mode when P_D exceeds the forced power supply. In order to be able to serve the heat demand of both heating circuits, the temperature of the main supply pipe must be at least as high as the maximum of the setpoints. Thus:

$$T_{supp,min} = max \ \{ \ Setp_{upp} \, , \ Setp_{low} \ \} \qquad [°C] \ (4.30)$$

with $T_{supp,min}$ the minimal temperature for the main supply pipe. Consequently, when the storage tank is being discharged, T_{supply} is a variable between T_{charge} and $T_{supp,min}$. The first time after a period of charging, the outlet of the storage tank maintains the temperature at which it was charged. However, due to heat losses, and especially when the tank has been depleted to a certain extent, the temperature at the outlet of the storage tank will drop. Then T_{supply} is determined by the mixing ratio of the water coming from the storage tank, with a temperature $T_{sto,top}$ and water from the power sources, with a temperature T_{charge}.

The temperature of the supply water affects the flow required to feed the heating circuits (see the denominator in the equations (4.25) and (4.26)) and, with it, the temperature of the water in the gathering pipe. On its turn, the temperature at which the power sources are fed (having the temperature of the gathering pipe) determines the flow through these devices and, as a consequence, the supply temperature.

Obviously, the chain of relations ends at its starting point. Because the connection of heating devices is based on a static computation scheme the flow through the storage tank that balances heat demand and heat production is computed by an iteration.

The temperature of the gathering pipe determines the mass flow through the combined heat and power engine and the boiler.

$$\varphi_{CHP} = \frac{P_{CHP}}{(T_{charge} - T_{gath}) \, c_p} \qquad [kgm^{-2}s^{-1}] \quad (4.31)$$

$$\varphi_{boiler} = \frac{P_{CO2}}{(T_{charge} - T_{gath}) \, c_p} \qquad [kgm^{-2}s^{-1}] \quad (4.32)$$

Obviously φ_{boiler} has to carry off the heat associated with carbon dioxide supply. The remainder of φ_{gath}, after φ_{CHP} and φ_{boiler} are withdrawn from the gathering pipe, flows into the storage tank. At the outlet, the same flow, having the temperature of the top of the storage tank is mixed with the water from the power sources, yielding a supply water temperature according to:

$$T_{supply} = \frac{\varphi_{power} T_{charge} + (\varphi_{gath} - \varphi_{power}) T_{sto,top}}{\varphi_{gath}} \qquad [°C] \quad (4.33)$$

with $\varphi_{power} = \varphi_{boiler} + \varphi_{CHP}$. As long as T_{supply} exceeds $T_{supp,min}$, the heating power of the storage tank and the forced heating power are sufficient to cover the heat demand of the greenhouse. However, in case the storage tank is almost depleted, the temperature of the water coming out of the tank drops and the supply temperature becomes too low to feed the heating circuits. Thus, the boiler has to produce additional power.

In the heating system depicted in Figure 4.22, the additional power from the boiler is supplied to the heating system by diverting a fraction of the discharge flow through the boiler, by means of mixing valve V_{add}.

This flow is computed by:

$$\varphi_{add} = \frac{\varphi_{gath} T_{supp,min} - \varphi_{power} T_{charge} - (\varphi_{gath} - \varphi_{power}) T_{sto,top}}{T_{charge} - T_{sto,top}} \qquad [kgm^{-2}s^{-1}] \quad (4.34)$$

The final power to be produced by the boiler is determined by:

$$P_{boiler} = P_{CO2} + \varphi_{add} \, c_p \, (T_{supp,req} - T_{sto,top}) \qquad [Wm^{-2}] \quad (4.35)$$

Note that the additional power is added to the power associated with CO_2-enrichment of the greenhouse air.

The storage tank is completely emptied when the temperature at the outlet is lower than or equal to the temperature in the gathering pipe. In that case the heating system switches back to charging mode, although in general just after a discharging period the charging flow will be zero.

4.5.3 Results

To show the behaviour of the heating system the heating power of the boiler, a number of temperatures and valve positions and the performance of the condenser is monitored during one day in spring (2 April). The greenhouse climate controller settings and building and equipment characteristics are described in Section 6.3. Figure 4.23 shows the course of the heating power of the boiler. The curve shows a peak around 06:00 hours and another one at 22:00 hours. The first peak originates from the greenhouse air temperature setpoint increment from night to day-level. The second peak marks the moment that the heat storage tank is empty. At that moment the boiler takes over the heat supply.

The constant level of the curve between 11:30 and 17:00 hours is caused by CO_2 supply with exhaust gases. At 18:00 hours the boiler is switched off.
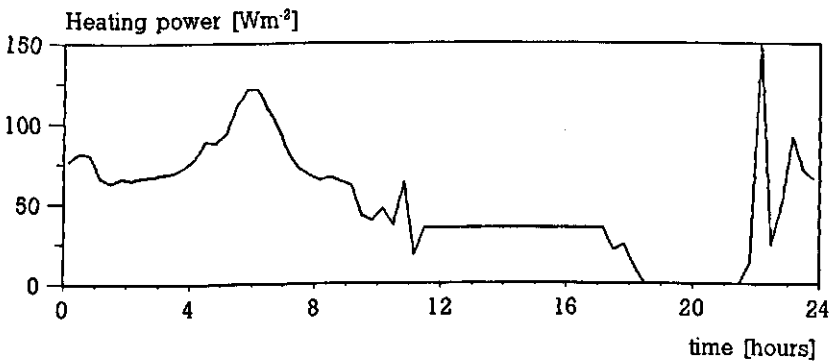
Figure 4.23 Heating power of the boiler.

In Figure 4.24a, from the dotted decreasing line can be seen that between 18:00 and 22:00 hours the heat demand of the greenhouse is covered by the heat storage tank. The storage tank has been filled in the preceding hours. During the charging period the mean storage tank temperature has increased from 36 °C to 60 °C. Thus, on this day, at the end of the charging period the tank was filled for only 44%. During the charging period the top of the tank increases to T_{charge} quite fast,

whereas the bottom of the tank remains at 35 °C.

From 11:00 till 15:30 hours, as can be seen in Figure 4.24b, the mixing valves of both the upper and lower heating circuit are closed. As a consequence, the water in the gathering pipe is not refreshed by return water from the heating circuits, and because the heating system model doesn't take account for heat losses in transport pipes, the temperature of T_{gath} remains constant at 30 °C (see Figure 4.24a). At 15:30 hours the mixing valve of the lower heating system opens to a mixing ratio of 0.15. From that moment, T_{gath} is governed by the return temperature of the lower heating circuit. First T_{gath} decreases to 28 °C, which is the temperature to which the lower heating circuit has cooled down in the preceding period, and then increases to about 40 °C. A similar course, but damped, can be found in the temperature at the bottom side of the storage tank because, during discharge, the water from the gathering pipe flows into the bottom side of the tank. Eventually the bottom side temperature becomes equal to T_{gath} (20:30 till 22:00 hours).
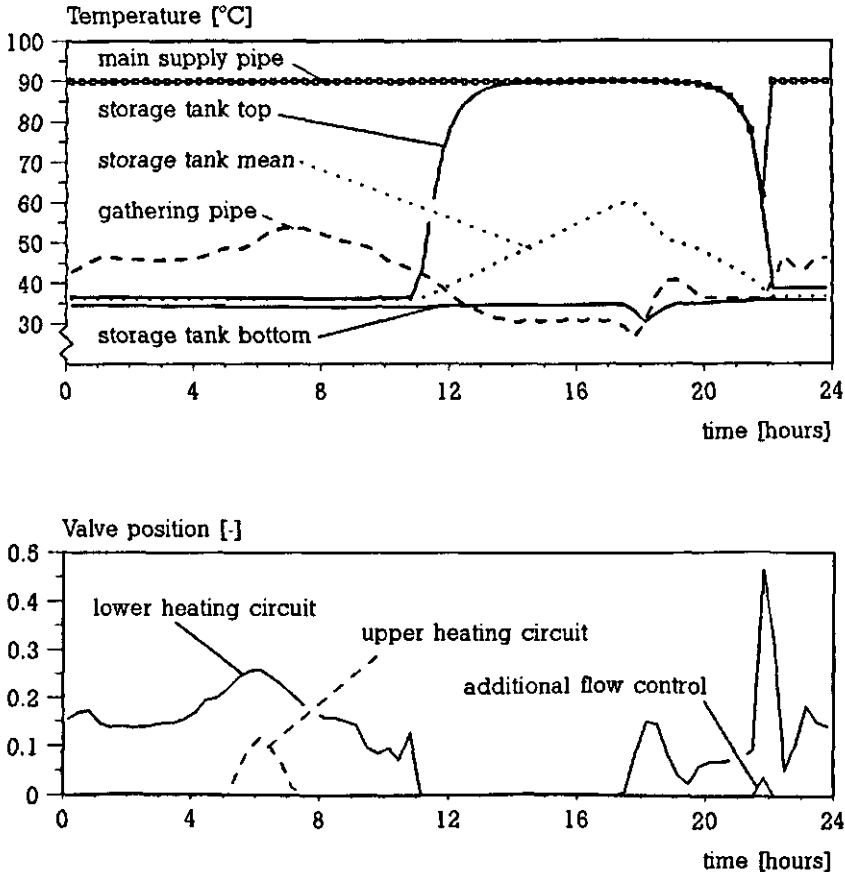
Figure 4.24 The course of temperatures (a) and valve positions (b) during one day

Starting at 20:00 hours, after the tank has been discharged for two hours, the temperature at the top of the tank starts to decrease. At 19:45 the temperature has become that low that the temperature setpoint for the lower heating circuit (not shown in the pictures) can no longer be realized. At that moment the valve V_{add} opens somewhat (see Figure 4.24b) to increase the temperature of a fraction of the water from the heat storage tank to 90 °C (see section 4.5.2.3). However, at 22:10 hours the temperature of the water withdrawn from the tank becomes lower than T_{gath}. On that moment the heating system switches to charging mode (with charging flow 0), meaning that the supply pipe temperature becomes 90 °C and V_{add} closes.

In Figure 4.24b can be seen that, for a short time (05:00 till 09:00 hours) the temperature of the upper heating circuit is controlled by V_{upp}. However, the upper heating circuit is used to carry off the heat gathered with the condenser as well. Thus, it can be expected that in the considered time span the condenser efficiency drops. Indeed, this appears to be the case, as can be seen in Figure 4.25. In this figure, the condenser efficiency is defined analogue to Figure 4.13. For the period that the boiler is switched off (18:00 till 22:00 hours) the condenser efficiency is not defined.
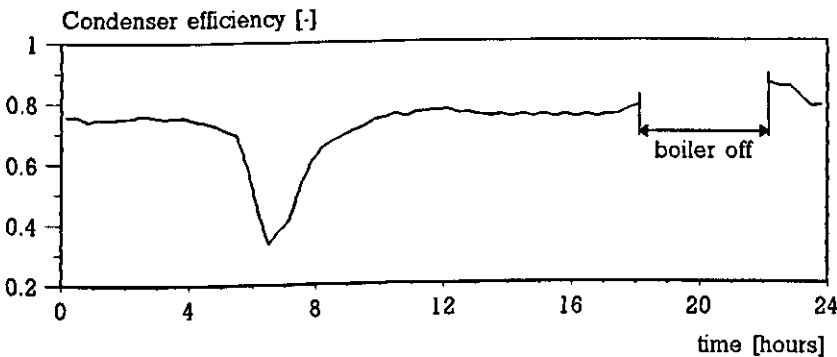
Figure 4.25 Condenser efficiency.

Finally, in Figure 4.26 the return temperature of the upper heating circuit is shown. Apart from the period between 05:00 and 09:00 hours, the upper heating circuit (and the return temperature) is governed by the heat production of the condenser. Note that the upper heating circuit cools down between 18:00 and 22:00. In this period the condenser does not produce heat because the boiler is turned off.

Return temperature upper heating circuit [°C]
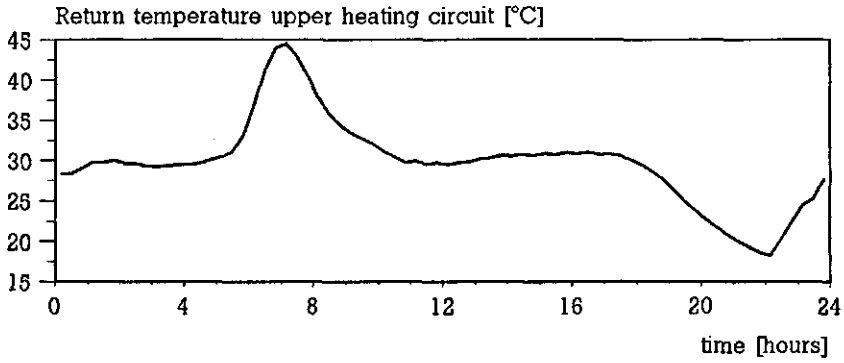
Figure 4.26 Return temperature of the upper heating circuit.

5. GREENHOUSE CLIMATE SIMULATION

5.1 INTRODUCTION

The simulation of greenhouse air temperature, humidity and carbon dioxide concentration provides the feed-back quantities for the greenhouse climate controller. In turn, these quantities are a result of climate control actions in the past. In this chapter the modelling of air temperature, humidity and carbon dioxide concentration, hereafter denoted as the greenhouse climate, is presented as a function of the actions of the greenhouse climate controller and the environment of the greenhouse.

As discussed in Chapter 3, the simulation of these three quantities is performed by numerical integration of their differential equations. In order to describe the differential equations, a large number of other quantities have to be defined. Some of these quantities are a result of numerical integration as well.

To keep the presentation conveniently arranged, the greenhouse climate simulation model is split into three sub-models: a thermal model, a water vapour model and a CO_2 model. These sub-models are discussed separately in Section 5.3 (the carbon dioxide model), Section 5.4 (the water vapour model) and the large section 5.5, where the thermal model is presented. However, before discussing the specific sub-models, the notational conventions applied are presented in Section 5.2.

5.2 NOTATIONAL CONVENTIONS

The greenhouse climate simulation model which is the subject of this chapter, is based on the definition of endogenous state variables, fluxes and boundary conditions, as formulated in Section 3.2. Because there is a high level of similarity between the equations that play a role in the models, a consequent notation for state variables and fluxes is adopted. In the sections below the conventions are presented.

5.2.1 State variables

In the greenhouse climate simulation model three types of state variables can be distinguished (see Figure 3.1). The majority of the state variables refer to temperatures. These variables are denoted by names beginning with a capital T, followed by a three characters subscript, which refers to the state variable in consideration (e.g. T_{air}). The other state variables comprise the partial pressures of vapour, denoted by the capitals VP, and the partial pressure of carbon dioxide. State varia-

67

bles in the CO_2 model are marked CO2. The subscripts are equal to the ones specifying the thermal state variables (e.g. VP_{air} and $CO2_{air}$).

Temperatures are expressed in K or °C, whatever is the most convenient. Partial vapour and carbon dioxide pressures are expressed in Nm^{-2} (which is equal to Pa).

5.2.2 Fluxes

The simulation model distinguishes heat and mass fluxes. Unless explicitly defined as being different, all fluxes are expressed per m^2 ground surface of the greenhouse. Most fluxes are the result of a difference between the level of state variables, but some fluxes are forced by boundary conditions or climate control actions. Forced heat fluxes are marked with a capital P, followed by a subscript. The subscript is made up of two parts, coding for the source and destination compartment of the flux (e.g. P_{AluCan}, which refers to a heat flux from artificial illumination to the canopy). Heat fluxes associated with condensation or evaporation of moisture begin with a capital L. Forced fluxes of carbon dioxide are denoted by a capital C, followed by the familiar subscript (e.g. C_{ConAir}, which refers to the carbon dioxide input from the greenhouse climate controller to the greenhouse air). Forced vapour fluxes do not occur in the present model.

Sensible heat fluxes are marked with a capital H, when they refer to convective or conductive exchange processes, and are marked with a capital R when radiative heat exchange is involved. The customary subscripts are suffixed (e.g. H_{AirCov} and R_{LowCan}).

Mass fluxes in the water vapour model are marked by the capitals MV (for example MV_{CanAir}). The fluxes in the CO_2 model are indicated with MC (e.g. MC_{AirOut}).

5.2.3 Exchange coefficients

All fluxes in the model that are computed from a difference in state variables have an exchange coefficient that governs the exchange process. Exchange coefficients for computing a convective or conductive heat flux are termed HEC, suffixed by the same subscript as the flux governed by the exchange process under consideration. For instance, the exchange coefficient for the heat exchange between the upper heating pipe and the greenhouse air is termed HEC_{UppAir}. With this exchange coefficient the equation for computing the convective heat release of the upper heating pipe to the air can easily be stated as:

$$H_{UppAir} = HEC_{UppAir} (T_{upp} - T_{air}) \qquad [Wm^{-2}] \ (5.1)$$

Radiative exchange processes are governed by the Stefan Boltzman equation. To stress that it is a non-linear relation, exchange coefficients involving radiative heat

exchange are termed REC. Again the suffixed subscript refers to the exchange process under consideration. Thus an equation expressing a radiative heat flux looks like:

$$R_{LowCan} = REC_{LowCan} \, (T_{low}^4 - T_{can}^4) \qquad\qquad [Wm^{-2}] \; (5.2)$$

However, all radiative exchange processes associated with the thermal screen linearized. To express this linearization, the exchange coefficients involving these radiative fluxes are categorized as HEC. Thus, for example, the heat exchange between upper heating pipe and the thermal screen is described by:

$$R_{UppScr} = HEC_{UppScr} \, (T_{upp} - T_{scr}) \qquad\qquad [Wm^{-2}] \; (5.3)$$

The exchange coefficients for mass exchange processes begin with VEC in equations on vapour exchange and with CEC where CO_2 exchange rates are being computed. Examples are:

$$MV_{AirCov} = VEC_{AirCov} \, (VP_{air} - VP_{cov}) \qquad\qquad [kgs^{-1}m^{-2}] \; (5.4)$$

and

$$MC_{AirTop} = CEC_{AirTop} \, (CO2_{air} - CO2_{top}) \qquad\qquad [kgs^{-1}m^{-2}] \; (5.5)$$

Evaporation and condensation of vapour are treated as mass exchange processes.

5.2.4 Exogenous variables

The greenhouse climate simulation model includes six exogenous state variables (or boundary conditions) that, in flux computations, act in a similar way as endogenous state variables. These six variables are T_{sky}, T_{out}, VP_{out}, $CO2_{out}$, T_{low}, T_{upp} and T_{so7} (see Figure 3.1). The fact that the temperatures of the upper and lower heating pipe are categorized as exogenous variables may surprise, since the pipe temperature was an endogenous state variable in Section 4.4.1. However, as was discussed in Section 4.4.1.4, the result of the heating circuit simulation is passed to the climate simulation model as the mean temperature of the pip segments representing the distribution loops. Thus, the pipe temperatures of the upper and lower heating circuit act as boundary conditions with respect to the thermal submodel of the greenhouse climate simulation.

Exogenous flux variables are the intensity of direct and diffuse solar radiation. Although these radiation intensities are forced fluxes they are referred to as I_{dir} and I_{dif} (and not with designations beginning with P), because they act in a very different type of equations.

5.2.5 Other variables

Structured naming only makes sense if equations or procedures have a high level of similarity. Since a high level of similarity lacks the relations which do not confine one of the types mentioned above, the naming of other variables that play a role in this study cannot be discussed in a general section.

5.3 THE CARBON DIOXIDE SUB-MODEL

The carbon dioxide sub-model includes the CO_2 concentration of the top compartment ($CO2_{top}$) and the greenhouse air compartment ($CO2_{air}$). However, when the thermal screen is opened, or not available, the air compartment and the top compartment are lumped together. The structure of the sub-model is presented first and subsequently the computation of the fluxes is discussed.

5.3.1 Structure of the carbon dioxide model

A graphic representation of the state variables and the fluxes distinguished in this sub-model is presented in Figure 5.1. The endogenous and exogenous state variables are represented analogue to Figure 3.1.
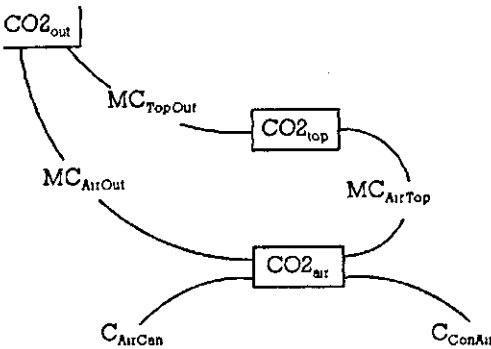
Figure 5.1 State variables, fluxes and the exogenous variable in the CO_2 model.

The two state variables of the CO_2 model are connected by MC_{AirTop}, describing the CO_2 transfer between the top compartment and the greenhouse air compartment when the screen is (partly) closed. The top compartment looses CO_2 to the outside air, described by MC_{TopOut}. The outside partial CO_2 pressure ($CO2_{out}$) is assumed to be constantly 34 Pa ($\approx$340 ppm). When the screen is opened, a direct

air exchange between the greenhouse air compartment and the outside air can occur. This exchange is described by MC_{AirOut}. Besides a CO_2 loss to the top compartment or the outside air, the greenhouse air compartment looses CO_2 to the canopy (C_{AirCrp}). The climate controller supplies CO_2 to the greenhouse air by means of C_{ConAir}. These last two mass flows are considered forced fluxes.

With the fluxes shown in the figure and the theory presented in Section 3.3 the differential equations for the state variables can be stated easily:

$$\frac{dCO2_{top}}{dt} = \frac{MC_{AirTop} - MC_{TopOut}}{M_C V_{top}/(R\ T)} \qquad [\text{Pas}^{-1}] \ (5.6)$$

and

$$\frac{dCO2_{air}}{dt} = \frac{C_{ConAir} - MC_{AirTop} - C_{AirCrp} - MC_{AirOut}}{M_C V_{air}/(R\ T)} \qquad [\text{Pas}^{-1}] \ (5.7)$$

The dependency of the capacity on the air temperature is neglected by using a constant temperature of 291 K. V_{air}, the volume of the CO_2 compartment is computed with the mean height of the greenhouse. The application of a constant value for V_{air} neglects the decrement of the air volume represented by $CO2_{air}$ when the screen is closed. However, since the top of the greenhouse contains only about 10% of the air volume, and the heat capacity of air is small already, the dynamics of the CO_2 concentration are of minor importance. Therefore this neglection is obliged. M_C is the molar mass of CO_2, (44 kgkmol^{-1}) and R the gas constant (8314 Jkmol^{-1}K^{-1}).

By (numerical) integration of Eqn. 5.7 the course of the CO_2-concentration in the greenhouse air can be determined in time.

As said, the capacity of the top compartment for CO_2 is only 10% of the capacity of the main air compartment. Consequently, the dynamics of this compartment is of a small time base compared to the mean dynamics of the other compartments. Therefore the CO_2 concentration in the top compartment is not computed by numeric integration but by a static equation, implying $dCO2_{top}/dt$ to be zero. After rewriting MC_{AirTop} with equation 5.5 and MC_{TopOut} with an analogue one, and after solving $CO2_{top}$ from this equation the expression yields:

$$CO2_{top} = \frac{CEC_{TopOut}\ CO2_{out} + CEC_{AirTop}\ CO2_{air}}{CEC_{TopOut} + CEC_{AirTop}} \qquad [\text{Pa}] \ (5.8)$$

5.3.2 Fluxes in the carbon dioxide model

In the CO_2 model three CO_2 exchange processes and two forced fluxes are considered to play a role. The exchange processes are related to the ventilation flux through the windows and to the air exchange rate through openings in the thermal screen. The forced fluxes are the CO_2 consumption of the canopy and the CO_2 supply by the greenhouse climate controller.

5.3.2.1 Exchange processes

The ventilation flux through the windows is denoted by f_{vent} and the air exchange rate through the thermal screen is denoted by f_{AirTop}. Both these air exchange rates are expressed in $m^3 m^{-2} s^{-1}$, where the surface refers to a m^2 floor area. f_{vent} and f_{AirTop} are defined in Section 5.5.2.

The CO_2 flux between the greenhouse and the outside air is presented as an example. Using the gas law for ideal gases and application of f_{vent} to describe the air flux between greenhouse and outside air outward CO2 flux is defined by:

$$MC_{AirOut} = \frac{M_C f_{vent}}{R} \left(\frac{CO2_{air}}{T_{air}} - \frac{CO2_{out}}{T_{out}} \right) \qquad [kgs^{-1}m^{-2}] \quad (5.9)$$

with M_C the molar mass of CO_2 (44 kgkmol^{-1}). The expression for MC_{AirOut} is not linear. Linearization of the expression by application of a mean temperature introduces an inaccuracy that goes up to some 15% for large temperature differences. Therefore, the definition of an exchange coefficient such as applied in Equation 5.5 is omitted. When the thermal screen is not opened, the model concept excludes MC_{AirOut} by assigning zero to the flux.

Contrary to the numeric computation of $CO2_{air}$, where fluxes govern the equation (see Eqn. 5.7), the algebraic computation of $CO2_{top}$ (Eqn. 5.8) requires linear equations for the fluxes (like Eqn. 5.5), rather than fluxes. Thus the non-linear relations for MC_{AirTop} and MC_{TopOut}, which can be stated analogue to Eqn. 5.9, have to be linearized in a CO_2 pressure difference. This linearization is performed by neglecting the density differences between the air temperatures, by using a mean temperature of 287 K in the equation for CEC_{AirTop} and 283 K in the equation for CEC_{TopOut}. The error made by this neglection goes up to 10%, but accepted because the CO_2-losses are small anyway during periods with a closed thermal screen. Thus the exchange coefficients are described by:

$$CEC_{AirTop} = \frac{M_C}{287 \, R} f_{AirTop} \qquad [kgs^{-1}m^{-2}Pa^{-1}] \quad (5.10)$$

$$CEC_{TopOut} = \frac{M_C}{283 \, R} f_{vent} \qquad [kgs^{-1}m^{-2}Pa^{-1}] \quad (5.11)$$

5.3.2.2 Forced fluxes

The CO_2 supply to the greenhouse air compartment by the greenhouse climate controller (C_{AirCon}) is an on/off flux. When on, the rate is determined by the amount of exhaust gases combusted in the boiler. Denoting the combustion rate of natural gas in m^3 per second per m^2 floor surface as ϕ^*, and with the CO2 content of exhaust gases of 1.76 kg per m^3 combusted gas (see Section 4.4.4.1) C_{AirCon} is defined by:

$$C_{ConAir} = \phi^* \, 1.76 \qquad\qquad [kgs^{-1}m^{-2}] \quad (5.12)$$

The second forced flux in the CO_2 model is the carbon dioxide fixation by the canopy (C_{AirCan}). This CO_2 assimilation process is driven by shortwave radiation. However, the relation between radiation and assimilation rate is quite complex. Therefore the discussion on this matter is presented in Appendix I.

5.4 THE WATER VAPOUR SUB-MODEL

The second sub-model concerns the humidity in the greenhouse. The water vapour model includes the partial vapour pressure of the top compartment (VP_{top}) and the greenhouse air compartment (VP_{air}). Analogue to the CO_2 model, the air- and top compartment are lumped together when the thermal screen is opened, or not available. In this section, the structure of the sub-model is presented first, followed by a computation of the fluxes.

5.4.1 Structure of the water vapour model

A graphic representation of the state variables and the fluxes in the water vapour model are presented in Figure 5.2. The partial vapour pressure of the greenhouse air compartment is increased by evaporation from the canopy and decreased by air exchange and condensation at the cover and screen.

Evaporation and condensation depend on the vapour pressure difference between air and the vapour pressure at a surface. The latter is defined by the saturated vapour pressure for its temperature (see Appendix H). Therefore, the vapour pressure at a surface is a result from the thermal sub-model. Thus, in the water vapour model the vapour pressure at the canopy, the screen and the cover act as boundary conditions. Consequently, in Figure 5.2 VP_{can}, VP_{scr} and VP_{cov} are placed in open boxes.

When the vapour pressure at the cover is lower than VP_{air} condensation takes place at the inner side of the cover. In modern greenhouses the condensate is drained. Therefore evaporation of moisture from the cover to the air (when the

cover temperature increases) can be neglected. When the thermal screen is closed, direct condensation of moisture from the greenhouse air below the screen to the cover (MV_{AirCov}), and the direct loss of moisture by ventilation (MV_{AirOut}) is prohibited.
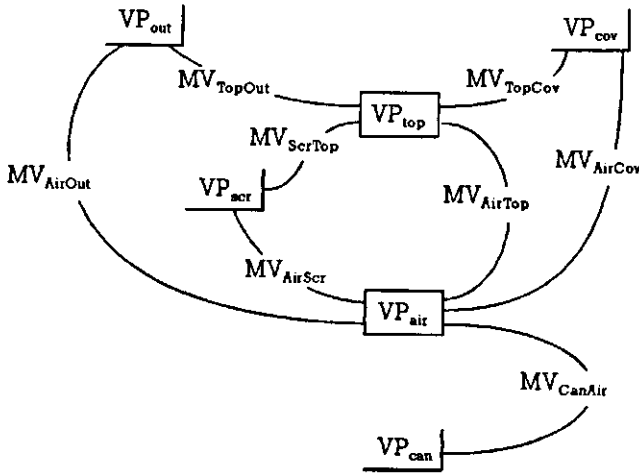
Figure 5.2 State variables, fluxes and boundary conditions in the water vapour model.

Because the screen cannot produce vapour, evaporation from the upper side of the thermal screen, accounted for by MV_{ScrTop}, is possible only when condensation takes place at the lower side of the screen, denoted by MV_{AirScr}. Obviously, when the screen is not porous, MV_{ScrTop} is always nil.

The capacity for moisture of the top compartment is very small. Therefore, the vapour pressure of the top compartment is computed by an algebraic equation, analogue to Eqn. 5.8.

$$VP_{top} = (VEC_{TopOut}VP_{out} + VEC_{AirTop}VP_{air} + \qquad\qquad [Pa] (5.13)$$
$$VEC_{TopCov}VP_{cov} + VEC_{ScrTop}VP_{top}) /$$
$$(VEC_{TopOut} + VEC_{AirTop} + VEC_{TopCov} + VEC_{ScrTop})$$

The vapour pressure of the greenhouse air is computed by numerical integration of the differential equation of the moisture content of the greenhouse air compartment. The differential equation for the moisture content of the greenhouse air compartment reads:

$$\frac{dVP_{air}}{dt} = \frac{1}{M_H V_{air}/(R\,T)} \; (MV_{CanAir} - MV_{AirTop} - \qquad [Pas^{-1}]\;(5.14)$$
$$MV_{AirScr} - MV_{AirCov} - MV_{AirOut})$$

The term that expresses the capacity for moisture is almost the same as the term for the capacity of the greenhouse air for CO_2, except for the molar mass, which holds for vapour (18 kgkmol^{-1}). Eqn. 5.14 shows that the capacity is a function of temperature. However, just like the case in the CO_2 model, the present model applies a constant capacity, holding for a temperature of 291 K and a mean greenhouse air volume above one m^2 floor surface.

Integration of Eqn. 5.14 yields the course of the vapour pressure of the greenhouse air in time.

5.4.2 Fluxes in the water vapour model

In the water vapour model all fluxes result from convective exchange processes. The computation of the mass flux from the greenhouse to the outside air by ventilation (MV_{AirOut}) is analogue to Eqn. 5.9.

$$MV_{AirOut} = \frac{M_H f_{vent}}{R} \; (\frac{VP_{air}}{T_{air}} - \frac{VP_{out}}{T_{out}}) \qquad [kgs^{-1}m^{-2}]\;(5.15)$$

with M_H the molar mass of vapour and f_{vent} the ventilation flux (m^{3}s^{-1}m^{-2}). When the thermal screen is not opened MV_{AirOut} is made zero.

As in the case of the CO_2 model, to compute the humidity of the top compartment, only the exchange coefficients are of interest. The exchange coefficients related to air exchange are defined analogue to Eqns. 5.10 and 5.11.

$$VEC_{AirTop} = \frac{M_H}{287\,R} \; f_{AirTop} \qquad [kgs^{-1}m^{-2}Pa^{-1}]\;(5.16)$$

$$VEC_{TopOut} = \frac{M_H}{283\,R} \; f_{vent} \qquad [kgs^{-1}m^{-2}Pa^{-1}]\;(5.17)$$

The mass transfer from the air to the screen and the cover (condensation) is governed by processes at the boundary layer at these surfaces. Because of the similarity of the transport mechanism for vapour and heat transfer through the boundary layer, the mass and heat transfer coefficients are correlated. The theory concerning this relation is presented in Appendix B. There a factor 6.4·10^{-9} kgKJ^{-1}Pa^{-1} is found between the heat and mass transfer coefficients.

Because the heat exchange coefficients are well described (see Appendix A), the mass transfer coefficients for condensation and evaporation at the screen and the cover can be calculated. Thus VEC_{AirScr}, VEC_{ScrTop}, VEC_{AirCov} and VEC_{TopCov} are computed by multiplying the corresponding heat exchange coefficient by 6.4·10^{-9}.

For example:

$$VEC_{AirCov} = 6.4 \cdot 10^{-9} \ HEC_{AirCov} \qquad [kgs^{-1}m^{-2}Pa^{-1}] \ (5.18)$$

The mass fluxes are computed from the mass transfer coefficients and vapour pressure differences with equations analogue to Eqn. 5.4. However, contrary to the mass fluxes resulting from air exchange, the evaporative fluxes and fluxes due to condensation are prohibited from being negative. This is because the model excludes evaporation from the cover and lower side of the screen. Condensation on the upper side of the screen is prohibited as well. The negative fluxes are prevented by making the mass transfer coefficients zero when the vapour pressure difference is negative.

By allowing a mass flux MV_{ScrTop}, the present model assumes that the thermal screen is capable of transporting water from the lower side to the upper side through the fabric. This fabric will be able to store some water. However, in the present model the storage of moisture in the screen is neglected. This implies that vapour that condenses at the screen is either evaporated at the upper side or drips from the screen. Another implication of the neglection of storage is that the rate of evaporation at the upper side of the screen is lower or equal to the rate of condensation at the lower side. To avoid the screen evaporating more than the amount of water that condenses at the lower side of the screen, VEC_{ScrTop} is restricted by:

$$VEC_{ScrTop} \leq VEC_{AirScr} \ \frac{VP_{air} - VP_{scr}}{VP_{scr} - VP_{top}} \qquad [kgs^{-1}m^{-2}Pa^{-1}] \ (5.19)$$

The vapour flux from the canopy to the greenhouse air originates from a phase interface somewhere inside the cavities of a leaf. Thus, the resistance to the transport of this vapour from the leaf to the greenhouse air consists of an internal resistance, formed by the leaf tissue and the stomata, and a boundary layer resistance (Stanghellini, 1987). The resulting mass transfer coefficient is the reciprocal of the sum of both resistances. The boundary layer resistance is computed from the resistance to heat transport. According to Appendix B the relation between the resistance to heat mass and heat transport reads

$$r_{b,V} = Le^{2/3} \ r_{b,H} \qquad [sm^{-1}] \ (5.20)$$

with Le the Lewis number (0.89 for vapour). The computation of the boundary layer resistance to heat transport is presented in Section 5.5.2 (page 87).

Contrary to the boundary layer resistance, which is determined by micro-climatic conditions, the internal resistance is actively regulated by the canopy. This regulation takes place by altering the aperture of the stomata. As can be seen in models describing the stomatal resistance (Bot, 1983; Stanghellini, 1987; Jolliet, 1991), the major factor in this control mechanism is the intensity of shortwave radiation.

Other factors, but less pronounced, are the CO_2 concentration of the greenhouse air, the temperature of the leaves and the vapour pressure deficit between the leaves and the ambient (Stanghellini, 1987). For tomatoes, Stanghellini described the internal resistance as a function of shortwave radiation, temperature, CO_2 concentration and vapour pressure deficit with a multiplicative equation.

$$r_{i,V} = r_{min} \, r(I_s) \, r(T_0) \, r(CO_2) \, r(e_0\text{-}e_a) \qquad\qquad [\text{sm}^{-1}] \quad (5.21)$$

r_{min} is the minimum possible canopy resistance. The symbols $r(I_s)$, $r(T_0)$, $r(CO_2)$ and $r(e_0\text{-}e_a)$ represent functions larger than unity, describing multiplicative resistance components on canopy transpiration due to unfavourable leaf temperatures, high irradiation levels, abundant CO_2 levels and large vapour pressure differences. The functions for the multiplication factors that were used in the model fitting procedure were:

$$r(I_s) \;=\; \frac{I_s + C_1}{I_s + C_2} \qquad\qquad [\text{-}] \quad (5.22)$$

$$r(T_0) \;=\; 1 + C_3(T_0 - T_m)^2 \qquad\qquad [\text{-}] \quad (5.23)$$

$$r(CO_2) \;=\; 1 + C_4(CO_2 - 200)^2 \qquad\qquad [\text{-}] \quad (5.24)$$

$$r(e_0\text{-}e_a) \;=\; 1 + C_5 \, (e_0 - e_a)^2 \qquad\qquad [\text{-}] \quad (5.25)$$

In these formulas I_s is the mean shortwave radiation flux, absorbed by the canopy (Wm^{-2}leaf), T_0 represents the canopy temperature and T_m the temperature at which the resistance is minimal (°C). CO_2 refers to the CO_2 concentration (ppm) and $(e_0 - e_a)$ represents the vapour pressure deficit (Pa). Stanghellini determined all variables for the daytime and the nighttime period (Table 5.1).

Table 5.1. Values and units of parameters in the model of Stanghellini for tomato and rose. The values for tomato were given by Stanghellini. The values for rose were validated on behalf of the present work.

		tomato		illuminated roses		
		daytime	nighttime	daytime	nighttime	
	r_{min}	82.0	658.5	140	180	sm^{-1}
$r(I_s)$	C_1	4.30	-	10	-	Wm^{-2}
	C_2	0.54	-	1.25	-	Wm^{-2}
$r(T_0)$	C_3	$2.3 \cdot 10^{-2}$	$0.5 \cdot 10^{-2}$	$1.3 \cdot 10^{-2}$	$0.35 \cdot 10^{-2}$	K^{-2}
	T_m	24.5	33.6	24.5	33.6	°C
$r(CO_2)$	C_4	$6.1 \cdot 10^{-7}$	$1.1 \cdot 10^{-11}$	0	0	ppm^{-2}
$r(e_0\text{-}e_a)$	C_5	$4.3 \cdot 10^{-6}$	$5.2 \cdot 10^{-6}$	$3.6 \cdot 10^{-6}$	$5.2 \cdot 10^{-6}$	Pa^{-2}

In this study, on behalf of the validation of the simulation model an illuminated rose canopy was used. During the validation of the model it appeared that results

improved when the evaporation of a rose canopy was diminished compared to a tomato stand. To achieve the diminished evaporation the stomatal resistance was increased by adaption of the variables r_{min}, C_1, C_2, C_3 and C_5. The results published by Stanghellini and the results of the model tuning with respect to illuminated roses are stated in Table 5.1.

Because in the present work the vapour pressure (deficit) is expressed in Pa, instead of kPa, the constant C_5 in Table 5.1 was multiplied by a factor 10^{-6} compared the value reported by Stanghellini.

For two of the functions Stanghellini added a restriction on the value of the function. She limited $r(CO_2)$ to 1.5 and $r(e_0-e_a)$ to 5.8. Now the mass transfer coefficient can be determined by:

$$VEC_{CanAir} = \frac{2 \rho c_p LAI}{\Delta H \gamma (r_{b,V} + r_{i,V})} \qquad [kgs^{-1}Pa^{-1}] \quad (5.26)$$

with ρ the density of air (1.23 kg m^{-3}), c_p the specific heat of air (1.0 J kg^{-1}), LAI the leaf area index, ΔH the latent heat of evaporation of water (2.45 10^6 J kg^{-1}) and γ the psychometric constant (65.8 Pa K^{-1}). The factor 2 accounts for the fact that a canopy leaf has two sides, whereas the LAI refers to one side only.

5.5 THE THERMAL SUB-MODEL

The third sub-model is the most extensive part of the greenhouse climate simulation model. It describes the thermal state variables.

5.5.1 Structure of the thermal model

The thermal model is shown in Figure 5.3. In the picture the same drawing conventions are applied as in Figure 5.1 and 5.2, but in order to keep a neatly arranged presentation the boxes for T_{Cov}, T_{Scr} and T_{Flr} are extended.

The majority of the fluxes distinguished in the thermal model originate from heat exchange processes between the endogenous and exogenous state variables. However, a number of the forced fluxes demand some explanation.

The greenhouse cover transmits most of the solar radiation, reflects a fraction back to the atmosphere and absorbs a small fraction in the glass and its supporting elements. The heat flux associated with this absorption is contributed to by P_{SunCov}. From the transmitted fraction, part is absorbed by opaque elements in the greenhouse (feet, girders etc.). Since these elements are not distinguished as separate entities, but directly release their heat to the greenhouse air, the energy flux associated with the absorption of these obstructing elements is assigned to the greenhouse air by a variable P_{SunAir}.
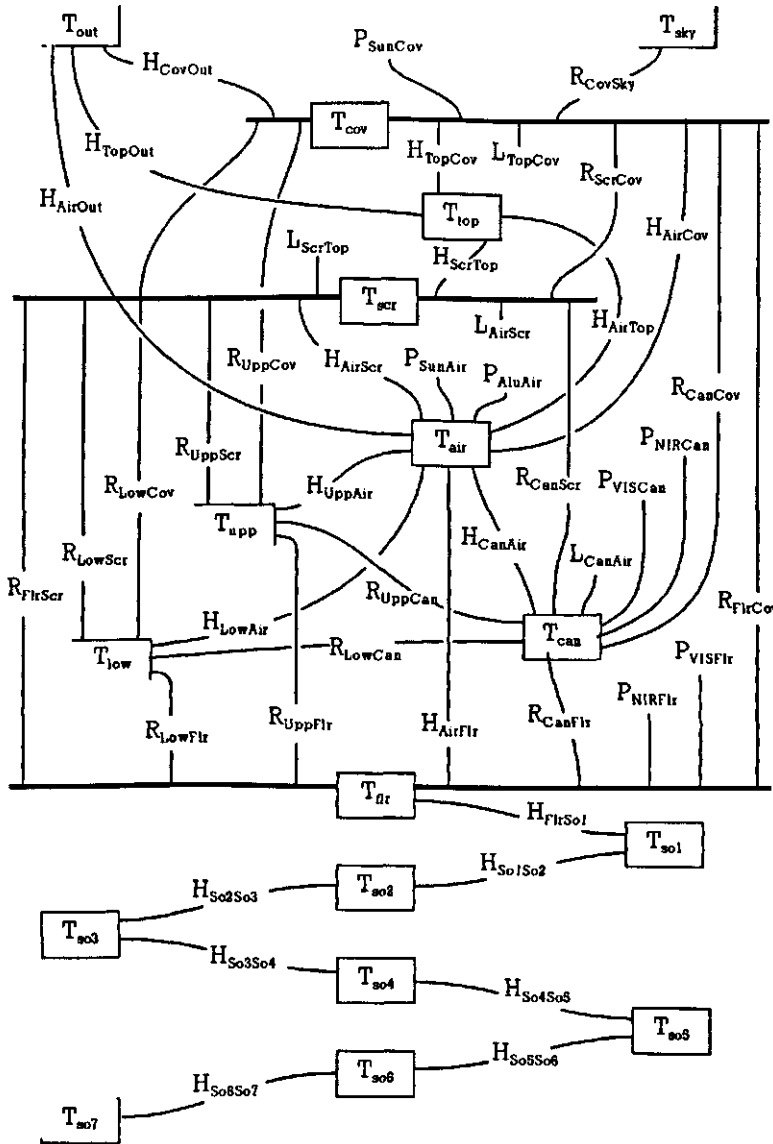
Figure 5.3 State variables, fluxes and boundary variables in the thermal model.

The canopy absorbs short-wave radiation from the sun and, if present, from artificial illumination. These short-wave heat fluxes are denoted P_{SunCan} and P_{AluCan} respectively. The short-wave fluxes to the canopy contribute to direct absorption, but

also for absorbtion from secondary reflections from the floor surface. Short-wave radiation that is not intercepted by the canopy is partly absorbed by the floor referred to by P_{SunFlr} and P_{AluFlr}, and partly scattered back to the sky above the canopy. Some of this radiation is intercepted by obstructing elements inside the greenhouse (some 10%), but the major part will leave the greenhouse envelope. Therefore the heat flux from short-wave radiation that is reflected by the canopy and floor back to the greenhouse ambient is neglected.

Besides generating short-wave radiation, artificial illumination supplies a significant amount of sensible heat. This heat flux is referred to by P_{AluAir}.

The temperature of the heating pipes is determined by the heating system model (see Section 4.4.1), and therefore considered as a boundary variable in the thermal model. The other boundary variables, except for T_{so7} are derived from hourly weather data. The temperature at 1.27 m below the floor of the greenhouse is computed by a periodic function reading

$$T_{so7} = 15.0 + 2.5 \sin(1.72 \cdot 10^{-2}(daynr - 140)) \qquad [°C] \ (5.27)$$

With *daynr* the number of the sequential day of the year, with 1 January as daynumber 1.

From Figure 5.3, the heat balances can be stated easily from the addition of all energy fluxes to a compartment in a net energy flux. For the cover this results in:

$$\frac{dT_{cov}}{dt} = \frac{1}{\rho_{cov}\, c_{p,cov}\, V_{cov}} H_{cov,net} \qquad [Ks^{-1}] \ (5.28)$$

with

$$H_{cov,net} = P_{SunCov} + H_{TopCov} + H_{AirCov} + R_{FlrCov} + \qquad [Wm^{-2}] \ (5.29)$$
$$R_{ScrCov} + R_{UppCov} + R_{LowCov} + R_{CanCov} +$$
$$L_{TopCov} + L_{AirCov} - H_{CovOut} - R_{CovSky}$$

The density of the greenhouse cover (ρ_{Cov}) is $2.6 \cdot 10^3$ kgm^{-3} (glass) and the specific thermal capacity ($c_{p,cov}$) is 840 Jkg^{-3}K^{-1}. The volume of the greenhouse cover compartment (V_{cov}) depends on the thickness of the glass (d) and the roof slope (ψ) according to $V_{cov} = d/\cos(\psi)$. Commonly d is $4 \cdot 10^{-3}$ m and ψ is 25°. As in the other sub-models, integration of the differential equation yields the course of the state variable in time. The fluxes mentioned in Eqn. 5.29 are discussed in the next sections.

As with the carbon dioxide and vapour sub-model, the state variable representing the temperature of the top compartment is computed by a static equation, because its heat capacity is very small. The net flux to the top compartment is stated in Equation 5.30.

$$H_{top,net} = H_{ScrTop} + H_{AirTop} - H_{TopCov} - H_{TopOut} \qquad [Wm^{-2}] \ (5.30)$$

The top compartment temperature that results from the requirement that the net

flux equals zero is found by implementing the flux relations (analogue to Eqn. 5.1) and yields:

$$T_{top} = (HEC_{ScrTop}T_{scr} + HEC_{AirTop}T_{air} + HEC_{TopCov}T_{cov} + \quad [K] (5.31)$$
$$HEC_{TopOut}T_{out})/(HEC_{ScrTop} + HEC_{AirTop} + HEC_{TopCov} +$$
$$HEC_{TopOut})$$

The net flux to the thermal screen is stated in Equation 5.32

$$H_{scr,net} = R_{FlrScr} + L_{AirScr} + R_{UppScr} + R_{LowScr} + \quad [Wm^{-2}] (5.32)$$
$$H_{AirScr} + R_{CanScr} - H_{ScrTop} - L_{ScrTop} - R_{SrcCov}$$

Because the capacity of the state variable representing the screen temperature is very small, like the top compartment, the screen temperature is computed by an algebraic equation. This implies that Eqn. 5.32 equals zero.

Some heat fluxes stated in Eqn. 5.32 (R and L) are not linear in T_{scr}. To perform easy calculation they are linearized. The linearization of the radiative heat exchange is discussed in Section 5.5.2. The linearization of the fluxes associated with condensation and evaporation (L_{AirScr} and L_{ScrTop} respectively) is performed by linearizing the saturated vapour pressure curve. This linearization states that

$$L_{AirScr} = 2.45 \cdot 10^6 \, VEC_{AirScr} \, (VP_{air} - (sT_{scr} + i)) \quad [Wm^{-2}] (5.33)$$

where s is the slope of the tangent at the saturated vapour pressure curve around T_{scr} and i its intercept. The slope of the tangent is computed from the derivative of the saturated vapour pressure curve (see Appendix H) and the intercept follows from $i = VP_{scr} - sT_{scr}$. In the expressions for s and i the last computed value for T_{scr} and VP_{scr} are applied. The expression for L_{ScrTop} is analogue to Eqn. 5.33.

After substitution of L_{AirScr} and L_{ScrTop} by equations such as Eqn. 5.33, the convective heat exchange terms by equations such as Eqn. 5.1 and the radiative heat exchange terms by equations like Eqn. 5.3, and after rearranging terms, the expression for T_{scr} yields:

$$T_{scr} = (\Delta H(VEC_{AirScr}(VP_{air}-i) + VEC_{ScrTop}(VP_{top}-i)) + \quad [°C] (5.34)$$
$$HEC_{AirScr}T_{air} + HEC_{UppScr}T_{upp} + HEC_{CanScr}T_{can} +$$
$$HEC_{LowScr}T_{low} + HEC_{FlrScr}T_{flr} + HEC_{ScrTop}T_{top} + HEC_{ScrCov}T_{cov})/$$
$$(\Delta H(VEC_{AirScr} + VEC_{ScrTop}) \, s + HEC_{AirScr} + HEC_{UppScr} +$$
$$HEC_{CanScr} + HEC_{LowScr} + HEC_{FlrScr} + HEC_{ScrTop} + HEC_{ScrCov})$$

with ΔH the heat of evaporation. The prevention of a greater evaporation than condensation was already accounted for in the computation of VEC_{ScrTop}.

When observing Equation 5.31 and 5.34, it appears that the equations are mutually

dependent because the first uses T_{scr} and the second uses T_{top}. Equations 5.31 and 5.34 can be considered as a set of two linear equations in T_{top} and T_{scr}, which should be solved simultaneously. However, because the contribution of T_{top} in the computation of T_{scr} is very small, in the present model the temperatures are computed sequentially, starting with T_{scr}.

The next state variable in the thermal model represents the greenhouse air temperature. Just like the case with the other sub-models, when the screen is opened the compartment also represents the air in the top of the greenhouse. The expression for the net flux to the greenhouse air can be read from Figure 5.3.

$$H_{air,net} = P_{AluAir} + P_{SunAir} + H_{UppAir} + H_{LowAir} + \qquad [Wm^{-2}] \ (5.35)$$
$$H_{CrpAir} - H_{AirFlr} - H_{AirTop} - H_{AirScr} - H_{AirOut} - H_{AirCov}$$

The rate of temperature change, resulting from this net flux is expressed in the same way as in Eqn. 5.28.

$$\frac{dT_{air}}{dt} = \frac{1}{\rho_{air} \, c_{p,air} \, V_{air}} \, H_{air,net} \qquad [Ks^{-1}] \ (5.36)$$

The capacity of the air compartment, the denominator in Eqn. 5.36 varies with temperature because the density ρ_{air} is temperature dependent. Nevertheless a constant density is applied ($1.20 \ kgm^{-3}$), holding for 20 °C and standard atmospheric pressure ($1 \cdot 10^5$ Pa). The specific thermal capacity ($c_{p,air}$) is set to a constant value as well ($1 \cdot 10^3 \ JK^{-1}kg^{-1}$). The volume of the air compartment (V_{air}) is equal to the volume applied in the computation of the capacity for vapour and CO_2 (see Section 5.3.1 and 5.4.1).

The canopy is the fifth state variable in the thermal model. The net heat flux to the canopy is defined by:

$$H_{can,net} = R_{UppCan} + R_{LowCan} + P_{VISCan} + P_{NIRCan} - \qquad [Wm^{-2}] \ (5.37)$$
$$H_{CanAir} - R_{CanCov} - R_{CanScr} - R_{CanFlr} - L_{CanAir}$$

which leads to a rate of temperature change according to

$$\frac{dT_{can}}{dt} = \frac{1}{Cap_{leaf} \, LAI} \, H_{can,net} \qquad [Ks^{-1}] \ (5.38)$$

The heat capacity of a square meter of canopy leaves (Cap_{leaf}) was estimated by Stanghellini (1987) at $1.2 \cdot 10^3 \ JK^{-1}m^{-2}$. The variable LAI defines the leaf area index, which is the total leaf surface per square meter floor surface.

The floor and soil below the greenhouse represents a massive thermal capacity with a poor thermal conductivity. The floor of the greenhouse is assumed to consist of concrete tiles with a thickness of 3 cm. The combination of the large heat flux from solar and thermal radiation and the poor conductivity of the floor yields

a large temperature gradient at the top of the floor. The surface temperature shows diurnal variations of some 10 °C. To be able to describe this temperature gradient the floor has to be considered in layers. Therefore the tiles are represented by two state variables, named T_{flr} and T_{so1}. T_{flr} represents the temperature of the top part of the tile, and T_{so1} describes the temperature at the bottom part. The top of the tile has a thickness of 1 cm and the bottom has a thickness of 2 cm. The thickness of the second floor compartment (T_{so1}) is allowed to be larger because the gradient in this part of the floor is much smaller than that at the top of the floor. The net heat flux to the floor compartment (T_{flr}) can be read from Figure 5.3

$$H_{flr,net} = R_{LowFlr} + R_{UppFlr} + H_{AirFlr} + R_{CanFlr} + \qquad [Wm^{-2}] \ (5.39)$$
$$R_{VISFlr} + R_{NIRFlr} - H_{FlrSo1} - R_{FlrScr} - R_{FlrCov}$$

The rate of temperature change as a function of the thermal capacity of the state variable and the net heat flux can be expressed analogue to for example Eqn. 5.28. The thermal capacity of the floor can be computed easily from the specific volumetric heat capacity of concrete ($2.0 \cdot 10^6$ Jm^3K^{-1}) and the thickness of the layer represented by T_{flr} (1 cm). The net heat flux to the lower part of the concrete tiles is governed by only two fluxes.

$$H_{so1,net} = H_{FlrSo1} - H_{So1So2} \qquad\qquad [Wm^{-2}] \ (5.40)$$

Because the volume of the lower part of the tile is double the volume of T_{flr}, its capacity is twice the capacity of T_{flr}. The computation of the net fluxes to the layer i (i=2..6) of the soil is similar to Eqn. 5.40.

$$H_{soi,net} = H_{Soi-1Soi} - H_{SoiSoi+1} \qquad\qquad [Wm^{-2}] \ (5.41)$$

The thermal capacity of the soil layers below the tiles is determined by the thickness of the soil compartments and their volumetric heat capacity. The thicknesses of the soil layers below the tiles increases with the following sequence:

$$th_{so2}=0.04, \ th_{so3}=0.08, \ th_{so4}=0.16, \ th_{so5}=0.32 \ \text{and} \ th_{so6}=0.64 \quad [m] \ (5.42)$$

The increment of the layer thickness with an exponential sequence is to limit the number of state variables and still describe a gradient in a volume with a large thermal capacity.

To compute the volumetric heat capacity of the soil it is assumed that the soil consists of 70% sand, 20% water and 10% air, holding for a tight sandy soil. Thus the cubic heat capacity of the soil is defined by:

$$\rho c_{p,soil} = 0.7 \, \rho c_{p,sand} + 0.2 \, \rho c_{p,water} + 0.1 \, \rho c_{p,air} = 1.73 \cdot 10^6 \quad [Jm^{-3}K^{-1}] \ (5.43)$$

Of course, with $\rho c_{p,sand} = 1.28 \cdot 10^6$ and $\rho c_{p,water} = 4.18 \cdot 10^6$, the contribution of the heat capacity of air in $\rho c_{p,soil}$ is negligible.

Finally, on behalf of the computation of the mean heat loss from the heating pipes (see Section 4.4.1.4) the net flux from the upper and lower heating circuit must be determined. From figure 5.3 these net fluxes read:

$$H_{upp,net} = -(R_{UppScr} + R_{UppCov} + \qquad\qquad\qquad \text{[Wm}^{-2}\text{] (5.44)}$$
$$H_{UppAir} + R_{UppCan} + R_{UppCrp})$$

and

$$H_{low,net} = -(R_{LowScr} + R_{LowCov} + \qquad\qquad\qquad \text{[Wm}^{-2}\text{] (5.45)}$$
$$H_{LowAir} + R_{LowCan} + R_{LowCrp})$$

The fluxes are signed negative to conform to the other expressions for net fluxes in this section. However, in the expression for α_{pip} (Eqn. 4.7, page 37), the net flux from a heating pipe is considered a heat loss and therefore treated as a positive value.

5.5.2 Fluxes in the thermal model

In the thermal model convective, conductive and radiative heat exchange processes can be found. Moreover there are a number of forced fluxes to be defined. All fluxes, or the exchange coefficients by which the fluxes can be computed with equations such as Eqn. 5.1, 5.2 or 5.3, are discussed in four separate sections.

5.5.2.1 Convective heat fluxes

In a greenhouse, convective heat exchange plays a role at the various surfaces and by the ventilation process.

Heat fluxes at the surfaces

Going from the top to the bottom of the conceptual greenhouse, the cover is the first surface. At the upper side, the greenhouse cover looses heat to the outside air. Bot (1983) devoted a substantial part of his research to the description of the heat exchange process at this saw-tooth surface. He found a satisfying description of the heat exchange coefficient as a function of the wind speed:

$$\alpha = \begin{cases} 2.8 + 1.2 \text{ Windsp} & | \text{ Windsp} < 4 \text{ m s}^{-1} \\ 2.5 \text{ Windsp}^{0.8} & | \text{ Windsp} \geq 4 \text{ m s}^{-1} \end{cases} \qquad \text{[Wm}^{-2}\text{glass K}^{-1}\text{] (5.46)}$$

Because the tilted cover yields a cover/floor surface ratio larger than 1 the heat exchange coefficient for the greenhouse cover to the air per m² floor surface reads:

$$HEC_{CovOut} = \alpha/\cos(\psi) \qquad\qquad [Wm^{-2}K^{-1}] \ (5.47)$$

The heat flux from the cover to the outside air (H_{CovOut}) can be computed with an equation analogue to Eqn. 5.1.

At the inner side of the cover, the heat exchange process is considered to be determined by free convection from an inclined surface. Thus, referring to Appendix A (see Eqn. A.4), the heat exchange coefficient at the inner side of the greenhouse cover is described by:

$$\alpha = 1.70 \ (\cos\psi)^{0.33} \ \Delta T^{0.33} \qquad\qquad [Wm^{-2}glass \ K^{-1}] \ (5.48)$$

Indeed, this value has a fair agreement with the results mentioned by Bot (1983), who found heat exchange coefficients ranging from 2 to 4 $Wm^{-2}glass \ K^{-1}$. Depending on the status of the thermal screen, the heat flux to the cover either originates from the top compartment, or from the main air compartment. However, the heat exchange process is the same. Thus, taking the larger surface due to the roof slope (ψ) compared to the floor surface into account the following relations are derived.

$$HEC_{TopCov} = 1.7 \ (T_{top} - T_{cov})^{0.33} \ \cos(\psi)^{-0.66} \qquad [Wm^{-2}K^{-1}] \ (5.49)$$

$$HEC_{AirCov} = 1.7 \ (T_{air} - T_{cov})^{0.33} \ \cos(\psi)^{-0.66} \qquad [Wm^{-2}K^{-1}] \ (5.50)$$

Below the cover, the next solid surface assigned to a state variable is that of the thermal screen. Because the porosity of the thermal screen subject to the present work[a] is very small, the screen can be considered to be a horizontal flat plate with respect to convective heat exchange. The heat exchange between the air below to the relative cold screen is an upward heat flux. The same holds for the exchange from the screen to the relative cold top compartment. The heat exchange coefficient for an upward heat flux to or from a plate is found from Eqn. A.4 (see Appendix A).

Taking account of the screen closure (SC), the heat exchange coefficients from the air to the screen and from the screen to the top are described by:

$$HEC_{ScrTop} = SC \ 1.7 \ (T_{scr} - T_{top})^{0.33} \qquad\qquad [Wm^{-2}K^{-1}] \ (5.51)$$

$$HEC_{AirScr} = SC \ 1.7 \ (T_{air} - T_{scr})^{0.33} \qquad\qquad [Wm^{-2}K^{-1}] \ (5.52)$$

SC is zero when the screen is opened and 1 when it is closed. However, to carry-off moisture, in common horticultural practice the screen is often opened slightly. In such cases the screen closure is 0.98.

Working downwards through the conceptual greenhouse, the upper heating pipe is the next solid element. The pipe is located in the free air above the canopy. In Appendix A, for such a heating pipe the heat exchange coefficient is determined

---

[a]The thermal screen applied in this work (LS-10^{+}) is a film strip fabric. The fabric is capable of transporting moisture.

at (see Eqn. A.6):

$$\alpha = 1.28 \ X^{-0.25} \ \Delta T^{0.25} \qquad \qquad [\text{Wm}^{-2}\text{pipe K}^{-1}] \ (5.53)$$

with X the characteristic dimension of the pipe, which is its diameter. With the introduction of the variable l_{upp}, denoting the length of upper heating pipes per m^2 floor surface and a variable d_{upp}, being the diameter of the pipe, the heat exchange coefficient of the upper heating pipe for heat exchange with the greenhouse air can be expressed as:

$$HEC_{UppAir} = 1.28 \ \pi \ d_{upp}^{0.75} \ l_{upp} \ (T_{upp} - T_{air})^{0.25} \qquad [\text{Wm}^{-2}\text{K}^{-1}] \ (5.54)$$

If the lower heating pipe hung in free air, similar to the upper heating pipe, the variable HEC_{LowAir} could be determined with an equation like Eqn. 5.54. However, since the lower heating pipe is situated near the ground and close to the canopy, the heat exchange process is likely to be somewhat hindered, compared to a pipe in free air. Therefore, instead of the theoretical value, as applied for the upper heating pipe, the results of measurements of Bot (1983) are used to describe the heat exchange coefficient. The best fit of his results for a pipe with a diameter of 51 mm yielded a heat exchange coefficient described by:

$$\alpha = 1.99 \ \Delta T^{0.32} \qquad \qquad [\text{Wm}^{-2}\text{pipe K}^{-1}] \ (5.55)$$

Indeed, as long as the temperature difference between pipe and air does not exceed 75 °C this heat exchange coefficient is smaller than the value computed by Eqn. A.6. The full equation that expresses HEC_{LowAir} reads:

$$HEC_{LowAir} = 1.99 \ \pi \ d_{low} \ l_{low} \ (T_{low} - T_{air})^{0.32} \qquad [\text{Wm}^{-2}\text{K}^{-1}] \ (5.56)$$

where l_{low} and d_{low} are defined analogue to l_{upp} and d_{upp}.

The canopy leaves are the fifth solid surface in the greenhouse. The expression for the heat exchange coefficient at the canopy leaves was derived by the work of Stanghellini (1987). By using artificial leaves, she determined the boundary layer resistance to heat transfer as a function of micrometeorological quantities. For tomato leaves she found:

$$r_H = \frac{1174 \ \ell^{0.5}}{(\ell \ | \ T_{crp} - T_{Air} | + 207 \ u^2)^{0.25}} \qquad [\text{sm}^{-1}] \ (5.57)$$

with r_H the boundary layer resistance for heat transfer (sm^{-1}), ℓ the characteristic dimension of a canopy leaf (the width) (m) and u the local air velocity (ms^{-1}). Obviously this relation shows a reasonable dependence of r_H on local air velocity and temperature excess of the leaf surface.

In greenhouses, the air velocities around the leaves are in the range of 0.04 to 0.1 ms^{-1} and the temperature difference between leaves and ambient are limited to some 2 K (Stanghellini, 1987). With a mean width of the canopy leaves of 0.05

m the resistance to heat transport will vary between 200 and 350 sm^{-1}.

Rather than a resistance, the thermal model uses an exchange coefficient to relate a heat flux to a temperature difference. A thermal diffusive resistance can be converted to a heat exchange coefficient by (Monteith, 1973):

$$\alpha = \rho c_{p,air} / r_H \qquad \text{[Wm}^{-2}\text{leaf K}^{-1}\text{]} \quad (5.58)$$

With the resistance (r_H) ranging between 200 to 350 sm^{-1}, α varies between 3.4 and 6 Wm^{-2}K^{-1}. Despite these variation the model uses a fixed heat exchange coefficient of 5 Wm^{-2}K^{-1}. The heat exchanging surface of the canopy is twice the LAI because sensible heat is released at the upper and the lower side of a leaf. Thus HEC_{CanAir} becomes:

$$HEC_{CanAir} = 2 \text{ LAI } 5 \qquad \text{[Wm}^{-2}\text{K}^{-1}\text{]} \quad (5.59)$$

The last surface distinguished in the thermal model is the greenhouse floor. The floor can be warmer or colder than the air above it. Since the Nu-Ra relation differs for these two cases, the convective heat exchange coefficient is determined by either of two equations.

With Equations A.4 and A.5 from Appendix A and a characteristic dimension of 3 m, as suggested in Appendix A, the heat exchange coefficient is defined by:

$$HEC_{AirFlr} = \begin{cases} 1.7 \, (T_{flr} - T_{air})^{0.33} & | \, T_{flr} > T_{air} \\ 1.3 \, (T_{air} - T_{flr})^{0.25} & | \, T_{flr} < T_{air} \end{cases} \qquad \text{[Wm}^{-2}\text{K}^{-1}\text{]} \quad (5.60)$$

Ventilation

Ventilation replaces greenhouse air by outdoor air. In most cases the exchange is governed by natural ventilation through windows, from which the aperture of the windows is controlled by the greenhouse climate controller. A small, uncontrollable, ventilation flux is caused by leakage since greenhouses are not completely airtight.

The computation of the air exchange rate f_{vent} (m^{3}m^{-2}s^{-1}), is based on the work of De Jong (1990). In his thesis he determined a relation to describe the impact of wind speed, temperature difference and opening angle on the air exchange rate for three window geometries.

In his work, each of the two main factors driving air exchange (temperature difference and wind) were studied separately and combined afterwards. It appeared that the combination could be performed by a vector-like summation.

$$\phi_{window} = (\phi_{temp}^2 + \phi_{wind}^2)^{0.5} \qquad \text{[m}^3\text{window}^{-1}\text{s}^{-1}\text{]} \quad (5.61)$$

The contribution of temperature driven ventilation (ϕ_{temp}) in the total ventilation flux is small but can be important during nighttime and in winter. ϕ_{temp} was

described by:

$$\phi_{temp} = C_f l/3 \, (\, | \, g \, ß \, \Delta T \, | \,)^{0.5} \, H^{1.5} \qquad\qquad [m^3s^{-1}window^{-1}] \;(5.62)$$

The constant C_f accounts for the discharge of energy caused by friction in the window opening. In the work of de Jong, it appeared to be 0.6 and was hardly affected by the window geometries subject to his work. l is the length of the window (m), as depicted in Figure 5.4. g is the gravitational acceleration (ms^{-2}) and ß the thermal expansion coefficient (1/283 K^{-1}). H is the height of the front opening of the window (m) (see Figure 5.4), expressed by $H = h(\sin(\psi) - \sin(\psi-\theta))$, with ψ the roof slope, θ is the opening angle of the window. In the model, Eqn. 5.62 is applied on both leeside ($\phi_{temp,l}$) and windward side ($\phi_{temp,w}$) windows.

To describe the wind speed driven ventilation, de Jong used 'Window Functions' that relate the air exchange rate through a window with the wind speed and the surface of the window ($G = \phi/(A_0 \, u)$, with u the wind speed (ms^{-1}) at reference height (1.5 m) and A_0 the surface of a window ($A_0 = l \, h$)). The window function $G_w(\theta)$ holds for windows at the windward side of the roof and $G_l(\theta)$ describes leeside ventilation.
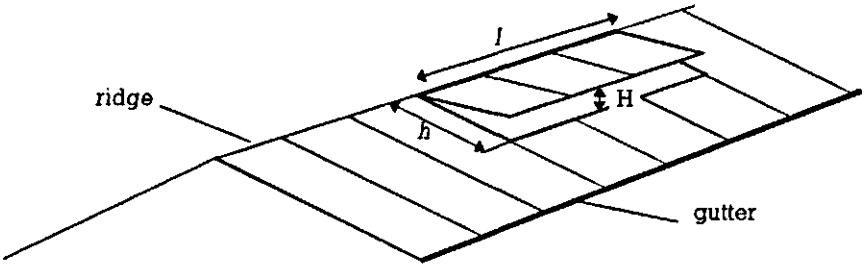
Figure 5.4 Window dimensions

With the window functions, the air exchange rate is defined by:

$$\phi_{wind} = ((G_l(\theta) + G_w(\theta)) \, A_0 \, u \qquad\qquad [m^3s^{-1}window^{-1}] \;(5.63)$$

In de Jong's measurements the ventilation fluxes didn't appear to be affected by wind direction. Moreover, for small opening angles of the windward ventilators ($\theta < 12°$), the experiments showed that windward ventilation could be considered as additional to leeside ventilation. De Jong's work does not mention whether the windward side ventilation can still be considered additive for large opening angles. However, during the period of the year that the greenhouse is heated, the wind-

ward side ventilators are hardly used. Thus, with respect to energy consumption, a possible (large) error in the total ventilation flux if both windward and leeside ventilators are opened with large angles is not a serious problem.

For the different window geometries studied by De Jong, the windows with an aspect ratio (*l/h*) of 1.825 show the most resemblance to windows in the most common type of greenhouse. Therefore the window functions that were determined for that case are applied in the present model. These window functions read:

$$G_l(\theta) = 2.29 \cdot 10^{-2} (1 - exp(-\theta/21.1)) \qquad \text{[-] (5.64a)}$$

$$G_w(\theta) = 1.2 \cdot 10^{-3} \, \theta \, exp(\theta/211) \qquad \text{[-] (5.64b)}$$

Combining Eqns. 5.61, 5.62, 5.63 and 5.64, and introducing a variable fr_{window}, denoting the number of windows per m^2 greenhouse, the air exchange rate from the greenhouse air to the outside air can be described by:

$$f_{vent} = \tfrac{1}{2} \, fr_{window} (\phi_{wind}^2 + (\phi_{temp,w} + \phi_{temp,l})^2)^{0.5} \qquad \text{[m}^3\text{s}^{-1}\text{m}^{-2}\text{] (5.65)}$$

The term $\tfrac{1}{2}$ accounts for the fact that ϕ_{wind} includes the air exchange through both leeside and windward-side windows, whereas fr_{window} counts all windows in the greenhouse. For a common Venlo type greenhouse, fr_{window} is 0.078 m^{-2}.

Due to the air exchange, indoor air with a heat content $\rho c_{p,air} T_{air}$ ($Jm^{-2}m^{-3}$) is replaced by outdoor air with a heat content $\rho c_{p,air} T_{out}$. Thus, when the difference in density of inside and outside air is neglected, the heat exchange coefficient for heat exchange by ventilation, is determined by:

$$HEC_{AirOut} = \rho c_{p,air} (f_{vent} + u \, f_{leakage}) \qquad \text{[Wm}^{-2}\text{K}^{-1}\text{] (5.66)}$$

The term $f_{leakage}$ takes account of leakage through cracks in the greenhouse construction. Obviously, the leakage is supposed to be linearly dependent on wind speed.

Air exchange through the screen

The direct heat exchange between the air compartment below and above the screen is due to the exchange of air between the two compartments. The exchange rate is expressed as a volume flux per m^2 floor surface ($m^3m^{-2}s^{-1}$).

The air exchange is based on two mechanisms. In the first place, air is transported through the openings in the fabric. In the second place, when the screen is opened a crack for dehumidification, air is exchanged through a relatively large opening. In both cases the air exchange is induced by pressure or density differences. Pressure differences originate from wind speed fluctuations inducing pressure fluctuations in the top compartment through opened windows or leakage. A density difference originates from a temperature difference across the screen.

Temperature-driven air exchange through fully closed screens is intensively studied by Balemans (1989). He measured the air exchange rate through the screen for 12 different types of fabrics as a function of the temperature difference across the material. Subsequently he fitted a function of the type $f_{screen} = K_s \Delta T^{0.66}$ through the data, where f_{screen} is the air flux through the screen ($m^3 m^{-2} s^{-1}$), K_s the 'screen flow coefficient' ($m^3 m^{-2} s^{-1} K^{-0.66}$) and ΔT the temperature difference across the screen (K). Table 5.1 lists some of his results.

Table 5.1 Screen-flow coefficients for various screen materials (extracted from Balemans, 1989).

Material type	Trade name	K_s ($m^3 m^{-2} s^{-1} K^{-0.66}$)
Knitted polyester	TD 55	$0.480 \cdot 10^{-3}$
Knitted polyester	TD 85	$0.372 \cdot 10^{-3}$
Woven polyester	Verzuu GPA bandjes	$0.203 \cdot 10^{-3}$
Film strip fabrics	LS 11	$0.161 \cdot 10^{-3}$
Non-woven	Tyvec gold standard	$0.243 \cdot 10^{-3}$

If the screen is opened slightly, the air exchange through this opening will dominate the air exchange through the screen. Unfortunately hardly any literature on this subject could be found. However, recently Miguel (1995) presented a theoretical model on air exchange through a crack induced by density difference. His model is based on the Navier-Stokes equation:

$$\phi_{crack} = \frac{L \, SO}{\rho_{mean}} (0.5 \, \rho_{mean} \, SO \, g \, (\rho_1 - \rho_2))^{0.5} \qquad [m^3 s^{-1}] \quad (5.67)$$

In this equation ϕ_{crack} is the flux of air through the crack ($m^3 s^{-1}$), L is the length of the opening in the screen (m), SO the screen opening (m), ρ_{mean} the mean density of air beneath and above the screen ($kg m^{-3}$), g the gravitational acceleration ($m s^{-2}$), ρ_1 the density of air above the screen ($kg m^{-3}$) and ρ_2 the density of air beneath the screen ($kg m^{-3}$). The comparison of the theoretical results and experimental data showed a good resemblance (Miguel, 1995). Also, a comparison of the results of the equation above with results from experiments on narrow, horizontal openings carried out by De Jong (1990) showed a good correspondence.
In a Venlo type greenhouse screens are usually located between the gutters and extend from one supporting element to the next. In Figure 5.5 a sketch of a thermal screen in a greenhouse construction is depicted.
Combining the air flow through the screen with the airflow through the crack, a single equation can be constructed.

$$f_{AirTop} = SC\ K_s\ \Delta T^{0.66} + \qquad\qquad\qquad [m^3s^{-1}m^{-2}]\ (5.68)$$

$$\frac{1\text{-}SC}{\rho_{mean}}\ (0.5\ \rho_{mean}W\ (1\text{-}SC)\ g\ (\rho_{air} - \rho_{top}))^{\ 0.5}$$

In this Equation f_{AirTop} refers to the exchange rate of air between the compartment beneath and above the screen. SC is a dimensionless number between 0 and 1 describing the fractional screen closure. The variable L has disappeared because ϕ_{crack} was divided by L×W. SO has disappeared, because it has been substituted by W(1−SC). For K_s a suitable value must be used from Table 5.1.
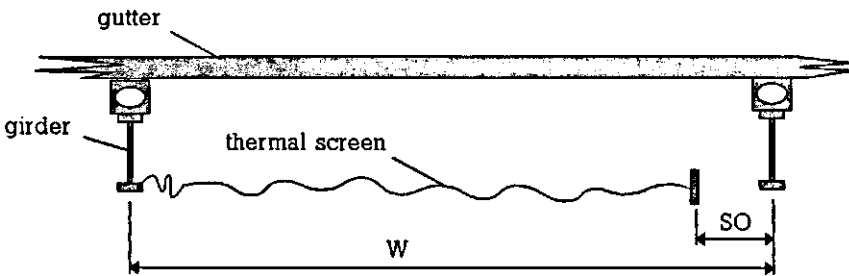
Figure 5.5 Sketch of a screen construction.

The effect of (wind speed driven) pressure fluctuation on air exchange through the screen and crack is even less well known than air exchange through the screen by temperature differences. However, in customary greenhouse operation the situation where screens are used and the windows are opened occurs when the climate controller opens the windows to carry off a heat surplus (due to artificial illumination or a minimum pipe temperature) or to decrease humidity. Thus the air exchange rate between the greenhouse air compartment through the crack to the top compartment and the outside air is part of a feed-back control loop. This means that deviations between model and reality are strongly attenuated. Therefore, in this work no further attention is devoted to this case.

The heat exchange coefficient from the main air compartment to the top compartment can be stated analogue to Equation 5.66.

$$HEC_{AirTop} = \rho c_{p,air}\ f_{AirTop} \qquad\qquad\qquad [Wm^{-2}K^{-1}]\ (5.69)$$

5.5.2.2 *Conductive heat fluxes*

In the model presented, conduction plays a minor role. Only the heat exchange between the soil layers is treated as a conduction process. The general equation for one-dimensional conduction reads:

$$\phi'' = -\lambda \frac{dT}{dx} \qquad\qquad [Wm^{-2}] \ (5.70)$$

Where ϕ'' is the heat flux density ($Wm^{-2}K^{-1}$), λ the thermal conductivity ($Wm^{-1}K^{-1}$) and dT/dx the temperature gradient (Km^{-1}). The negative sign expresses that the (positive) direction of the heat flux is opposite to the temperature gradient.

In discrete simulation models, the continuous gradient is replaced by a temperature difference. To do so, the continuous conducting medium is split up into several discrete compartments and the gradient is discretized by dividing the temperature difference between the compartments by the distance between the centres of the compartments. Then the equation becomes:

$$H = \frac{\lambda}{d} \ (T_1 - T_2) \qquad\qquad [Wm^{-2}] \ (5.71)$$

where H is the conductive exchange (Wm^{-2}), d the distance between the centres of the two heat exchanging compartments (m) and T_1-T_2 the temperature difference (K). The term λ/d corresponds with a heat exchange coefficient as applied in Eqn. 5.1.

The distances between the centre of the floor compartment and the first soil compartment is $1.5 \cdot 10^{-2}$ m (see Eqn. 5.42, page 83). With the thermal conductivity of concrete ($1.7 \ Wm^{-1}K^{-1}$) the conductive heat exchange coefficient between the floor and the first soil layer (HEC_{FlrSo1}) can be computed easily.

The heat exchange from the first soil layer to the second (H_{So1So2}) is partly governed by conduction through concrete, and partly by conduction through the soil. To account for a different thermal conductivity, a mean conductivity is used. This mean conductivity is computed from the reciprocal of the weighed mean of $1/\lambda_{concrete}$ and $1/\lambda_{soil}$. The weighing factors are the fractional contribution of the different constituents in the distance between the centres of the compartments under consideration.

Although the conductivity of a soil will vary considerably between soil types, and depends strongly on water content, the present model applies a constant value of $0.85 \ Wm^{-1}K^{-1}$, which is derived from Houter (1989). Using the layer thicknesses mentioned in Eqn 5.42 the weighed mean thermal conductivity of the media comprising the second and third soil layer is $1.02 \ Wm^{-1}K^{-1}$.

With the thicknesses of the other layers (Eqn. 5.42), which are all made up entirely of soil, the conductive heat exchange coefficients HEC_{So2So3} up till HEC_{So5So6} can be easily computed.

To determine the heat loss from the bottom soil layer, represented by T_{so6}, to the boundary variable in the soil (T_{so7}), half the thickness of the sixth soil layer is applied as the distance across which the temperature gradient is discretized.

5.5.2.3 Radiative heat fluxes

Radiation is an important heat exchange mechanism. With respect to the present greenhouse climate simulation model two radiative fluxes in different wavelength regions are important. The first is short-wave radiation, which acts as a forced energy flux on the greenhouse system. Therefore, short-wave radiation is discussed in Section 5.5.2.4. The second is long-wave radiative heat exchange in the wavelength region between 5 and 50 µm.

Long-wave radiative heat is exchanged between opaque surfaces in the greenhouse and between the greenhouse cover and the sky. The opaque surfaces are those from the cover, the screen, the heating pipes, the canopy and the floor. Thus there are 22 radiative heat fluxes to be determined (6+5+4+3+2+1 inside the greenhouse and for the radiation from the cover to the sky). The surface temperatures of the heat exchanging bodies, the emission and reflection coefficients in the long-wave band, and the mutual view factors play a role in this computation.

Going from the top downwards through the conceptual greenhouse, the radiative heat exchange between sky and cover is the first to be defined. The sky is assumed to radiate as a black body. Its (virtual) temperature (T_{sky}) is one of the boundary conditions in the model and is passed to the model by the weather data. Of course a measured value for T_{sky} is preferred, but when a sky temperature is missing in set of weather data, the sky temperature can be estimated from other meteorological quantities by an approach presented in Appendix F.

From Appendix E, the equation describing the radiative heat exchange between cover and sky reads:

$$R_{CovSky} = \varepsilon_{cov,up} \, F_{CovSky} \, A_{cov} \, \sigma \, (T_{cov}^4 - T_{sky}^4) \qquad \text{[Wm}^{-2}\text{]} \quad (5.75)$$

The emission coefficient (ε) is given an extra index (up) because for coated cladding materials, the emission coefficient of upper and lower side of the material can be very different. Due to the tilted greenhouse cover the view factor F_{CovSky} is smaller than 1. However, the product $F_{CovSky} \cdot A_{Cov}$ is 1 because the sky encloses the greenhouse cover. Thus equation 5.75 reduces to:

$$R_{CovSky} = \varepsilon_{cov,up} \, \sigma \, (T_{cov}^4 - T_{sky}^4) \qquad \text{[Wm}^{-2}\text{]} \quad (5.76)$$

To shorten the expressions presented, the radiative heat exchange processes are referred to by their exchange coefficient rather than by the description of the heat flux. Using the conventions presented in Section 5.2.3 (Eqn. 5.2 in particular) the radiative heat transfer coefficient from the cover to the sky is defined by:

$$REC_{CovSky} = \varepsilon_{cov,up}\, \sigma \qquad\qquad [Wm^{-2}K^{-4}]\ (5.77)$$

For ordinary glass $\varepsilon_{cov,up}$ is 0.84 (Out & Breuer, 1995). The lower side of the cover faces the screen, when it is closed, or four other surfaces in the greenhouse, when the screen is opened (the surface of the upper and lower heating pipe, the canopy and the soil). When the screen is positioned somewhere between both extremes, all five surfaces exchange thermal radiation with the cover. In that case the computation of view factors is very complex. However, to reduce this complexity, and without making severe neglections because the screen is hardly ever in a position far away from the extremes, the view factors between cover and other bodies are supposed to be linearly dependent on the screen closure.

The radiative heat exchange between cover and screen is computed by the linearized equation for radiative heat exchange (see Appendix E), since the screen temperature is determined by an algebraic equation (see Eqn. 5.34). Thus the heat flux is determined by:

$$R_{ScrCov} = \frac{\varepsilon_{scr}\, \varepsilon_{cov,do}\, F_{ScrCov}\, A_{scr}}{1 - \rho_{scr}\rho_{cov,do}F_{ScrCov}F_{CovScr}}\, 4\sigma T_m^{\,3}(T_{scr} - T_{cov}) \quad [Wm^{-2}]\ (5.78)$$

The cover occupies all of the upper hemisphere of the screen. Therefore F_{ScrCov} equals 1. However, the radiating surface of the screen depends on its closure, and thus A_{scr} equals SC (the fractional screen closure). T_m is the mean temperature of T_{scr} and T_{cov} (K). The most convenient way to determine the view factor from cover to screen, required in the denominator, is using the reciprocity theorem (Pitts, 1986):

$$F_{ScrCov}\, A_{scr} = F_{CovScr}\, A_{cov} \Rightarrow F_{CovScr} = F_{ScrCov}\, A_{scr}/A_{cov} \qquad [-]\ (5.79)$$

Because of the tilting roof pane, the radiating cover surface (A_{cov}) is $1/\cos(\psi)$. Thus, F_{CovScr} equals $A_{scr}\cos(\psi)$. The screen surface (A_{scr}) equals SC. Because the screen considered is not aluminized, the emission coefficient will be close to 1. Together with the low reflection coefficient of the glass ($\rho_{cov,do} = 1-\varepsilon_{cov,do} = 0.16$), the denominator in Eqn. 7.78 will be close to 1. Therefore, this denominator is omitted. After substitution of F_{ScrCov} and A_{scr} the linearized radiative heat exchange for the heat exchange between cover and screen is found. This reads:

$$HEC_{ScrCov} = \varepsilon_{scr}\, \varepsilon_{cov,do}\, SC\, \tfrac{1}{2}\sigma\, (T_{scr} + T_{cov})^3 \qquad [Wm^{-2}K^{-1}]\ (5.80)$$

When the screen is opened, the cover faces the upper heating pipes, the canopy and, through the spaces in canopy, the lower heating pipes and the floor. To contribute to the screen, all expressions for the radiative exchange processes from the cover to the bodies beneath the screen are premultiplied by $(1-SC)$. Thus the radiative heat exchange between cover and upper heating pipe is described by:

$$REC_{UppCov} = (1-SC) \frac{\varepsilon_{upp}\, \varepsilon_{cov,do}\, F_{UppCov}\, A_{upp}\, \sigma}{1 - \rho_{upp}\, \rho_{cov,do}\, F_{UppCov}\, F_{CovUpp}} \qquad [Wm^{-2}K^{-4}] \quad (5.81)$$

The view factor of an infinitely long pipe to an infinite cover is 0.5, since half the hemisphere around the pipe is located above the pipe. However, the upper heating circuit consists of a network of parallel pipes. Thus, a small part of the hemisphere of a heating pipe is occupied by the neighbouring pipes. From the work of Sparrow and Cess (1970) it can be derived that the view factor of a pipe with a diameter of 0.051 m to a neighbouring pipe on the left and on the right side at a distant of 1.6 m is 0.01. Therefore, a fraction 0.005 of the upper part of the hemisphere is occupied by the neighbouring pipes. This is such a small fraction that it can be neglected. Thus the view factor of the upper heating pipe to the screen (F_{UppCov}) is 0.5

Using the reciprocity theorem, F_{CovUpp} can be defined by $F_{CovUpp} = F_{UppCov} A_{upp}/A_{cov}$. With A_{upp} being about 0.1, F_{CovUpp} becomes about 0.05. The emission coefficient of heating pipes (white painted) is about 0.88 (American institute of physics handbook, 1972). Thus, ρ_{upp} is about 0.12. With the small values in the multiplicative term in the denominator of Eqn. 5.81 it is obvious that the denominator can be omitted yielding:

$$REC_{UppCov} = (1-SC)\, 0.5\, \varepsilon_{upp}\, \varepsilon_{cov,do}\, l_{upp}\, \pi\, d_{upp}\, \sigma \qquad [Wm^{-2}K^{-4}] \quad (5.82)$$

The next opaque element of the greenhouse construction in the top-down view is the canopy. In general terms the radiative heat exchange coefficient between the cover and the canopy is analogue to Eqn. 5.81.

$$REC_{CanCov} = (1-SC) \frac{\varepsilon_{can}\, \varepsilon_{cov,do}\, F_{CanCov}\, A_{can}\, \sigma}{1 - \rho_{can}\, \rho_{cov,do}\, F_{CanCov}\, F_{CovCan}} \qquad [Wm^{-2}K^{-4}] \quad (5.83)$$

Because both reflection coefficients in the denominator are close to zero, and the view factors are smaller than one by definition, a simplification of the relation by a denominator equal 1 is allowed.

The view factor for radiation between canopy and cover is determined by application of the reciprocity theorem on the view factor for radiation from cover to canopy. From the previously defined view factor from upper heating pipe to cover (0.5) the view factor from cover to pipe can be computed using the reciprocity theorem. For an endless cover, F_{CovUpp} can be computed to be $0.5\, \pi\, d_{upp} l_{upp}\, \cos(\psi)$. Thus, by definition, the hemisphere occupied by the other opaque elements beneath the upper heating pipes is stated by $(1 - 0.5\, \pi\, d_{upp} l_{upp})\cos(\psi)$. Since the radiative exchange takes place at obstructing canopy surfaces, the view factor from the cover to the canopy can be determined by the fraction of the hemisphere not masked by the heating pipes which is occupied by the canopy. This fraction is related to the leaf area index by multiplication of the LAI with the long-wave extinction coefficient in an exponential function (see Appendix D). Thus the view

factor of the cover to the canopy becomes

$$F_{CovCan} = (1 - 0.5 \, \pi d_{upp} l_{upp}) \, (1 - exp(-k_l \, LAI)) \, cos(\psi) \qquad [-] \ (5.84)$$

where k_l is the long-wave extinction coefficient. The view factor F_{CanCov} can be found from the reciprocity theorem yielding

$$F_{CanCov} = F_{CovCan} \, A_{cov} / A_{can} \qquad [-] \ (5.85)$$

The radiating surface of the canopy stand is very large (twice the LAI) but most thermal radiation is re-radiated within the stand. Thus an effective radiating surface must be determined. This surface is described by the integral of the long-wave extinction function (Stanghellini, 1987).

$$A_{can} = 1 - exp(-k_l \, LAI) \qquad [m^2] \ (5.86)$$

After combining Eqns. 5.84, 5.85 and 5.86, and stating that $A_{cov} = 1/cos(\psi)$, the view factor from canopy to cover appears to be

$$F_{CanCov} = (1 - 0.5 \, \pi d_{upp} l_{upp}) \qquad [-] \ (5.87)$$

Combining Eqn. 5.86 with the simplified equation 5.83 the radiative heat exchange coefficient between canopy and cover is:

$$REC_{CanCov} = (1-SC) \, \varepsilon_{can} \, \varepsilon_{cov,do} \, F_{CanCov} \, (1-exp(-k_l \, LAI)) \sigma \qquad [Wm^{-2}K^{-4}] \ (5.88)$$

The emission coefficient of the canopy (ε_{can}) is taken to be 1, meaning that the leaves are considered as black bodies (Stanghellini, 1987).

The fourth opaque surface beneath the cover is formed by the pipes of the lower heating circuit. Just like the reasoning applied in the definition of REC_{CanScr}, the view factor for radiation from the cover to the lower heating pipe is determined by the computation of the view factor for radiation from the lower heating pipe to the cover. To determine the latter it is recalled that the simulation model conceptualizes that the lower heating pipe 'sees' five opaque surfaces. These are the floor, the neighbour pipes, the canopy, the upper heating pipes and the cover or screen. By definition the sum of these view factors is one. Thus, the most convenient way to determine the most difficult view factor is to compute the others and to consider the most difficult one as the rest factor.

The view factor to the neighbouring pipes can be computed with the formulas presented by Sparrow and Cess (1970). It appears that F_{LowLow} is about 0.02. According to the same reasoning as in the discussion on REC_{UppCov}, it can be stated that F_{LowFlr} equals 0.49. If there is no canopy, the view factor for radiation from the lower heating pipe to the upper heating pipe is about 0.005. This fraction is already small and becomes even smaller when the canopy has grown to a certain extent. Therefore the radiation exchange between the upper and lower heating pipes is neglected. Consequently, without a canopy, the view factor from pipe to cover equals 0.49. Because the canopy obstructs the exchange with the cover, the view

factor for the heat exchange between lower pipe and cover becomes

$$F_{LowCov} = 0.49 \, exp(-k_l \, LAI) \qquad\qquad [-] \, (5.89)$$

The denominator in the full equation of the type stated in Appendix E as equation E.11 is close to one. Thus the radiative heat exchange between lower heating pipe and cover can be stated as:

$$REC_{LowCov} = (1\text{-}SC) \, \varepsilon_{low} \, \varepsilon_{cov,do} \, \pi d_{low} \, l_{low} \, F_{LowCov} \, \sigma \qquad [Wm^{-2}K^{-4}] \, (5.90)$$

With F_{LowCov} stated by Equation 5.89. The emission coefficient of the lower heating pipes (ε_{low}) is equal to ε_{upp}.

The last opaque element exchanging radiation with the cover is the floor. The floor 'sees' the lower and upper heating pipes, the cover and the canopy. To compute the view factor from the floor to the cover, the absence of a canopy is again assumed first. A part of the full hemisphere of the floor is masked by the lower heating pipe. This part is expressed by $0.49 \, \pi d_{low} l_{low}$. The remainder of the hemisphere is either empty, obstructed by the canopy or obstructed by the upper heating pipe. Thus the view factor from floor to cover is determined by:

$$F_{FlrCov} = (1\text{-}0.49 \, \pi d_{low} l_{low}) \, exp(-k_l \, LAI) \, (1\text{-}0.5 \, \pi d_{upp} l_{upp}) \qquad [-] \, (5.91)$$

Because the canopy occupies a large part of the hemisphere of the floor for the major part of the year (resulting in a low view factor to the cover), and the reflection coefficient of the cover for long-wave radiation is low (about 0.1), multiple reflections are negligible. Therefore the equation describing the radiative heat exchange coefficient does not contain the extensive denominator.

$$REC_{FlrCov} = (1\text{-}SC) \, \varepsilon_{flr} \, \varepsilon_{cov,do} \, F_{FlrCov} \, \sigma \qquad\qquad [Wm^{-2}K^{-4}] \, (5.92)$$

The emission coefficient of the floor, consisting of concrete tiles, is assumed to be comparable to that of brick. For brick an emission coefficient of 0.89 was found (American institute of physics handbook, 1972).

The next opaque element for which the radiative exchange processes are described is the thermal screen. Because it's temperature is computed by an algebraic equation, all fluxes are linearized. The radiative exchange coefficient between screen and cover was already stated in Equation 5.80

Because in all previously derived radiative exchange coefficients the cover acts as a horizontal surface, from geometrical point of view the closed thermal screen is comparable to the cover. Thus the expressions for the heat fluxes are similar, except that the term (1-SC) must be substituted by SC. Moreover, because of the algebraic solution for the screen temperature requires linear exchange coefficients all expressions for the radiative heat exchange with the screen are linearized.

$$HEC_{UppScr} = SC\; 0.5\; \varepsilon_{upp}\varepsilon_{scr}\pi d_{upp}l_{upp}\; \tfrac{1}{2}\sigma(T_{upp}+T_{scr})^3 \qquad [Wm^{-2}K^{-1}]\; (5.93)$$

$$HEC_{CanScr} = SC\; \varepsilon_{can}\varepsilon_{scr}F_{CanScr}(1-e^{-kl\; LAI})\; \tfrac{1}{2}\sigma(T_{can}+T_{scr})^3 \qquad [Wm^{-2}K^{-1}]\; (5.94)$$

$$HEC_{LowScr} = SC\; \varepsilon_{low}\varepsilon_{scr}\pi d_{low}l_{low}F_{LowScr}\; \tfrac{1}{2}\sigma(T_{low}+T_{scr})^3 \qquad [Wm^{-2}K^{-1}]\; (5.95)$$

$$HEC_{FlrScr} = SC\; \varepsilon_{flr}\; \varepsilon_{scr}\; F_{FlrScr}\; \tfrac{1}{2}\sigma(T_{sol}+T_{scr})^3 \qquad [Wm^{-2}K^{-1}]\; (5.96)$$

The view factors F_{CanScr}, F_{LowScr} and F_{FlrScr} are equal to ones previously defined as F_{CanCov}, F_{LowCov} and F_{FlrCov} respectively.

The next opaque element in the greenhouse is the upper heating pipe. From this element two of the heat exchange processes (R_{UppCov} and R_{UppScr}) were already defined.

To compute the heat exchange between upper heating pipe and canopy, it is re-called that a fraction 0.5 of the hemisphere around the heating pipe is considered to face downward (see the discussion on REC_{UppCov}). Part of that fraction is occu-pied by canopy leaves. Thus the view factor for radiation from the upper heating pipe to the canopy is defined by

$$F_{UppCan} = 0.5\; exp(-k_1\; LAI) \qquad [-]\; (5.97)$$

With this view factor, and given the fact that multiple reflections between canopy and pipe are omitted because the canopy is practically black, the expression for the radiative heat exchange coefficient becomes

$$REC_{UppCan} = \varepsilon_{upp}\; \varepsilon_{can}\; F_{UppCan}\; \pi d_{upp}l_{upp}\; \sigma \qquad [Wm^{-2}K^{-4}]\; (5.98)$$

The next solid surface below the canopy leaves is composed of the lower heating pipes. However, radiation exchange between the upper and lower heating pipes is not included in the model because, even when there is no canopy, the view factor from the upper to the lower pipe is only about 0.01. When the canopy has grown to a certain extent, the view factor becomes even smaller.

The flux to the floor surface is the last radiative heat flux from the upper heating pipe that has to be defined. Taking into account that the canopy and the lower heating pipe mask the floor surface, the view factor of the upper heating pipe to the floor is defined by

$$F_{UppFlr} = 0.5\; (1-\pi d_{low}l_{low})\; exp(-k_1\; LAI) \qquad [-]\; (5.99)$$

Again the denominator in the extensive definition of the radiative exchange coeffi-cient is close to one. Thus remains:

$$REC_{UppFlr} = \varepsilon_{upp}\; \varepsilon_{sol}\; F_{UppFlr}\; \pi d_{upp}l_{upp}\; \sigma \qquad [Wm^{-2}K^{-4}]\; (5.100)$$

For the canopy, the fourth opaque element in the top-down approach to the green-house construction, the majority of radiative fluxes have already been described. Only the radiative heat exchange with the lower heating pipe and the floor have

to be defined.

Due to similarity of configuration, the upward radiation from the lower heating pipe to the canopy is described by the same type of equation as the downward radiation of the upper heating pipe to the canopy. Thus, analogue to Eqn. 5.98, the radiative heat exchange between lower heating pipe and canopy is described by

$$REC_{LowCan} = \varepsilon_{low}\, \varepsilon_{can}\, F_{LowCan}\, \pi d_{low} l_{low}\, \sigma \qquad [Wm^{-2}K^{-4}] \quad (5.101)$$

The view factor F_{LowCan} is defined by:

$$F_{LowCan} = 0.49\,(1 - exp(-k_1\, LAI)) \qquad\qquad [-] \quad (5.102)$$

The expression for the radiative heat exchange coefficient between canopy and soil is derived in the same way as the expression for REC_{CanCov}.

$$REC_{CanFlr} = \varepsilon_{can}\varepsilon_{sol}(1-0.49\,\pi d_{low}l_{low})(1-e^{-k_1\, LAI})\,\sigma \qquad [Wm^{-2}K^{-4}] \quad (5.103)$$

The final radiative heat exchange coefficient to be determined describes the thermal radiation exchange between the floor and the lower heating pipes. This exchange process is similar to the heat R_{UppCov}. Thus, analogue to Equation 5.82:

$$R_{LowFlr} = 0.49\,\varepsilon_{low}\,\varepsilon_{sol}\,\pi d_{low}l_{low}\,\sigma(T_{low}^{4} - T_{sol}^{4}) \qquad [Wm^{-2}K^{-1}] \quad (5.104)$$

5.5.2.4 Forced fluxes

In the thermal model the forced fluxes originate from short-wave radiation and from latent heat associated with condensation and evaporation.

Short-wave radiation

The short-wave radiation to which a greenhouse is exposed originates almost exclusively from the sun. Sometimes additional short-wave radiation is generated by artificial illumination. Compared to the yearly energy content of solar radiation, the contribution of artificial light is very small but nevertheless, during winter, additional lighting can have an important impact on actual canopy growth and development and on the actual greenhouse energy budget.

Solar radiation to which the greenhouse is exposed, contains wavelengths in a band between 0.3 and 3 µm. This wavelength band can be split in three spectral parts. The first part is Ultra violet (UV), ranging from 0.3-0.4 µm. The other two are visible light, ranging from 0.4 - 0.7 µm and the Near Infra Red (NIR), consisting of wavelengths between 0.7 and 3 µm. The visible light corresponds with radiation of interest for biological growth.

The fraction UV is between 6 and 10% and visible light contributes for 45 to 60%

to the intensity of radiation (Coulson, 1975). However, for plant growth modelling purposes it is common use to neglect these variations and to assign 50% of the solar radiation to visible light. Even the fraction UV is generally neglected so the other 50% is attributed to NIR (Monteith, 1973).

Besides the spectral division, solar radiation can be divided into direct and diffuse radiation. Principally, direct radiation reaches the earth surface with a certain angle of incidence, given by solar position. This angle varies during the day and seasons. In Appendix J an algorithm is presented that expresses the angle of incidence of solar radiation as a function of time, latitude and longitude.

Diffuse radiation is omnidirectional and has a distribution function for the intensity of radiation over the hemisphere. In the literature several distribution functions can be found (Coulson, 1975; Morris and Lawrence, 1971). In this study the standard overcast sky is applied (see also Appendix C). Direct and diffuse solar radiation are considered to be two sets of input data.

In the model, solar radiation induces the forced fluxes P_{SunCov}, P_{SunAir}, P_{SunCan} and P_{SunFlr}. The heat flux P_{SunCov} contributes to the absorption of radiation by the covering structure. This flux is assumed to be linearly dependent on the intensity of solar radiation.

$$P_{SunCov} = a_{cov} (I_{dif} + I_{dir}) \qquad [Wm^{-2}] \quad (5.105)$$

The absorption coefficient of the construction was computed by the light transmission model described in Appendix C. For direct radiation this coefficient was about 0.04 and slightly affected by solar elevation and azimuth. From the diffuse radiation to which the greenhouse is exposed also 4% was absorbed by the cover. The present model discards the small variations of a_{cov}.

Solar radiation that hits the greenhouse cover and which is not absorbed by the cover is either reflected back to the atmosphere or transmitted through the cover. For direct radiation, the transmitted fraction depends strongly on elevation and azimuth. The model presented in Appendix C calculates this transmitted fraction. In the Appendix an example is given of transmission data for a modern Venlo type greenhouse. In the equations in this work the transmissivity of the construction for direct radiation is referred to by τ_{dir}.

The diffuse transmissivity can be computed from the direct transmissivity after the definition of the distribution function for the intensity of radiation from the sky vault. Assuming a standard overcast sky and adopting the computed data for direct transmissivity, yields a diffuse transmissivity of 0.79 (see Appendix C). The transmissivity for diffuse radiation is denoted by τ_{dif}.

However, after passing the covering structure, quite a lot of light obstructing elements are present within the enclosure. Here one can think of girders, luminaries, energy screen packages, feet etc.. The fraction of transmitted light intercepted by those obstructions is denoted a_{obs}. Eventually, this absorbed radiation

will be released to the greenhouse air. Therefore a forced flux P_{SunAir} is introduced reading:

$$P_{SunAir} = a_{obs} (I_{dif} \tau_{dif} + I_{dir} \tau_{dir}) \qquad [Wm^{-2}] \quad (5.106)$$

Obviously, by applying τ_{dif} and τ_{dir}, a_{obs} acts on the transmitted fraction of the solar radiation. In the present model a_{obs} for a greenhouse without a screen and without artificial illumination is assumed to be 0.06. A thermal screen is assumed to increase this value with 0.04, and the luminaries of artificial lighting intercept an additional portion of 0.02. The amount of light that is passed by the cover and not obstructed by construction elements in the greenhouse is either absorbed by the canopy, absorbed at the floor or reflected. The absorption of solar radiation by a canopy stand is discussed thoroughly in the thesis prepared by Goudriaan (1977). He showed that the absorption can be expressed by an exponential function of the LAI. It appears that the absorption of direct radiation differs from diffuse radiation. This difference is expressed by defining extinction coefficients for both diffuse and direct radiation. Besides the distinction between diffuse and direct radiation, the absorption of NIR differs significantly from the absorption of visible light. Thus, the model computes two short-wave fluxes to the canopy, defined by:

$$P_{VISCan} = (I_{dif}(1-a_{obs})\tau_{dif}+P_{AluVIS})a_{Can,Vdif} \qquad [Wm^{-2}] \quad (5.107)$$
$$+I_{dir}\tau_{dir}(1-a_{obs})a_{Can,Vdir}$$

$$P_{NIRCan} = (I_{dif}(1-a_{obs})\tau_{dif}+P_{AluNIR})a_{Can,Ndif} \qquad [Wm^{-2}] \quad (5.108)$$
$$+I_{dir}\tau_{dir}(1-a_{obs})a_{Can,Ndir}$$

In the equations artificial illumination (denoted by P_{AluVIS} and P_{AluNIR}) is treated as diffuse radiation. These fluxes are defined in the last part of this Section.

The background of the computation of the absorption coefficients for diffuse and direct VIS and NIR ($a_{Can,Vdif}$, $a_{Can,Vdir}$, $a_{Can,Ndif}$ and $a_{Can,Ndir}$ respectively) is presented in Appendix D. It appears that for a common greenhouse canopy they can be expressed as:

$$a_{Can,Vdif} = (0.95 - 0.9 \, exp(-0.85 \, LAI)) \qquad [-] \quad (5.109)$$

$$a_{Can,Vdir} = (0.94 - 0.95 \, exp(-k \, LAI)) \qquad [-] \quad (5.110)$$
$$\text{with } k = 0.88 + 2.6 \, exp(-0.18 \, \beta)$$

$$a_{Can,Ndif} = (0.65 - 0.65\ exp(-0.27\ LAI) \qquad\qquad [-]\ (5.111)$$

$$a_{Can,Ndir} = (a - b\ exp(-k\ LAI) \qquad\qquad [-]\ (5.112)$$

$$with\ a = 0.67 - 0.06\ exp(-0.08\ \beta)$$
$$b = 0.68 - 0.50\ exp(-0.11\ \beta)$$
$$k = 0.25 + 0.38\ exp(-0.12\ \beta)$$

In Eqns. 5.110 and 5.112 β represents the solar elevation angle.

Radiation that is not absorbed nor reflected by the canopy is absorbed at the floor of the greenhouse. This absorbtion was computed with the model outlined in Appendix D by registering the amount of radiation not absorbed by the canopy and not reflected back to the greenhouse ambient. This amount, must be absorbed by the floor. By assuming an shortwave absorbtion coefficient of the floor of 0.25 for VIS and 0.6 for NIR, the following relations as a function of LAI and solar elevation angle were found.

$$a_{Flr,Vdif} = exp(-0.92\ LAI) \qquad\qquad [-]\ (5.113)$$

$$a_{Flr,Vdir} = exp(-k\ LAI) \quad with\ k = 0.90 + 0.83\ exp(-0.12\ \beta) \qquad [-]\ (5.114)$$

$$a_{Flr,Ndif} = (0.05 + 0.91\ exp(-0.50\ LAI) \qquad\qquad [-]\ (5.115)$$

$$a_{Flr,Ndir} = (a + b\ exp(-k\ LAI) \qquad\qquad [-]\ (5.116)$$

$$with\ a = 0.05 + 0.06\ exp(-0.08\ \beta)$$
$$b = 0.92 - 0.53\ exp(-0.18\ \beta)$$
$$k = 0.48 + 0.54\ exp(-0.13\ \beta)$$

again with β the solar elevation angle. The absorption coefficients defined in equations 5.113 till 5.116 can be used in equations like 5.107 and 5.108 to yield P_{VISFlr} and P_{NIRFlr}.

The upward reflections of the canopy stand and the reflections at the floor that are not intercepted by the canopy are partly intercepted by obstructing elements in the greenhouse, partly reflected back to the canopy and floor, but for the major part are scattered back to the atmosphere. Because the intercepted fraction is not more than some 30% of the already small reflections this secondary intercepted radiation is neglected.

Latent heat fluxes

Within the thermal sub-model the latent heat fluxes are treated as forced fluxes because their magnitude is determined by the water vapour sub-model. In the thermal model there are four latent heat fluxes. These fluxes are computed by:

$$L_{TopCov} = \Delta H \; MV_{TopCov} \qquad\qquad [Wm^{-2}] \; (5.117)$$

$$L_{ScrTop} = \Delta H \; MV_{ScrTop} \qquad\qquad [Wm^{-2}] \; (5.118)$$

$$L_{AirScr} = \Delta H \; MV_{AirScr} \qquad\qquad [Wm^{-2}] \; (5.119)$$

$$L_{CanAir} = \Delta H \; MV_{CanAir} \qquad\qquad [Wm^{-2}] \; (5.120)$$

with ΔH the heat of evaporation ($2.45 \cdot 10^6$ Jkg^{-1}).

Sensible heat loss from luminaries

The electric power consumed by luminaries of the artificial illumination is only partly converted to short-wave radiation. Typically, 17% of the electric power is converted to NIR and 25% is converted to visible light (Philips, 1990). Thus, 58% of the electric power is exchanged to the greenhouse by means of convection or by long-wave radiation. To contribute to this energy input a variable P_{AluAir} is introduced. The definition of this variable simply reads:

$$P_{AluAir} = fr_{SenAlu} \; P_{Artif} \qquad\qquad [Wm^{-2}] \; (5.121)$$

in which fr_{SenAlu} is the fraction of the electric power not converted to short-wave radiation. P_{Artif} denotes the electric power uptake of the artificial illumination (Wm^{-2}). It is clear that P_{AluVIS} and P_{AluNir} are calculated analogue to P_{AluAir}.

6 RESULTS

6.1 INTRODUCTION

As stated in Chapter 3, the primary energy consumption of a greenhouse is a result of the interaction between heating devices, requested greenhouse air conditions, properties of the building and greenhouse climate control. In Chapter 4 and 5 a tool to describe these interactions was developed, comprising an integrated simulation model of greenhouse climate conditions and the greenhouse heating system.

In this chapter, first the quality of the simulation model to describe the dynamics of the greenhouse climate, its climate control actions and energy demand is demonstrated by means of comparisons between measurements and results of simulations. After the quality of the model has been proved, the tool developed is used to study energy conserving measures. In this study, the usual process of cultivating tomatoes serves as a horticultural context.

6.2 COMPARISONS BETWEEN SIMULATION MODEL AND MEASUREMENTS.

A research facility at the IMAG-DLO site was used to test and adjust the simulation model. In this facility measurements were carried out on aggregated greenhouse air conditions (air temperature, humidity and CO_2 concentration), control actions (window apertures, heating pipe temperatures, screen positions, CO_2 supply and illumination), and required heating power. Moreover, data on daily water consumption were gathered.

Although the number of measured entities was limited, the long-term character of the measurements (some years) generated a vast amount of information on the dynamic behaviour of the greenhouse climate, its controller and heating system. In this section, first the experimental set-up is described, followed by the parametrization of the model that corresponds to the geometry of the research facility. Thereafter comparisons of small time scale measurements (10 minute mean values) are made over a short period (three successive days). Comparisons spanning a long period (year round) are made with large time scale measurements (daily averages). Finally some concluding remarks are made.

6.2.1 Experimental set-up

To compare model computations with experimental data, the first compartment of the research facility has been used. A sketch of the floor-plan of the facility is presented in Figure 6.1. It can be seen that the facility comprises four compartments of 192 m² each. In Figure 6.2 a cross-section through a compartment is shown.

The research facility is a Venlo-type greenhouse with a roof slope of 25° and a gutter height of 5 m. Twelve ventilators were mounted in the roof (6 at the leeside and 6 at the windward side of the roof segments). Thus, the number of windows per m² greenhouse area (fr_{window} in Eqn. 5.65) was 12:192 = 0.0625. The ventilators were 3 m wide and 0.86 m high, making the area of a window 2.64 m² (A_0 in Eqn. 5.63). Fully opened, the window pointed 5° upward. The leakage of the compartments ($f_{leakage}$ in Eqn. 5.66) was estimated on $1.5 \cdot 10^{-4}$ m³m⁻²s⁻¹/(ms⁻¹).
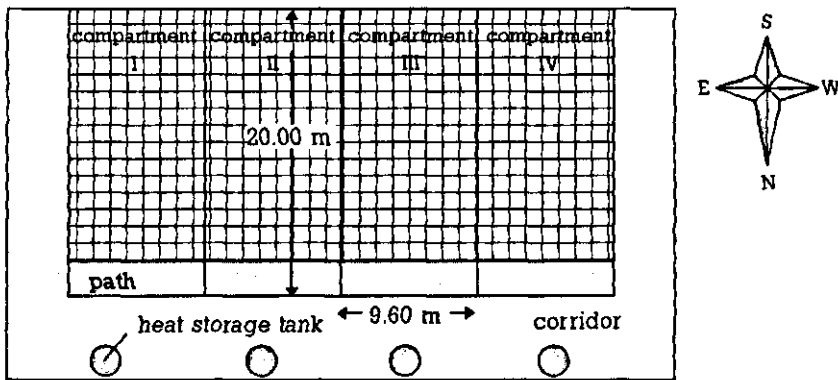
Figure 6.1 Floor plan of the research facility.

In the compartments, roses were grown on movable benches just above the lower heating pipes. Because the benches were movable, practically the entire floor of the growing area was occupied by the canopy. The path at the head of the compartment occupied 10% of the floor surface. The benches consist of a pair of translatable girders carrying small gutters, which were positioned perpendicular on the girders. Thus the benches have an open structure. The gutters support rockwool in which the roses are rooted. The roses were planted in January 1992. All measurements applied in the comparisons are from February 1993 or later, so in all simulations the canopy in the greenhouse is considered to be a full grown rose stand.
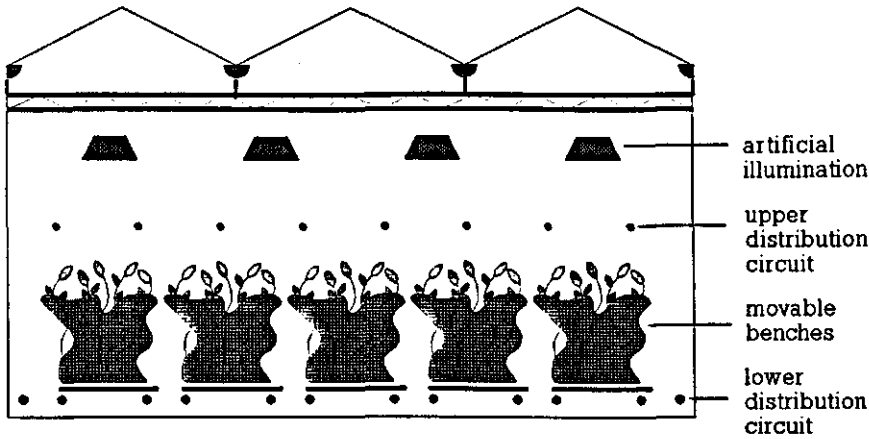
Figure 6.2 Cross-section of a compartment.

From mid-August to the end of April supplementary lighting was applied in the first and fourth compartment. With 16 SonT-Agro luminaires in each compartment, and the electric power demand of the lamps being 475 W, the electric power demand was 44 Wm^{-2} the intensity of shortwave radiation to the canopy was 11 Wm^{-2}. During nighttime, the lamps were switched on, 5 hours after sunset. During daytime the lamps were on when the (outside) intensity of global radiation dropped beneath 75 Wm^{-2}. When on, the illumination was switched off one hour before sunset to imply a natural dusk.

The compartments were heated with two heating circuits. The lower heating pipes consisted of 6 heating loops, each with a length of 42 m and positioned just above the floor. The pipes had a droplet shape and had a wet cross-section of $6.25 \cdot 10^{-4}$ m^2 (the variable $\frac{1}{4}\pi d_{in}^2$ in Section 4.4.1.1). Documentation on this piping material reports the heat exchange coefficient of the pipe to be comparable to the heat exchange coefficient of a circular pipe with a diameter of 51 mm (van Leeuwen, 1992). Thus, with respect to heat exchange processes, the lower heating pipe is treated like a 51 mm circular pipe. The flow through the lower heating circuit was 1.9 m^3 per hour. The lower heating pipes acted as the primary circuit.

The upper heating pipes were hung at a height of about 2 meters and only used during periods with a high heat demand. The parameters of this secondary circuit were already described in Section 4.4.1.2).

To allow for a detailed comparison between model and experimental data the sensors were scanned every two minutes and, after averaging 5 samples, stored as 10 minute mean values in daily datafiles. With respect to the outside weather conditions the air temperature and humidity, virtual sky temperature, wind speed and

intensity of global and diffuse solar radiation were measured. The wind direction was registered, but not stored since this quantity is not required in the present model.

Inside the greenhouse, temperatures and humidity and CO_2 concentration of the air were measured. The temperature measurements comprised the air and the supply and return temperatures of both heating circuits. From the heating circuits, also the heat demand was measured. Furthermore the heat production of the boiler and the heat production associated with carbon dioxide supply and combined heat and power was measured. Finally, information on climate controller output on window apertures, the position of the thermal screen, the status of artificial illumination and the amount of CO_2 artificially supplied to the greenhouse was stored.

To overcome scaling problems related to the small dimensions of the research facility as compared to horticultural practice, the boiler was implemented by a hardware simulation by means of valves that control a hot water supply to the heating system of each research compartment. Also, the combined heat and power of the research facility was not a real engine, but implemented by a hardware simulation by means of a heat exchanger.

The heat associated with carbon dioxide supply also acts as a forced heat input and, therefore, is comparable to heat from CHP. Hence, the reject heat of carbon dioxide supply was brought into the heating system at the same place as the reject heat from CHP.

6.2.2 Detailed comparisons

To have a high resolution comparison, a detailed study of the performance of the simulation model was performed taking a period of only three days. Thus the sample interval for the comparisons can be as small as 10 minutes. However, some quantities, such as heating power and CO_2 supply appeared to be fluctuating in such a way that both the measured and simulated values had to be filtered first to make them suitable for interpretation.

The comparisons are made with respect to temperatures, humidity, CO_2 concentration of the greenhouse air, the heating power and controller actions (window aperture, thermal screens, artificial illumination and CO_2 supply).

The three days period under consideration used to provide the measurements for the comparisons started on 7 January 1995. This period was selected because it consisted of a sequential period with large variations of weather types. The course of the outside air temperature in the selected period is shown in Figure 6.3.
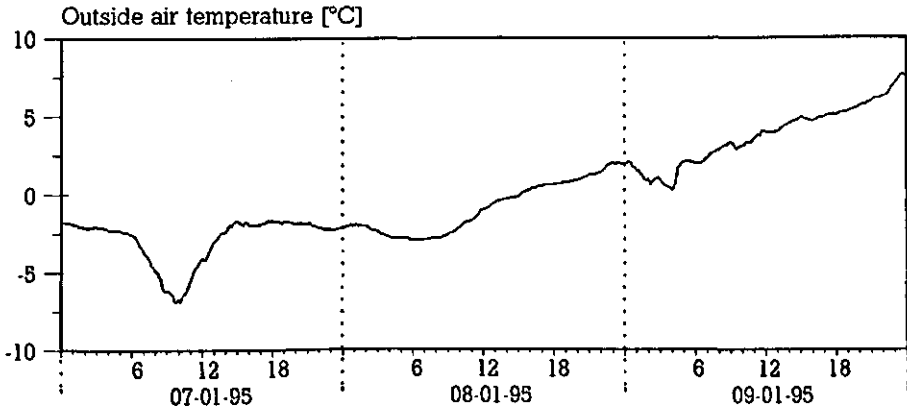
Figure 6.3 Outside air temperature.

Figure 6.3 shows that for about half the period, the outside air temperature remained below freezing point. On 9 January, the temperature becomes quite high. The temperature drop during the morning of the seventh was caused by the fact that a clouded night was followed by a bright day. Figure 6.4, where the intensity of global radiation is shown, confirms the bright day. Figure 6.5, showing the sky temperature, very clearly supports the assumption of a clouded night. The sharp decrease of sky temperatures on 7 January, starting some hours before sunrise, can only be caused by a clearing sky. At about 16:00 hours of the first day cloudiness again increases. The rest of the measuring period consisted of dull days, except for some clearing up on the third day.
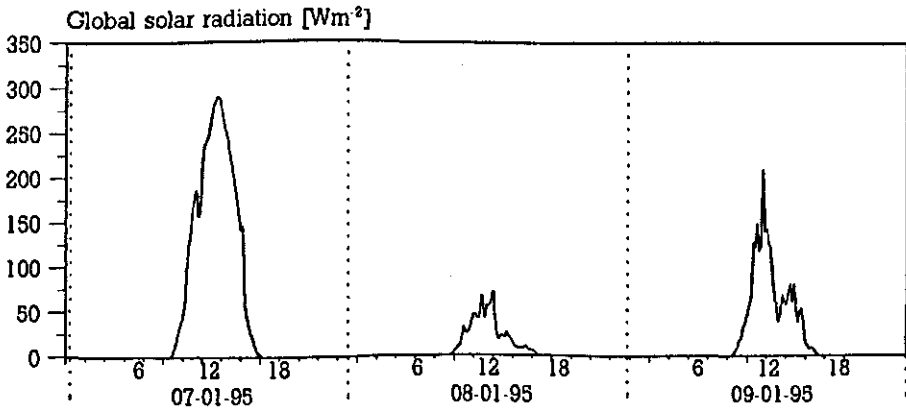
Figure 6.4 Global solar radiation.
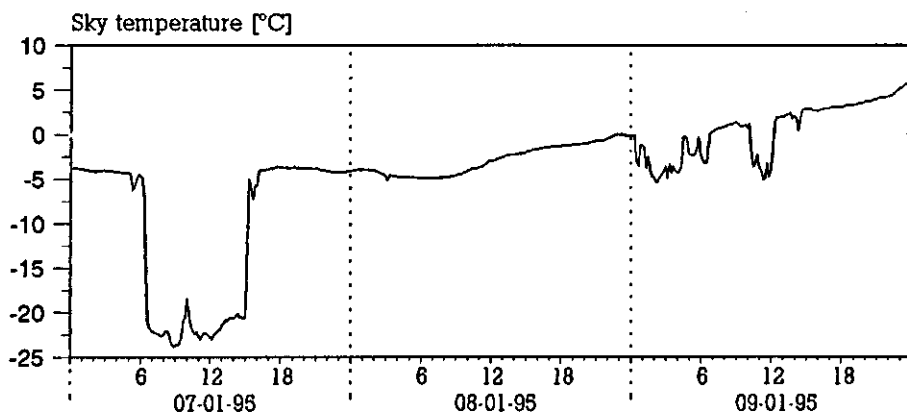
Sky temperature [°C]

Figure 6.5 Sky temperature.

The course of wind speed is shown in Figure 6.6. On the first day there is hardly any wind, but it speeds up on the other days, especially on 9 January.
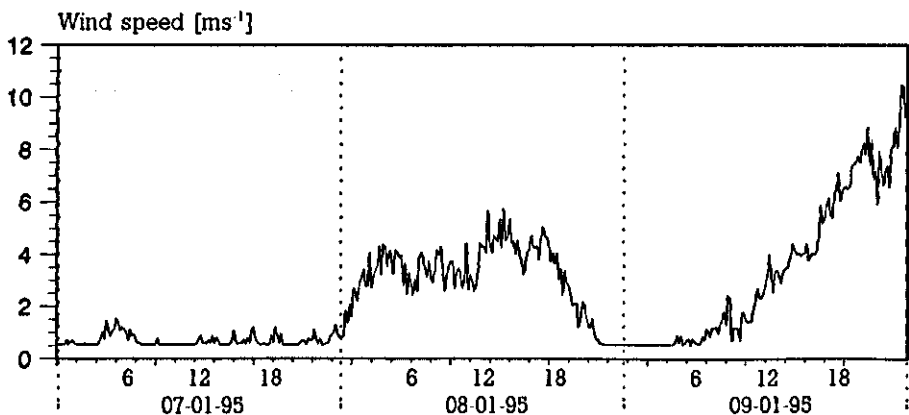
Wind speed [ms⁻¹]

Figure 6.6 Wind speed

The outside vapour pressure is not shown because this quantity only plays a minor role in the period under consideration (see the discussion on the comparison of measured and simulated window aperture, page 115).

The comparison of the measured and simulated greenhouse air temperature of the greenhouse compartment exposed to the outside weather conditions as mentioned above yielded the results shown in Fig. 6.7 till Fig. 6.15.

Figure 6.7 shows that most of the time the measured and simulated greenhouse air

temperature agree pretty well. Except for the early morning of the second day, the difference between measurement and model does not exceed 0.5 °C. Also the dynamics of simulated and measured data agree quite well. The fast fluctuations of the simulated temperature between 4:00 and 8:00 on the second day originate from screen position variations during that time interval (see Figure 6.14). In reality the screen position was constant during that period and therefore the measured temperature did not show these variations.
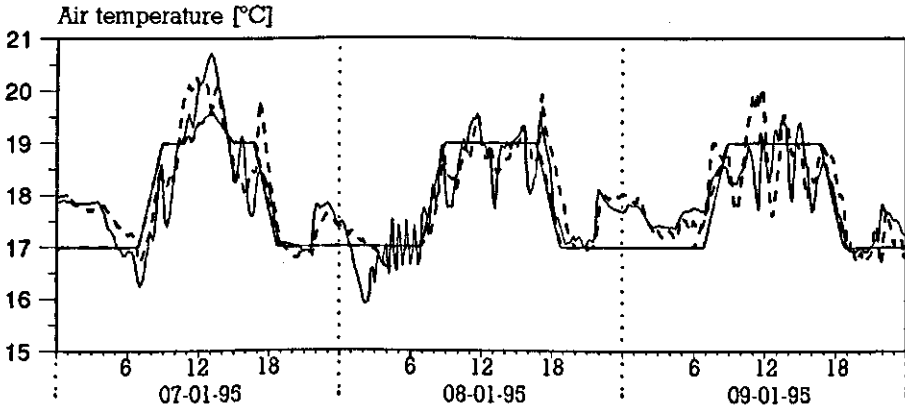
Figure 6.7 Air temperature setpoint (——) and measured (- - -) and simulated (——) air temperature.

The simulated and registered setpoint for the air temperature coincided, because the algorithm applied in the research facility to determine the setpoint was copied into the climate controller of the model. Note that on the first day the daytime setpoint (19 °C) is incremented with about 0.7 °C, due to the light dependent temperature setpoint increment.

Observing Figure 6.7 it is striking that both the simulated and measured greenhouse air temperature significantly exceeds the setpoint for large sections of the period, although the outside temperatures are much lower than the requested inside temperature. This must be attributed to the application of a minimum pipe temperature. This minimum pipe temperature can be clearly seen in Fig. 6.8a and b, where strikingly constant temperatures can be noticed, especially during the night. The minimum pipe temperature for the daytime can be noticed only in the morning of the third day. On the first day this minimum pipe temperature has been lowered due to the high level of global radiation and on the second day the pipe temperatures are too high to be able to see the effect of the lower bound.

The comparison of the measured and simulated supply side temperature of the lower heating circuit shows a good similarity. However, the simulated temperature

maxima of the upper heating circuit are smaller than the measured values, but the dynamics are still comparable.
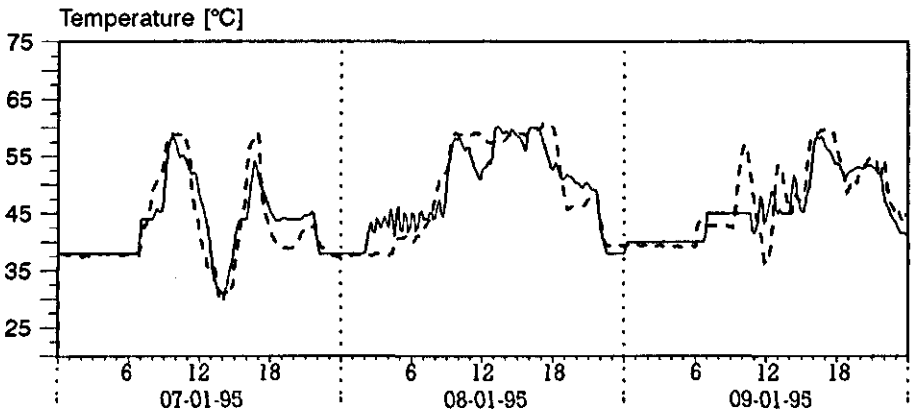
Figure 6.8a Measured (- - -) and simulated (———) temperatures just behind the mixing valve of the lower heating circuit.
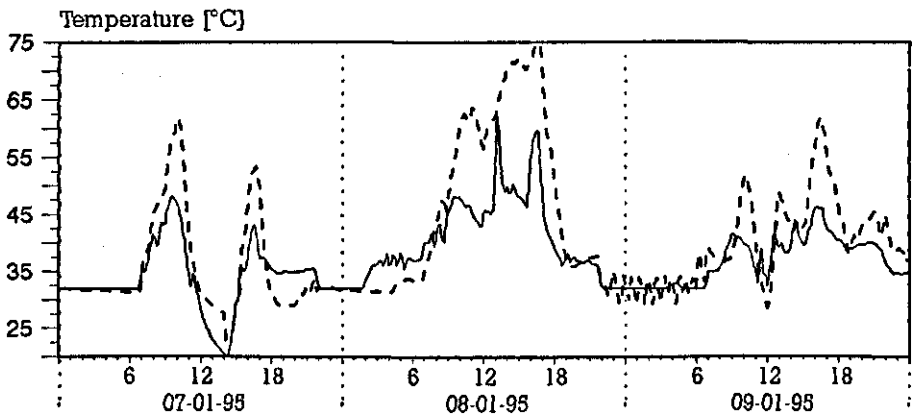
Figure 6.8b Measured (- - -) and simulated (———) temperatures just behind the mixing valve of the upper heating circuit.

Contrary to the custom that only the primary heating system is bounded by a minimum pipe temperature, in the period under consideration the upper heating circuit was also bound to a minimal value. This explains why even the temperature of the secondary heating circuit was not lowered during the periods when the air temperature exceeded the setpoint.

Obviously, expressed in the lower temperatures simulated for the upper heating

circuit, the model underestimates the heat demand for some periods during the daytime of the second and third day. Figure 6.9, where the heating power is depicted, shows this more clearly.
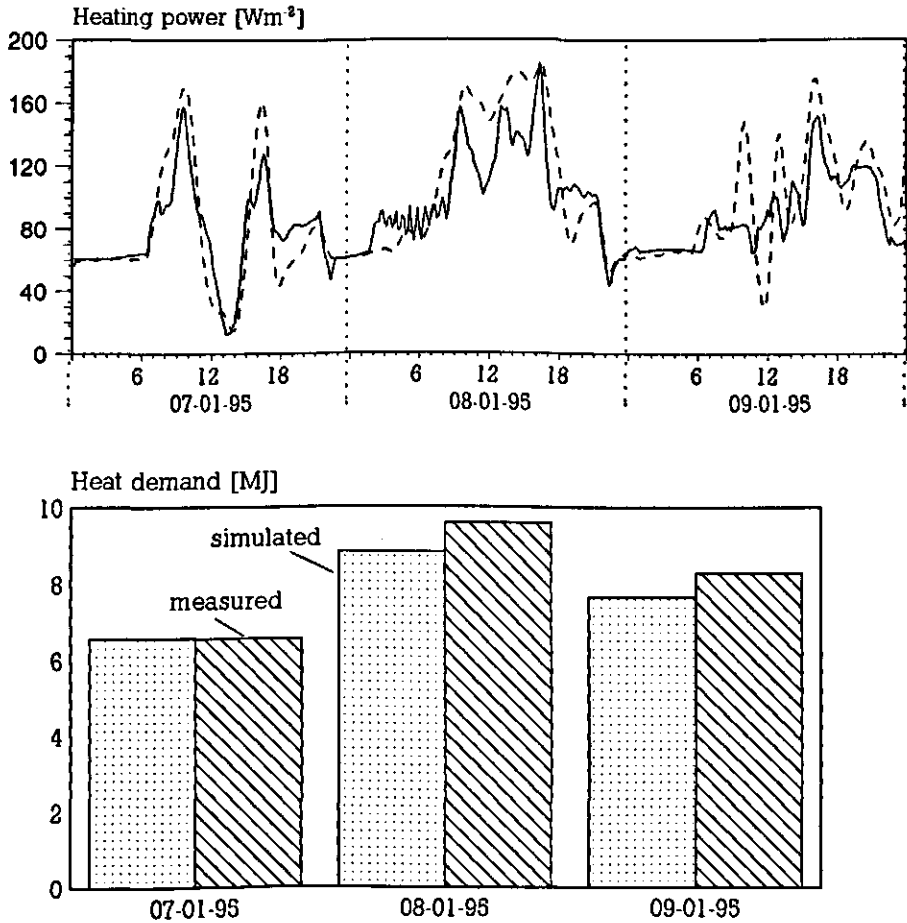
Figure 6.9 Measured (- - -) and simulated (——) heating power demand (a) and total daily heat demand (b). The curves in (a) were smoothed by a 6-cell moving average filter.

The differences in computed and measured heat consumption on the second and third day are almost 10%. One of the explanations for these differences is the fact that the real climate controller induces more overshoots than the simulated one, as can be seen in Figure 6.7.
In Figure 6.10 can be seen that the vapour pressure deficit was described very well.

Vapour pressure deficit [gkg⁻¹]
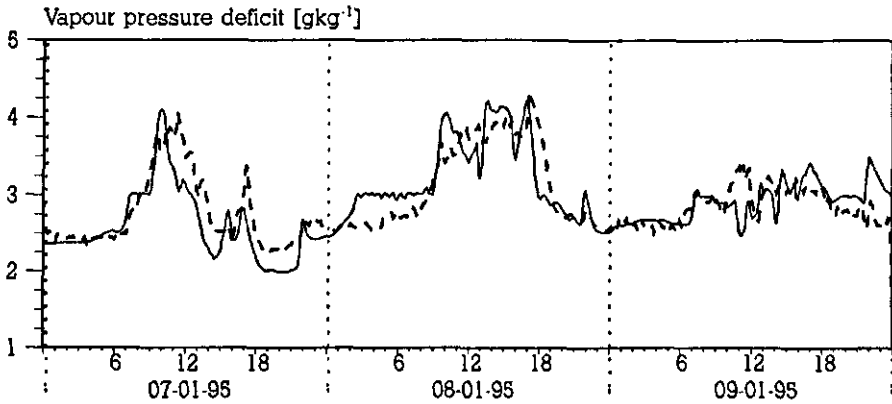
Figure 6.10 Measured (- - -) and simulated (——) vapour pressure deficit.

Combining Figure 6.7 and 6.10 with Figure 6.11, which shows the window aperture, demonstrates the importance of the simulation of humidity. The humidity controller opens the windows proportional to the violation of the humidity setpoint which was 3 gkg⁻¹ during the night and 3.5 gkg⁻¹ during the day. The combination of the figures shows that the window aperture during daytime of the third day is governed by the humidity controller, rather than by temperature control.
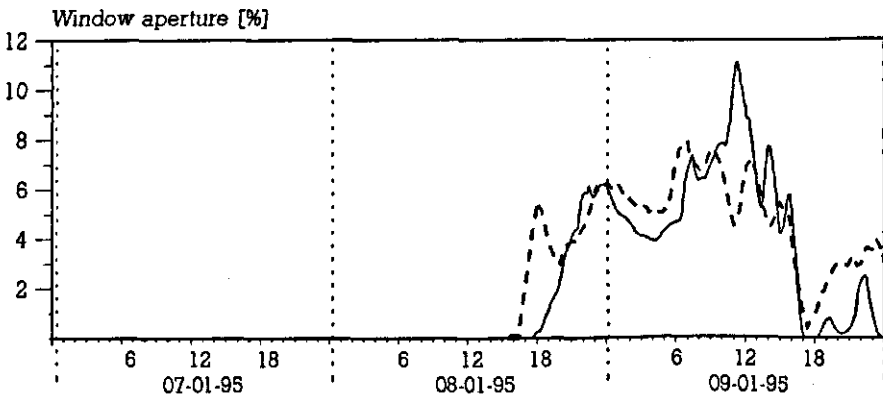
Window aperture [%]

Figure 6.11 Registered (- - -) and simulated (——) window apertures. The curves in (a) were smoothed by a 6-cell moving average filter.

In Figure 6.11, it is significant that the windows are not opened during the first part of the period under consideration. This has to do with the prevention of

window control during a period of frost in order to eliminate the risk of severe damage due to opening a window frozen fast by ice.

The fact that during the evening of the third day simulated windows were opened to a smaller extent than the measured aperture is a result of the lower humidity computed by the simulation model for that time.

The third important entity of the greenhouse air is the CO_2 concentration. In Figure 6.12 the computed values are shown together with the measured values. The controller maintains the CO_2 concentration at 900 ppm during daytime and during the night when the artificial illumination is switched on. Unfortunately, the decay of the CO_2 concentration in the research facility can hardly be seen because for most of the nighttime without illumination the measuring device is switched off. It is switched off to prevent the device sucking in sulphur, which is evaporated in the greenhouse air during the first hours of the night to avoid diseases (*erysiphaceae*). However, the first part of the decay-curves after the CO_2 supply is stopped and the response of the CO_2 concentration on the re-start of CO_2 supply is very similar.
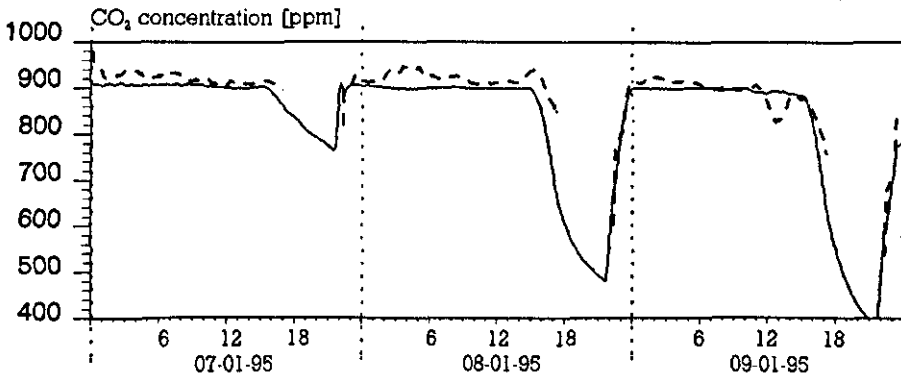
Figure 6.12 Measured (- - -) and simulated (——) CO_2 concentration.

In the research facility the CO_2 supply is performed by a valve that controls the addition of pure CO_2. The valve is either activated or closed. If activated, the valve passes $1.9 \cdot 10^{-6}$ kg CO_2 m^{-2}s^{-1}. The mean supply rate resulting from this on-off control is depicted in Figure 6.13. The data of the curve have been smoothed by a 20 cells moving average filter.

The dynamics of the simulated and registered supply rate are very similar but on the second day the total amount of CO_2 supplied in the simulation model is significantly higher. An explanation for the fact that the matching is quite good on the first and last day and worse on the second day is probably the existence of a

strong CO_2 gradient in the canopy region. Because the canopy was planted on movable benches and the CO_2 measuring device sucked its air samples from a fixed location, it is conceivable that the samples were taken from a region with a relatively high CO_2 concentration on one day and from a region with a different regime on another.
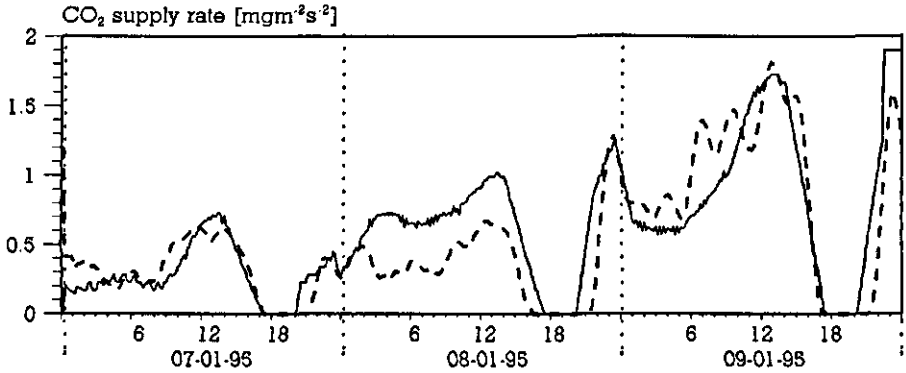
Figure 6.13 Registered (- - -) and simulated (——) CO_2 supply rate.

Finally, Figure 6.14 shows the status of the thermal screen and Figure 6.15 show the status of the artificial illumination. In both model and reality the thermal screen is hardly ever closed completely on these three days. The crack in the screen is to carry off moisture when the vapour pressure deficit is lower than 3 gkg^{-1} (the nighttime humidity setpoint). This can be seen very clearly in the simulation results where in the early morning of the second day the vapour pressure deficit is kept constant at 3 gkg^{-1} by a constantly changing screen position.

Only in the early morning of 7 and 8 January is the humidity criterion satisfied (which is 3.5 gkg^{-1} for the daytime, including two hours before sunrise). Then the screen is fully closed for a small time.

As can be seen in Figure 6.3 the outside temperature remained higher than 5 °C during the evening of the last day. This prevented the screen from being closed.
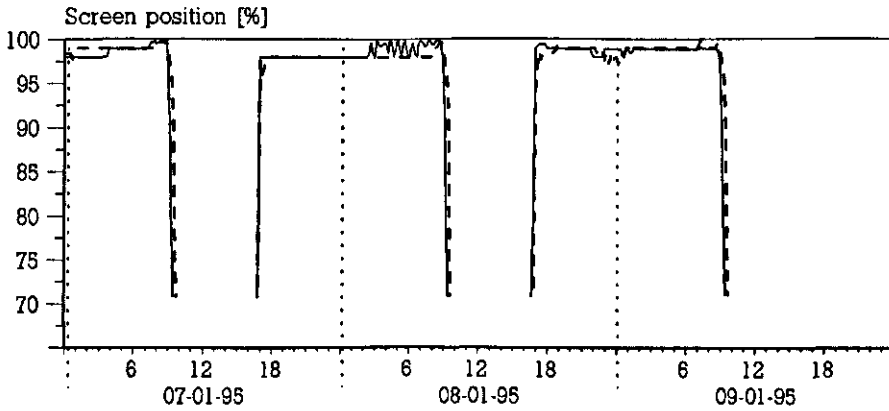
Figure 6.14 Registered (- - -) and simulated (——) screen position.
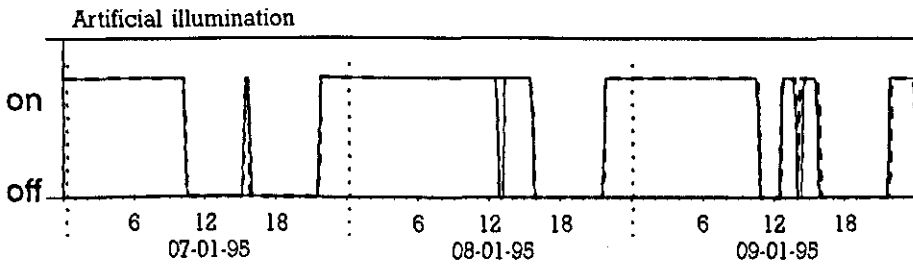
Figure 6.15 Registered (- - -) and simulated (——) status of artificial illumination

The artificial illumination can be expected to follow the registered status almost exactly, because its status is controlled by the same algorithm as applied in the research facility. The only case where deviations may occur is during daytime when the intensity of solar radiation fluctuates around the intensity at which the lights are switched on and off. This occurs once on the second day.

6.2.4 Comparisons for a year round period

The experimental data that serve as a reference for the long-time comparisons were gathered for the time span of a year. This year started on 1 February 1993. To limit the amount of graphs, the showed comparisons are restricted to temperature, heat demand and water consumption. Figure 6.16 shows the measured and simulated daily mean greenhouse air temperature.
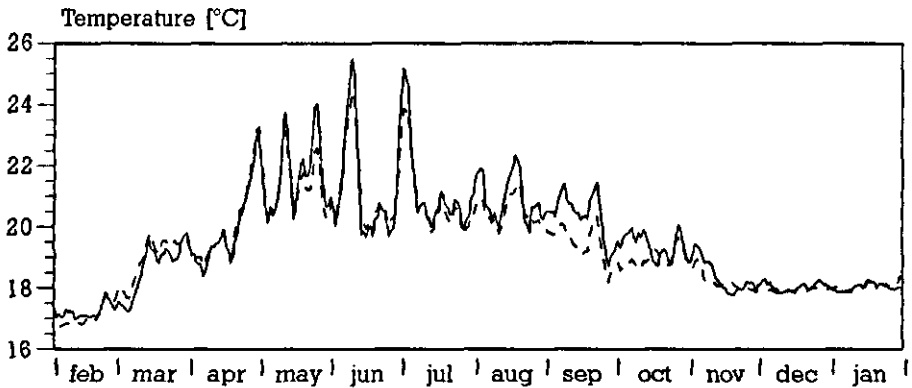
Figure 6.16 Measured (- - -) and simulated (——) daily mean greenhouse air temperature. The daily values were smoothed by a 4 cell moving average filter.

In general the simulated temperature is quite similar to the measured values, but during warm periods the model tends to compute higher temperatures. Since in those periods the windows are fully opened, it is likely that the ventilation capacity of the real greenhouse at maximal window aperture is more than the air exchange rate resulting from De Jong (1990) (see Section 5.5.2.1).

In Figure 6.17 the measured and simulated daily heat demand of the greenhouse are depicted. The agreement between model and measurement is good. Only during the quite extreme cold period at the end of November does the model show an important lower heat demand. The total heat demand computed by the model, 1743 MJm^{-2}, is a bit lower than the measured total, which was 1782 MJm^{-2} (a difference of 2%).

In Figure 6.17, it is interesting to see that during summer the heat demand is still about a quarter of the heat demand in winter, whereas the mean difference between the requested greenhouse air temperature and the outside air temperature is far much smaller in summer than in winter (see Fig. 6.18). This high heat demand in summer must be attributed to the minimum pipe temperature, which was 40 °C during the day (but diminished on global radiation) and 45 °C during the night.
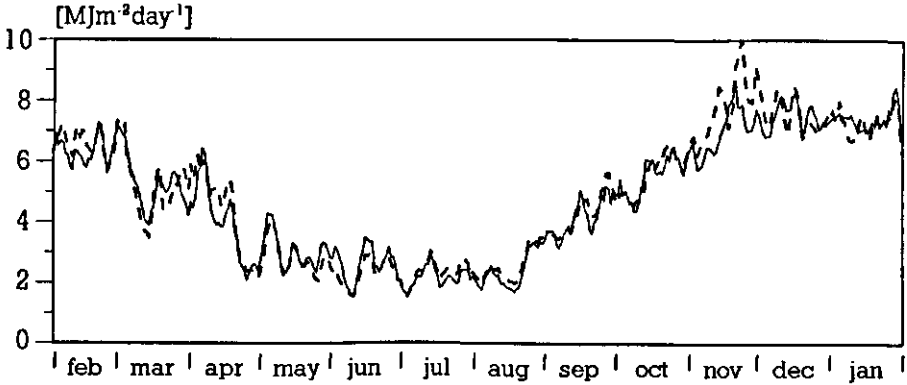
Figure 6.17 Measured (- - -) and simulated (——) daily mean heat demand. The daily values were smoothed.
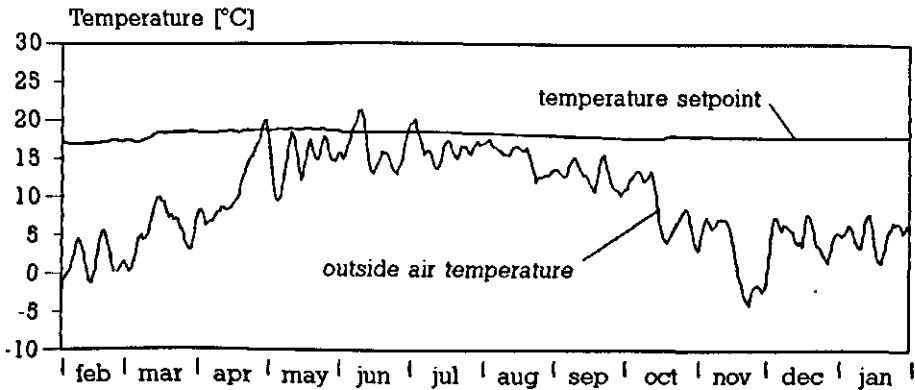
Figure 6.18 Outside daily mean air temperature and daily mean greenhouse air temperature setpoint.

The third measured quantity that is compared to the simulated values is the daily water consumption.

Obviously the model tends to compute a higher daily evaporation than registered. The most important differences occur in March, the second half of April and May. A possible explanation for these differences is the fact that the response of stomatal resistance to environmental factors such as temperature and vapour pressure deficit of the greenhouse climate is not constant during the year. From horticultural practice it is well known that at the end of winter, roses have very thin leaves with a limited evaporation capacity. In the present work it was not possible to quantify this effect and thus the coefficients applied to determine the stomatal resistance remain constant throughout the year. This resulted in a serious over estimation of the evaporation at the end of winter and spring.

Water consumption [kgm⁻²day⁻¹]
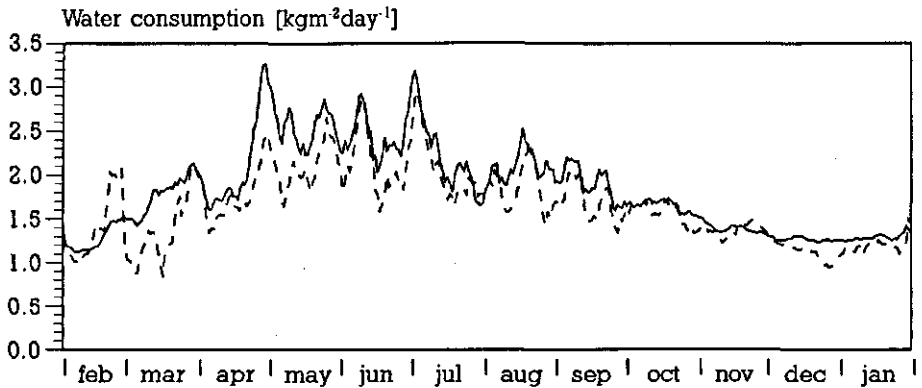
Figure 6.19 Measured (- - -) and simulated daily water consumption

6.2.4 Conclusions on the model evaluation

The resemblance between the measurements and model computations is good. On a small-time scale the dynamics of the modelled quantities are very much the same as the measured values, although sometimes distinct differences can be noticed, especially as far as carbon dioxide supply is concerned. The greenhouse climate controller actions of the model were in line with the actions of the controller of the research facility that served as a reference.

On a year round time scale, the temperatures and heat demand of the greenhouse are well described by the model. The computed yearly heat demand was only 2% less than the measured heat demand. Moreover, the deviation between computed and measured heat demand was concentrated in a short period of extreme cold weather. The simulated daily mean greenhouse air temperature deviated only during very warm periods from the measured values. Then the simulated temperature is higher than the measured value. This was attributed to an under-estimation of the ventilation capacity.

The daily water consumption was over-estimated by the model.

6.3 EVALUATION OF ENERGY SAVING TECHNIQUES

In Chapter 2 three groups of energy saving measures were formulated to be studied. In the present section these measures are determined by means of the application of the simulation model developed. In all computations the growth of a tomato canopy in the Netherlands in a modern greenhouse of 1 hectare serves as a horticultural reference. In Section 6.3.1 the requested greenhouse climate with respect to the growth of tomato is outlined briefly. The parametrization of the large greenhouse is very much alike the construction of the research facility discussed in Section 6.2.1. However, in Section 6.3.2 some typical scale affected variables are re-parametrized to suit a commercial greenhouse. In Section 6.3.3 the weather conditions to which the greenhouse in the simulations is exposed are presented.

In Section 6.3.4 the three clusters of energy saving options which were mentioned in Chapter 2 are evaluated.

6.3.1 Requested greenhouse climate conditions for the growing of a tomato crop

The growth of crops in modern protected cultivation is a highly professionalised activity. Skilful and well-educated people continuously adapt the greenhouse controller settings in order to create a favourable environment for canopy growth. Obviously, these continuous adaptations result in a vagary course of climate controller setpoints. However, in order to simplify the definition of the requested greenhouse climate conditions for the greenhouse that serves as a reference in the major part of this chapter, a broad outline of the course of climate controller setpoints is applied.

The reference greenhouse starts its growth season in December when the young tomato plants are planted. During the first three weeks the daytime and nighttime temperature setpoint are 18 °C. The light dependent temperature setpoint increment is 2 °C for outside solar radiation in the range from 50 to 250 Wm^{-2}. During the first months of the growth, no minimum pipe temperature is applied. The maximum carbon dioxide concentration is set to 700 ppm. Carbon dioxide is supplied by exhaust gases from the combustion of natural gas at a rate of 40 m^3 gas per hectare per hour. Heat surpluses from CO_2 supply are stored in a heat storage tank. When the storage tank is completely charged the combustion for carbon dioxide supply is stopped.

The humidity setpoint is set to 85% RH. If the actual humidity in the greenhouse exceeds the setpoint the windows are opened proportional to the excess with 2% window opening per percent excess of the RH.

The secondary heating circuit accompanies the primary circuit when the tempera-

ture of the latter exceeds 55 °C. The windows are opened when the air temperature exceeds the setpoint by 0.5 °C. The opening angle is proportional to the excess, with a proportional band with a minimum of 4 and increases linearly to 8 on temperature difference between air temperature setpoint and outside temperature. The maximal proportional band is reached when the outside temperature is 8 °C below the air temperature setpoint.

After the first period of three weeks the daytime temperature setpoint is increased to 19 °C and the nighttime temperature setpoint is lowered to 17 °C. All other settings are left unaltered.

On the first of April the daytime and nighttime minimum pipe temperature are set at 45 °C and 40 °C respectively. During daytime, the minimum pipe temperature is lowered linearly towards the air temperature setpoint for outside global radiation in the range between 100 and 300 Wm^{-2}. All other settings are left unaltered.

On 1 September the humidity setpoint is lowered to 80 %RH.

The growth season ends on 11 November. On that day the nighttime air temperature and all minimum pipe temperature setpoints are lowered to 5 °C. Humidity control and carbon dioxide supply are abandoned. To provide a comfortable temperature during daytime, when a lot of work is being carried out in the greenhouse, the daytime temperature setpoint is set to 15 °C.

On 26 November the air temperature setpoints are increased to 18 °C.

6.3.2 Geometry of a large commercial greenhouse

The Venlo-type greenhouse, which is commonly applied in the Netherlands is built from a repeated sequence of 3.20 m wide roof segments. The 1 hectare greenhouse subject in this study is composed of 30 of these roof segments, and thus, the length of the greenhouse is 104 meter. The floor to gutter height is assumed to be 3.5 meter. Therefore, the sidewall/surface ratio of the greenhouse is 0.15. The gutter orientation is north-south.

One window per eight glass panels is mounted in each side of the greenhouse cover. The glass panels are one meter wide. Thus the number of ventilating windows per m^2 greenhouse surface equals 1:12.8 = 0.078. The windows are two glass panels wide and half the ridge-gutter distance long. The roof slope is 25°. Hence the area of one window equals 1.8 m^2.

When the windows are closed the leakage of the greenhouse is assumed to be $1.25 \cdot 10^{-4}$ m^3 per m^2 greenhouse per unit wind speed (ms^{-1}). This figure is a mean of the leakages determined by De Jong (1990) in four commercial greenhouses. The greenhouse has a lower heating circuit with four pipes per roof segment and an upper heating circuit with half as many pipes. The capacity of the circulation pumps in the upper and lower heating circuits are 30 m^3 per hour and 90 m^3 per

hour respectively. The diameter of the lower heating pipes is 51 mm. The upper heating pipes have a diameter of 28 mm. The upper heating circuit serves both as a secondary heating circuit and as a heat dispenser for the condenser. If the heating system comprises a combined heat and power engine (see Section 6.3.4.3), the condenser is used by both the boiler and the CHP engine.

The greenhouse boiler has a heating capacity of 2.5 MW. The conversion efficiency of the boiler is 0.85 with respect to the upper heating value of natural gas, which is a customary value for modern boilers (Handboek Verwarming Glastuinbouw, 1995).

Heat surpluses are temporary stored in a storage tank of 80 m^3.

6.3.3 Weather data

Outside weather conditions have a considerable impact on the course of heat demand of a greenhouse. Therefore, in order to judge the possible energy-saving options for situations in the Netherlands, the simulation model has to be fed with typical weather data for the Netherlands. The definition of such a typical weather cannot be based on mean levels of meteorological quantities, but also has to include their dynamics. Such a set of weather data for the Netherlands can be found in the SEL-year (Breuer & Van de Braak, 1989). The SEL-year is a composition of twelve sets of real monthly weather data. Each set of monthly data in the SEL-year has been selected from 17 sets of real weather data for that month. The 17 sets were gathered between 1970 and 1986 in De Bilt by the Royal Dutch Meteorological Institute. The selection was made in such a way that the temperature and radiation data are in fair agreement with mean weather characteristics for the month under consideration in the Netherlands. This means that, for example, the weather data measured in January 1971, serve as typical weather for January, whereas the SEL weather data for February were measured in 1973.

The data file contains records of hourly weather data that consists of temperature, radiation and humidity. The SEL-year does not provide information on the sky temperature. Because the model requires this virtual temperature, the algorithm presented in appendix F has been used (Eqn. F.6). The fraction of the sky covered with clouds was estimated comparing diffuse and direct radiation with the maximal intensity of global radiation for each hour in the datafile. Also the data on rain fall, present in the SEL-year have been applied to estimate the cloudiness. Finally, the slope of the course of nighttime temperatures were applied to get an indication of cloudiness.

In Figure 6.20 the mean monthly temperatures and monthly radiation totals of the SEL-year are compared to the same quantities between 1990 and 1994.

The pictures show a large variation of monthly values, but indeed the SEL-year appears to represent the weather data in a reasonable way.

(a)
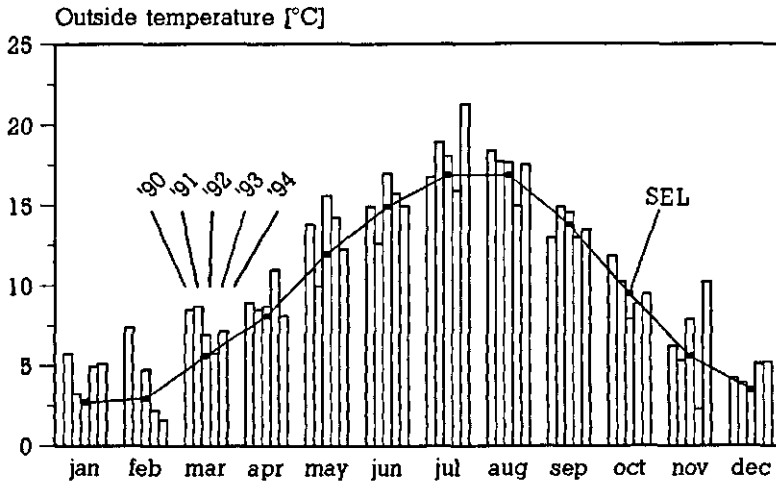
(b)
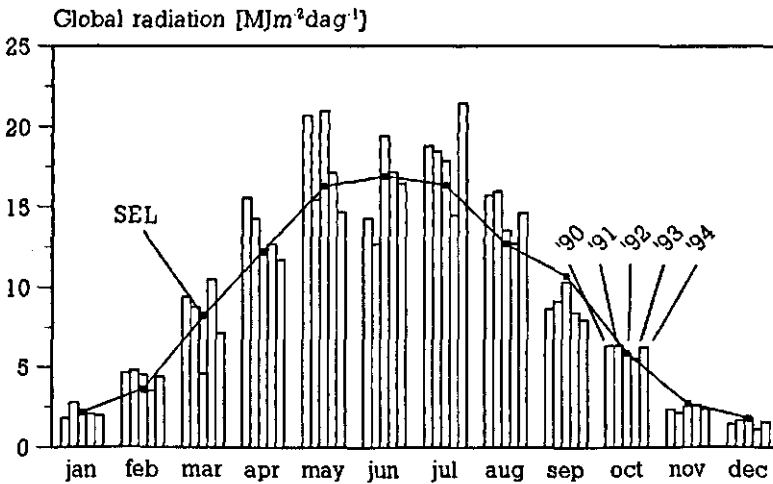
Figure 6.20 Mean monthly temperatures (a) and monthly totals of global radiation (b) in the SEL-year data set compared to measurements in De Bilt between 1990 and 1994

6.3.4 Energy saving prospectives

In the document on the MJA a large number of energy saving measures are suggested in order to decrease the energy consumption of glasshouse horticulture. In this section, the prospectives of six of the proposed measures will be evaluated. In Chapter 2, the proposed measures were arranged in three clusters. The first item concerns relatively simple improvements to the heating system. With respect to this item the effect of the insulation thickness of the boiler, insulation of transport pipes and the connection of the expansion vessel of the heating system are studied. The second item concerns improvements to the greenhouse building. The heat loss from the building can be decreased by eliminating cracks in the cover, by the application of thermal screens and by the application of alternative cladding materials.

The third item involves the application of energy-saving heating devices. Here the energy saving effects of a condenser, a short-term heat storage facility and a combined heat and power engine will be studied.

6.3.4.1 Simple improvements of the heating system

The first requirement for an efficient application of heat is to prevent heat release in places where there is no need for heating. This can be achieved by insulating the boiler and transport pipes. Also the connection of the expansion vessel affects the extent of unnecessary heat loss.

In the following the simulation model (or a part of it) is applied to compute a theoretical value for the energy savings that can be expected from these measures.

Insulation of the boiler

Contrary to all other options discussed in this section, the complete greenhouse climate simulation model is not required to compute the energy savings from the insulation of the boiler. This is because, in order to avoid condensation inside the boiler, the temperature of the water in a boiler is kept at a constant level of 90 °C throughout the year. Thus the boiler sub-model, presented in Section 4.4.3, suffices.

In the sub-model the heat loss from the boiler surface is a function of the temperature difference between the water inside the boiler and the temperature of the environment and insulation thickness. In Figure 4.11 the relation between the overall heat exchange coefficient and the insulation thickness was shown. Multiplication of the heat exchange coefficient with the surface of the boiler and the appropriate temperature difference yields a heat loss. Multiplying the heat loss

with the time span of a year gives the yearly energy loss.

To show the effect of insulation thickness, a boiler insulated with 2 cm of rock-wool was compared to a boiler insulated with 6 cm of rockwool. Assuming the mean (air and radiation) temperature of the environment of the boiler to be 20 °C, the results for a boiler with a diameter of 2.3 m and a length of 4.6 m are stated in Table 6.1. The assumed dimensions are typical for a boiler of 2.5 MW.

Because in horticultural practice energy savings are mostly expressed in m^3 natural gas, the energy savings are expressed in both m^3 of natural gas in GJ. To convert the savings from GJ to m^3 a conversion efficiency of 0.9 with respect to the upper heating value was used.

Table 6.1 Yearly energy loss of a boiler at 90 °C with a length of 4.6 m and a diameter of 2.3 m to an environment at 20 °C for an insulation thickness of 2 cm rockwool and 6 cm rockwool.

insulation thickness	energy loss of the side wall	energy loss of front and rear side	total energy loss	
	$GJ\ year^{-1}$	$GJ\ year^{-1}$	$GJ\ year^{-1}$	$m^3 year^{-1}$
2 cm	105	24	129	4316
6 cm	42	11	53	1773

From the table it can be seen that a boiler insulated with only 2 cm of rockwool has a yearly energy loss of 129 GJ. An increment of the insulation up to 6 cm decreases the yearly energy loss to 53 GJ.

Comparing losses computed by application of the boiler model with empirical data as presented by Nawrocki & van der Velden (1991) the latter appear to be much larger. In their work the weekly energy loss contributed to the boiler was fitted into an empirical formula reading:

$$L = -182 + 1272 \frac{C_{boiler}}{d_{insu}} \qquad (6.1)\ [m^3\ week^{-1}]$$

where L is the weekly energy loss in m^3 of natural gas, C_{boiler} the maximal heating capacity of the boiler in MW and d_{insu} the insulation thickness of the side wall in cm. Multiplication of the figures in Eqn. 6.1 with a factor 1.65 turns the equation into a relation that expresses the yearly energy loss in GJ per year.

Application of the empirical formula to compute the effect of the increment of the insulation thickness from 2 to 6 cm results in an energy saving effect of 1749 GJ per year. Thus, the empirical formula gives an energy saving that is 23 times larger than the theoretical approach.

The major part for the large difference between the result of Eqn. 6.1 and the theoretical value must be attributed to the peculiarity that heat losses that are not expected to be dependent on insulation thickness (losses from valves, pumps, the

feet of the boiler, the front and rear side), are somehow included in the term that describes the dependency of the energy loss on insulation thickness. What's more, the constant, from which it would be expected that it takes account of insulation independent losses, is negative.

Observing the difference between the theoretic computations and the peculiarities of the empirical relation posed by Nawrocki & Van der Velden, additional measurements accompanied by a more detailed model on the heat losses from the boiler should be carried out to give a plausible relation to compute the energy loss from a boiler.

Insulation of transport pipes

The heat release of transport pipes in a greenhouse can play a positive or a negative role in the realization of a uniform temperature distribution in the greenhouse. Generally speaking, the heat release is included in the design to compensate for heat losses near walls, but transport pipes can also disturb the temperature distribution. In the latter case, insulation of the transport pipes has a positive effect on the homogeneity of the greenhouse air temperatures and saves energy as well.

To compute the energy saving, it is sufficient to know the frequency distribution of the temperature excess of the transport pipes relative to their environment and the heat loss of pipes as a function of insulation and temperature excess. In this section, first the frequency distribution curves are presented. Then the heat loss of pipes with and without insulation as a function of temperature excess is determined. Finally, the energy-saving effect of insulating the pipe types distinguished is computed.

The energy-saving achieved by insulation is computed for six types of transport pipes, namely the main supply and gathering pipe (see Fig. 4.3) and the transport sections of the supply and return sides of both the heating circuits (see Fig. 4.4). The frequency distribution of the temperature excesses of these six pipe types were determined by the simulation model. The results are presented in Figure 6.21 and 6.22.

Figure 6.21 shows that the main supply pipe is at 90 °C for most of the time. Only during discharge of the heat storage tank does its temperature decreases to the setpoint of the lower heating circuit. The temperature of the gathering pipe is a weighed mean temperature of the water returning from the upper and lower heating circuits. Comparison of the dashed curve in Fig. 6.21 and the dashed curves in Fig. 6.22 shows that the return temperature of the lower heating circuit dominates the temperature of the water in the gathering pipe. This is not surprising since the upper heating circuit withdraws water from the main supply pipe only during periods with a high heat demand. Moreover, the maximal

contribution of the upper heating circuit to the flow through the gathering pipe is only ¼.
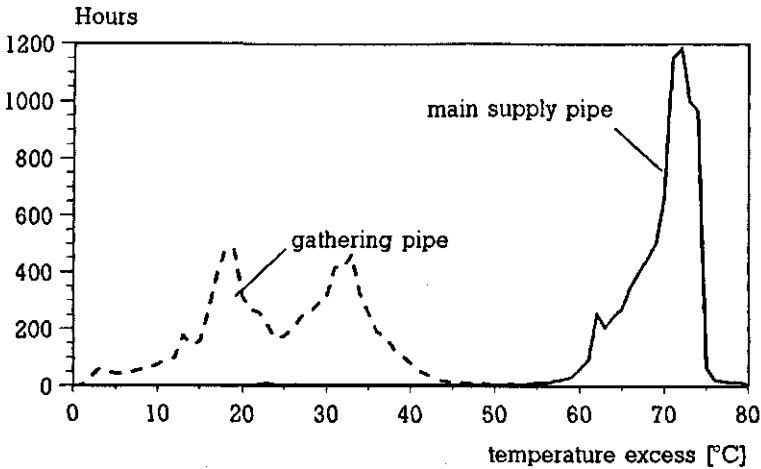
Figure 6.21 Frequency distribution of pipe temperature excess relative to the greenhouse air of the main supply pipe and the gathering pipe.
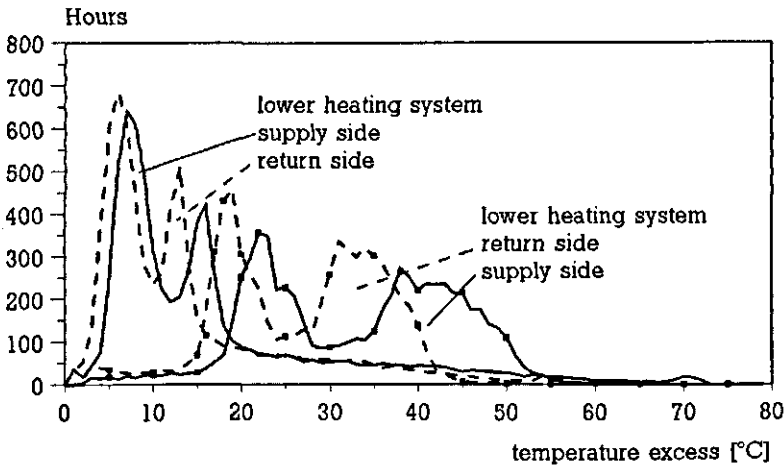
Figure 6.22 Frequency distribution of pipe temperature excess relative to the greenhouse air of the supply and return side of the heating circuits.

Figure 6.22 shows that the upper heating circuit has rather small temperature excesses most of the time. This is due to the fact that most of the time the pipe temperatures of the upper heating circuit are a result of heat produced by the condenser. The majority of the time, the upper heating circuit is about 7 °C higher than the air temperature. During this time the heat produced by the condenser ori-

ginates in the boiler that combusts gas for the carbon dioxide supply. The second peak in the frequency distribution curve of the upper heating circuit (around an excess of 14 °C) is the result of the minimum pipe temperature in the lower heating circuit.

The effect of the minimum pipe temperature on the temperature in the lower heating circuit can be seen in the first peak of the supply side temperature excess of this heating circuit, located around a temperature excess of 23 °C. This temperature excess is caused by a minimum pipe at 40 °C and an air temperature at 17 °C. These are the nighttime controller settings between April and November. Near to the first peak, a second, somewhat lower peak, at a temperature excess of 25 °C can be observed. This peak must be attributed to the daytime minimum pipe temperature of 45 °C, accompanied by an air temperature of 20 °C. This peak is lower than the first, because during daytime the minimum pipe temperature is decreased on outside global radiation (see the climate controller definition on page 122) and the air temperature often exceeds 20 °C. The dashed return temperatures follow the supply temperatures with a temperature difference (due to the heat release in the distribution loops) that increases as the temperature excess increases.

On a one hectare greenhouse, the supply and return pipes of the upper and lower heating circuits are commonly made from piping material with a diameter of 90 mm and 180 mm respectively. The diameter of the main supply and gathering pipe is also 180 mm. The convective heat exchange coefficient of these pipes was computed using the theory presented in appendix A as a function of pipe temperature. The air temperature was assumed to be 20 °C. The radiative heat loss of these pipes was computed by assuming an emission coefficient of 0.84 and an optically black environment at 20 °C. In Figure 6.23, the total heat loss, being the sum of both heat exchange mechanisms, is expressed per meter pipe as a function of temperature excess for both pipe diameters.

The heat loss per meter pipe as a function of the temperature excess of the 180 and 90 mm pipes after insulation with 3 cm rockwool covered by aluminum plates is shown in Figure 6.24. The thermal conductivity of rockwool was set to 0.04 $Wm^{-1}K^{-1}$ (Polytechnisch zakboekje, 1987) and the emission coefficient of the aluminum covering was set to 0.3 (Handbook of Chemistry and Physics, 1968). Comparing the y-axes of Figures 6.23 and 6.24 shows a decrease of heat release with a factor of around 10.

The energy saving that results from the insulation of the pipes can now be determined by the sum of the multiplication of the savings achieved for each temperature excess with the yearly duration of that temperature excess for a particular type of pipe.

In Table 6.2 the results of this computation for the six types of transport pipes are stated.
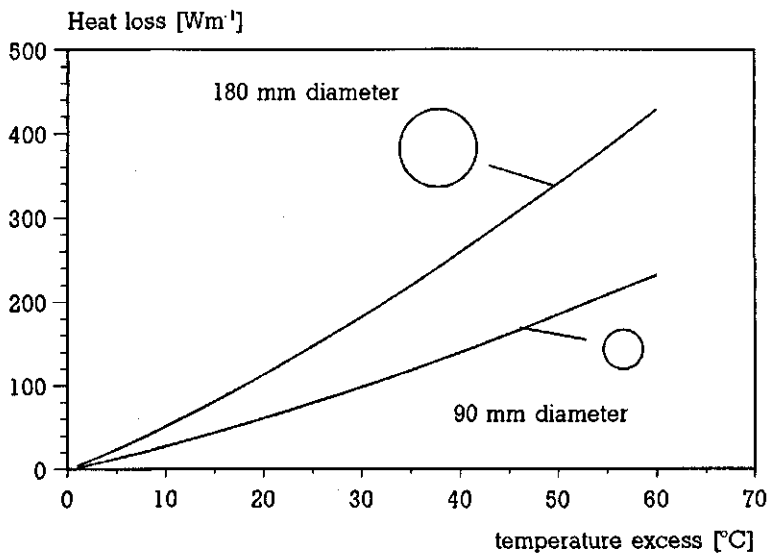
Figure 6.23 Heat loss per meter pipe for two pipe diameters as a function of temperature excess.
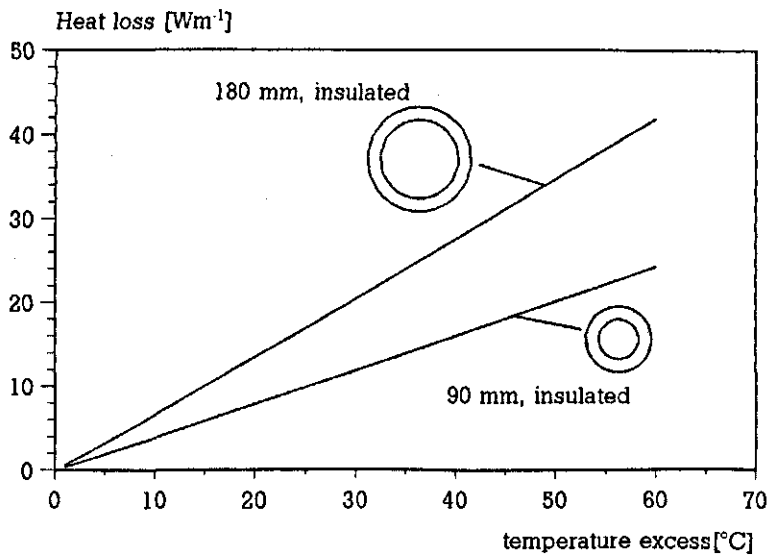
Figure 6.24 Heat loss per meter pipe of a 90 mm and 180 mm pipe isolated with 3 cm rockwool and wrapped with aluminium plates to an environment at 20 °C as a function of water temperature excess inside the pipe.

Table 6.2 Decrement of the yearly energy loss per meter pipe due to insulation for six types of transport pipes. The transport pipes of the upper heating circuit have a diameter of 90 mm. The other pipes have a diameter of 180 mm. Insulation was performed with 3 cm rockwool, covered with aluminum plates.

type of transport pipe	energy loss of un-insulated pipe	energy loss after insulation	energy saving per meter pipe due to insulation	
	$GJm^{-1}year^{-1}$	$GJm^{-1}year^{-1}$	$GJm^{-1}year^{-1}$	$m^{3}m^{-1}year^{-1}$
main supply pipe	15.28	1.45	13.84	437
gathering pipe	4.44	0.50	3.93	214
low. heating circ. supply	5.01	0.54	4.47	141
return	2.58	0.29	2.28	72
upp. heating circ. supply	2.09	0.25	1.84	58
return	1.06	0.14	0.93	29

The results of Table 6.2 can be applied to answer the question whether or not it is economically attractive to insulate transport pipes at places where the heat release is not wanted or not necessary.

Connection of the expansion vessel

If an expansion vessel is connected to a part of the heating system with predominantly high temperatures, a relatively simple measure to conserve energy is to change the connection of the expansion system to a part of the heating system with low temperatures (van der Velden *et.al.*, 1993).

Heat losses from the expansion system emanate from the inflow of water into the expansion vessel (when the mean temperature of the water in the heating system increases) which is returned at a lower temperature (when the mean temperature of the heating system drops). Insulation of the vessel in order to decrease its heat loss is discouraged by installers because it has been experienced that current expansion vessels do not withstand a continuously high temperature.

The computation of the amount of energy conserved by changing the place of attachment of the expansion system cannot be computed with frequency distribution curves like Fig. 6.21 and 6.22, because the inflow and residence time of the water in the vessel also have to be known. Instead, the heat losses from the expansion vessel were computed by the simulation model which was evaluated once with the vessel connected to the hottest part in the heating system (the pipe segment that transports the water from the boiler to the main supply pipe) and once with the vessel connected to the gathering pipe.

The comparison of the heat losses of a relatively hot and a relatively cold expansion vessel are studied for two cases. The first case concentrates on the reference

greenhouse, with a heat storage tank of 80 m^3ha^{-1}. For this greenhouse the expansion vessel has to have a volume of 3 m^3. In the second case the effect of the connection place of the expansion vessel of a greenhouse without a heat storage tank is studied. The expansion vessel in the second case is much smaller, namely 0.5 m^3. The dimensions of the storage vessels were computed from the volume difference of the entire water content of the system at 90 °C and at 20 °C.
The computed daily energy losses are plotted for both options in Figure 6.25.
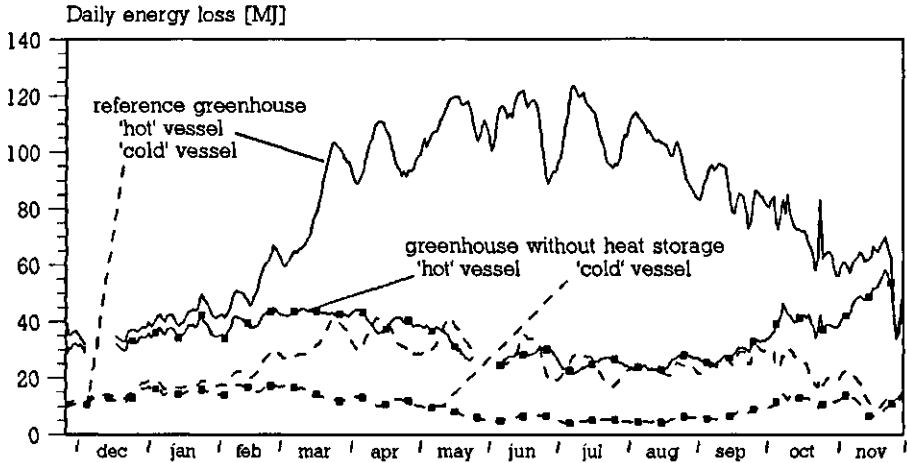
Figure 6.25 Daily energy losses of a 'cold' (dashed lines) and a 'hot' (full lines) connected expansion system for the reference greenhouse, and for a greenhouse without a heat storage tank.

Of course, the energy losses from the large volume expansion vessel of the greenhouse with the storage tank are more than the losses from the expansion vessel of the other greenhouse. For the greenhouse with the heat storage tank the losses are concentrated in the summer, because in that period the heat storage tank is used intensively. An intensively used storage tank implies large volume differences of the water in heating system because a massive amount of water in the storage tank is heated and cools down every 24 hours. For the greenhouse without a storage tank the energy losses in winter are larger than the losses in summer because the temperature variations of the heating circuits are larger in winter.
In Table 6.3 the yearly cumulated energy losses for both connection options are stated. From the table can be concluded that the energy saving achieved by changing the connection of the expansion vessel from the hottest part to the coldest part is about 9 GJ for a greenhouse with a small vessel and increases up to 20 GJ when the greenhouse is equipped with a heat storage tank. However, the energy saving effect found with the simulation model is much smaller than the results

reported by Van der Velden & Nawrocki (1991). It could be deduced from their work that they estimated the yearly extra heat losses of a 'hot' expansion vessel compared to a 'cold' one at 270 GJ. This value was not related to the size of the heat storage facility, nor to the water content of the rest of the heating system.

Table 6.3 Yearly energy loss from a 'hot' and a 'cold' connected expansion vessel for the reference greenhouse and a greenhouse without a heat storage tank.

	'hot' expansion vessel	'cold' expansion vessel	energy saving by changing the attachment	
	GJ year^{-1}	GJ year^{-1}	GJ year^{-1}	m^{3}year^{-1}
reference greenhouse (storage tank of 80 m^3)	29.2	8.9	20.3	642
greenhouse without a storage tank	12.8	3.8	9.0	284

The empirical value is much larger than the differences computed by the simulation model. However, the value presented by Van der Velden and Nawrocki is rather unlikely, since a heat loss of 270 GJ requires that the mean expansion vessel temperature is about 80 °C hotter than the 'cold' vessel, throughout the year. This figure was computed assuming an expansion vessel with a volume of 3 m^3 (enough for a greenhouse of one hectare with a 80 m^3 storage tank), an outside surface of 11 m^2 (about the size of the one depicted in Fig. 4.21) and an overall heat exchange coefficient of 12 Wm^{-2}K^{-1} (which is quite high).
Having noticed the large discrepancy between the results of the simulation model and the empirical data and the questionable results presented by Van der Velden & Nawrocki, additional measurements should be carried out prior to the development of a more detailed simulation model.

Conclusions

Among the simple improvements to the heating system, the insulation of the boiler and the insulation of transport pipes are the measures that are most likely to yield the highest energy savings. However, because changing the attachment of the expansion vessel is quite easy, the priority sequence of measures to save energy from simple improvements will probably start with the connection of the expansion vessel.

6.3.4.2 Improvement of the building

The transmission of solar radiation by the greenhouse cover is of utmost importance for a high productive horticulture. Therefore, at present, greenhouses are covered with glass. However, the thin glass panes (4 mm) have a low thermal resistance and a high emission coefficient for long-wave radiation. Consequently the heat losses through the covering structure are large. Also, in order to have a high transparency, the mechanism to control the aperture of ventilating windows is made as small as possible. However, this delicate mechanism is vulnerable. Therefore, there is quite a risk that when the mechanism is not periodically adjusted, some windows can no longer be closed completely.

In this section the energy saving effects of adjusting the window aperture control mechanism and measures to decrease the heat losses at the cover are studied. The latter is achieved by a number of measures, including the application of a thermal screen and alternative cladding materials.

An important disadvantage of a thermal screen and of current alternative cladding materials is the decreased transparency of the covering structure. This leads to a decreased biomass production. Therefore, when studying the difference in energy consumption which results from applying different energy saving measures that affect the transparency of the cover, the energy consumption must be corrected for possible production losses. Thus, with respect to these measures, the energy-saving effect is expressed in terms of specific energy consumption (the energy consumption per unit of production), instead of the energy consumption per m^2. In the present model, the computation of production is limited to the first step of biomass production, being the photosynthesis. Therefore the specific energy consumption is defined as the yearly primary energy consumption divided by the yearly sum of photosynthesis. The specific energy consumption is expressed as $MJkg^{-1}$.

Another aspect of the improved insulation of the greenhouse is its effect on humidity. In a customary, single glass cladded greenhouse, in winter, a large amount of moisture condenses at the cover. Thus, the greenhouse air is continuously dehumidified. Sometimes, this (uncontrolled) dehumidification results in an unfavourably dry indoor climate, but more often condensation prevents the humidity exceeding the setpoint.

If the insulation of the greenhouse increases, which is accompanied by higher cover temperatures (alternative cladding materials) or an obstructed vapour transport to the cover (a thermal screen), condensation diminishes. Thus, windows have to be opened more frequently to carry off moisture. So, part of the benefits of increased insulation are lost by the necessity of increased ventilation. Increased (controlled) ventilation is also necessary when the air tightness of the greenhouse is improved by better closing windows. To give an impression of the order of magnitude of the amount of energy consumed as a result of ventilation on behalf

of humidity control, in all tables of the following sections the portion of the energy consumption associated with controlled dehumidification is presented. For each case, the portion is determined by comparing the results of two simulations. For each second simulation all settings are equal to the first, except for the set-point for the humidity controller, which is increased from 85% RH to 100% RH, resulting in the absence of humidity control.

Improved air tightness

An important source of leakage in a greenhouse is the fact that sometimes windows cannot be closed. In a greenhouse, a large number of ventilators are coupled to one mechanism that controls the aperture. Therefore, a slovenly tune up of the mechanism can easily mean that a number of ventilators cannot be closed completely. To give an impression of the energy loss due to such a shortcoming to the ventilators the simulation model is applied once with perfectly closing windows, and once for a case where 20% of the windows remain open with a slit of 1 cm ($\cong 0.72°$, $\cong 2\%$).

The results are presented in Table 6.4. The considered measure is not likely to affect production. Therefore the correction for effects on photosynthesis can be omitted. Consequently the energy consumption is expressed in $GJm^{-2}year^{-1}$.

Table 6.4 Yearly energy consumption and energy saving of a greenhouse with well closing windows compared to a greenhouse with a slit of 1 cm in 20% of the windows when the windows are meant to be closed.

	energy consumption $GJm^{-2}year^{-1}$	portion for dehum. $MJm^{-2}year^{-1}$	%	energy saving $MJm^{-2}year^{-1}$	%
cracks	2.045	216	11	-	-
reference	2.013	219	11	32	1.6

The computations show that the small cracks in 20% of the windows induce an increment of energy consumption of only 32 MJ per m^2 per year (1.6%). As expected, the portion of the energy consumption for dehumidification decreases when the uncontrolled ventilation of the greenhouse grows, although in the considered case the effect is hardly noticeable.

Application of a thermal screen

The effect of an overhead thermal screen on heat demand depends on the characteristics of the screen and the horticultural environment in which the screen is applied. As far as this study is concerned, only the characteristics of an LS-10^{+} screen tissue were available, because this type of screen was applied in the research facility (see Section 5.5.2.1 and Section 6.2). Thus, only one screen option is evaluated and compared to the reference situation (without a screen).

If a screen is present, it is closed when the outside air temperature drops below 8 °C, which is a customary closing condition for nurseries that intensively apply a thermal screen. After a closure, the screen starts to open 20 minutes before sunrise and, after having paused three times at intermediate positions, is fully opened at sunrise. In the last two weeks of November, when the canopy is removed from the greenhouse the thermal screen is closed every night.

When a screen is present in the greenhouse, the interception of radiation by construction elements within the greenhouse enclosure (the variable a_{obs} in Section 5.5.2.4) is enlarged to 10% (against 6% for the reference greenhouse).

The daily heat consumption for the reference greenhouse with and without a screen are showed in Figure 6.26. Of course the energy saving effect of the screen is limited to the cold period of the year, because the screen only closes when the outside temperature drops below 8 °C.

The year round decrement of energy consumption was 0.47 $GJm^{-2}year^{-1}$ (23%).
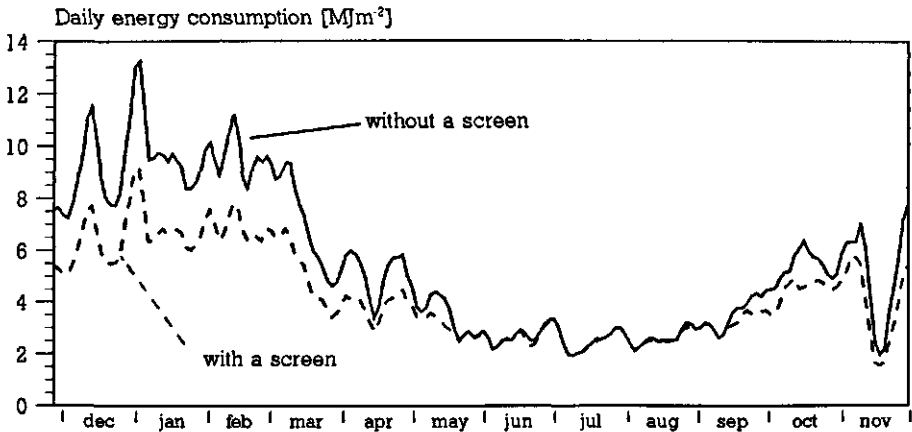
Figure 6.26 Daily heat demand of a greenhouse with, and a greenhouse without an overhead thermal screen.

The negative impact on biomass production of the increased interception of light by the construction related to the thermal screen is showed in Figure 6.27. In sum-

mer, where the amount of light is large, the decrease of photosynthesis is limited due to the non-linear response of photosynthesis on radiation level.

In winter, the relative decrement of photosynthesis is even more than the relative increment of obstructing elements, although the photosynthetic response on radiation is about linear at low radiation levels. This is caused by the larger impact of the dark respiration on the daily photosynthesis.
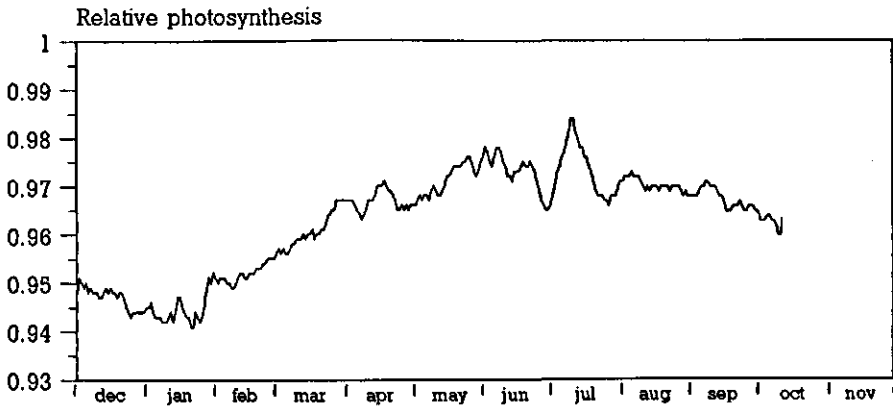
Figure 6.27 Relative daily dry matter photosynthesis of a greenhouse with a thermal screen compared to a greenhouse without a screen.

Indeed, Figure 6.27 shows that in winter the relative photosynthetic activity in the greenhouse with a screen drops to 6% (whereas the screen is assumed to intercept 4% of the solar radiation) of the photosynthetic activity of the reference greenhouse. In summer the decrement of assimilation rate is about 3%.

As argued in the introduction to this section, the energy saving of the thermal screen is corrected for this decrement of production by representing the savings in terms of specific energy consumption, expressed in $MJkg^{-1}$. This resulted in the figures presented in Table 6.5

Table 6.5 Specific energy saving of a greenhouse with an overhead screen compared to the reference greenhouse

	energy consumption $MJkg^{-1}$	portion for dehum. $MJkg^{-1}$	%	spec. energy saving $MJkg^{-1}$	%
reference	218	24	11		-
greenhouse with thermal screen	175	26	15	43	20

From Table 6.5 it can be seen that the specific energy saving due to the described application of an LS-10$^+$ screen is 43 MJkg^{-1}, which is 20% of the specific energy consumption of the reference greenhouse.

Because the screen obstructs moisture transport to the cover, the uncontrolled moisture loss decreases in favour to controlled dehumidification. In a greenhouse with a thermal screen the humidity is controlled in first instance by opening the screen somewhat. Only when the humidity remains at an unacceptable high level after the screen has been opened, are the windows opened. However, this will not occur frequently because, as soon as the screen is opened a little, large amounts of vapour can condense against the cover, due to its low temperature. Thus, because the number of occasions that the windows have to be opened to carry off vapour is comparable for a greenhouse with and a greenhouse without a thermal screen, the absolute portions of the specific energy consumption for dehumidification are about the same (240 GJm^{-2}year^{-1} and 220 GJm^{-2}year^{-1} respectively). However, due to the specific energy decrement of 20% the relative portion of energy consumption for dehumidification is larger for the greenhouse with a thermal screen.

Coated cladding material

Because of the high transmissivity for shortwave radiation and the long durability, as far as greenhouses are concerned, glass is the cladding material most applied in the Netherlands. However, on days with clear skies, the radiative heat loss of a glass-covered greenhouse can be quite large due to the high emission coefficient of glass for thermal radiation.

Coated glass may reduce the emission coefficient. Currently, HORTIPLUS® is the only coated glass pane used in horticulture. The emission coefficient for thermal radiation of HORTIPLUS, providing the glass is dry, is 0.25 (0.84 for ordinary glass) (Out & Breuer, 1995).

During rainfall, the effect of the coating vanishes. Thus, if the effect of rainfall on the emission coefficient is neglected, the energy-saving effect of this coating will be over-estimated. However, during rainy periods the sky temperature will be about equal to the air temperature and therefore the effects of the neglection will be small. Model computations showed that, when the rain effect is not taken into account, the resulting energy consumption of the greenhouse is 3% less than the energy consumption computed for the greenhouse when the rain-effect has been taking into account. Fortunately, information on rainfall is present in the SEL-year. Thus the rain-effect could be included in the model.

The decrement of yearly primary energy consumption due to the application of HORTIPLUS was computed to be 0.36 GJm^{-2}year^{-1} (18%).

An important disadvantage of HORTIPLUS is the diminished transmissivity for

short-wave radiation. In Figure 6.28 the transmission and reflection coefficient for short-wave radiation of both ordinary glass and HORTIPLUS are shown as a function of the angle of incidence.
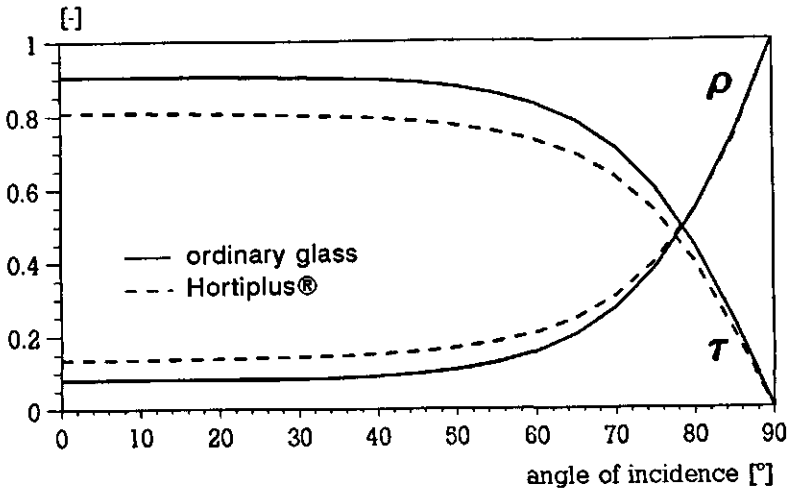
Figure 6.28 τ and ρ for short-wave radiation of both ordinary glass and HORTIPLUS as a function of the angle of incidence (computed with the theory presented by Out & Breuer, 1995).

The model to compute the transmissivity of a greenhouse covering structure, presented in Appendix C, showed that, due to the application of HORTIPLUS, the transmissivity of the reference greenhouse for diffuse radiation from a standard overcast sky dropped from 0.79 to 0.70. The direct transmissivity figures dropped about 11% as well (although somewhat more for low elevation angles).

Due to the reduced amount of light inside the greenhouse, the biomass production was reduced. The mean decrement of production appeared to be 12% in winter and about 7% in summer. The simulation model computed the yearly photosynthesis in the reference greenhouse cladded with HORTIPLUS on 0.92 compared to the greenhouse cladded with ordinary glass.

The effects of HORTIPLUS on the specific energy consumption, taking account for the decrement of production is shown in Table 6.6. The table shows that the specific energy saving effect of HORTIPLUS is limited to 10%. An important reason for the small effect is the amount of energy required for dehumidification.

The large portion of the energy consumption for dehumidification (38.3 MJkg^{-1} or 325 MJm^{-2}year^{-1}) is caused by the fact that condensation at the coated cover is much less than the condensation at an ordinary cover. This is a result of the higher glass temperature of coated cladding material, due to the reduced radiative heat loss. To compensate for a reduced condensation, the greenhouse with HORTIPLUS

has to carry off moisture by means of ventilation. This way of dehumidification requires more energy because, when ventilating, both latent and sensible heat is lost to the atmosphere.

Table 6.6 Specific energy consumption and specific energy saving of a greenhouse cladded with HORTIPLUS compared to the reference greenhouse.

	energy consumption $MJkg^{-1}$	portion for dehum. $MJkg^{-1}$	%	spec. energy saving $MJkg^{-1}$	%
reference	218	24	11		-
HORTIPLUS	195	38	20	23	10

Double glazing

Besides the application of coated glass panes, the heat loss at the cover can be reduced by other measures as well. Double glazing is one of those options.

To compute the effect of double glazing on energy consumption and photosynthesis the greenhouse climate simulation model has been extended with a second glass pane. This meant that a state variable (T_{cov2}) and two heat fluxes (H_{CovCov} and R_{CovCov}) were added to the thermal sub-model. In the extended model, the net flux to T_{cov} changes in (compare with Eqn. 5.29):

$$H_{cov,net} = P_{SunCov} + H_{TopCov} + H_{AirCov} + R_{FlrCov} + \qquad [Wm^{-2}] \ (6.2)$$
$$R_{ScrCov} + R_{UppCov} + R_{LowCov} + R_{CanCov} +$$
$$L_{CovTop} + L_{AirCov} - H_{CovCov} - R_{CovCov}$$

The net flux to the upper glass pane was stated by:

$$H_{cov2,net} = P_{SunCov2} + H_{CovCov} + R_{CovCov} - \qquad [Wm^{-2}] \ (6.3)$$
$$H_{CovOut} - R_{CovSky}$$

The derivative dT_{cov2}/dt was computed analogue to Eqn. 5.28. The forced fluxes P_{SunCov} and $P_{SunCov2}$ were computed by:

$$P_{SunCov} = a_{cov} (1 - a_{cov}) I_{glob} \qquad [Wm^{-2}] \ (6.4)$$
$$P_{SunCov2} = a_{cov} I_{glob} \qquad [Wm^{-2}] \ (6.5)$$

To account for the doubled obstruction of the glass panes, for the diffuse and direct transmissivity the values of τ_{dir} and τ_{dif}, as defined in Section 5.5.2.4 were squared.

The convective heat exchange coefficient HEC_{CovCov} was set to 3 $Wm^{-2}K^{-1}$, which was mentioned by Schinkels (1980) to be a customary value for ordinary double glass panes. The radiative heat exchange coefficient (REC_{CovCov}) was determined

by the application of Equation E.7, using an emission coefficient of 0.84 (Out & Breuer, 1994).

After having extended the simulation model, computations were carried out to determine the energy saving and biomass production effects. The results are stated in Table 6.7

Table 6.7 Specific energy consumption and specific energy saving of a greenhouse with a double glass covering compared to the reference greenhouse

	energy consumption MJkg^{-1}	portion for dehum. MJkg^{-1}	%	spec. energy saving MJkg^{-1}	%
reference	218	24	11		-
Double glass	175	49	28	43	20

For the double glazed cover, the model computed that the yearly energy demand dropped to 1.36 MJm^{-2}year^{-1} and that the photosynthesis dropped with a factor 0.16. Still the specific energy saving (43 MJkg^{-1}) is almost doubled, compared to the former alternative.

In line with the tendency in the former cases that the relative portion of energy consumption for dehumidification increases for better insulated buildings, the double glass cover applies almost 30% of its energy consumption for humidity control (49 MJkg^{-1} or 380 MJm^{-2}year^{-1}). This high proportion is caused by the fact that in a double glazed greenhouse, there is hardly any condensation.

Polymer coating

In the work of Out & Breuer (1995) applications of polymer coatings were mentioned as improving the optical properties of glass. These coatings do not decrease the long-wave emissivity, but increase the short-wave transmissivity (by decreasing the reflection coefficient). This property appeared not to be affected when such a polymer is added to a glass pane with an oxide coating such as HORTIPLUS. Samples of glass panes with such a double coating were tested by Out & Breuer and they reported that these samples had a short-wave diffuse transmissivity, comparable to the diffuse transmissivity of ordinary glass, while the long-wave emission coefficient remained 0.25.

Another possibility is to add the polymer coating onto clear glass to be used in double glass constructions. In the application proposed by Out & Breuer, the coated sides of the glass panes were facing each other. In doing so, they reported the transmissivity of a double glass pane to be about equal to the short-wave transmissivity of an ordinary single glass pane.

A third possibility is to construct a double glass pane from panes that each have a double coating. This cladding material has the light transmission properties of

ordinary double glass, discussed in the former item, but the radiative heat exchange coefficient REC_{CovCov} becomes a factor 0.2 compared to the radiative heat exchange between the untreated glass panes.

In Table 6.8, the results of the effects of the polymer coating for all three applications is listed.

Table 6.8 Specific energy consumption and specific energy saving of a greenhouse with various applications of polymer coatings compared to the reference greenhouse.

	energy consump. $MJkg^{-1}$	portion for dehum. $MJkg^{-1}$	%	spec. en. saving $MJkg^{-1}$	%
reference	218	24	11		-
HORTIPLUS+polymer coating	178	36	20	40	18
coated double glass	151	41	27	67	31
double-coated double glass	134	53	40	84	39

The table shows another increment of the energy savings, compared to the cases discussed previously. It is interesting to see that the absolute portions of energy for dehumidification for the first and second application of the polymer coating is less than the portions computed in the former cases. This effect must be attributed to the increased entrance of solar radiation into the greenhouse. Thus, in the polymer coated greenhouses the latent and sensible heat loss to the atmosphere by ventilation is more often derived from the sun, than from the heating system.

The energy consumption related to dehumidification per m^2 greenhouse was computed to be 330 $MJm^{-2}year^{-1}$ for the HORTIPLUS+polymer coating, 460 $MJm^{-2}year^{-1}$ for the coated double glass and 670 $MJm^{-2}year^{-1}$ for the double-coated double glass.

Conclusions

The effect on energy consumption of windows that, due to the slovenly adjustment of their mechanisms, remain a little open when they were meant to be closed, is small. When 20% of the windows have an opening of 1 cm, the energy consumption of the greenhouse is only 1.6% more than the energy consumption it would have when the ventilation mechanism was well adjusted.

The other measures which can be used to diminish the heat losses from the building, and which were studied in this section, can affect biomass production through a diminished transparency of the greenhouse. The model computed decrements of photosynthesis between 3% (a thermal screen) and 16% (double glass). The effect of production loss was taken into account by judging the energy saving measures on specific energy consumption, defined as the yearly primary energy

consumption divided by the yearly sum of photosynthesis. The results showed specific energy savings ranging form 10% (HORTIPLUS) to 39% (double-coated double glass).

Besides information on the specific energy savings of alternative cladding materials and the thermal screen, the simulation model has been used to compute the portion of the total energy demand required for dehumidification. It appeared that a decreasing heat loss through the covering structure resulted in a growing portion of the primary energy demand being required for humidity control. For HORTI-PLUS this portion is 20% ($325 \text{ MJm}^{-2}\text{year}^{-1}$), but for the greenhouse covered with double-coated double glass, 40% of the energy consumption is related to humidity control ($460 \text{ MJm}^{-2}\text{year}^{-1}$). The reference greenhouse uses 11% ($220 \text{ MJm}^{-2}\text{year}^{-1}$) of its energy consumption for dehumidification. From the growing amount of energy consumed for dehumidification, it can be concluded that the decrement of energy consumption of greenhouses can (highly) be over-estimated if dehumidification is not taken into account.

6.3.4.3 Energy conserving heating devices.

To cover the heat demand of greenhouses, primary energy has to be converted into heat. Also, to enhance production, natural gas is combusted to produce CO_2. Finally, primary energy is applied to produce electricity. Thus, in horticulture, three conversion processes with respect to natural gas (the conversion to heat, to CO_2 and to electricity) can be distinguished. An increased efficiency of these conversion processes serves the target of energy conservation.

The condenser enhances the conversion process of natural gas to heat. The effect of a condenser will be studied by making a comparison of a greenhouse with such a device (the reference greenhouse) with one that omits a condenser. Moreover, apart from the reference connection (see Figure 4.3) an alternative connection of the condenser to the heating system will be analyzed.

The heat storage tank is an important device to save the reject heat from the conversion of natural gas to CO_2 and to electricity. Thus, in fact it enhances these conversion processes. The effects of such a storage tank are studied as a function of its storage capacity.

The combined heat and power engine is the third energy conserving heating device. This device contributes to energy saving because it improves the conversion efficiency of natural gas to electricity by enabling the application of the reject heat. However, for this device, the benefits are only noticed when primary energy saving elsewhere is attributed to the electricity production in the greenhouse.

Condenser

In most greenhouses the condenser is connected to a heating circuit which is preferably applied by this heating device only (Van der Velden, 1995). In the reference greenhouse, the upper heating circuit serves this function. Only during cold periods, when the temperature setpoint of the lower heating circuit exceeds 55 °C, hot water is passed to the upper heating circuit, taking the decreasing efficiency of the condenser for granted.

The condenser is a part of the heating system of the reference greenhouse. Thus the energy savings of the device can be studied by removing the condenser from the heating system and then comparing the yearly heat demand computed by a simulation without the condenser with the 2.013 $GJm^{-2}year^{-1}$ that holds for the reference greenhouse.

In the reference greenhouse, the condenser is connected to the upper heating system (see Chapter 4). This means that return water from the upper heating circuit is led through the condenser. The condenser heats this water and pushes it into the supply side of the upper heating circuit. However, in this configuration, during periods where the heat demand is governed by a minimum pipe temperature, the heat gained from the exhaust gases is not used in an efficient way, because only the lower heating circuit requires heating power. Therefore, the performance of the condenser is studied in an alternative configuration as well. In this alternative configuration, during periods where the minimum pipe temperature constrains the temperature of the lower heating circuit, the water to the condenser is withdrawn from the return pipe of the lower heating circuit. Thus the condenser contributes to the heat demand of the lower heating circuit. The condenser switches back to the upper heating circuit when the setpoint for the lower heating circuit exceeds the actual minimum pipe temperature with 1 °C. The hydraulic scheme that enables this alternative control of the condenser is shown in Figure 6.29.

In the alternative configuration, the valve that controls the selection between the one or the other heating circuit is always moved to one of the extreme positions. The results of the model computation for the greenhouse without a condenser and for the heating system with the alternative heating system configuration are stated in Table 6.9. The boiler was assumed to be tuned on an air factor (λ) of 1.2 (see Section 4.3.4.1).

The computations show that the condenser in the reference configuration saves 7% compared to a greenhouse without a condenser. With the alternative configuration the savings are increased to 9%. This means that if the heat demand is not governed by the realisation of a greenhouse air temperature, feeding the condenser with relatively warm water (return water from the lower heating circuit instead of the upper heating circuit) is advantageous, in spite of a diminished condenser efficiency.
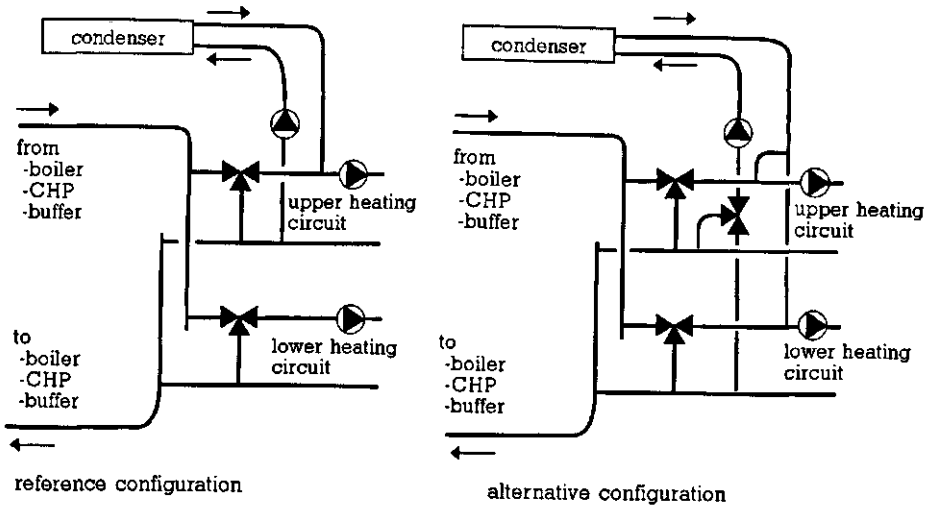
Figure 6.29. Hydraulic scheme of the reference and alternative connection of the condenser to the heat heating circuits.

Table 6.9 Yearly energy consumption of the reference heating system (with a condenser) and a heating system with an alternative connection of the condenser, compared to a greenhouse without a condenser.

	energy consumption $GJm^{-2}year^{-1}$	energy saving $MJkg^{-1}$	%
greenhouse without condenser	2.165		-
reference greenhouse	2.013	151	7
greenhouse with alternative condenser configuration	1.973	192	9

As an illustration, Figure 6.30 shows the decrement of mean condenser efficiency in the alternative configuration compared, to the reference configuration. In this Figure, an efficiency 1 means that all heat which is present in the exhaust gases, relative to the heat content of the ambient air is gathered (like in Fig.4.13).

From the data shown in Figure 6.30 it was computed that the mean conversion efficiency of the condenser was 0.77 for the reference configuration and 0.74 for the alternative configuration. Figure 6.30 shows that the condenser runs at an efficiency of between 0.75 and 0.85 for most of the time. From Figure 4.13 it can be seen that, to reach such an efficiency, the water fed to the condenser has to be below 35 °C. Indeed, as shown in Figure 6.22, the temperature of the return water of the upper heating circuit hardly exceeds a temperature excess of 15 °C above the greenhouse air temperature.

The low efficiencies at 0.25 and 0.30 originate from periods with a high heat demand, where the upper heating circuit acts as a secondary circuit.
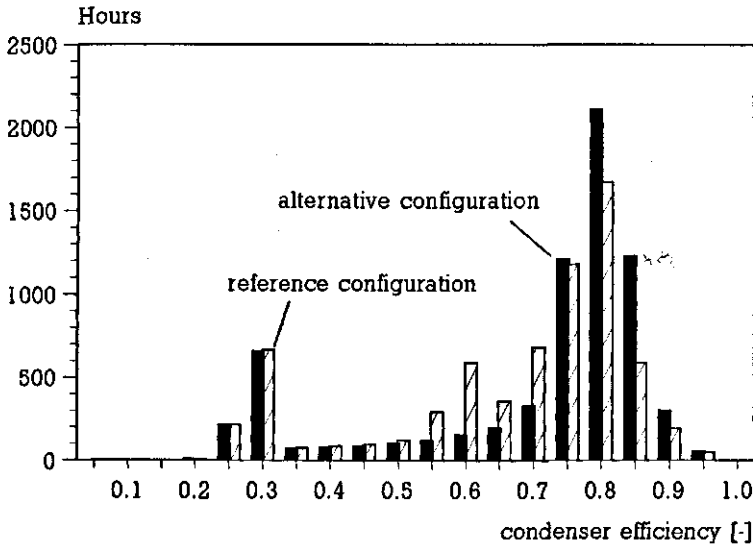
Figure 6.30 Frequency distribution of condenser efficiencies. The condenser effi-ciency expresses the fraction of heat recovered from the heat content of the exhaust gases.

Short-term heat storage

A short-term heat storage facility saves energy if it carries heat from a period with heat surpluses to a period with a heat demand. The energy is stored as hot water in a tank (see Section 4.4.6). In the present heating system, heat surpluses can be caused by the boiler, when it runs to produce CO_2, or by the reject heat of electricity production by combined heat and power.

The energy conservation achieved with a heat storage tank depends on the alternative for storage. If heat production can be decreased when it exceeds the demand (by stopping the CHP engine or the CO_2 production), a storage tank does not conserve energy, but, as will be shown, has other advantages. If the alternative to storage is to raise the heat supply to the greenhouse, forcing additional ventilation, the temporary storage of heat avoids energy losses.

With respect to CO_2 production, the fact whether a storage tank saves primary energy depends on the CO_2 supply strategy. In the reference supply strategy (see Section 6.3.1), CO_2 production is stopped when the greenhouse lacks a (sufficient) heat demand. Thus, the heat storage tank does not contribute to the decrement of primary energy consumption in the reference greenhouse. Rather, the storage tank affects specific energy consumption because, since it can absorb heat surpluses, the CO_2 supply can be increased (resulting in an increased photosynthesis). However, in present horticulture it is also quite common to supply CO_2 irrespective of

the heat demand. In that situation a heat storage tank serves the energy conservation objective. Moreover, as will be shown, it even slightly enhances photosynthesis. The effects of the storage tank on yearly absolute energy consumption, yearly photosynthesis and specific energy consumption will be studied for both the supply strategies.

When a heat storage tank is used in greenhouses with artificial illumination powered by CHP, the storage tank is used by both the CHP engine (when it is switched on for lighting) and the boiler (when producing CO_2). A CHP engine on behalf of artificial lighting is normally operated irrespective the heat demand, because the illumination controller has the highest priority. Thus, with respect to heat surpluses, this case is comparable to the second CO_2 supply strategy (CO_2 supply irrespective of the heat demand). Consequently, the storage tank will have an energy saving effect. However, because the storage tank can be used by the boiler as well, providing the reference CO_2 supply strategy is applied (CO_2 supply as long as the reject heat can be used or stored), an increasing heat storage tank will result in an increment of CO_2 supply. Thus, again the effects of the storage tank can be judged with respect to absolute energy consumption, yearly photosynthesis and specific energy consumption.

When CHP is used to produce electricity for the public grid (discussed in the next section), the device normally does not produce surpluses, because it is common practice to stop the engine when the heat demand is too small (Oversloot, 1992).

Effects of a storage tank in relation to CO_2 supply

To study the effects of heat storage in relation to CO_2 supply, again the horticultural context of the greenhouse growing tomatoes used in the previous sections serves as a reference. However, to study the effects for both extremes with respect to CO_2 supply strategies (stopping the supply when there is no heat demand or CO_2 supply irrespective of the heat demand), besides the reference supply strategy, the simulation model was employed using the second CO_2 supply strategy.

Simulations were carried out for 6 storage tank values (5, 20, 40, 60, 80 and 100 m^3ha^{-1}) for both the supply strategies and three exhaust gas supply rates. The supply rates were set to a combustion of 25, 50 and 75 m^3 of natural gas per hectare per hour. The first value is less than the supply rate used in the reference situation (40 $m^3ha^{-1}hr^{-1}$, see Section 6.3.1). The highest supply rate is significantly more, but certainly not unusual in present horticultural practice.

Figure 6.31 and 6.32 show the results with respect to energy consumption and yearly photosynthesis.

Figure 6.31 clearly shows that a heat storage tank decreases the energy consumption only when the second supply strategy is applied. This could be expected because the storage tank prevents reject heat being carried off by increased venti-

lation. The larger the tank, the more heat surpluses can be absorbed. Of course, in the second supply strategy, the amount of heat to be carried off is greater when the supply rate is higher. Thus the effects of a heat storage tank are larger for increasing supply rates.
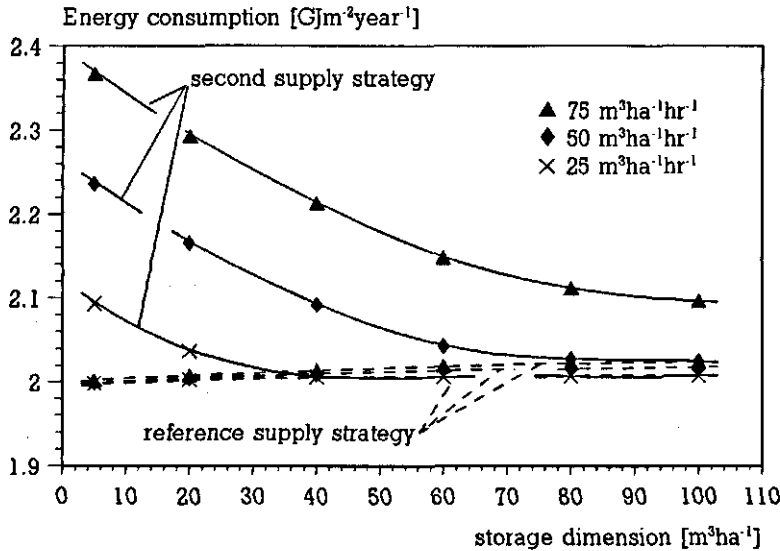
Figure 6.31 Energy consumption of the reference greenhouse as a function of heat storage dimension for three levels of CO_2 supply and for two supply strategies. The reference supply strategy prohibits the combustion of gas for CO_2 supply when the greenhouse lacks a heat demand and the storage tank is completely filled. The second strategy supplies CO_2 irrespective of the heat demand.

Figure 6.31 shows that the tank does not yield an energy conservation for the reference supply strategy. The energy consumption can even be seen to increase with the storage tank dimension. This increment is caused by an increased energy loss from the storage tank. Again the effect, which is an increment of energy consumption this time, is greater for higher supply rates. Of course the increased energy loss will occur with respect to the second strategy as well, but that cannot be seen in the graph because the increased losses are less than the savings from the storage tank.

Figure 6.32 shows that the effect of the storage tank dimension is much larger for the reference supply strategy than for the second strategy as far as photosynthesis is concerned. The results of the reference strategy differ significantly from the results of the second strategy for a particular supply rate for low storage tank dimensions. This is caused by the fact that, for the reference strategy, the amount of CO_2 that can be supplied is strongly limited by the heat demand in the period

that the boiler produces CO_2 (the daytime). As the dimension of the storage tank increases, the differences between the strategies become smaller. If the storage tank is so large that it can always absorb the heat surpluses, the CO_2 supply is never prohibited for both supply strategies. However, for the highest supply rate, even for the largest storage tank a difference between the supply strategies persist. Moreover, the difference will remain even when the tank becomes larger because it can be seen from the figure that the dashed curve for the 75 $m^3ha^{-1}hr^{-1}$ supply rate has almost flattened out. It can be deduced from this fact that the daily amount of heat produced by a boiler for that supply rate exceeds the diurnal demand. Indeed, the combustion of 75 $m^3ha^{-1}hr^{-1}$ during some 16 hours (in summer) yields 3.8 MJ, whereas the mean daily consumption in summer for the reference greenhouse is less than 3 MJ (see for instance Figure 6.26).

Also remarkable in Figure 6.32 is the declining increment of photosynthesis for the increasing level of CO_2 supply rate. Finally, the figure shows that for the second strategy too, the yearly photosynthesis increases for increasing storage tank dimensions, especially for the highest supply rate. This is caused by diminished losses of CO_2 because extra ventilation, carrying off reject heat, is needed less frequently as the storage tank increases in size.
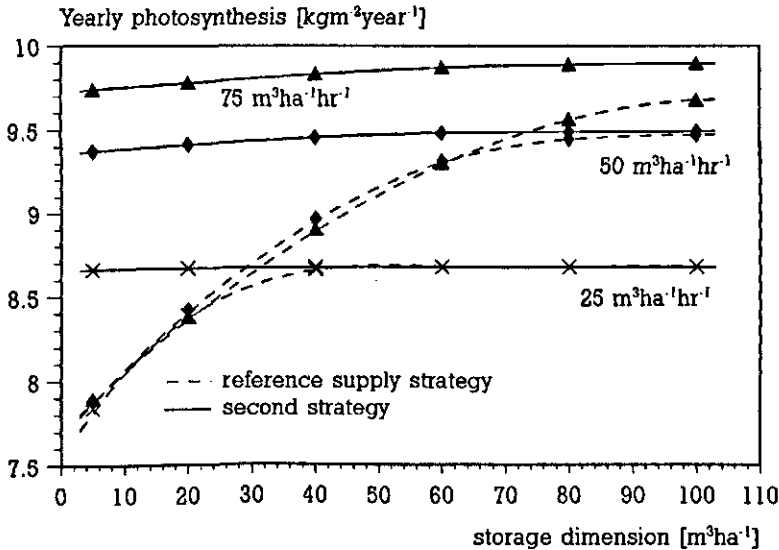
Figure 6.32 Yearly photosynthesis of a tomato crop as a function of heat storage dimension for three levels of CO_2 supply and for two supply strategies.

As in Section 6.3.4.2, the effects of photosynthetic activity and energy consumption can be combined into a single number describing specific energy consumption. This number is shown as a function of the storage facility dimension in Figure 6.33 for both extremes.

Specific energy consumption [MJkg^{-1}]

storage dimension [m^{3}ha^{-1}]
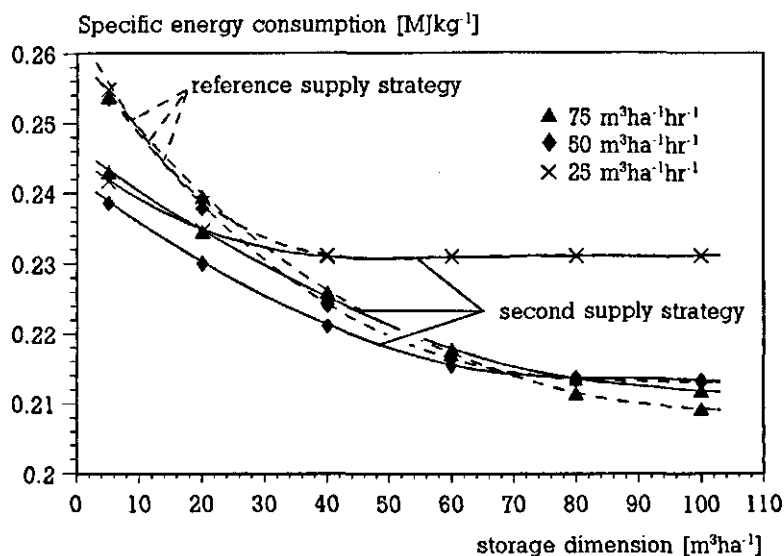
Figure 6.33 Specific energy consumption of the reference greenhouse as a function of heat storage dimension for three levels of CO_2 supply and for two supply strategies.

All curves in Figure 6.33 tend to decrease when the heat storage tank increases. Also, it appears that the supply strategy becomes less important for increasing heat storage tanks. The decrement of specific energy consumption ranges up to 20% for the reference CO_2 supply strategy.

For small storage tanks the second supply strategy yields a significantly lower specific energy consumption than the reference strategy. Moreover, the supply rate at 50 m^{3}ha^{-1}hr^{-1} yields the lowest value for that supply strategy, unless the storage tank exceeds 80 m^{3}ha^{-1}. This must be attributed to the declining extra photosynthesis (see Figure 6.32) when the supply rate is increased.

In general, the supply of CO_2 irrespective of the heat demand results in the lowest energy demand per unit of photosynthesis. However, when the storage tank exceeds 70 m^{3}ha^{-1}, the highest supply rate starts to yield the lower specific energy consumption, providing the reference supply strategy is applied.

Effects of heat storage for a greenhouse with a CHP engine for artificial lighting

A greenhouse growing roses with artificial illumination was simulated to study the effect of heat storage with respect to combined heat and power for private electricity production. Except for the illumination, the greenhouse construction was assumed to be the same as the one hectare greenhouse that served as a reference in the preceding sections. Illumination was applied between 8 August and 27

April. The lamps were switched on when outside solar radiation intensity dropped below 75 Wm^{-2}. During the period from one hour before sunset till 5 hours after sunset the lamps were not allowed to be switched on. This illumination control strategy was equivalent to the strategy applied in the research facility discussed in Section 6.2.1. Using this strategy, artificial illumination is in use for about 3000 hours per year (3041 hours in the SEL-year) in the Netherlands.

By assuming the same amount of luminaires per m^2 as in the research facility, artificial lighting consumes 44 Wm^{-2} of electrical power. Typically, a CHP engine as applied in horticulture, has a thermal power which is a factor 1.6 of its electric power (Klimstra, 1991). This yields a thermal power of 70 Wm^{-2}.

The air temperature setpoints were set to 19 °C during daytime and 17 °C for the night, throughout the year. The light dependent temperature setpoint increment was parametrized according to the settings mentioned in Section 6.3.1.

From 1 April to 1 October, the minimum pipe temperature for the lower heating circuit was 45 °C during the day and 40 °C during the night. At high levels of solar radiation, the minimum pipe temperature was lowered according to the settings mentioned in Section 6.3.1. The humidity setpoint was 85% RH except for the period between 1 September to 1 December, where the setpoint was lowered to 80% RH. CO_2 was supplied by combusting natural gas at a rate of 40 $m^3ha^{-1}hr^{-1}$. The CO_2 supply was stopped when the greenhouse lacked a heat demand and the storage tank was completely charged.

With the settings mentioned above, the climate controller setpoints for the growth of roses are comparable to the settings for the tomato crop, except for the settings holding for the period when the tomato crop was removed and the first three weeks after a new crop is planted. This period runs from 11 November to 21 December.

As in the case of the greenhouse growing tomatoes, the nursery growing roses was supposed not to have a thermal screen.

The effect of the storage tank was determined by simulating year round energy consumption and photosynthesis for the same six storage tank volumes applied in the former section. The results of the simulations with respect to primary energy consumption, yearly photosynthesis and specific energy consumption are shown in the Figures 6.34, 6.35 and 6.36 respectively.

The fact that an increased storage tank saves primary energy shows that the CHP engine produces heat irrespective of the heat demand. However, because the decrement of the primary energy consumption is small (for the largest heat storage tank about 7% of the energy consumed when the greenhouse is not equipped with a heat storage tank), the heat surpluses caused by the combined heat and power engine are limited.

Energy consumption [GJm^{-2}year^{-1}]

storage dimension [m^{3}ha^{-1}]
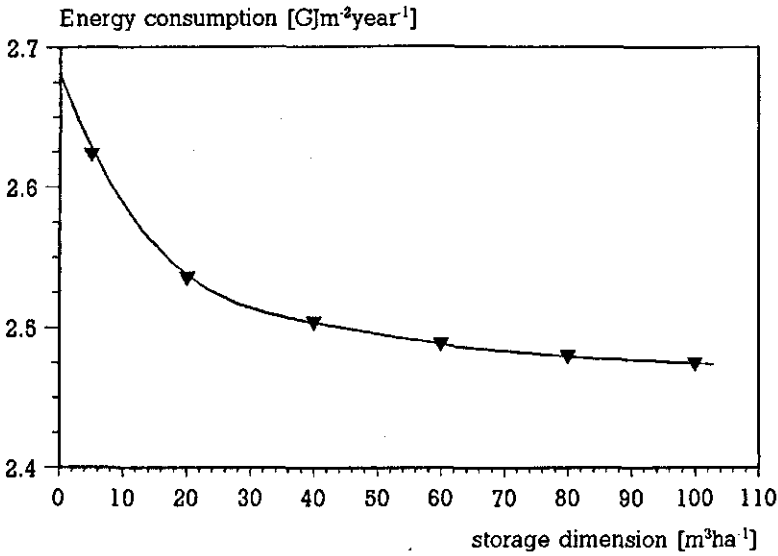
Figure 6.34 Primary energy consumption of a greenhouse using artificial lighting powered by on-site CHP as a function of heat storage dimension.

Yearly photosynthesis [kgm^{-2}year^{-1}]

storage dimension [m^{3}ha^{-1}]
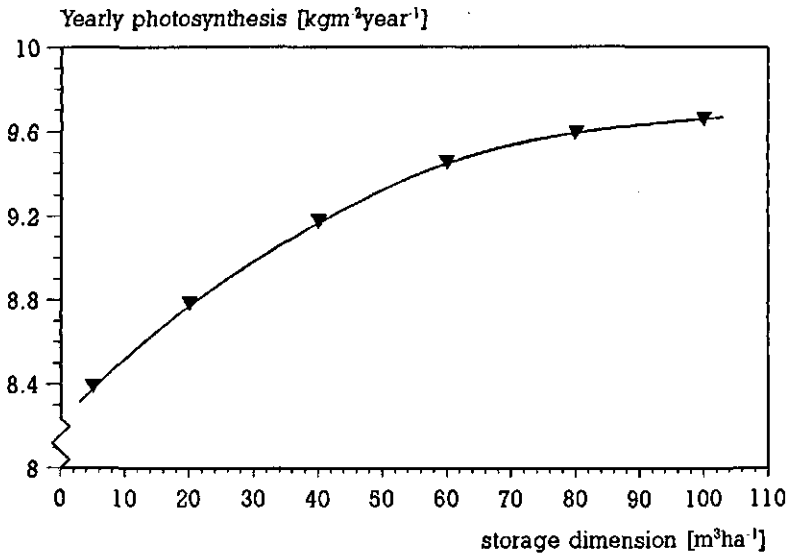
Figure 6.35 Yearly photosynthesis of an illuminated rose canopy as a function of heat storage dimension. CO_2 is supplied according to the reference strategy (stopping the supply if the greenhouse lacks a heat demand and the storage tank is completely filled).

As can be seen in Figure 6.35, with respect to yearly photosynthesis, the storage tank has a considerable impact (up to 18%). The curve in Figure 6.35 is compara-

ble to the dashed curve for the 50 m³ha⁻¹hr⁻¹ supply rate in Figure 6.32. This is not surprising, since it describes the same effect. However, the curve of Figure 6.35 lies about 0.5 kgm⁻²year⁻¹ higher. This is caused by the fact that the rose canopy grows throughout the year, whereas the tomato hardly assimilates when it is just planted and is removed from the greenhouse in November.

Again, the figures for energy consumption and production can be combined to yield the specific energy consumption. The specific energy consumption is shown in Figure 6.36. Obviously, the application of a large storage tank reduces the specific energy consumption by some 20%. This Figure is comparable to the decrement achieved when the storage tank is applied for surpluses from the boiler due to CO_2 supply.

Figure 6.36 also shows that the level of the curve is significantly higher than the levels of the curves presented in Figure 6.32. This is caused by the fact that the application of artificial illumination results in high primary energy demands. However, as will be discussed in the next section, if the lamps were powered by the public grid, the actual primary energy consumption would be even higher. This is because then the primary energy applied by the power plant that produces the electricity should be taken into account.
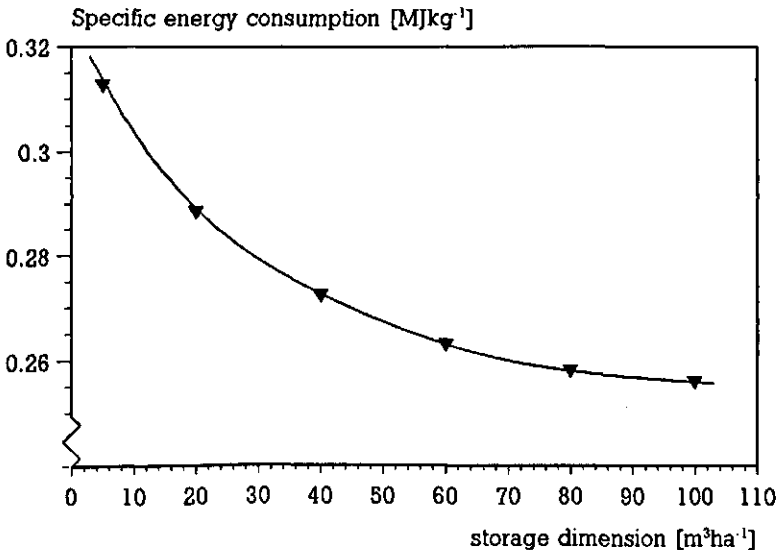
Figure 6.36 Specific energy consumption of a greenhouse using artificial illumination as a function of heat storage dimension.

Combined heat and power

Application of combined heat and power at a nursery raises its primary energy consumption. However, the electricity produced replaces electricity production of large power plants. Because, unlike the case with CHP, as a rule the reject heat of those large power plants is not used, on a national scale, the energy conservation objective can still be served.

Of course the net effect of CHP depends on the conversion efficiencies of the production processes compared. The decrease of natural gas consumption in a power plant per unit of electric energy produced with on-site CHP can be expressed by:

$$G_{prim,pp} = -\frac{E_{chp}}{\eta_{pp}\,35.16\cdot10^6} \qquad\qquad [m^3]\ (6.6)$$

in which $G_{prim,pp}$ represents the (decrease of) gas consumption at the power plant (m^3), E_{chp} the electricity production by combined heat and power (J), η_{pp} the conversion efficiency of the power plant and $35.16\cdot10^6$ the upper heating value of natural gas of Slochteren quality at standard pressure and temperature (Jm^{-3}). For modern gas fired power plants the conversion efficiency is about 0.45 of the upper heating value (0.5 of the lower heating value).

The year round electricity production of a CHP engine is (providing the engine runs on full capacity only) the product of electric power and the number of running hours. In a horticultural context the number of running hours depends mainly on the thermal power of the engine.

To determine the relation between thermal power and the number of running hours the simulation model has been applied for 5 levels of thermal power (20, 40, 60, 80 and 100 $W_{th}m^{-2}$). The horticultural context of the simulations was described by the reference greenhouse and its set of horticultural settings (see Section 6.3.1, 6.3.2 and 6.3.3). To get an impression of the contribution of CHP to heat production the mean daily heat production of the engines is shown in Fig. 6.37. The horticultural context is included in the figure by the grey shaded total mean daily heat demand of the greenhouse.

The fact that even the engine of 100 $W_{th}m^{-2}$ never covers the total heat demand is attributed to the carbon dioxide supply, which forces the boiler to produce heat. Also, during peak heat demands, which cannot be seen in the figure because of the smoothings that were applied to the data (a 10 cells moving average filter), the boiler supplies heat now and then. Obviously, in summer the heat associated with CO_2 supply severely diminishes the contribution of CHP.

The relative contribution of the heating devices in greenhouse heat production are tabulated in Table 6.11.

The table clearly shows the decreasing additional contribution of the CHP engine as the thermal power becomes greater. The amount of heat released by CO_2 pro-

duction is constant, because the CO_2 supply has a higher priority than the production of electricity. The increment of the contribution of the condenser is caused by the higher amount of exhaust gases per unit of thermal energy from a CHP engine, compared to the amount of exhaust gases per unit of thermal energy from a boiler.
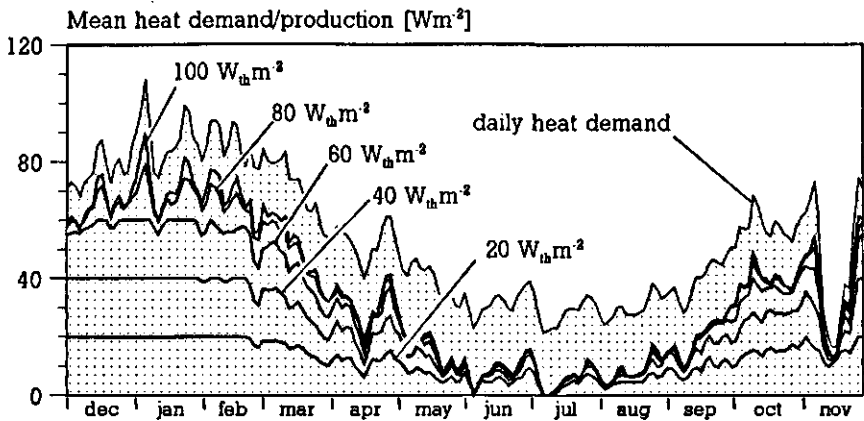
Figure 6.37 Daily heat demand of the reference greenhouse and daily heat production of CHP for 5 thermal power levels. In order to present a readable picture the daily mean values were smoothed by a 10 cells moving average filter.

Table 6.11 Total yearly heat production of the heating devices and the percentage of contribution for the reference greenhouse with 5 differently sized CHP engines.

| | thermal power [Wm^{-2}] | | | | | |
	0	20	40	60	80	100
CHP	0	20%	36%	49%	58%	63%
boiler	70%	49%	32%	19%	9%	4%
condenser	10%	11%	12%	12%	13%	13%
CO_2 supply	20%	20%	20%	20%	20%	20%
total	100%	100%	100%	100%	100%	100%

To compute the extra gas consumption and the electricity production for the five cases a thermal and an electric conversion efficiency must be employed. Typically, the thermal conversion efficiency of currently applied engines is 0.47 with respect

to the upper heating value (0.53 with respect to the lower heating value). The electric conversion efficiency is typically a factor 1.6 smaller (Klimstra, 1991). From the total heat produced by the CHP engine, as computed with the model, the electricity production can be computed and, by means of Eqn. 6.6, the savings of natural gas at the power plant. The gas consumption of the CHP engine and the boiler can be computed from their conversion efficiencies which are the previously mentioned 0.47 and 0.85 with respect to the upper heating value of natural gas. Table 6.12 shows the electricity production, gas consumption of the nursery, savings at the power plant and net savings of natural gas for the five levels of thermal power.

Table 6.12 Electricity production, gas consumption of the nursery, savings at the power plant and net savings of natural gas for five thermal power levels.

	thermal power [Wm^{-2}]					
	0	20	40	60	80	100
electricity production [MJm^{-2}]	0	240	433	585	693	747
nursery gas consumption [$m^3m^{-2}year^{-1}$]	57	67	75	80	84	86
power plant gas saving [$m^3m^{-2}year^{-1}$]	0	15	27	37	44	47
net energy consumption [$m^3m^{-2}year^{-1}$]	57	52	47	43	41	39
energy saving	0%	9%	18%	25%	28%	32%

Table 6.12 shows that the application of CHP has a considerable impact on the gas consumption of the nursery. However, on a national scale, this extra gas consumption is amply compensated by savings elsewhere. Thus, for a large combined heat and power engine, the net energy consumption drops to less than 70% of the energy consumption of the reference greenhouse.

In the control strategy subject to the simulated cases, the CHP engine does not affect canopy growth. Thus, the specific energy consumption drops parallel to the decrement of net energy consumption.

The computations show that from March up until the end of the growth season, the contribution to the heating of the greenhouse is less than the potential contribution for all devices. This is due to the reject heat from CO_2 supply which causes the CHP engine to switch off. This means that, if the exhaust gases of the engine were clean enough to be used for CO_2 supply, the contribution made by a CHP engine to the heat demand can be increased strongly. A look at Figure 6.37 shows that the CHP engine with a thermal power of 20 $W_{th}m^{-2}$ (12.5 $W_{el}m^{-2}$) would run almost 8760 hours a year and the 40 $W_{th}m^{-2}$ engine (25 $W_{el}m^{-2}$) would run about 8500 hours a year. With these running hours an electricity production of 390 MJ for the 20 $W_{th}m^{-2}$ engine and 765 MJ for the 40 $W_{th}m^{-2}$ engine would be achieved.

Thus, if CO_2 could be supplied from CHP engines, the net energy saving by application of the 20 $W_{th}m^{-2}$ engine would increase from 9% to 16%. For the 40 $W_{th}m^{-2}$ engine the net energy saving would increase to 33%, which is comparable to the results achieved for the largest engine if CO_2 is supplied with the boiler. Indeed, currently a number of full-scale experiments are being carried out with devices that clean the exhaust gases to such an extent that they can serve as a horticultural CO_2 source.

Conclusions

The application of a condenser in the reference heating system, where the boiler runs at a conversion efficiency of 0.85 with respect to the upper heating value and the condenser is fed with water from the upper heating circuit, results in a primary energy saving of 7%. An alternative configuration, where the condenser was fed with water from the lower heating system during periods where its temperature was governed by a minimum pipe temperature, increased the primary energy saving to 9%. This higher energy saving was achieved despite the fact that due to the alternative configuration the mean condenser efficiency decreased from 0.77 to 0.74. The explanation by the fact that in the reference configuration the heating power of the condenser during periods where the heat demand is governed by a minimum pipe temperature is useless. In the alternative configuration, due to the valve that enables a connection of the condenser to the lower heating circuit, the heating power of the condenser contributes to the heat demand of the lower heating circuit.

The computations with respect to the two condenser configurations shows that the customary recommendation to connect the condenser to a special heating circuit does not necessarily achieves the highest energy saving. This because, when the configuration lacks a connection to the lower heating circuit, the gathered heat during periods where a minimum pipe dominates the temperature of the lower hating circuit is useless.

The energy saving effect of a heat storage tank principally depends on the alternative for heat storage. Only if the alternative is to carry off the heat surplus by forcing a higher pipe temperature, a heat storage tank will result in primary energy saving. In the computations on this alternative, the simulations show that savings of up to 13% can be reached if the surpluses are caused by CO_2 supply by combusting 75 m^3 natural gas per hectare per hour irrespective of the heat demand. For lower supply rates, the surpluses without a storage tank are less and so are the maximal savings. For a supply rate of 50 $m^3ha^{-1}hr^{-1}$ the maximal saving is 10% and for a supply rate of 25 $m^3ha^{-1}hr^{-1}$ the saving is limited to 6%.

If the alternative to the storage of heat surpluses is to prevent the surplus by stopping the CO_2 supply, a storage tank can even increase the primary energy con-

sumption of a greenhouse, although the increment is always less than 2%. This increment of energy consumption is caused by the heat losses from the storage tank surface.

However, besides an energy saving effect, a heat storage tank affects the yearly photosynthesis as well. This effect is most pronounced for the CO_2 supply strategy that stops the supply on a surplus (the reference supply strategy). Because the storage tank absorbs the surpluses, the availability of a storage tank enlarges the possibility of supplying CO_2. This results in an increased production. The maximal increment of yearly photosynthesis was computed to be 14% for the low supply rate. Application of a large heat storage tank on the reference supply strategy with a supply rate of 50 $m^3ha^{-1}hr^{-1}$ showed a increment of photosynthesis of 25%. The maximal increment of yearly photosynthesis by a heat storage tank in a greenhouse applying the reference supply strategy is even 28% for the high supply rate (75 $m^3ha^{-1}hr^{-1}$).

For the alternative supply strategy the heat storage tank results in a higher yearly photosynthesis as well. This is because, due to the storage tank, extra ventilation to carry off surpluses occurs less frequently. Thus, the loss of CO_2 will be less and photosynthesis will be enhanced. However, the effect is much less than the effects described in the former paragraph. The maximal increment of photosynthesis for a large storage tank was only 2.2% for the highest and 1.6% for the 50 $m^3ha^{-1}hr^{-1}$ supply rate. For the low supply rate the increment of yearly photosynthesis was not worthmentioning.

The energy saving figures and the increment of yearly photosynthesis can be combined to a specific energy consumption figure, describing the amount of primary energy required per unit of photosynthesis. The computation of this figure shows that, in general, for the reference growth of a tomato canopy, the alternative CO_2 supply strategy (supply irrespective of the heat demand) uses less primary energy per unit of photosynthesis than a strategy that stops the supply when the greenhouse lacks a heat demand. Moreover, if a storage tank is applied with a capacity less than 80 m^3h^{-1}, the 50 $m^3ha^{-1}hr^{-1}$ supply rate, irrespective of the heat demand, shows a lower specific energy consumption than both the other supply rates.

The curves of the specific energy consumption as a function of heat storage dimension show that, for a particular supply rate, the differences between both supply strategies tend to disappear as the storage tank increases. Only for the highest supply rate the specific energy consumption of the reference supply strategy appears to yield an even lower specific energy consumption if the heat storage tank dimension exceeds 70 m^3ha^{-1}.

The computations of the effects of a heat storage tank on a nursery with artificial illumination powered by an on-site combined heat and power engine shows both an important energy saving effect and an increment of yearly photosynthesis. The energy saving effect is caused by the fact that the CHP engine runs irrespective

of the heat demand. The production increment is a result of the fact that the storage tank is also used by the boiler when it supplies CO_2 according to the reference strategy with a supply rate of 40 $m^3ha^{-1}hr^{-1}$.

Combining the energy saving and production increment in the specific energy consumption, the decrement of specific energy consumption appears to range upwards to 24% compared to a situation without a storage tank.

The application of combined heat and power, enlarges the gas consumption of greenhouses significantly. However, because the electricity produced at the greenhouse site decreases electricity production elsewhere, CHP can still save energy. This is the case if its overall conversion efficiency of natural gas to electricity and heat is larger than the conversion efficiency of public power plants. Since a greenhouse applies (most of) the reject heat of a CHP engine, in general this condition will be served.

Thus, to compute the energy saving from combined heat and power, the decrease of energy consumption at public power plants due to the electricity production at the greenhouse site must be subtracted from the energy consumption of the greenhouse. This yields energy savings that, depending on the capacity of the CHP engine, range up to 32% for an engine with a thermal power of 100 $W_{th}m^{-2}$.

If exhaust gases of the device can be cleaned sufficiently to allow them to be used for CO_2 supply, a comparable saving can be achieved by an engine with a thermal power of only 40 $W_{th}m^{-2}$.

6.3.5 Conclusions on the evaluation of energy-saving prospectives

Because energy conserving measures have the greatest impact on horticultural production with a high energy demand, the growth of tomato, planted in December and removed in November has been chosen as a reference. Indeed, the reference greenhouse, described in Sections 6.3.1, 6.3.2 and 6.3.3, has a much higher primary energy input (2.0 $GJm^{-2}year^{-1}$) than the average value for horticulture (±1.4 $GJm^{-2}year^{-1}$, see Figure 2.5) in the Netherlands.

Three items on energy conservation were studied for this reference greenhouse. The first item concentrates on the boiler house. Three of the energy conserving measures mentioned by the MJA with respect to the boiler house were evaluated. Because there are still quite a number of boilers that are poorly insulated in horticultural practice (Velden, 1995), in the first place the energy savings were computed for the increment of the boiler insulation thickness from 2 cm to 6 cm. The boiler model shows that, for a 2.5 MW boiler, this measure decreases the yearly energy loss from the boiler with 76 GJ. For the reference greenhouse this saving is less than 0.4% of its primary energy consumption. However, because it is a simple measure, it can still be advantageous.

In the second place, the energy saving of the insulation of transport pipes was studied. Six pipe types were distinguished with respect to diameter and function in the heating system. The computations show a large difference in the effect of insulation between the one and the other pipe. For the pipe with the highest mean temperature (the main supply pipe), insulation yields an energy saving of 14 GJ per meter pipe insulated per year. Insulating the gathering pipe (see Fig. 4.3 for the terminology) yields 3.9 $GJm^{-1}year^{-1}$. Insulating the transport section of the supply side of the lower and upper heating circuit saves 4.5 and 1.8 $MJm^{-1}year^{-1}$, respectively. The energy savings of insulation of the return transport pipes yields about half the savings achieved at their supply side.

The third energy saving measure in the boiler house is the changing of the connection of the expansion vessel if it is connected to a section in the heating system where a high temperature predominates (the main supply pipe) to a part of the heating system with relatively low water temperatures (the gathering pipe). The computations on this subject show that the savings depend to a large extent on whether the greenhouse is equipped with a heat storage tank. For a greenhouse without a storage tank, the savings are 9 $GJyear^{-1}$, whereas the savings for the reference greenhouse, having a heat storage tank of 80 m^3 can be up to 20 $GJyear^{-1}$.

The second item of energy saving measures involves the decrement of energy losses from the greenhouse cover. The studied measures involved the decrement of leakage through windows, the application of a thermal screen and the application of alternative cladding materials (coated glass panes and double glazing).

The prevention of unnecessary leakage through windows appeared to decrease the heat demand by only 1.6%. This figure was achieved by computing the difference with respect to primary energy consumption between the reference greenhouse and an equal greenhouse except for 20% of the windows that remain 1 cm open when they were meant to be closed.

The application of a thermal screen, which was closed during the night when the outside temperature dropped beneath 8 °C, yields an energy saving of 23%. However, because the screen construction decreases the transparency of the greenhouse, the yearly photosynthesis appears to become 4% less. The specific energy consumption was computed to combine these effects in a single figure. The specific energy consumption is defined as the yearly primary energy consumption per unit of yearly photosynthesis. For a thermal screen, the specific energy consumption decreases with 20% compared to the reference greenhouse (without a screen).

With respect to coated cladding materials, the currently available tin-oxide coating (HORTIPLUS) and three options for the application of an experimental polymer coating were studied.

The application of a tin-oxide coating yields a decrement of primary energy consumption of 18%. On the other hand, due to the important impact of the coating

on transmissivity, the yearly photosynthesis decreases by 8%. Thus, the specific energy consumption decreases by only 10%. However, with experiments on small glass samples, Out & Breuer (1995) reported that the negative effect of the tin-oxide coating on transparency can be almost cancelled out by bringing a polymer coating onto the tin-oxide coating. This leads to a specific energy saving equal to the decrement of primary energy consumption (which is 18%).

Out & Breuer also suggested applying the polymer coating onto the glass panes of double glass greenhouse cladding. This gives a double glass pane a transparency equal to that of a single glass pane. Thus, the decrement of specific energy consumption by the application of a polymer-coated double glass cover, becomes equal to the decrement of primary energy consumption for an ordinary double glass cover. For ordinary double glass the decrement of primary energy consumption appears to be 31%.

Without the polymer coating the yearly photosynthesis drops to 84% of the reference greenhouse. Thus, for ordinary double glass a large amount of the benefits of energy saving are lost when its effect on specific energy consumption is judged. The savings of an ordinary double glass cover are then limited to 20%.

The ultimate suggestion with respect to primary energy saving, as posed by Out & Breuer is to make a double glass cover consisting of glass panes coated with both the tin-oxide and the polymer coating. This cladding material has a transparency comparable to that of ordinary double glass but achieves an energy saving of 48%. After combining the energy saving effect and the decrement of production the double-coated double glass pane yields a decrement of specific energy consumption of 39%.

An interesting aspect of the decrement of the overall heat exchange coefficient of the greenhouse cover is that the (absolute and relative) portion of energy demand related to dehumidification increases as the insulation of the cover improves. This effect originates from the fact that the temperature of the inner side of the cover increases as its heat loss at the outside becomes less. When the mean inner cover surface temperature increases, the condensation of moisture against the cover decreases. Thus windows have to be opened more frequently to carry off moisture. When a thermal screen is applied, the absolute portion of the energy demand for dehumidification increases only slightly. This is because, by slightly opening the screen condensation against the cover is still possible.

For the coated and double glass cladding materials condensation is severely diminished, resulting in a growth of the portion of energy demand related to dehumidification ranging from 20% (tin-oxide coated glass) to 40% (double-coated double glass) of the specific energy consumption.

The third item of energy saving measures was the application of energy conserving heating devices. With respect to this item a condenser, a heat storage tank and a combined heat and power engine were studied.

The condenser was applied in two configuration alternatives. In the first configuration (termed the reference configuration) the condenser was attached to the upper heating circuit. The upper heating circuit was also applied as a secondary heating circuit, meaning that during periods with a high heat demand, hot water was added to the upper heating circuit. This way of operating the upper heating circuit results in a somewhat decreased condenser efficiency, but it avoids the necessity for an additional heating circuit.

In the reference configuration the condenser decreases the primary energy consumption of the reference greenhouse by 7% compared to a greenhouse without a condenser. The mean condenser efficiency is 0.77. The results show that the negative impact of the fact that, during cold periods hot water is added to the upper heating circuit, is not of great importance.

In the alternative configuration, the condenser could be connected to both the upper and lower heating circuit. This configuration prevents the heating power of the condenser being dissipated at the upper heating system during periods when the temperature of the lower heating system is governed by a minimum pipe temperature. In the alternative configuration the condenser saves 9% compared to the primary energy consumption of a greenhouse without a condenser. This higher saving is achieved despite the fact that the mean efficiency of the device drops from 0.77 to 0.74. This seeming inconsistency is explained by the fact that in the alternative configuration, during periods when a minimum pipe dominates the lower heating circuit, at least some heat is recovered from the exhaust gases. The condenser in the reference configuration gathers more heat during those periods but the dissipation of that heat in the upper heating circuit does not decrease the heat demand at the mixing valve of the lower heating circuit. Thus, if a greenhouse applies a minimum pipe temperature it will be favourable to creating the possibility of connecting the condenser to the heating circuit on which (during some periods) a minimum pipe temperature holds.

The computations on the effects of a heat storage tank show that, depending on the CO_2 supply strategy, either primary energy savings or the increment of yearly photosynthesis dominates the effect of the device. Energy is saved if CO_2 is supplied irrespective of the heat demand. If the CO_2 supply strategy avoids heat surpluses having to be carried off by extra ventilation (termed the reference supply strategy), the application of a storage tank induces an increased CO_2 supply, which enhances photosynthesis. To combine both effects, like in previous subjects of study, the energy saving effect is expressed by the relation between the heat storage dimension and specific energy consumption. After combination, it appears that in general, for a heat storage tank smaller than 70 m^3 and for a particular

supply rate, the supply strategy irrespective of the heat demand requires less primary energy per unit of yearly photosynthesis than the reference supply strategy. Moreover, if CO_2 is supplied by combusting 50 m^3 of natural gas per hectare per hour the specific energy consumption is lower than for the 25 m^{3}ha^{-1}hr^{-1} supply rate and the 75 m^{3}ha^{-1}hr^{-1} supply rate. However, the lowest specific energy consumptions were calculated for the reference supply strategy at a rate of 75 m^{3}ha^{-1}hr^{-1}, combined with a heat storage tank larger than 80 m^{3}ha^{-1}.

As far as the CO_2 supply strategy irrespective of the heat demand is concerned, the maximal decrement of specific energy consumption appears to be 15%, holding for the highest supply strategy. For the reference supply strategy (avoiding surpluses having to be carried off) the maximal specific energy saving of the storage tank is larger, namely 22%. The larger effect must be attributed to the high value of the specific energy consumption for this supply strategy if there is no storage facility.

Providing the application of the reference CO_2 supply strategy, the effect of a heat storage tank on a greenhouse with combined heat and power that produces electricity for its artificial illumination affects both the primary energy consumption and the yearly photosynthesis. The energy saving effect is due to the fact that the CHP engine runs irrespective of the heat demand. The production increment is a result of the increased CO_2 supply because the storage tank can also be used to store surpluses form the boiler when producing CO_2. For a greenhouse about equal to the reference greenhouse except for the illumination and the climate controller settings in November and December, the maximal decrement of specific energy consumption is 24% compared to the situation without a storage tank.

The third topic of the study on energy-saving heating devices concerned the application of a CHP engine that produces electricity for the public grid. In this case energy savings are achieved because electricity production with a high overall conversion efficiency at the greenhouse site replaces electricity production at a lower conversion efficiency elsewhere. Taking account of energy savings due to diminished primary energy consumption at public power plants, the reference greenhouse appear to be able to achieve energy savings of up to 32%, holding for a CHP engine with a thermal power of 100 W$_{th}$ per m^2 greenhouse (and an electric power of 63 W$_{el}$m^{-2}).

If the exhaust gases of the device can be cleaned to such an extent that they are suitable for CO_2 supply, a comparable saving is achieved for an engine having a thermal power of only 40 W$_{th}$m^{-2}.

7. CONCLUSIONS AND DISCUSSION

Under an official agreement with the government - the MJA - horticulture in the Netherlands has set itself the task of halving its primary energy consumption per unit of production by the end of the millennium, compared to its value in 1980. The quantity that describes the actual primary energy consumption per unit of production as a percentage to that holding for 1980 data is referred to by the ENSEC (Economically Normalized Specific Energy Consumption), defined as a formula in Eqn. 2.1. Thus, the target of the MJA is to achieve an ENSEC = 50 by the end of the century.

In the early 1980[s] the ENSEC decreased rapidly, reaching 60 in 1985, but then increased again to about 68. By the end of 1993 the ENSEC was 66. When the tendencies with respect to primary energy consumption and production value of the last five years are extrapolated toward the year 2000, the ENSEC at the end of the century is above 70. Thus, to reach the objective of the MJA, the tendency of the last years has to change drastically.

To achieve this, either production (the denominator of Eqn. 2.1) should increase or the primary energy consumption (the nominator) should decrease. However, with respect to the governmental objective to decrease the level of absolute CO_2 production, as cited in the MJA, a decrement of the nominator is much more favourable. This is because if the ENSEC is decreased by enhancement of production the absolute level of the primary energy consumption will severely violate the general governmental objective for the decrement of CO_2-exhaust. Therefore, the measures proposed in the MJA for the decrement of the ENSEC opt for a decrement in primary energy consumption. In this study, the perspectives of nine of these measures are analyzed.

The evaluation of the impact of the proposed measures in full-scale greenhouses is difficult because it is very hard to eliminate all other factors than the subject of survey. Moreover, full-scale experiments are expensive because the evaluations should span at least a year and, due to the large number of factors that determine energy-saving effects, a large number of experiments is required. Therefore the application of a computer model capable of computing the effects of energy conserving measures as a function of relevant parameters is to be preferred to full-scale measurements.

In order to be able to create enough, and physically interpretable parameters, a deterministic simulation model has been built by assembling a greenhouse climate controller with a greenhouse climate simulation model and a model that describes the greenhouse heating system devices. The model concerning the heating system devices comprised a description of the heating circuit, the boiler, the condenser, the expansion vessel, combined heat and power and a short-term heat storage faci-

lity. All sub-models for the heating system were developed for the present study. The model describing the greenhouse climate was based on the state-of-the-art as presented in the literature.

Prior to the application of models related to the computations of effects that can be expected from energy-saving measures, their results must first be shown to have a satisfying resemblance with reality.
From the sub-models describing the heating system, the heating circuit simulation and the sub-model for the heat storage facility were validated with measurements carried out on a research facility at IMAG-DLO. Both sub-models appeared to simulate the physical behaviour of these heating system components very well.
The sub-models for the boiler and the expansion vessel were not compared with measurements but with aggregated results presented in the literature. These comparisons showed large differences between modelling results and the results reported in literature. However, because it is reasonable to have considerable doubts about the results presented in the literature, the developed models were judged to be applicable with respect to the present work.
The assembled model, when compared to detailed measurements carried out on a semi-practical greenhouse (a research facility at IMAG-DLO) showed a good resemblance. Compared to long-term measurements on the same facility, the model described the yearly energy consumption with an accuracy of 2%.
When simulation models are to be applied in configurations that differ from the situation(s) in which it is validated, there should be no parameters that lack a physical interpretation. Moreover, such models should have not too many parameters that are difficult to measure or estimate. Both conditions were satisfied with the present model. Only a few parameters on mechanisms that cannot be readily measured (the impact of attachments on the overall heat exchange coefficient of heating pipes, the discretization of the velocity profile in a storage tank, canopy evaporation and the heat exchange through the thermal screen) were determined by iteration of model results with measurements.

To analyze the energy-saving options with the model developed a greenhouse of 1 hectare producing tomatoes in the Netherlands was taken as a reference. Of course, this reference greenhouse is only one example from the wide variety of greenhouses that can be found. If a different reference situation was chosen, which can be found easily, even among greenhouses growing tomatoes, many of the results presented in this work would change. Moreover, the model assumes that the heating system is well engineered. In practice, a heating system displays numerous shortcomings. Here one can think of a shortcut between the main supply pipe and the gathering pipe that prevents the storage tank being cooled down to the return water temperature of the heating circuit. Another shortcoming frequently encountered is the coupling of the storage tank to the heating system by pipes that are not

wide enough. This severely limits the heating power of the tank.

However, the computations on the reference greenhouse give a good impression of the tendencies of the energy saving measures. The studied topics were selected from the measures proposed in the MJA and were arranged in three items.

The first item comprised relatively simple improvements in the boiler house, involving the increment of insulation thickness of the boiler, the insulation of transport pipes and the replacement of the place of connection of the expansion vessel. The computations show that the energy savings achieved by these measures are small. Nevertheless, since the proposed measures are easy, and therefore relatively cheap to carry out, they can still be advantageous.

The second item of energy saving measures studied with the simulation model concerned the decrement of energy losses from the greenhouse cover by the decrement of leakage through windows, the application of a thermal screen and the application of alternative cladding materials (coated glass panes and double glazing).

Under the circumstances created to study the effect of the prevention of leakage through windows, the decrement of heat demand was small (1.6%). The other measures show energy savings ranging from 18% (a tin-oxide coating) up to 47% (an option using double glass where each glass is coated with a tin-oxide coating and a particular polymer coating). However, the thermal screen and most of the alternative cladding materials result in a decreased transparency of the greenhouse. This results in a decrement of photosynthesis. To combine the energy saving effect with the loss of production, the qualities of the thermal screen and the alternative cover materials are judged according to their impact on the decrement of the specific energy consumption. The specific energy consumption is defined as the yearly amount of primary energy required per unit of yearly photosynthesis. With respect to specific energy consumption, the achieved savings range from 10% (a tin-oxide coated cover) to 39% (double coated double glass).

An interesting aspect of increased insulation properties of the greenhouse cover is the increase of the energy demand of the greenhouse related to dehumidification. This effect was explained by the decreasing condensation against the inner side of the cover as the cover has a higher thermal resistance. Because the greenhouse climate controller does not allow the relative humidity in the greenhouse to exceed 85% RH, a decreased condensation is compensated for by increased ventilation. Thus, part of the benefits of the diminished heat loss from the cover is lost by extra ventilation.

The absolute amount of energy associated with dehumidification by opening windows is 240 $MJm^{-2}year^{-1}$ for an ordinary cladded greenhouse, 320 $MJm^{-2}year^{-1}$ for a greenhouse with HORTIPLUS and 380 $MJm^{-2}year^{-1}$ for a greenhouse with double glass. For the cover with the lowest heat loss (double-coated double glass) the

energy demand associated with dehumidification even becomes 450 $MJm^{-2}year^{-1}$ (40% of it primary energy consumption).

The large portions of energy associated with dehumidification stress the importance of the description of the vapour household in a greenhouse by the simulation model. Moreover, the fact that decreased condensation is compensated by extra ventilation means that savings are (highly) over-estimated if computed with the fraction that the heat flux through the insulating covering material has decreased compared to ordinary glass.

Judgement of energy saving properties by means of the effects on specific energy consumption rates primary energy saving equivalent to increment of production. This agrees with the definition of the ENSEC. However, with respect to practical horticulture the business economics effect of a decrement of the specific energy consumption by enhancing production is much larger (4 to 5 times) than if the same decrement of specific energy consumption is achieved by energy saving (providing that the costs related to the decrement are equal). This is due to the fact that the nominator affects the costs, whereas the denominator affects the benefits of production.

The third item of energy saving measures analyzed in this study concerned the application of a condenser, a short-term heat storage facility and a combined heat and power engine. It was shown that it is advantageous to be able to feed the condenser with return water from both heating circuits rather than with a connection to the low temperature heating circuit alone.

The energy-saving effects of the heat storage tank on a greenhouse without a CHP engine was shown to depend strongly on the CO_2 supply strategy. For a greenhouse that supplies CO_2 irrespective of the heat demand, a storage tank can decrease the primary energy consumption by up to 12%. If the supply strategy prevents heat surpluses having to be carried off by extra ventilation, the storage tank does not save primary energy, but rather enhances production. For this case, the model shows that the yearly photosynthesis can be increased by up to 25%.

The combination of both the effects by means of the computation of the specific energy consumption shows that the decrement of specific energy consumption can be up to 22%. For small heat storage tanks the supply strategy irrespective of the heat demand yielded a lower specific energy consumption than the supply strategy that prevents heat surpluses having to be carried off. Indeed, this CO_2 strategy is widely applied in present-day horticulture. In this context, it must be recalled that the business economics effect of the decrement of specific energy consumption by an increment in production is larger than the effect of the same decrement of specific energy consumption by primary energy saving.

If a heat storage tank is applied to a greenhouse using artificial illumination powered by an on-site CHP engine, providing the storage tank can be used by both the CHP engine and the boiler, the major benefits are related to CO_2 supply.

A large storage tank (80 m^3ha^{-1}) gives a 7% decrement of primary energy consumption but the extra production due to increased CO_2 supply (providing a CO_2 supply strategy that prevents extra ventilation is used) appears to be 18%. The resulting decrement of primary energy consumption can be up to 20%.

If a combined heat and power engine is used for the production of electricity for the public grid, energy savings can only be noticed when the decreased primary energy consumption at public power plants is subtracted from the significantly increased energy demand at the greenhouse site. In doing so, the reference greenhouse appears to be able to achieve energy savings of up to 32%, holding for a CHP engine with a thermal power of 100 W_{th} per m^2 greenhouse (and an electric power of 63 $W_{el}m^{-2}$). If exhaust gases of the device can be cleaned to such an extent that they are suitable for CO_2 supply, a comparable saving is achieved for an engine having a thermal power of only 40 $W_{th}m^{-2}$.

One aspect that has not been taken into consideration in the study on CHP for the public grid is the fact that the economic value of the electricity produced is not constant. During peak demands of electricity, the contribution of CHP engines (not necessarily in horticulture) can mean that large public power plants will not have to be switched on for just short times. This means that, because of the high value of electricity, during periods of high public electricity demand, it will be advantageous to assign a higher priority to CHP than to CO_2. Inclusion of this control strategy will lead either to a decreased energy saving (when the reject heat cannot be stored or applied in the greenhouse) or a decrement of CO_2 supply (in case the CHP engine prevents the boiler to produce CO_2). Thus, this strategy will lead to some increase of specific energy consumption. However, from a business economics point of view such a strategy can be very advantageous.

With respect to the energy savings figures resulting from an application of CHP to serve the public grid, it must be mentioned that by expressing the savings as in Section 6.3.4.3, all benefits of electricity production with CHP engines are attributed to horticulture. From a wider perspective (national scale) when comparing the primary energy consumption of public power plants producing electricity and horticultural boilers producing heat with the CHP alternative, the absolute savings, of course, are the same but the percentages become less.

Finally, it must be concluded that the simulation model developed has proved to be is a useful tool to judge the potentials of particular energy saving measures in a horticultural context.

REFERENCES

ALDRICH, R.A. and J.R. Sharp, 1989, *The IER vertical south roof greenhouse*. In: Energy saving in Protected Cultivation. ed. B.J. Bailey, Acta Horticulturae 245, Bedford.

American Institute of Physics Handbook, 3rd ed. 1972, McGraw-Hill Book Co, New York

BALEMANS, L., 1989. *Assessment of criteria for energetic effectiveness of greenhouse screens*. Ph.D. Dissertation, Agricultural University, Gent, 157 pp.

BAKKER, J., 1994. *Vraagtekens bij doel minimumbuis*. Vakdeel glasgroente, Groente & Fruit, 4(1994)2, pag 10-11

Basisgegevens aardgassen, 1980, N.V. Nederlandse gasunie, Groningen

BERRY, J. and O. Bjorkman, 1980. *Photosynthetic response and adaptation to temperature in higher plants*. Annual Review on Plant Physiology, 31:491-543

BOT, G.P.A. and J.J van Dixhoorn, 1978. *Dynamic modelling of greenhouse climate using a minicomputer*. Acta Horticulturae 76: 113-120

BOT, G.P.A., 1983. *Greenhouse climate: from physical processes to a dynamic model*. Ph.D. Dissertation, Agricultural University, Wageningen, 240 pp.

BREUER, J.J.G., and N.J. van de Braak, 1989, *Reference year for Dutch greenhouses.*, Acta Horticulturae nr 248, pag. 101-108

BRUNT, D., 1939, *Physical and Dynamical Meteorology*. Cambridge University Press.

CBS, 1994a, *Glastuinbouw 1992*. sdu/uitgevrij, 's-Gravenhage

CBS, 1994b, *Statistisch jaarboek 1994*. sdu/uitgevrij, 's-Gravenhage

COULSON, K.L., 1975, *Solar and Terrestrial Radiation*, Academic Press, New York

FRANCE, J. and J.H.M. Thornley, 1984, *Mathematical models in agriculture*. Butterworks, London

GEBHART, B., 1971, *Heat transfer*. 2nd ed. McGraw-Hill, New York

GIJZEN, H., 1992, *Simulation of photosynthesis and dry matter production of greenhouse crops*. Simulation report 28, CABO-DLO, Wageningen

GIJZEN, H., J.G. Vegter and E.M. Nederhoff, 1990, *Simulation of greenhouse crop photosynthesis: validation with cucumber, sweet pepper and tomato*. Acta Horticulturae 268:71-80

GOUDRIAAN, J., 1977, *Crop micrometeorology: a simulation study*. Simulation Monographs. Pudoc, Wageningen

GOUDRIAAN, J., 1986, *A simple and fast numerical method for the computation of daily totals of crop photosynthesis*. Agricultural and forest meteorology, 38:249-254

GOUDRIAAN, J., 1988, *The bare bones of leaf-angle distribution in radiation models for canopy photosynthesis and energy exchange*. Agricultural and forest meteorology, 43:155-169

HAM, P.J., 1984, *Mollier-h/x-diagrammen voor vochtige lucht, geconstrueerd door middel van de computer*. Klimaatbeheersing 13(1984)6

Handbook of chemisry and physics, Editor: R.C. Weast, 49th edition, The chemical rubber co., 1968

Handboek Verwarming Glastuinbouw, 1995, Editors: J.B. Verveer and C.D. Becqué, Nutsbedrijf Westland

HASHIMOTO, Y., G.P.A. Bot, W. Day, H.J. Tantau and H. Nonami, 1993, *The computerized Greenhouse*, Academic Press, San Diego

HENTEN, E.J. van and J. Bontsema, 1991, *Optimal control of greenhouse climate*. Proceedings of the IFAC/ISHS Workshop, Matsuyama, Japan. 27-32

HENTEN, E.J. van, 1995, *Greenhouse climate control, an optimal approach*, Ph.D. Dissertation, Agricultural University, Wageningen, 327 pp.

HOFSTEDE, G.J., 1992, *Modesty in modelling: on the applicability of interactive planning systems with a case study in pot plant cultivation*. Diss. Wageningen Agricultural University, Wageningen, The Netherlands

HOUTER, G. 1989, *Simulatie van het CO_2-verbruik in de glastuinbouw (modelbeschrijving)*. Proefstation voor Tuinbouw on de Glas, Naaldwijk

HOUTER, G. 1991, *ECP-model: Simulatiemodel voor energieverbruik, CO_2-verbruik en kg-produktie in de glastuinbouw (Eindverslag)*. Proefstation voor Tuinbouw on de Glas, Naaldwijk

JOLLIET, O. and B.J. Bailey, 1991. *The effect of climate on tomato transpiration in greenhouses: measurements and model comparison*. Agricultural and Forest Meteorology 1991, 58:43:62

JONG, T. de, 1985. *Metingen aan en simulatie van het kasklimaat*. M.Sc. Dissertation, Agricultural University, Wageningen

JONG, T. de, 1991. *Natural ventilation of large multispan greenhouses*. Ph.D. Dissertation, Agricultural University, Wageningen

LJUNG, L., 1987, *System identification: theory for the user*. Prentice-Hall, New Jersy, 519 pp.

KLEINBACH, E.M., W.A. Beckman and S.A. Klein, 1993, *Performance study of one-dimensional models for stratiefied thermal storage tanks*. Solar Energy, 50(1993)2, pp. 155-166

KLIMSTRA, J., 1991. *De energiehuishouding van warmte/kracht-installaties 2*. Gas, 4(1991), pp. 166-171

Kwantitatieve informatie voor de glastuinbouw 1992-1993, Groenten, Snijbloemen, Potplanten, 1992, Informatie en Kennis Centrum Akker- en Tuinbouw, Afdeling Bloemisterij/Afdeling Glasgroente en Bestuiving, Aalsmeer/Naaldwijk.

MAVROS, P., V.Belessiotis and D. Harambopoulos, 1994. *Stratified energy storage vessels: characterization of performance and modeling of mixing behaviour*. Solar Energy, 52(1995)4, pp. 327-336

Meerjarenafspraak tussen de Nederlandse glastuinbouwsector en de Staat vertegenwoordigd door de Ministers van Economische Zaken en Landbouw, Natuurbeheer en Visserij over de verbetering van de energie-efficiëntie, 1992, Landbouwschap, Den Haag

MEIJNDERT, J., 1983, *Juiste keuze maken bij toepassing rookgascondensor*. Vakblad voor de bloemisterij 38(1983)3, pp. 72-75.

MIGUEL, A.F., N.J. van de Braak and G.P.A Bot, 1995, *Mass flow through materials with pores and openings: II-natural convection*, submitted for publication in International Journal of Heat and Mass Transfer.

MONSI, M. and Saeki, T., 1953, *Uber den Lichtfaktor in den Pflanzengesellschaften und seine Bedeutung für die Stoffproduktion.* Japanese Journal on Botany, 14:22-52

MONTEITH, J.L., 1961, *An emperical method for estimating long wave radiation exchanges in the Britsh Isles.* Quarterly Journal of the Royal Meteorological Society, 87, 171

MONTEITH, J.L., 1973, *Principles of environmental physics.* Edward Arnold, London, 241 pp.

MORRIS, C.W. and Lawrence, J.H., 1971, *The anisotropy of clear sky diffuse solar radiation.* Transactions of the ASHRAE 77 (2): 136-142

MUIJZENBERG, E.W.B. van den, 1980, *A history of greenhouses.* Institute of Agricultural Engineering (IMAG-DLO), Wageningen, 435 pp.

MYNENI, R.B., J. Ross and Asrar, G., *A review of the theory of photon transport in leaf canopies*, Agricultural and Forest Meteorology, 45(1989)1-153

Nationaal milieubeleidsplan-plus, (in Dutch), SDU, 's-Gravenhage, 1989

NAWROCKI, K.R. and N.J.A. van der Velden, 1991, *Gebruiksrendementen aardgasgestookte ketels in de glastuinbouw; gissen is missen, meten is (z)weten.* IMAG-DLO, Nota 91-55, 81 pp.

Novem Energiegids, Van Haalen & Partners, Sittard, 1994

OUT, P.G., and J.J.G. Breuer, 1995, *Effect van gecoat glas op de lichttransmissie en het energieverbruik van tuinbouwkassen*, IMAG-DLO, Wageningen, rapport 95-1

OVERSLOOT, H.P., 1992, *Optimale integratie van WK-systemen in bestaande verwarmingssystemen met warmtebuffers in de glastuinbouw.* TNO-rapport B-92-1048, Delft,

PALM, W.J., 1986, *Control systems engineering.* Wiley, New York, 695 pp.

PITS, D.R. and L.E. Sissom, 1986, *Heat transfer.* Schaum, Singapore, 325 pp.

Polytechnisch zakboekje, Editors: M.R. Creemers *e.a.*, PBNA. Arnhem, 1987

RIJSDIJK, A., 1993. *Minimumbuis ter discussie.* Vakdeel glasgroente, Groente & Fruit, 3(1993)45, pag 24-25

SCHINKEL, W.M.M., 1980, *Natural convection in inclined air-filled enclosures*, Phd Thesis TUD, Delft, 342 pp.

SELLERS, W.D., 1965, *Physical Climatology.* University of Chicago Press.

SEGINER, I., A. Angel, S. Gal and D Kantz, 1986, *Optimal CO_2-enrichment strategy for greenhouses. A simulation study.* Journal of Agricultural Engineering Research, 34:285-304.

SEGINER, I. and A. Sher, 1993, *Optimal greenhouse temperature trajectories for a multi-state-variable tomato model.* In The Computerized Greenhouse, Academic Press, New York, 340 pp.

SLUIS, B.J. van der, K.R. Nawrocki and N.J.A. van der Velden, 1992, *Dekkingsgraden van restwarmte in de glastuinbouw.* Landbouw-Economisch Instituut, Den Haag, 68 pp.

173

SPARROW, E.M. and R.D. Cess, 1970, *Radiation heat transfer*. Brooks/Cole publishing Co, Belmont, California.

SPITTERS, C.J.T., H. van Keulen and D.W.G. van Kralingen, 1989, *A simple and universal crop growth simulator: SUCROS87*. In: R. Rabbinge, S.A. Ward and H.H. van Laar (eds.). Simulation and system management in crop production. PUDOC, Wageningen, pp 147-181

SPRENGER, E. and W Hönmann, 1983, *Taschenbuch für Heizung und Klimatechnik*. Oldenburg, München.

STANGHELLINI, C., 1987, *Transpiration of greenhouse crops, an aid to climate management*. Ph.D. Dissertation, Agricultural University, Wageningen: 150 pp.

SWINBANK, W.C., 1963. *Long wave radiation from clear skies*. Quarterly Journal of the Royal Meteorological Society, 89, 339

TAKAKURA, T. 1992. *Climate under cover*. Kluwer Academic Publishers, Dordrecht, 155 pp.

UDINK TEN CATE, A.J., 1983. *Modeling and (adaptive) control of greenhouse climates*. Ph.D. Dissertation, Agricultural University, Wageningen: 159 pp.

VELDEN, N.J.A. van der and B.J. van der Sluis, 1993, *Energie in de glastuinbouw van nederland in 1991; ontwikkelingen in de sector en op de bedrijven*. LEI-DLO, Den Haag, 85 pp.

VELDEN, N.J.A. van der, B.J. van der Sluis and A.P. Verhaeg, 1995, *Energie in de glastuinbouw van nederland; ontwikkelingen in de sector en op de bedrijven t/m 1993*. LEI-DLO, Den Haag, 76 pp.

VERHOEVEN, A.T.M., F.L.K. Kempkes and N.J.A. van der Velden, 1995, *Warmte/kracht-installaties in de glastuinbuow; gebruiksrendementen en dekkingsgraden*. LEI-DLO, Den Haag,76 pp.

VERMEULEN P., 1987, *Kosten en baten CO_2 doseren in de zomer: CO_2 doseren met warmteopslag is rendabel*, Vakblad voor de bloemisterij (1987)4, p. 40-43.

VERMEULEN, P. and H. van de Beek, 1992, *Beslissingsmodel voor CO_2 in de glastuinbouw; investeringsselectie & doseertaktiek; aanvullend CO_2 doseren en warmteopslag; kwantitatieve informatie*. PTG-verslag nr 14, Naaldwijk, 88 pp.

Vademecum voor de glastuinbouw 1978, 1978, Landbouw economisch instituut, Den Haag.

YOO H. and E. Pak, 1993, *Theoretical model of the charging process for stratified thermal storage tanks*. Solar Energy, 51(1993)6 pp. 513-519

APPENDICES

APPENDIX A: CONVECTIVE HEAT EXCHANGE

In his thesis, Balemans (1989) presented a thorough review of the literature on convective heat exchange. Therefore, this appendix is based on the results presented in his work.

Typically, convective heat exchange processes in a greenhouse are governed by free convection. Only the convective heat exchange at the outside of the greenhouse cover can be considered to be forced by wind speed. Thus, except for the heat losses at the cover, the Nusselt number describing the exchange process can be defined as a function of the Raleigh number (Ra). The Raleigh number is defined by

$$Ra = g \, \beta \, \Delta T \, X^3/(\nu \, a) \qquad \text{[-] (A.1)}$$

With g the gravitational acceleration (9.8 ms^{-2}), β the thermal expansion coefficient (K^{-1}), ΔT the temperature difference (K), X the characteristic dimension (m), ν the kinematic viscosity (m^{2}s^{-1}) and a the thermal diffusivity (m^{2}s^{-1}). Taking $\beta = 1/283$ K^{-1}, $\nu = 1.42 \cdot 10^{-5}$ m^{2}s^{-1} and a$= 1.8 \cdot 10^{-5}$ m^{2}s^{-1} the Raleigh number appears to be

$$Ra = 1.30 \cdot 10^8 \, \Delta T \, X^3 \qquad \text{[-] (A.2)}$$

The temperature differences between the heat exchanging surfaces range between around 5 °C for the enclosing surfaces of the greenhouse envelope and up to 50 °C for the heat release from the heating pipes. The Raleigh number characterizing the heat exchange at the enclosures of the greenhouse air (floor, screen and cover) lies in the order of magnitude of $1 \cdot 10^9$. The Raleigh number for the heat exchange process from the heating pipes lies in the order of magnitude of $1 \cdot 10^6$. For the upward heat release from a horizontal surface in the considered order of magnitude for Ra, Balemans reports on two authors, presenting the same relation for Nu as a function of Ra, namely Nu $= 0.14$ Ra$^{0.33}$.

On an inclined surface, such as the greenhouse cover, a first approximation is to multiply the Ra number in the Nu-Ra relation with a factor cos(ψ), where ψ is the angle with the horizontal. Thus the driving force, *i.e.* the gravitational acceleration, for which the Ra number takes account, is attenuated. Indeed, Gebhart (1971) shows that this approach yields satisfactory results.

A downward heat flux (which may occur at the floor surface in the morning), holding for the considered value of Ra, is mentioned by only one author, who reports Nu $= 0.27$ Ra$^{0.25}$.

The Nu-Ra relation for heat release at the heating pipes is derived from Monteith (1973). He mentions a relation reading Nu $= 0.48$ Gr$^{0.25}$. Tor air, this relation can be rewritten as Nu $= 0.50$ Ra$^{0.25}$.

The simulation model uses a heat exchange coefficient (expressed in $Wm^{-2}K^{-1}$), which can be found from the Nusselt number by stating that

$$\alpha = Nu \; \lambda/X \qquad\qquad\qquad [Wm^{-2}K^{-1}] \; (A.3)$$

With λ the thermal conductivity of air ($0.024 \; Wm^{-1}K^{-1}$) and X the characteristic dimension.

Combining Eqn. A.2, Eqn. A.3 and the theoretic Nu-Ra relations the heat exchange coefficient for an upward heat flux is stated by:

$$\alpha_{up} = 1.70 \; (\cos \psi)^{0.33} \; \Delta T^{0.33} \qquad\qquad [Wm^{-2}K^{-1}] \; (A.4)$$

Note that the characteristic dimension has disappeared from the equation and that for a horizontal plate $\cos(\psi) = 1$. Unfortunately, the downward heat flux and the heat exchange coefficient for the heating pipe does not omit the characteristic dimension.

$$\alpha_{down} = 0.70 \; X^{(-0.25)} \; \Delta T^{0.25} \qquad\qquad [Wm^{-2}K^{-1}] \; (A.5)$$

$$\alpha_{pipe} = 1.28 \; X^{(-0.25)} \; \Delta T^{0.25} \qquad\qquad [Wm^{-2}K^{-1}] \; (A.6)$$

The characteristic dimension of a heating pipe is simply the diameter of the pipe, but it is questionable what should be used as a characteristic dimension of a greenhouse floor. A first approximation could be to take half the diameter of the Bernard-cells in which the air circulates. Assuming the Bernard-cells to cover an area with a diameter of about 6 meters the characteristic dimension would be 3. Substituting this characteristic dimension in Equation A.5 makes the heat exchange coefficient for the downward heat flux at small temperature differences comparable to the heat exchange coefficient for the reverse case.

APPENDIX B: RELATION BETWEEN MASS AND HEAT TRANSFER

Mass transfer to or from objects suspended in a moving airstream is analogous to heat transfer by convection. Where for heat exchange the Nusselt number describes the rate of heat exchange by $H = Nu\ \lambda\ \Delta T/X$, mass transfer can be described by a similar equation $M = Sh\ D\ \Delta c/X$, with M the mass transfer rate per unit surface area ($kgm^{-2}s^{-1}$), Sh the Sherwood number, D the molecular diffusivity (m^2s^{-1}), Δc the vapour concentration difference (kgm^{-3}) and X the characteristic dimension (m) (Monteith, 1973). Because of the analogy between heat and mass transfer, the Sherwood number can be computed from Nu with the relation $Sh = Nu\ (a/D)^m$, with a the thermal diffusivity (m^2s^{-1}). The power m equals 0.25 for laminar conditions and 0.33 when the transfer process is turbulent. The ratio a/D is also referred to as the Lewis number (Le). For water vapour in air Le is 0.89. In the former section the Raleigh number for the heat exchange at the horizontal (or slightly inclined plates) indicated a turbulent exchange process. Thus the mass transfer rate can be defined as a function of Nu by:

$$M = Nu\ (0.89)^{0.33}\ D\ \Delta c/X \qquad\qquad [kgm^{-2}s^{-1}]\ (B.1)$$

After substituting Nu by an expression of α the characteristic dimension disappears from the equation and λ appears in the denominator.

$$M = \alpha\ (0.89)^{0.33}\ D/\lambda\ \Delta c \qquad\qquad [kgm^{-2}s^{-1}]\ (B.2)$$

Equation B.2 relates the mass transfer rate to a concentration difference, but the simulation model defines the humidity as a vapour pressure, expressed in Pa (Nm^{-2}). Therefore a conversion from vapour pressure difference to concentration difference must be performed, which can be realized by application of the gas law.

$$\Delta c = \frac{M}{R} \left\{ \frac{P_1}{T_1} - \frac{P_2}{T_2} \right\} \qquad\qquad [kgm^{-3}]\ (B.3)$$

with M the molecular weight (18 $kgkmol^{-1}$ for water vapour), R the universal gas constant (8314 $Jkmol^{-1}K^{-1}$), P_1 and P_2 the vapour pressures of the mass exchanging entities (Nm^{-2}) and T_1 and T_2 their temperatures (K). Considering that the temperature differences will not be very large, a mean temperature of 287 K for both T_1 and T_2 can be used to make the concentration difference dependent on a vapour pressure difference only. At a temperature of 287 K and with $D = 2.2 \cdot 10^{-3}$ and $\lambda = 2.5 \cdot 10^{-2}$ and after combination of Eqn. B.3 and B.2 the mass transfer rate is described as a function of vapour pressure difference and related to the heat transfer coefficient by:

$$M = \alpha\ 6.4 \cdot 10^{-9}\ \Delta P \qquad\qquad [kgm^{-2}s^{-1}]\ (B.4)$$

APPENDIX C: TRANSMISSIVITY OF A GREENHOUSE COVERING STRUCTURE

Short-wave solar radiation which encounters a greenhouse is either reflected, transmitted or absorbed by the covering structure. For direct radiation the transmitted (and reflected) fraction depends strongly on the angle of incidence between the ray of incoming radiation and the intercepting glass panes. Diffuse radiation comes from all directions in the hemisphere. The intensity of diffuse radiation from a specified solid angle in the hemisphere can be defined by a distribution function. In the literature several of these functions are mentioned (Coulson, 1975; Morris and Lawrence, 1971). Most of these functions define the intensity irrespective of the actual solar position. Only the circumsolar distribution function relates the intensity of diffuse radiation to the angular distance from the sun.

Irrespective of the assumed distribution function the diffuse transmissivity can be computed by a numeric integration of a large number of direct transmissions, each given the weight in accordance with the distribution function. Thus, here the direct transmissivity of the greenhouse for direct radiation is determined first.

C.1 Direct transmissivity

To compute the transmitted radiation as a function of the angle of incidence, the theory discussed in the following article can be applied. This paper was reprinted with the kind permission of the publisher.

Determination of Direct Transmission of a Multispan Greenhouse Using Vector Algebra

H. F. de Zwart

Agricultural Research Department, Institute for Agricultural Engineering (IMAG-DLO), P.O. Box 43, NL-6700 AA Wageningen, The Netherlands

The transmission of a multispan infinite greenhouse cover for direct radiation is calculated as a function of greenhouse geometry and solar position. The calculation allows for the shading effect of the main construction elements. The solution method is based on vector algebra. It appears that the use of vectors that denote the orientation of the planes in the greenhouse cover leads to a clear, and easy to understand calculation scheme. Therefore, the method presented here can be applied to other situations as well. Due to the compact and unambiguous notation, and assuming the availability of software suitable for vector algebra, programming effort is considerably diminished.

The results of the solution method are compared with the model of Bot, which employs similar assumptions, but based on goniometric expressions. Calculations were made for the direct transmissivity of a venlo-type greenhouse and similar results were obtained.

1. Introduction

Shortwave solar radiation entering the greenhouse is an important energy source. For plant growth, solar radiation is the only source, or in cases where artificial illumination is used, the major source of PAR (Photosynthetic Active Radiation). Many modellers have developed and published schemes to calculate the transmissivity of a greenhouse, as a function of its geometry and orientation.[1-9]. Some of these models are concerned with light transmission of small, single span greenhouses.[2,3] Others have calculated the transmission of large multispan greenhouses, assuming an infinite cover.[1,4] More recent papers present models with more general and comprehensive calculation schemes.[6-9]

An important objective of many models is to determine a 'figure of merit' for the transmissivity of different greenhouse constructions. The shape and orientation of covering structures were compared and improved.[6-9] Because of this interest in global behaviour, the focus has changed from a detailed description of transmission to a more general approach. Another objective in building a transmission model is to get accurate information on the transmissivity of a greenhouse at each moment of the day.[2,4] This transmissivity, as a function of solar position, can be used in simulation models of canopy crop growth[2] or greenhouse climate models.[4] For this reason Bot[4] developed an extensive model holding for an infinite greenhouse cover. However, his model requires much programming effort, owing to the large amount of extensive goniometric expressions. The determination of the shading effects of construction elements in his model is especially complicated.

The model presented in this paper follows the outline of Bot's model but performs the

Notation

B	bar distance vector	R_{2p}	projection of R_2 on D
$C_1 \ldots C_4$	vector to corner points of the cross section of a glazing bar	t_{t1}	transmissivity of the f_1 fraction of D
D	vector from one gutter to the next	t_{t2}	transmissivity of the f_2 fraction of D
d	gutter distance. m	$U_1 \ldots U_3$	three gutter corner points
$E_1 \ldots E_3$	three ridge corner points	ω	solar elevation, deg
h	height of ridge above gutter, m	$e_1 \ldots e_3$	fraction of the three ridge corner point shadows with respect to D
f_1, f_2	fractions of the light beam		
G	gutter direction vector	$\mu_1 \ldots \mu_3$	fraction of the three gutter corner point shadows with respect to D
$\mathbb{I}$	three-dimensional light beam vector		
I	two-dimensional light beam vector (projection in the xz-plane)	λ	multiplication factor between D and R_p
i	angle of incidence, deg	λ_2	multiplication factor between D and R_{2p}
L_1, L_2	two-dimensional light beam vector projected in the $y\mathbb{N}_1$ and $y\mathbb{N}_2$ plane respectively	ν	multiplication factor between B and the projections of $C_1 \ldots C_4$
N_I	normal on the two-dimensional light beam vector I	ψ	roofslope. deg
		ρ	reflection coefficient
$\mathbb{N}_1, \mathbb{N}_2$	normal on pane $\mathbb{R}_1$ and $\mathbb{R}_2$ respectively	ρ_{inward}	reflection on inner sides of the $\mathbb{R}_2$ panes
n	number of spans passed by the light beam	τ	transmission coefficient
		τ_1, τ_2	transmission coefficient of a pane $\mathbb{R}_1$ and pane $\mathbb{R}_2$
$\mathbb{R}_1, \mathbb{R}_2$	set of two vectors describing a glass pane	τ_{b1}, τ_{b2}	transmissivity of the bars in the $\mathbb{R}_1$ and $\mathbb{R}_2$ pane
R_1, R_2	projection of $\mathbb{R}_1$ and $\mathbb{R}_2$ in the xz-plane respectively	τ_{cover}	total transmissivity of the cover
		ζ_g	azimuth of the greenhouse. deg
R_p	projection of a pane on d	ζ_s	azimuth of the sun. deg

calculation in a much more efficient way by the use of vector algebra. Moreover, vector algebra improves the understanding of the method and the calculation of shading by construction elements is simplified.

This paper treats only the direct transmission. Diffuse transmissivity can be calculated by taking the weighted average of the direct transmissivities. Distribution functions to determine the relative weight to be assigned to the direct transmissivities for the different angles of incidence can be found in the literature.[4,7,10]

2. Theory

2.1. *A greenhouse in vector notation*

In general. a greenhouse cover is constructed of repeating roof elements. Due to this regularity the cover can be characterized by three parameters (see *Fig. 1*). The *azimuth*

Fig. 1. Basic greenhouse geometry with ζ_g the azimuth, ψ the roofslope and d the gutter distance

(ζ_g) indicates the angle between the gutter of the greenhouse and the north–south direction. The *roofslope* (ψ) and the *gutter distance* (d) determine the geometry of the roofpane.

To solve the transmission problem all directional indications (greenhouse construction and incident light beams) are expressed as vectors in a coordinate system related to the greenhouse (see *Fig. 2*). The light beam vector, $\mathbf{l}$, is defined as:

$$\mathbf{l} = \begin{pmatrix} \sin(\zeta_s - \zeta_g)\cos(\omega) \\ \cos(\zeta_s - \zeta_g)\cos(\omega) \\ -\sin(\omega) \end{pmatrix} \tag{1}$$

With ζ_s azimuth of the sun, ζ_g azimuth of the greenhouse. e solar elevation.

Due to symmetry, only light from the third quadrant of the *xy*-plane needs to be

Fig. 2. Vectors in the greenhouse co-ordinate system with $\mathbf{l}$, the light beam vector, ω, the solar elevation, ζ_s and ζ_g, the azimuth of the sun and the greenhouse respectively. $h = \frac{1}{2}d\tan(\psi)$

studied. Light entering from other directions can be mirrored to the third quadrant. The two roof parts are panes in a three-dimensional space. Each of these panes (R_1 and R_2) can be described by a set of two vectors.

$$R_1 = \begin{pmatrix} \tfrac{1}{2}d \\ 0 \\ h \end{pmatrix} \begin{pmatrix} 0 \\ 1 \\ 0 \end{pmatrix} \qquad R_2 = \begin{pmatrix} -\tfrac{1}{2}d \\ 0 \\ h \end{pmatrix} \begin{pmatrix} 0 \\ 1 \\ 0 \end{pmatrix} \tag{2}$$

where $h = \tfrac{1}{2}d \tan(\psi)$, is the height of the ridge above the gutter. The second vector of each pane is the gutter direction vector, G. The transission and reflection of a glass pane depends on the angle of incidence with the normal of the glass panes. The normals N_1 and N_2, corresponding with R_1 and R_2 are given by:

$$N_1 = \begin{pmatrix} h \\ 0 \\ -\tfrac{1}{2}d \end{pmatrix} \qquad N_2 = \begin{pmatrix} h \\ 0 \\ \tfrac{1}{2}d \end{pmatrix} \tag{3}$$

2.2. *Calculation of the transmission through the glass panes*

Given both the normal to each plane and the incident light vector the angle of incidence (i) can be calculated using an adapted cosine rule.

$$i = \arccos\left(\frac{\mathrm{abs}\{(I, N)\}}{|I|\,|N|}\right) \tag{4}$$

where (I, N) means the scalar product of I and N. $|I|$ and $|N|$ mean lengths of I and N respectively ($|N| = \sqrt{(N, N)}$). *The adaption is the 'abs' operator, providing an angle of incidence between 0 and $\tfrac{1}{2}\pi$.*

If the angle of incidence (i) is known, the reflection (ρ), transmission (τ) and absorption coefficient (α) can be determined. The theory of transmission and reflection of transparent surfaces is not relevant in the discussion of the vector approach to the transmission problem. Therefore only a graphical representation of ρ and τ is presented here for glass, the most used cladding material (see *Fig. 3*). These graphs were determined by using the Fresnel equations (e.g. Corson and Lorraine,[11] Jelimenko[12]).

2.3. *Transmission of a greenhouse construction*

With a high solar position the direct sunlight partly passes through the roofpanes R_1 and R_2. This situation is depicted in *Fig. 4*. The picture is a two-dimensional projection of the greenhouse on the xz-plane. Because the previously defined vectors to determine the greenhouse construction and light incidence were calculated in an orthonormal co-ordinate system, the transition to the new two-dimensional orthonormal system can be performed by just leaving out the y co-ordinate of the vectors. In so doing, the second vector describing the panes R_1 and R_2 [see Eqn (2)] disappears and the following new, two-dimensional vectors are derived.

$$R_1 = \begin{pmatrix} \tfrac{1}{2}d \\ h \end{pmatrix} \qquad R_2 \begin{pmatrix} -\tfrac{1}{2}d \\ h \end{pmatrix} \qquad I = \begin{pmatrix} \sin(\zeta_s - \zeta_g)\cos(\omega) \\ -\sin(\omega) \end{pmatrix} \tag{5}$$
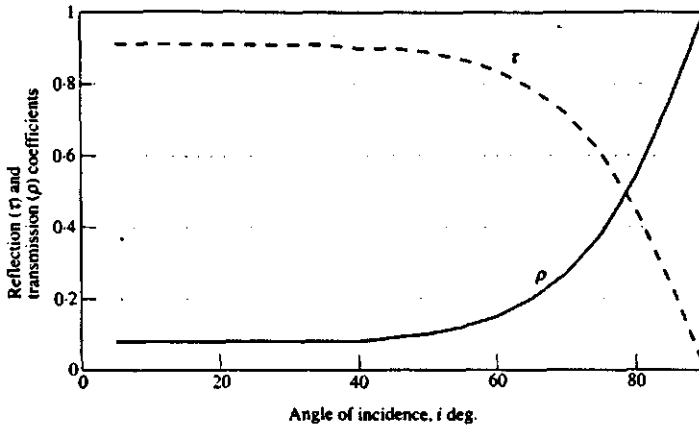
Fig. 3. Reflection (ρ) and transmission coefficient (τ) of a 4 mm thick glass pane, as a function of angle of incidence

The transmission pattern is repeated for every gutter-to-gutter distance. Therefore, the calculation is performed on the direct transmission entering one roof-section only.

The transmission is the sum of the light transmitted by the panes R_1 and R_2. By using Eqn (4) the angles of incidence can be determined and a transmittance for both the panes can be ascertained. The separation of the beam between two ridges into a part through R_1 and a part through R_2 is determined by the fractions f_1 and f_2 (see *Fig. 4*).

A careful study of *Fig. 4* shows that the part of the light beam through R_2 is the projection of R_2 along the direction of I on D, where D is the vector pointing from one gutter to the next.

$$D = \begin{pmatrix} d \\ 0 \end{pmatrix} \tag{6}$$

The projection is defined by:

$$R_p = \lambda D \tag{7a}$$

with

$$\lambda = \frac{(N_I, R)}{(N_I, D)} \tag{7b}$$
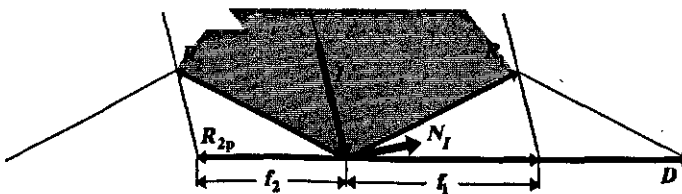
Fig. 4. Transmission and reflection on the greenhouse cover at high solar positions. R_{2p} is the projection of the vector R_2 on D, N_I is the normal to I

Where N_I is the normal of I in the xz-plane, calculated by:

$$N_I = \begin{pmatrix} \sin(\omega) \\ \sin(\zeta_s - \zeta_g)\cos(\omega) \end{pmatrix} \tag{8}$$

As can be seen in *Fig. 4* the fraction f_2 is the length of the projection of R_2, marked R_{2p}, with respect to D. f_2 can be calculated by:

$$f_2 = |R_{2p}|/|D| \tag{9}$$

However, the signed length ratio was, in fact, already defined by the term λ in Eqn (7b). When the multiplication factor for the projection of R_2 on D is denoted λ_2, f_2 can be calculated by:

$$f_2 = \mathrm{abs}(\lambda_2) \tag{10}$$

The absolute value provides f_2 a positive number. The fraction f_1 is the fraction of light through the panes R_1. It is the complement of f_2.

$$f_1 = 1 - f_2 \tag{11}$$

For the case where the solar elevation angle (projected in the xz-plane) exceeds the roofslope, the transmission of the greenhouse cover can be expressed as:

$$\tau_{cover} = f_1\tau_1 + f_2\tau_2 \qquad \{\lambda_2 < 0\} \tag{12}$$

where τ_1, and τ_2 transmission coefficients of R_1 and R_2 respectively [with an angle of incidence calculated by Eqn (4)]

Reflections at the outer sides of the covering glass panes, marked by a grey shading in *Fig. 5*, are directed away from the cover. This holds for both panes R_1 and R_2 as long as the projected angle of incidence exceeds three times the roofslope. When the projected angle of incidence lies between ψ and three times the roofslope the reflections from R_2 interact with R_1. However, the large angle of incidence with R_1 results in a high secondary reflection on that glass pane. Thus the amount of light reflected by R_2, followed by transmission through R_1 is negligible. Therefore, no further attention is paid to the reflections of the outer sides of the cover at high solar positions.

The next situation is when the light beam intercepts the greenhouse with an angle smaller than the roofslope. This is shown in *Fig. 5*. In this case, all radiation first passes
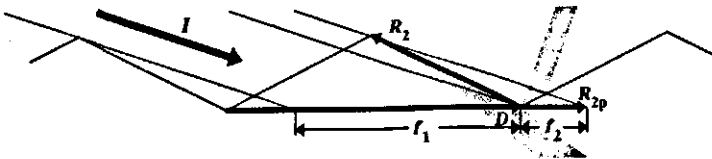
Fig. 5. Transmission and reflection of a light beam with an angle of incidence smaller than the roofslope
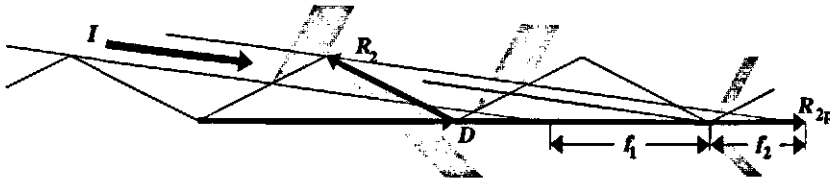
Fig. 6. Transmission and reflection of light coming in at very low elevation angles.

through R_1. After passing through R_1 part is transmitted by R_2, followed by passing through another pane R_1. Although R_{2p} is now pointing in the same direction as D, the fraction of the light passing these three panes is still represented by R_{2p}. Therefore, f_2 and f_1 can still be calculated by Eqns (10) and (11).

Fig. 6 shows a situation where the solar elevation has dropped to such an angle that all light passes more than one glass pane before reaching the greenhouse floor. It will be noted from *Fig.* 6 that R_{2p} has grown longer than D itself. However, the beam of light falling in between two ridges can still be divided into two parts. The part f_1 is transmitted twice by a R_1 pane and once by a R_2 pane. The other part (f_2) is transmitted by three R_1 and two R_2 panes. It can be shown that f_2 can be expressed as:

$$f_2 = \text{fractional}\,(\lambda_2) \tag{13}$$

Where "fractional" means the fraction part of the expression in the brackets [e.g. fractional $(1\cdot23) = 0\cdot23$]. f_1 is still determined by Eqn (11).

Both the expressions for f_2, namely Eqns (10) and (13), can be combined to derive a general expression.

$$f_2 = \text{fractional}\,[\text{abs}\,(\lambda_2)] \tag{14}$$

As demonstrated in *Figs* 5 and 6, the amount of roof sections passed by a light beam increases when the angle of incidence decreases. It can also be seen that light reflected on the inner side of the panes, R_2 (coloured grey) contributes to the amount of light coming into the greenhouse. A suitable indication of the number of passed glass panes is λ_2, as calculated by Eqn (7b). The situation of *Fig.* 5 is typical when λ_2 is between 0 and 1. *Fig.* 6, where the entire beam passes through the panes R_1 and R_2, before it splits in f_1 and f_2, is typical for the situation where $1 \leqslant \lambda_2 < 2$. It appears that the situation changes with the truncated value of λ_2. Therefore, a new number (n) is introduced with the definition:

$$n = \text{trunc}\,(\lambda_2) \tag{15}$$

where the operator "trunc" is supposed to generate the integer part of the number λ_2. Given n, the transmission for the f_1 and f_2 part of the beam can be determined.

$$
\begin{aligned}
t_{11} &= \tau_1^{n-1}\,\tau_2^{n} \\
t_{12} &= \tau_1^{n+2}\,\tau_2^{n+1}
\end{aligned}
\qquad \{\lambda_2 \geqslant 0\} \tag{16}
$$

Besides the transmitted light, some light also enters the greenhouse by reflection against the inner side of the passed R_2 panes (see the down-directed, grey-coloured reflection beams in *Figs* 5 and 6). The fraction of the outside light beam reflected inward is

expressed by:

$$\rho_{\text{inward}} = \rho_2\left(\left(\sum_{j=1}^{n} \tau_1^j \tau_2^{j-1}\right) + f_2 \tau_1^{n+1} \tau_2^n\right) \tag{17}$$

where ρ_2 denotes the reflection coefficient of R_2 [with an angle of incidence calculated with Eqn (4)]. The first term between the large brackets contributes to the attenuation of the entire beam due to the multiple passing of R_1 and R_2 panes. The second term expresses the extra attenuation of the f_2 fraction, which passes two panes more than the f_1 fraction.

Now the total transmission can be determined from

$$\tau_{\text{cover}} = f_1 t_{t1} + f_2 t_{t2} + \rho_{\text{inward}} \tag{18}$$

The calculation scheme presented is suitable as long as the projected solar elevation (the angle between D and I) is not too small, because n grows to infinity as the projected solar elevation tends to 0. However, the shadowing of construction parts at low elevation angles prohibits transmission anyway. Therefore, it is recommended that the transmission calculation should be discontinued when $\lambda_2 > 10$.

2.4. *Shadowing of ridges and gutters*

In the previous section a theoretical greenhouse cover was observed, consisting of glass panes only. In practice, construction elements support the cover (see *Fig. 1*). Therefore, a cross-section along the cover, with exaggerated ridges and gutters, looks more like Fig. 7. In the figure, six corner points (E_1, E_2, E_3 and U_1, U_2, U_3) play a role in the shadowing problem. The corner points are projected on the horizontal plane, yielding (e_1, e_2, e_3 and μ_1, μ_2, μ_3). These projections can be calculated with Eqn (7b), just like the calculation of λ_2, being the projection of R_2. In the constructed situation of *Fig. 7*, the value of all ε and μ are positive, due to the choice of the $(0,0)$ co-ordinate.

From the picture it is obvious that the fraction shaded by the gutter can be expressed as $\mu_3 - \mu_1$. The width of the beam coming in between the two ridges can be determined by $e_3 - e_1$. Thus, the unmasked part of the light beam can be determined simply by
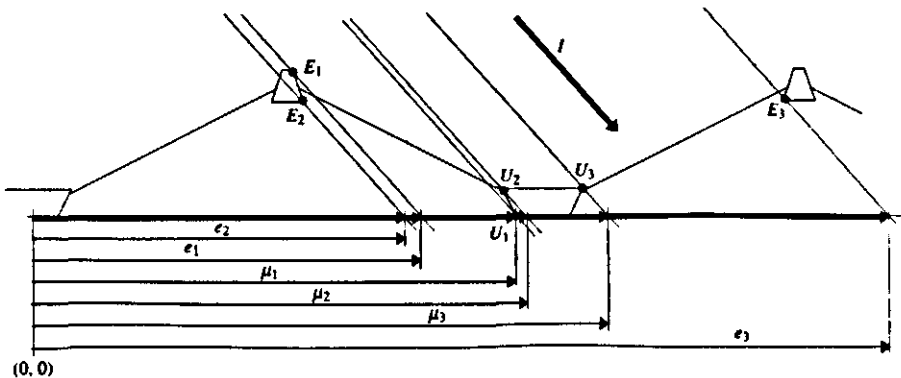
Fig. 7. Cross-section of a greenhouse ridge-gutter system
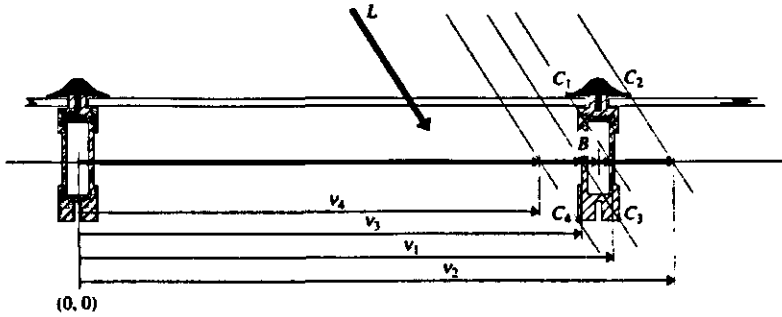
Fig. 8. Cross-section of a greenhouse covering pane. B is the bar-distance vector. C_1, C_2, C_3 and C_4 are corner points

comparing the lengths of a set of corner point projections. In the situation shown in *Fig. 7*, the unmasked fraction is the width of the beam, diminished by the width of the gutter shadow. Even a (partial) coincidence of the shades of a ridge and a gutter can be detected easily by analysing the lengths of the projections.

2.5. *Shadowing by glazing bars*

The shadowing by glazing bars can be calculated by analogy with the shadowing of ridges. A cross-section of a covering pane is shown in *Fig. 8*. The vector L is a projection of the three-dimensional light beam vector I (*Fig. 2*) in the two-dimensional orthonormal plane containing the normal of a glass pane [described by Eqn (3)] and the gutter direction vector G [defined in Eqn (2)]. Given these vectors, the projection L_1 of I in the plane $\langle N_1 \rangle \langle G \rangle$ is:

$$L_1 = \begin{pmatrix} G^T/|G| \\ N_1^T/|N_1| \end{pmatrix}(I) \tag{20}$$

The projection of L_2 in the plane $\langle N_2 \rangle \langle G \rangle$ can be determined in an analogous way. The superscript T means the transpose of a vector (i.e. turning a column vector into a row vector, or vice versa).

Once L_1 is determined, the relative length of the projection of the corner-points along L_1 on B with respect to B is given by:

$$v_x = \begin{pmatrix} N_{L1}, C_x \\ (N_{L1}, B) \end{pmatrix} \qquad x \in \{1, 2, 3, 4\} \tag{21}$$

N_{L1} denotes the normal vector on L_1. From the picture it is obvious that the shade of the bar spans the area enclosed by v_4 and v_2. Thus, the unmasked fraction of the bar-distance is calculated by $1 - (v_2 - v_4)$. In general the "transmissivity" of the bars in a pane can be determined by

$$\tau_b = 1 - (\max \{v_1, v_2, v_3, v_4\} - \min \{v_1, v_2, v_3, v_4\}) \tag{22}$$

Once τ_{b1} is calculated for the roofpanes R_1 and τ_{b2} for the panes R_2, Eqn (12) becomes:

$$\tau_{cover} = f_1 \tau_1 \tau_{b1} + f_2 \tau_2 \tau_{b2} \qquad \{\lambda_2 < 0\} \tag{23}$$

For low elevation angles ($\lambda_2 \geqslant 0$) the transmittivity of the panes, taking account of the
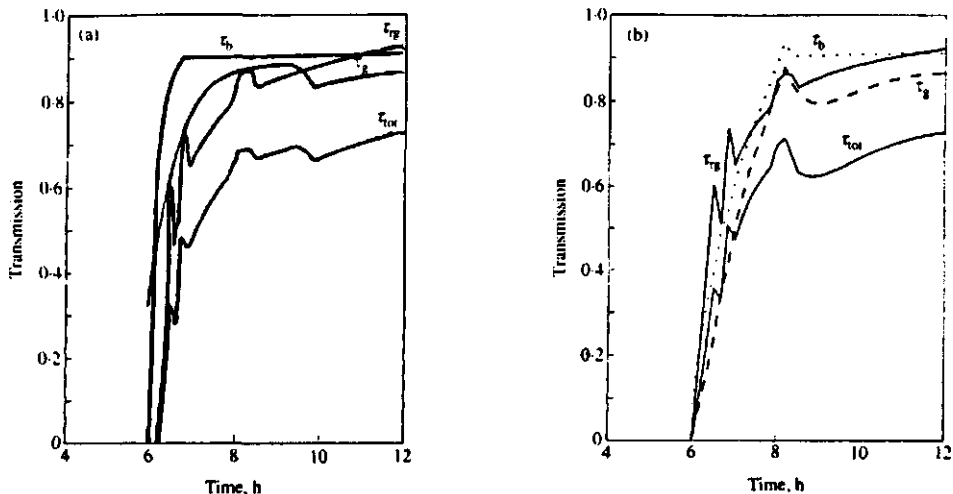
Fig. 9. *Direct transmissivity of a venlo-type greenhouse presented by Bot[4] (Fig. 9a) and calculated by vector algebra (Fig. 9b). τ_b denotes the transmission of the bars, τ_g the transmission by the glass panes, τ_{rg} the unmasked fraction of the ridge-gutter system, and τ_{tot} denotes the total transmissivity for direct radiation. The result holds for a north–south oriented greenhouse at 52° latitude on 22 March (equinox).*

masking by glazing bars, is determined by:

$$t_{f1} = (\tau_1 \tau_{b1})^{n+1}(\tau_2 \tau_{b2})^n$$
$$t_{f2} = (\tau_1 \tau_{b1})^{n+2}(\tau_2 \tau_{b2})^{n+1} \qquad \{\lambda_2 \geqslant 0\} \qquad\qquad (24)$$

Multiplying (23) or (24) by the fraction not masked by the ridge or gutter, yields the final direct transmissivity of the construction.

3. Results

The theory above has been used to calculate the direct transmissivity of a venlo-type greenhouse. The results were compared with the results derived by Bot. The results of both models are shown in *Fig. 9*. The calculation of the transmission of the roof-gutter system (τ_{rg}), as calculated by Bot[4] and shown in *Fig. 9a*, showed especially good resemblance with τ_{rg}, as calculated with the method presented in Section 2.4. (*Fig. 9b*).

However, there were significant differences for τ_b (the transmissivity of the bars) and τ_g (the transmissivity of the glass solely) found by Bot, and those calculated with vector algebra. The sharp decrease of τ_g in *Fig. 9b*, at about 0800 hrs, marks the point where the angle of the light beam falls on the upper side of the $\mathbb{R}_2$ panes (since $\lambda_2 < 0$) with a large angle of incidence. The reflection of this beam is cast on the neighbouring pane $\mathbb{R}_1$, and, after being transmitted by the $\mathbb{R}_1$ pane, contributes to the amount of light in the greenhouse. Contrary to the neglect of these reflections in the model presented here, the model of Bot accounted for this effect. After about 1000 hrs, where the solar elevation is more than twice the roofslope, the reflections on the outer side of $\mathbb{R}_2$ are directed away from the greenhouse (as depicted in *Fig. 4*) and the results for τ_g of both the models coincide. The difference in the curves of τ_b are caused by a different definition of the

transmissiviity of bars. Bot defines τ_b as the unmasked fraction of the projection of one roof section. The model presented here accounts for the increased shading by bars when the light passes multiple roof sections. as is the case at low elevation angles.

4. Conclusions

The use of vector algebra to determine the direct transmissivity of a greenhouse yields easy-to-use relationships. One formula [Eqn (7b)] can be applied to determine the length ratios of projections of all kinds of vectors. With Eqn (20) the light beam vector can be projected easily into any plane of the greenhouse construction. Thus the shades of all kinds of solid bodies of the construction and within the greenhouse can be studied. The results of the transmission calculation based on vector projections were compared with the results of the transmission model presented by Bot,[4] which is built on goniometric expressions. The results of both models were similar for the direct transmissivity of a venlo-type greenhouse.

The theory in this paper has been presented on the basis of a venlo-type greenhouse. However, as long as ridges and gutters are parallel to one another the method can be used for other types of greenhouses, such as houses with asymmetric roofshapes as well.

References

[1] **Stoffers, J. A.** Lichtdoorlatendheid van met vlakke materialen bedekte warenhuizen. [in Dutch]. Wageningen. IMAG. ITT publ. 14. 1967, 35 pp.

[2] **Kozai, T.; Goudriaan, J.; Kimura, M.** Light transmission and photosynthesis in greenhouses. Wageningen Centre for Agricultural Publishing and Documentation (Pudoc) 1987. 99 pp.

[3] **Thomas, R. B.** The use of specularly-reflecting back walls in greenhouses. Journal of Agricultural Engineering Research 1978, **23:** 85–97

[4] **Bot, G. P. A.** Greenhouse climate: from physical processes to a dynamic model. Ph.D. Dissertation. Agricultural University, Wageningen, 1983. 240 pp.

[5] **Critten, D. L.** A computer model to calculate the daylight integral and transmissivity of a greenhouse. Journal of Agricultural Engineering Research 1983, **28:** 61–76

[6] **Critten, D. L.** A theoretical assessment of the transmissivity of conventional symmetric roofed multispan E–W greenhouses compared with vertical south roofed greenhouses under natural irradiance conditions. Journal of Agricultural Engineering Research 1985, **32:** 173–183

[7] **Critten, D. L.** A general analysis of light transmission in greenhouses. Journal of Agricultural Engineering Research 1986, **33:** 289–302

[8] **Rosa, R.** Solar and thermal radiation inside a multispan greenhouse. Journal of Agricultural Engineering Research 1988 **40:** 285–295

[9] **Rosa, R.** Solar irradiation inside a single span greenhouse. Journal of Agricultural Engineering Research 1989, **43:** 221–229

[10] **Litlefair, P. J.** The luminance distribution of an average sky. Lighting and research technics 1981, 13(4): 192–198

[11] **Corson, D. R.; Lorraine, P.** Introduction to electromagnetic fields and waves Ch. 11: 361–372. San Fransisco, C. C. Freeman and Cy. San Fransisco. 1962, 552 pp.

[12] **Jefimenko, O. O.** Electricity and magnetism, Ch. 8: 233–258. New York, Appleton-Century-Crofts. 1966, 591 pp.

The theory presented in the article was applied to compute the transmissivity of a Venlo type greenhouse with a gutter distance of 3.20 meter (d in the paper) and a roof slope of 25° (ψ in the paper). The cladding material was 4 mm thick and the bar to bar distance was set to 1 m. The ridge was very small, namely 2×2 cm, which implied that the vectors E_1, E_2 and E_3 were (1.61 0.76)', (1.61 0.74)' and (4.79 0.74)' respectively. The gutter of a real greenhouse is usually not rectangular, but nevertheless approximated by a 6×6 cm square. Thus the corner points U_1, U_2 and U_3 were (3.23 0.06)', (3.17 0.06)' and (3.17 0.00)' respectively. The bars in the roof were of about the same size as the ridge, which implied that C_1, C_2, C_3 and C_4 were (0.99 0.02)', (1.01 0.02)', (1.01 0.00)' and (0.99 0.00)' respectively.

Table C.1 shows the results of the computations for a greenhouse from which the gutter direction points North-South.

Table C.1 Transmissivity of a greenhouse covering structure as a function of azimuth and elevation.

azimuth	elevation										
	0°	3°	5°	8°	10°	15°	20°	25°	30°	40°	60°
0°	.000	.069	.151	.263	.336	.486	.598	.678	.735	.800	.646
10°	.000	.226	.298	.339	.384	.500	.599	.674	.729	.795	.844
20°	.000	.277	.398	.510	.532	.556	.616	.675	.724	.788	.841
30°	.000	.295	.413	.553	.608	.651	.650	.683	.721	.783	,839
40°	.000	.284	.414	.559	.625	.717	.702	.699	.721	.777	.837
50°	.000	.268	.411	.554	.623	.722	.765	.724	.728	.773	.835
60°	.000	.256	.404	.548	.620	.724	.775	.753	.737	.770	.834
70°	.000	.245	.400	.547	.618	.724	.777	.781	.748	.770	.834
80°	.000	.241	.404	.533	.621	.727	.779	.801	.758	.772	.834
90°	.000	.245	.412	.562	.629	.733	.783	.809	.764	.775	.836

C.2 Diffusive transmissivity

The simplest distribution function describing diffuse radiation is the uniform overcast sky. Such a distribution, being one in all directions, holds for a heavy clouded day. Other distribution functions, such as 'standard overcast sky' (Coulson, 1975) and 'hemispherical radiation' (Morris and Lawrence, 1971) give more weight to radiation from the zenith than to radiation coming from low elevation angles. A 'circumsolar radiation' distribution (Morris and Lawrence, 1971), representative for sunny days, gives extra weight to the sector of the hemisphere around the sun. Bot (1983) analyzed the effects of these distribution functions on the resulting

diffuse transmissivity of the greenhouse. He found significant variations. Nevertheless the model discussed here uses a single diffuse transmissivity number, based on the standard overcast sky according to Coulson (1975). Due to the symmetry of the greenhouse the integration over the hemisphere can be performed by:

$$\tau_{diff} = \frac{\int_0^{\frac{1}{2}\pi} \int_0^{\frac{1}{2}\pi} \tau_{dir}(\beta,\omega) \; (1 + 3\sin(\beta))/4) \; \sin(\beta)\cos(\beta) \; d\beta \; d\omega}{\frac{1}{2}\pi \int_0^{\frac{1}{2}\pi} (1 + 3\sin(\beta))/4) \; \sin(\beta)\cos(\beta) \; d\beta} \qquad \text{[-] (C.1)}$$

in which β is the elevatation and ω is the azimuth.

In Eqn. C.1 the term $(1 + 3\sin(\beta))/4$ represents the distribution function for a standard overcast sky. Obviously it rates radiation coming perpendicular to the earth's surface 3 times compared to radiation coming from just above the horizon. The integral above has been approximated by a numerical integration with steps of 10° in both azimuthal and elevational direction yielding

$$\tau_{diff} = 0.79 \qquad \text{[-] (C.2)}$$

APPENDIX D: LIGHT ABSORBTION BY A CANOPY STAND

Downward directed short-wave radiation, propagating through a canopy stand on its way down, is made extinct by absorbtion and reflection at the canopy leaves. The description of the resulting radiation profile was thoroughly discussed in the Ph.D. thesis of Goudriaan (Goudriaan, 1977). His work elaborated on the idea introduced by Monsi & Saeki, to describe the extinction of light in a canopy by an exponential curve (Monsi & Saeki, 1953).

For idealized canopy stands, characterized by leaves with an equal reflection and transmission coefficient, arranged in a horizontal or spherical leaf angle distribution, planted in a non-reflecting soil, Goudriaan derived analytic solutions to describe the profile of radiation. However, if one or more of these assumptions are violated an analytic solution can no longer be given. For those cases a numerical procedure was presented.

In greenhouses the soil is mostly covered with a reflecting sheet, and the canopy architecture tends to a planophile leaf angle distribution. Therefore, in this work the numerical approach along the routes posited by Goudriaan is applied. The model assumptions are stated briefly, followed by a presentation of results.

D.1 Model description

The basis of the model is the concept of a canopy as a series of stratified layers. The surface covered by leaves in each layer is supposed to be randomly distributed within the layer. Therefore, in each layer the chance that a ray of light is intercepted by a leaf is the same.

For each layer a radiation balance is constructed, consisting of upward and downward fluxes. The downward flux in a layer is computed from the downward flux transmitted by the layer above, supplemented by upward radiation which is reflected downward by that layer. Transmission takes place through the space which is not occupied by leaves, and through the leaf tissue. The computation of the fraction of light intercepted and redistributed by transmission and reflection takes account of the dependency of the intercepting surface on the directional characteristics of the radiation. This means that radiation entering the canopy stand on low angles of elevation is extincted more rapidly than radiation entering from the zenith. In order to be able to compute this elevational dependency the leaf angle distribution function has to be known. Azimuthal preference of the canopy leaves is left out of consideration.

All reflections and transmission through the leaf tissue are assumed to generate isotropically distributed diffuse radiation. This assumption is simple, but supposed to be realistic enough (Gutschick and Weigel, 1984), especially for light transmitted by the tissue (Myneni et.al., 1989). Thus reflection and transmission gene-

rate diffuse fluxes, even if the radiation entering the canopy stand would have a direct component only.

The last layer in the model represents the soil surface, which does not transmit short-wave radiation, but reflects part of it isotropically back into the canopy.

D.2 Results with the model

A numerical model, based on the theory presented by Goudriaan was built and applied to compute the absorbtion of short-wave radiation in a canopy stand for both visible wavelengths (VIS) and the near infra red region (NIR). Moreover, an extinction coefficient for VIS and long-wave radiation is determined. All computed quantities are determined for diffuse radiation and for direct radiation in four classes of solar elevation.

The computations hold for a canopy with a planophile leaf angle distribution. The relative frequency of leaves having a leaf angle with the horizon in one of the nine distinguished elevation classes is displayed in Figure D.1
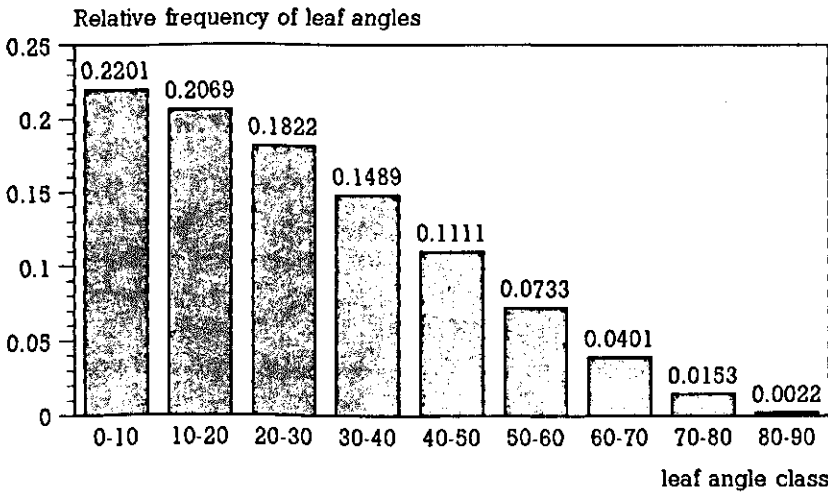
Figure D.1 Relative frequency of leaf angles of a canopy with a planophile leaf angle distribution function in nine elevation classes.

For VIS, the transmission coefficient of the tissue was set to 0.10, which is an appropriate mean value for green leaves in this part of the spectrum (Goudriaan, 1973). For NIR the transmission coefficient is much larger, namely 0.46. The leaf reflection coefficients for VIS and NIR are set to 0.05 and 0.38 respectively. The reflection coefficient of the floor was assumed to be 0.25 for both VIS and 0.40

for NIR. Diffuse radiation was assumed to be represented by the uniform distribution function.

The absorbtion of radiation plays a role in the thermal sub-model that determines the greenhouse energy budget and in the CO_2 sub-model, where the VIS profile determines the assimilation rate. In both contexts the same theory on the radiation profile within the canopy holds, but because the quantities of interest differ for the two cases the required quantities are determined in two sections.

D.2.1 Absorbtion of short-wave and long-wave radiation in a canopy stand

To compute the absorbtion of radiation by the canopy, the radiation absorbed by the soil surface and the upward radiation flux at the top of the canopy (being a resultant of numerous reflections within the canopy) was subtracted from the downward radiation flux to which the canopy was exposed. Figure D.2 shows the result of this subtraction for a diffuse radiation flux in the VIS and the NIR part of the spectrum. Both the eight values of the LAI for which the canopy absorbtion was computed and a smooth curve fitted through these points are displayed.
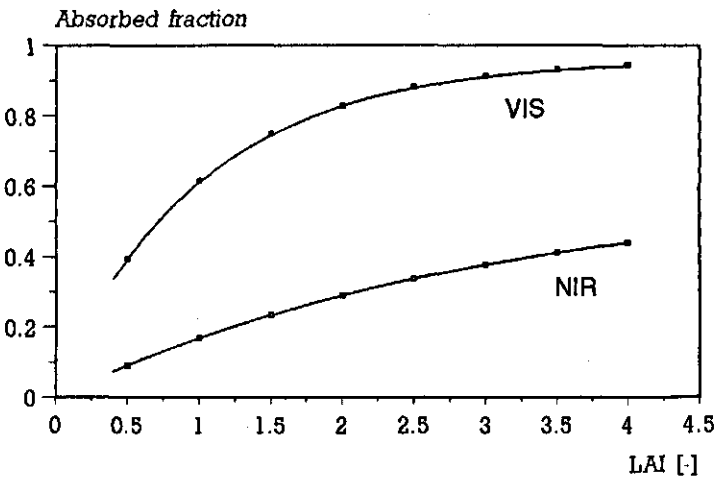
Figure D.2 Canopy absorbtion of diffuse VIS and NIR for eight values of the LAI and as a smooth fitted curve.

The smooth curve in Figure D.2 for VIS is described by $0.95 - 0.9 \, exp(-0.85 \, LAI)$ and the curve describing the absorbtion of radiation in the near infra red band of wavelengths reads $0.65 - 0.65 \, exp(-0.27 \, LAI)$.

For direct radiation the absorbed fraction depends on both LAI and solar elevation angle. Figure D.3 shows the computed fractions of direct radiation absorbed by the canopy and again a number of fitted curves.
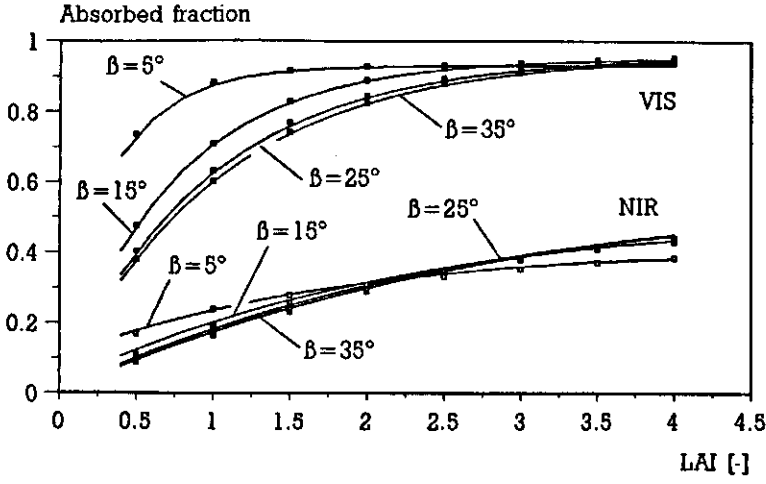
Figure D.3 Canopy absorbtion of direct VIS and NIR for eight values of the LAI and for solar elevation angles ranging from 5° to 65° with steps of 10°. Through the points a number of curves are fitted.

The full curves in Figure D.3 for radiation in the visible band of wavelengths are described by $0.95 - 0.9 \, exp(-k_{VISdir} \, LAI)$, with $k_{VISdir} = 0.88 + 2.6 \, exp(-0.18 \, \beta)$. The curves holding for near infra red direct radiation in Figure D.3 are described by $a - b \, exp(-k_{NIRdir} \, LAI)$, with the coefficient $a = 0.67 - 0.36 \, exp(-0.095 \, \beta)$, the coefficient $b = 0.68 - 0.50 \, exp(-0.11 \, \beta)$ and $k_{NIRdir} = 0.25 + 0.38 \, exp(-0.12 \, \beta)$. For long-wave radiation canopy leaves are assumed to be black (Stanghellini, 1987). Thus the absorbtion of long-wave radiation can be computed with the theory outlined above, after setting the reflection and transmission coefficients 0, and studying the absorbtion of diffuse radiation. Figure D.4 shows the absorbtion of long-wave radiation, both as computed points and as a fitted curve. The smooth curve is described by $1 - exp(-0.94 \, LAI)$. The factor 0.94 is referred to as the long-wave extinction coefficient (k_l).

Absorbed fraction
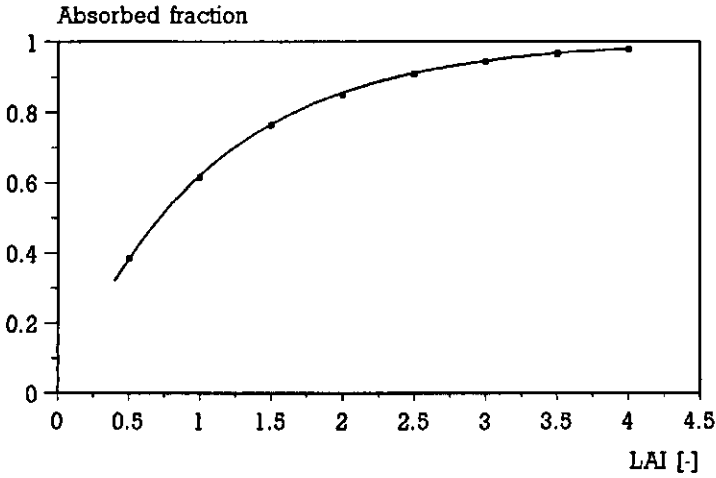
Figure D.4 Absorbtion of long-wave radiation for eight values of the LAI and as fitted curve.

D.2.2 Radiation profile within a canopy stand

Because of the strong non-linearity of the photosynthesis response curve the total assimilation rate of a canopy can not be deducted from the total amount of absorbed radiation, but must be computed by integration of the contribution of leaves throughout the canopy stand. To compute the photosynthetic activity at arbitrary height in the canopy the local intensity of radiation to which the leaves are exposed has to be known. Therefore the radiation profile has to be determined. The intensity of radiation at each layer in the model can be stated as the sum of the computed upward and downward radiation flux for that layer. The results of these computations for diffuse radiation are shown in Fig. D.5 for a number of LAI's. Obviously the intensity of radiation to which the leaves at the top of the canopy are exposed exceeds the downward diffuse flux. This is a result of upward reflections. For very small canopies this increment of the amount of radiation appears to be more than ten percent.

The computed radiation profiles shown in Figure D.5 can be approximated quite well with exponential curves of the form

$$I(x) = I_0 \, a \, exp(-k \times LAI) \hspace{3cm} [Wm^{-2}] \; (D.1)$$

where $I(x)$ denotes the intensity of radiation at relative canopy depth x ($0 \leq x \leq 1$), I_0 denotes the radiation flux at the top of the canopy (Wm^{-2}), a a multiplication factor taking account for the increment of radiation intensity at the top of the

canopy due to upward reflections and k an extinction coefficient. In Figure D.6, for a canopy with a LAI=1 and a canopy with a LAI=3, the approximating exponential curves are shown as full lines, together with a number of points. The points are elements of the curves shown in Fig. D.5.
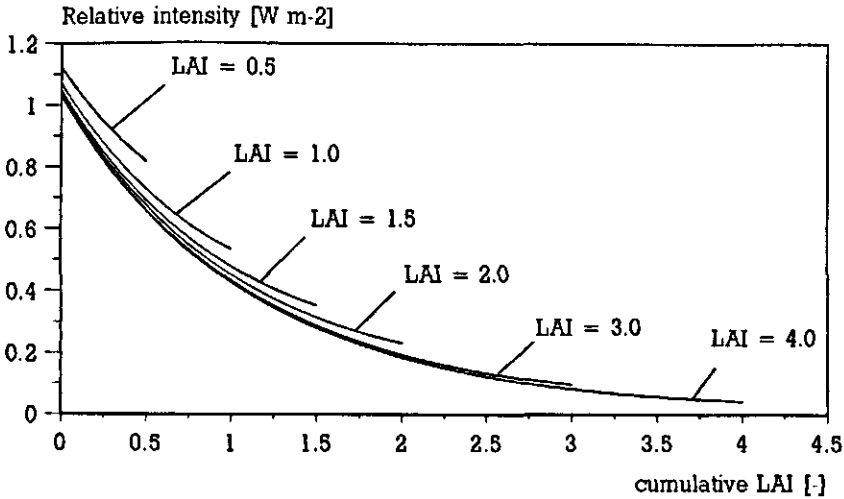
Figure D.5 Computed radiation intensity as a function of the cumulative LAI, expressed as a fraction of the diffuse downward radiation flux at the top of the canopy for a number of values of the actual LAI of the canopy.
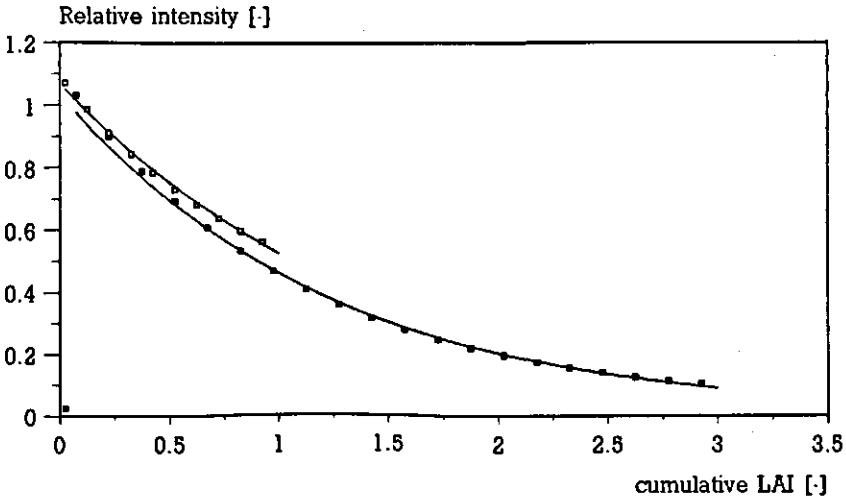
Figure D.6 Fitted radiation profiles for diffuse radiation

The curves in Figure D.6 are described using Eqn. D.1 with a and k according to $a = 1.04 + 0.24$ *exp*(-2 LAI) and $k = 0.85 - 0.27$ *exp*(-0.69 LAI).

The radiation profiles for direct radiation do not depend on the canopy size only, but on the solar elevation angle as well. In figure D.7 the profiles computed for four solar elevation angles and for two canopy sizes are shown.
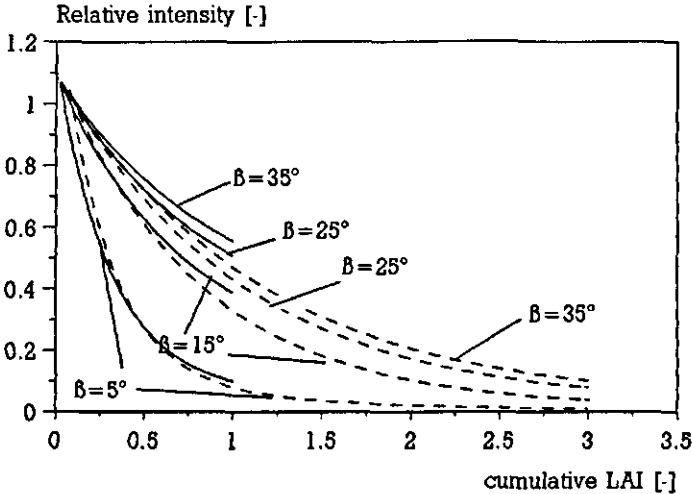
Figure D.7 Computed radiation profiles for direct radiation entering the canopy with an elevation angle of 5°, 15°, 25°, and 35° for a canopy with a LAI=1 (——) and a LAI=3 (– – –)

Just like the profiles for diffuse radiation, after determination of the parameters a and k, the curves in Fig. D.7 can be approximated with Eqn. D.1. The curves for direct depend on two variables, namely the LAI of the canopy and the solar elevation angle.

Figure D.8 shows the computed radiation intensity profiles (the square points) and the radiation profiles approximated by an exponential function of the type of Eqn. D.1, holding for a canopy with a LAI=2. Obviously, the approximation is better for higher elevation angles than for the low elevation angle of 5°. For direct radiation the dependency of the parameter a on the canopy size could be described by $a = 1.06 + 0.26$ *exp*(-2 LAI). The parameter k depended on both canopy size and solar elevation angle. After introducing three intermediate parameters, k was described by $k = p + q$ *exp*(r β). The parameters p, q and r contribute for the canopy-size effect according to $p = 0.76 - 0.87$ *exp*(-1.84 LAI), $q = -0.95$ LAI +4.83 and $r = 0.02$ LAI -0.17.
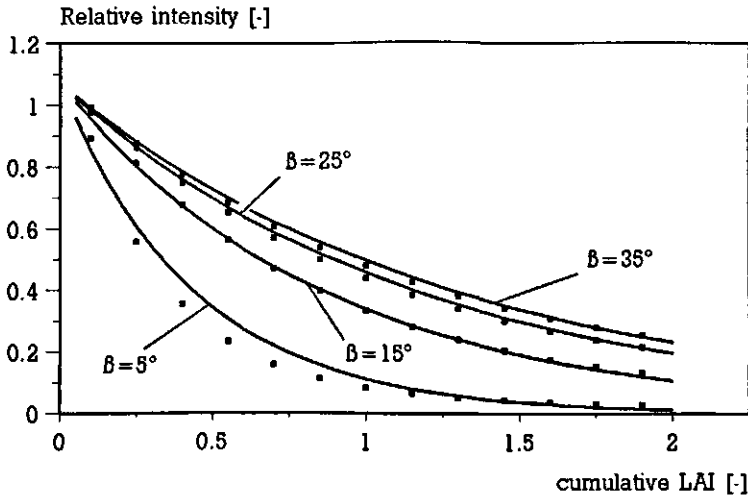
Figure D.8 Fitted and computed radiation profiles for direct radiation.

The intensities of the radiation flux from direct radiation inside the canopy, as showed in the Figures D.7 and D.8, do not consist of direct radiation only but, due to scattering of the radiation, are a mixture of direct and diffuse radiation. Moreover, leaves are either sunlit, meaning that they are exposed to the full intensity of the direct flux, or are in shade, where they receive diffuse radiation only. Thus, the sunlit leaves are exposed to radiation at a much higher intensity the rest of the leaves. Because the photosynthetic response is strongly non-linear (see Appendix I), the pure direct radiation flux at the sunlit leaves must be distinguished from the total radiation intensity in the canopy.

To compute the pure direct radiation intensity, the model described in Section D.1 was applied, after setting the transmission and reflection coefficients of the canopy leaves 0. This yielded a radiation profile showed in Figure D.9. Again, the figure shows points computed with the model and curves described by Eqn. D.1. For all curves in Fig. D.9, the parameter a is 1 because, by definition, scattering does not add pure direct radiation. Moreover, since soil reflections do not affect the pure direct radiation profile the canopy size does not affect the radiation profile (apart from the fact that the curve for a canopy with a small LAI ends earlier the the curve holding for a larger canopy).

The parameter k subject to Eqn. D.1 in order to describe the profiles shown in Figure D.9 reads $k = 0.89 + 0.26 \, exp(-0.16 \, \beta)$. This parameter k is referred to in Appendix I as k_{sunlit}.

Relative intensity [-]
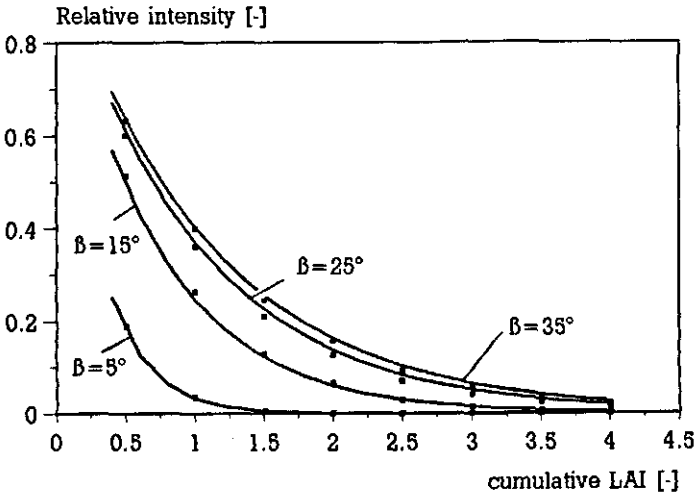
Figure D.9 Fitted and computed profiles for pure direct radiation

APPENDIX E: LONG-WAVE RADIATION

The emission of radiation by a black body is described by the Stefan-Boltzmann equation:

$$E_b = \sigma\, T^4 \qquad\qquad [Wm^{-2}]\ (E.1)$$

Where E_b is the emissive power density of the black body (Wm^{-2}), σ the constant of Stefan-Boltzmann ($5.67 \cdot 10^{-8}\ Wm^{-2}K^{-4}$) and T the absolute surface temperature of the body (K). However, most natural bodies are not black and radiate less than E_b. Therefore a factor ε, the emissivity of a body is introduced. It is defined as the fraction radiated energy compared to the radiative energy emitted by a black body at the same temperature.

$$\varepsilon(v) = E(v)/E_b(v) \qquad\qquad [Wm^{-2}]\ (E.2)$$

When $\varepsilon(v)$ is constant for all wavelength's v, the body is called a grey body. Real bodies having a constant emission coefficient over the whole spectrum hardly exist but when only a part of the spectrum is being considered, a single value for ε can be applied. Since radiative heat exchange between elements in the greenhouse takes place in such a limited spectrum (5 - 50 μm), it is common in simulation models to assume a constant emission coefficient for thermal radiation (Takakura, 1992).

Besides emittance, the absorbtion of radiation is just as important in radiative heat exchange. A black body absorbs all incident radiation, regardless of spectral and directional characteristics. Thus the absorbtion coefficient $\varepsilon(v)$ emission coefficient $\alpha(v)$ of a black body is 1 over the whole frequency range.

In general the absorbtion coefficient of a natural body is less than 1. It can be proved that for any particular body, the functions $\varepsilon(v)$ and $\alpha(v)$ are equal. This rule is known as Kirchhoff's law (Pitts, 1986). The remainder of the radiative energy to which a body is exposed is either reflected or transmitted.

In radiation exchange, when there are more bodies interacting with each other, each body acts both as an emitter and as an absorber. In the following, the calculus of such a radiative exchange is derived.

Consider two parallel infinite opaque surfaces, having different emissivities and different temperatures. The upper face of s_2 only radiates to s_1. The lower face of s_1 only radiates to s_1.

$$\underline{\quad s_1 \qquad\qquad\qquad\qquad\qquad T_1\ \varepsilon_1 \quad}$$

$$\overline{\quad s_2 \qquad\qquad\qquad\qquad\qquad T_2\ \varepsilon_2 \quad}$$
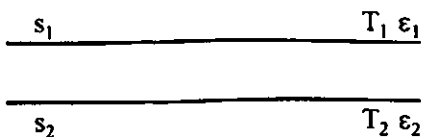
Suppose an amount of energy E_1 is radiated from s_1 in the direction of s_2. A fraction α_2 of this energy is absorbed by s_2 and the rest is reflected to s_1. Thus p_1

receives a fraction ρ_2 back from itself. From this reflected energy an amount $E_1\rho_2\rho_1$ scattered back to s_2 which again reflects to s_1 and so on. The total radiative energy transfer from s_1 to s_2 is:

$$q''_{1,2} = \alpha_2 E_1 + \alpha_2 \rho_1 \rho_2 E_1 + \alpha_2 \rho_1^2 \rho_2^2 E_1 + \ldots + \alpha_2 \rho_1^n \rho_2^n E_1 \quad [Wm^{-2}] \text{ (E.3)}$$

The other surface (s_2) is radiating in the same way to s_1. The total radiative energy transfer from s_2 to s_1 reads:

$$q''_{2,1} = \alpha_1 E_2 + \alpha_1 \rho_2 \rho_1 E_2 + \alpha_1 \rho_2^2 \rho_1^2 E_2 + \ldots + \alpha_1 \rho_2^n \rho_1^n E_2 \quad [Wm^{-2}] \text{ (E.4)}$$

Both the expressions are a series resulting in:

$$q''_{1,2} = \frac{\alpha_1 E_2}{1 - \rho_1 \rho_2} \qquad\qquad q''_{2,1} = \frac{\alpha_2 E_1}{1 - \rho_1 \rho_2} \qquad [Wm^{-2}] \text{ (E.5)}$$

The net radiation from s_1 to s_2, being $q''_{1,2} - q''_{2,1}$ is given by:

$$Q''_{1,2} = \frac{\alpha_2 E_1 - \alpha_1 E_2}{1 - \rho_1 \rho_2} \qquad [Wm^{-2}] \text{ (E.6)}$$

With the assumption that the radiating surfaces are grey for the part of the spectrum where the majority of energy is radiated, E can be replaced by $\varepsilon \sigma T^4$. Also, assuming opaque surfaces and a comparable wavelength distribution of emitted and absorbed radiation, the relation $\rho = (1-\alpha) = (1-\varepsilon)$ holds. Then Eqn. E.6 can be simplified to:

$$Q''_{1,2} = \frac{\sigma (T_1^4 - T_2^4)}{(1/\varepsilon_1) + (1/\varepsilon_2) - 1} \qquad [Wm^{-2}] \text{ (E.7)}$$

Where $Q''_{1,2}$ represents the net radiation flux from p_1 to p_2.
If the temperature differences are small, this fourth-order equation can be linearized to:

$$Q''_{1,2} = \frac{4 \sigma T_m^3 (T_1 - T_2)}{(1/\varepsilon_1) + (1/\varepsilon_2) - 1} \qquad [Wm^{-2}] \text{ (E.8)}$$

Where T_m represents the mean temperature between T_1 and T_2.
The situation becomes more complicated when the radiation exchanging surfaces are not infinite. Radiation of both surfaces is directed to the total hemisphere but the intersection of the other surface with the hemisphere is just a fraction. This fraction of the total radiation emitted by s_4 to which s_3 is exposed is called the view factor of s_4 to s_3 (Notation F_{43}). Likewise the view factor F_{34} is the fraction of the hemisphere of s_3 that intersects s_4.
Figure E.1. shows a sketch of the series of emission, absorbtion, and reflection between two finite sized surfaces.

absorbtion by s_4

s_3

$\rightarrow E_3$

$F_{3,4} E_3 \rightarrow$
$\leftarrow \rho_4 F_{3,4} E_3$

$\rightarrow \alpha_4 F_{3,4} E_3$

$\leftarrow \rho_4 F_{3,4} F_{4,3} E_3$
$\rightarrow \rho_4 \rho_3 F_{3,4} F_{4,3} E_3$

$\rho_4 \rho_3 F_{3,4}{}^2 F_{4,3} E_3 \rightarrow$
$\leftarrow \rho_4{}^2 \rho_3 F_{3,4}{}^2 F_{4,3} E_3$

$\rightarrow \alpha_4 \rho_4 \rho_3 F_{3,4}{}^2 F_{4,3} E_3$

$\leftarrow \rho_4{}^2 \rho_3 F_{3,4}{}^2 F_{4,3}{}^2 E_3$
$\rightarrow \rho_4{}^2 \rho_3{}^2 F_{3,4}{}^2 F_{4,3}{}^2 E_3$

$\rho_4{}^2 \rho_3{}^2 F_{3,4}{}^3 F_{4,3}{}^2 E_3 \rightarrow$

$\rightarrow \alpha_4 \rho_4{}^2 \rho_3{}^2 F_{3,4}{}^3 F_{4,3}{}^2 E_3$
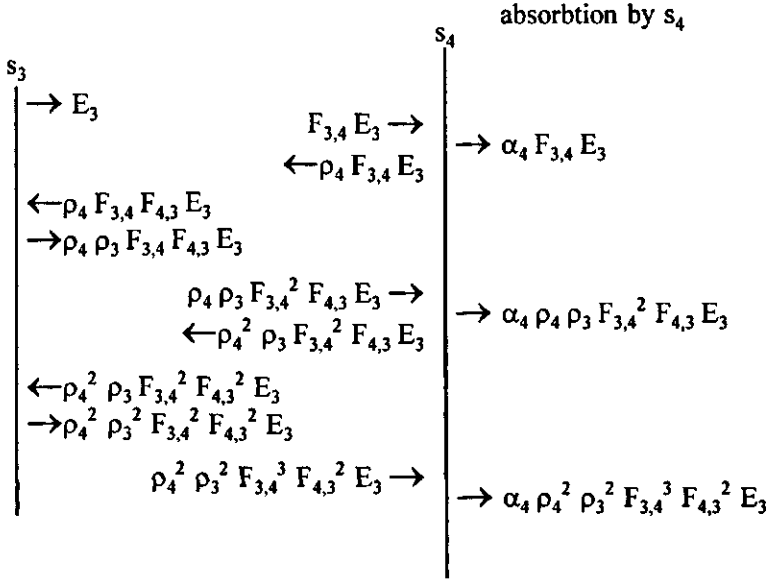
Figure E.1 Radiative energy transfer from the finite sized surface s_3 to the finite sized surface s_4.

From this sketch the following series can be derived describing the radiative energy flow from s_3 to s_4.

$$q_{3,4} = \alpha_4 F_{3,4} E_3 + \alpha_4 \rho_4 \rho_3 F_{3,4}{}^2 F_{4,3} E_3 + \alpha_4 \rho_4{}^2 \rho_3{}^2 F_{3,4}{}^3 F_{4,3}{}^2 E_3 + ... \qquad \text{[W] (E.9)}$$

E_3 is determined by $A_3 \varepsilon_3 \sigma T_3{}^4$. The term A_3 is added because now we are not interested in energy flux densities but in the total energy flux. This is a consequence of the finite dimensions of s_3 and s_4. If $0 < (\rho_3 \rho_4 F_{3,4} F_{4,3}) < 1$ this series converges to:

$$q_{3,4} = \frac{\alpha_4 F_{3,4} A_3 \varepsilon_3 \sigma T_3{}^4}{1 - (\rho_3 \rho_4 F_{3,4} F_{4,3})} \qquad \text{[W] (E.10)}$$

The radiative energy flux from s_4 to s_3 can be determined analogue. After using the property that for finite body $A_3 F_{3,4}$ equals $A_4 F_{4,3}$ and that α equals ε (Pitts, 1986) the net radiation from s_3 to s_4, being $q_{3,4} - q_{4,3}$ yields:

$$Q_{3,4} = \frac{\varepsilon_3 \varepsilon_4 F_{3,4} A_3 \sigma}{1 - (\rho_3 \rho_4 F_{3,4} F_{4,3})} (T_3{}^4 - T_4{}^4) \qquad \text{[W] (E.11)}$$

If necessary or for small temperature differences Equation E.11 can be linearized analogue to Equation E.8.

APPENDIX F: ESTIMATION OF THE SKY TEMPERATURE

The hemisphere around the greenhouse is a gaseous medium consisting of particles all having a certain temperature and therefore a certain electromagnetic energy emittance. All particles together, at different altitudes in the sky, generate a downward radiation flux. On the other hand the opaque elements on earth emit thermal radiation into the hemisphere. The net effect is a heat loss to the atmosphere.
This net heat loss can be measured by a pyrgeometer and, combined with the temperature of the emitting element of the measuring device, a fictive sky temperature (T_{sky}) can be computed.

$$T_{sky} = (T_{device}^4 - R_{net}/\sigma)^{0.25} \qquad \text{[K] (F.1)}$$

with T_{device} the temperature of the measuring device, R_{net} the net radiative heat loss and σ the Stefan-Boltzmann constant ($5.67 \cdot 10^{-8}$ Wm^{-2}K^{-4}). Obviously the emitting element of the measuring device is assumed to be black. The sky is optically black by definition.
If the sky temperature is not available in a set of meteorological data, several approximation algorithms can be found in the literature (Monteith, 1961; Sellers, 1965; Swinbank, 1963). However, contrary to the approach embedded in Eqn. F.1, where a fictive temperature is calculated in meteorological literature it is customary to express the downward long-wave radiation flux as a function of a fictive emissivity of the sky from which the temperature is set to the temperature at reference height (2 m). Thus the downward flux R_d is defined by

$$R_d = \varepsilon_{sky} \sigma T_{air}^4 \qquad \text{[Wm}^{-2}\text{] (F.2)}$$

Meteorological literature concerning the radiative heat exchange to the sky concentrates on the parametrization of ε_{sky}. It appears that ε_{sky}, as applied in Eqn. E.2, is well correlated with the vapour pressure at reference height. Brunt (1939) suggested a relation for clear skies of the type $\varepsilon = \alpha + \beta \downarrow e$, with e the vapour pressure. The parameters α and β differ from region to region. For moderate latitudes Monteith (1973) mentions

$$\varepsilon_{sky,clear} = 0.53 + 6 \cdot 10^{-3} \, VP_{air}^{0.5} \qquad \text{[-] (F.3)}$$

where the vapour pressure is expressed in Pa.
The cold atmosphere is (partly) screened by optically black clouds with higher temperatures for cloudy skies. Monteith (1973) mentions the following empirical expression

$$\varepsilon_{sky} = \varepsilon_{sky,clear}(1 + n \, c^2) \qquad \text{[-] (F.4)}$$

where c denotes the fraction of the sky covered by clouds and n contributes to the different impact of the height of the clouds. For high clouds (for example cirrus

types) the impact is low (n=0.04) and for low clouds (for example stratus, cumulus) the apparent emissivity is much more affected, expressed by n = 0.2.

Monteith (1973) derived a more convenient expression for the British Isles, where low clouds predominate over other cloud types. This empirical relation reads:

$$R_d = (1 - c)\, \varepsilon_{sky,clear}\, \sigma T_{air}^4 + c(\sigma T_{air}^4 - 9) \qquad [Wm^{-2}]\ (F.5)$$

with c the clouded fraction of the sky. Because in the Netherlands low clouds are common as well, Equation F.5 can be applied to estimate the downward radiative flux.

Expressing the downward flux with Equations such as F.2 and F.5 implies the calculation of the net thermal radiation by subtracting R_d from an upward flux R_u. The applied reasoning obliges the upward flux R_u to be computed by $R_u = \varepsilon \sigma T^4$ (with appropriate values for ε and T).

The radiative exchange processes in this study are computed using the theory presented in Appendix E. This approach computes the radiative heat exchange as a function of temperature difference. Therefore, in the context of this work a fictive sky temperature is computed by solving the black body temperature from the equation $\sigma T_{sky}^4 = R_d$. Thus, using Equation F.5 the sky temperature can be estimated by

$$T_{sky} = ((1-c)\varepsilon_{sky,clear} T_{air}^4 + c(T_{air}^4 - 9/\sigma))^{0.25} \qquad [K]\ (F.6)$$

APPENDIX G: GAUSSIAN INTEGRATION

Basically the Gaussian integration method estimates the mean value of a function to be integrated within an interval of interest. With this mean value the integral of the function on this domain is simply the mean value multiplied by the width of the domain.

To estimate the arithmetic mean of the function, the Gauss method samples the function on well chosen points. The more points are evaluated, the better the estimation of the integral.

Suppose a function is to be sampled at only one place within the interval. The best place to sample the function is in the middle of the interval. Indeed, polynomials up to the first order are integrated exactly by this method.

When two function evaluations in the interval are taken the Gauss method selects these points in such a way that polynomials up to the third order are integrated exactly. Suppose a function $y = ax^3 + bx^2 + cx + d$ has to be integrated in the interval $-\frac{1}{2} < x < \frac{1}{2}$. Because the length of the interval is 1 the integral of the function is the same as the mean of the derivative. When the two evaluation points are chosen symmetric around 0 the sum of the odd powered terms of the polynomial become 0 because the polynomial is symmetric in $x = 0$. The analytic integral of the third order function in the interval $<-\frac{1}{2},\frac{1}{2}>$ is $b/12 + d$. The mean of the two evaluations of the function to be integrated at $x = -\gamma$ and $x = \gamma$ is $b\gamma^2 + d$. The Gauss integration method states that $b\gamma^2 + d$ has to be the same as $b/12 + d$. Therefore γ is found to be $1/\sqrt{12}$.

The third order Gaussian integration performs three function evaluations to estimate the mean of the function and calculates the integral up to a fifth order polynomial exactly. The three evaluation points are placed symmetric around 0, resulting in the points $x = 0$, $x = -\gamma$ and $x = \gamma$. Contrary to the second order case it is not the arithmetic mean of the three function evaluations to represent the mean value of the function but a weighted mean. To find the two unknowns (γ and the weighing term for the mid-point w), two equations can be defined.

$$\frac{(-\gamma)^2 + 0 \cdot w + (\gamma)^2}{1 + w + 1} = \int_{-\frac{1}{2}}^{\frac{1}{2}} x^2 \, dx = 1/12 \tag{G.1a}$$

$$\frac{(-\gamma)^4 + 0 \cdot w + (\gamma)^4}{1 + w + 1} = \int_{-\frac{1}{2}}^{\frac{1}{2}} x^4 \, dx = 1/80 \tag{G.1b}$$

The solution of this set of equation yields:

$$\gamma = \sqrt{0.15} \Rightarrow \text{evaluation points: -0.387, 0, 0.387} \tag{G.2}$$

$$w = 1.6 \Rightarrow \text{weight of each evaluation: 1, 1.6, 1} \tag{G.3}$$

Besides as a method to integrate polynomials, Gaussian integration is also suitable to compute the integral of exponential functions, although for exponential functions the result is an approximation. Below gives an example by means of the computation of the integration of a non-polynomial function e^x.

$$\int_1^4 e^x \, dx \quad \text{with the analytical solution } e^4 - e^1 = 51.880 \qquad (G.4)$$

To use the three points Gaussian integration routine, three points relative to the middle of the interval have to be determined.

$$x_1 = 2.5 - 0.387 \cdot 3 = 1.339 \quad x_2 = 2.5 \quad x_3 = 2.5 + 0.387 \cdot 3 = 3.661 \qquad (G.5)$$

Where 2.5 is the middle of the interval to be integrated (<1,4>) and 3 is the length of the interval. Now the estimation of the mean function value can be determined:

$$y = \frac{e^{1.339} + 1.6 \, e^{2.5} + e^{3.661}}{1 + 1.6 + 1} = 17.280 \qquad (G.7)$$

The last step is to multiply the estimated mean derivative by the length of the interval.

$$17.280 \cdot 3 = 51.840 \qquad (G.8)$$

Comparing the numerical-found value with the analytical value shows that Gaussian integration gives a very good estimate of the integral of an exponential function.

APPENDIX H: APPROXIMATION OF SATURATED VAPOUR PRESSURE

The saturated vapour pressure is dependent on its temperature. Many handbooks present tables on this quantity. Figure H.1 shows the saturated vapour pressure curve for a temperature interval between -5 and 35 °C.
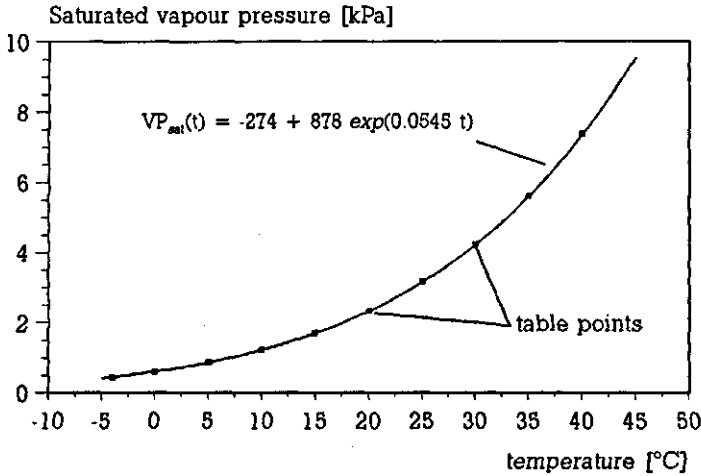
Figure H.1 Saturated vapour pressure curve

To be able to compute the saturated vapour pressure at any temperature an exponential curve was fitted through the table points. The curve-fitting resulted in the expression:

$$p_{satu}(t) = -274.36 + 877.52 \ exp(0.0545 \ t) \qquad \text{[Pa] (H.1)}$$

In the Figures H.2 and H.3 the absolute and relative deviations of the vapour pressures computed by Eqn. H.1 compared to the values through which the curve was fitted.

From Figure H.3 can be seen that in the most important part of the curve, namely the interval between 15 and 25 °C, the error of Eqn. H.1 is less than 1%.

Besides the saturated vapour pressure the model also requires the derivative of the saturated vapour pressure function. The derivative of Eqn. H.1 is easy to determine and yields:

$$p_{satu}(t)' = 47.82 \ exp(0.0545 \ t) \qquad \text{[PaK}^{-1}\text{] (H.2)}$$

Absolute deviation [Pa]
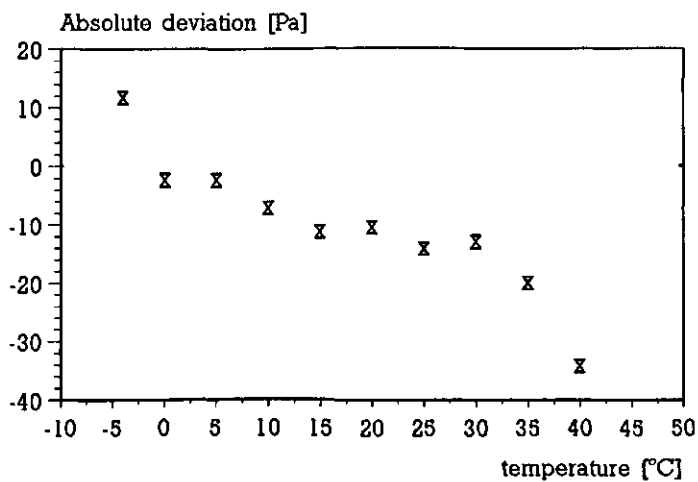
Figure H.2 Absolute deviation of the results of eqn. H.1 compared to table-values.

Relative deviation [%]
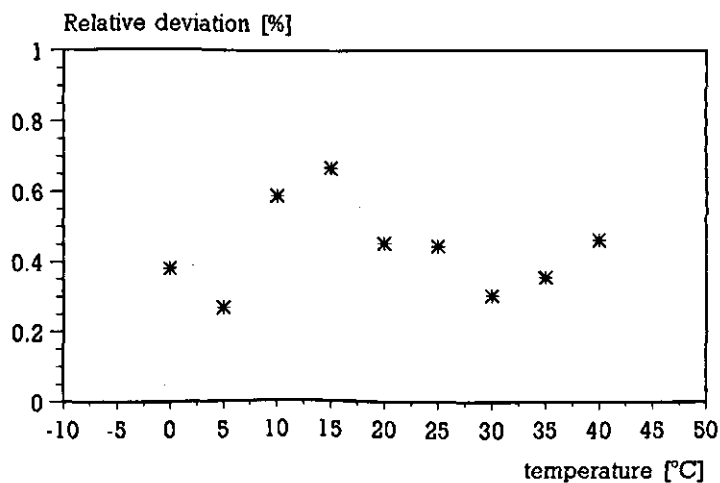
Figure H.3 Relative deviation of the results of H.1, compared to table-values.

APPENDIX I: PHOTOSYNTHESIS

Given light in an appropriate spectral range, a canopy extracts CO_2 from its ambient in order to produce starch as an energy source for its growth and development. This chemical assimilation of sucrose from carbon dioxide and water is called photosynthesis. In the greenhouse climate simulation model the CO_2 consumption reflated to photosynthesis is referred to by the variable MC_{AirCan}. Because photosynthesis is strongly non-linear the mean radiation intensity on canopy leaves gives insufficient information to compute the assimilation rate. Thus, in order to compute the canopy photosynthesis, the integral of the assimilation rates of the individual leaves must be based on local light intensities.

In this section, first the leaf assimilation rate is related to the local radiation intensity. Then an approach to determine the distribution of light in the canopy stand is presented, followed by a calculus for the canopy photosynthesis.

I.1 CO_2 fixation in a canopy leaf

The rate of CO_2-assimilation is an increasing function of radiation intensity. For low radiation intensities the response is almost linear, but at higher levels the process becomes saturated. Thus photosynthesis, as a function of irradiation, shows a maximum. It is described by (Gijzen, 1992):

$$\text{assim}(VIS_{abs}) = P_m \left\{ 1 - \exp\left(\frac{-\varepsilon\ VIS_{abs}}{P_m}\right) \right\} \qquad [\text{mgm}^{-2}\text{leaf s}^{-1}] \ (I.1)$$

In this function $\text{assim}(VIS_{abs})$ denotes the photosynthesis per m^2 leaf, P_m the maximal photosynthesis ($mgCO_2 s^{-1}m^{-2}$), ε the initial light-use efficiency ($mgCO_2 J^{-1}$) and VIS_{abs} the intensity of absorbed Photosynthetic Active Radiation (Wm^{-2}). The initial light use efficiency depends on the leaf temperature according to (Gijzen, 1992):

$$\varepsilon = \varepsilon_0\ \frac{C_a - \Gamma}{C_a + 2\Gamma} \qquad [\text{mgCO}_2\text{J}^{-1}] \ (I.2)$$

The variable ε_0 is the potential light-use efficiency in the absence of oxygen and is reported to be 0.017 mg CO_2 (J VIS)$^{-1}$ (Gijzen, 1992). The variable C_a is the CO_2 concentration of the ambient, expressed in $\mu l\ l^{-1}$, which is equivalent to a CO_2 concentration expressed in ppm. Γ is called the CO_2 compensation point and depends on leaf temperature. For air with a normal oxygen concentration (about 210 ml l^{-1}) Γ is described by (Gijzen, 1992):

$$\Gamma = 42.7 + 1.68(T_1 - 25) + 0.012(T_1 - 25)^2 \qquad [\mu l\ l^{-1}] \ (I.3)$$

In this equation the variable T_1 represents the leaf temperature (°C).

The maximal rate of photosynthesis (P_g) depends on another three variables. It is described by:

$$P_g = R_d + \min\{P_n, P_{mm}\} \qquad \text{[mgm}^{-2}\text{leaf s}^{-1}\text{] (I.4)}$$

R_d is the dark respiration of the leaf ($mgCO_2m^{-2}s^{-1}$), P_n denotes the rate of net photosynthesis and P_{mm}, the endogenous capacity, limits the maximal rate of photosynthesis. The dark respiration is commonly determined by the Q_{10}-factor.

$$R_d = R_{d,20} \, Q_{10}^{\,0.1(T-20)} \qquad \text{[mgm}^{-2}\text{leaf s}^{-1}\text{] (I.5)}$$

where $R_{d,20}$ represents the dark respiration of a leaf of 20 °C. Gijzen mentions a value of 0.05 mg CO_2 m^{-2} s^{-1}. The Q_{10}-factor describes the increment of the dark respiration due to a 10 °C temperature increase. Gijzen uses the value $Q_{10} = 2$. The rate of net photosynthesis (P_n) depends on a CO_2 concentration difference and the resistance to diffusion of CO_2.

$$P_n = \frac{1.8(C_a - \Gamma)}{1.37\, r_{b,V} + 1.6\, r_s + r_c} \qquad \text{[mgm}^{-2}\text{leaf s}^{-1}\text{] (I.6)}$$

The term 1.8 converts ppm to mg CO_2. The multiplication by 1.37 converts the boundary layer resistance to vapour transport $r_{b,V}$, which was determined in Section 5.4.2, to a resistance to CO_2 transport. Gijzen (1992) reported the stomatal resistance to vapour transport (r_s) to be 50 sm^{-1} for a wide range of canopies. The third resistance (r_c) in the series is a chemical resistance. In the work of Gijzen, this resistance is calculated from a chemical conductance (C_c). In his work C_c depends on temperature. It grows linearly from 0 to 0.004 in the leaf temperature range from 5 to 25 °C. On temperatures above 25 °C C_c decreases linearly until the value 0 is reached at 40 °C. The value for r_c is the reciprocal of C_c.

The last parameter in the photosynthesis model is the maximal endogenous capacity (P_{mm}). According to Gijzen, P_{mm} is temperature dependent. P_{mm} is zero for temperatures beneath 5 and above 40 °C. Between 5 and 30 °C P_{mm} grows linearly from 0 to 2.5 mg $CO_2m^{-2}s^{-1}$. In the temperature range from 30 to 40 °C P_{mm} decreases linearly from 2.5 to 0.

I.2 From leaf assimilation rate to canopy photosynthesis

A canopy consists of numerous leaves that each intercept radiation at a certain intensity and thus induce a CO_2 consumption. With respect to the greenhouse climate simulation model the CO_2 consumption of all these individual leaves has to be combined to a canopy assimilation rate.

A fast and commonly used method to perform the computation of canopy photosynthetic activity from leaf photosynthesis is the Gaussian Integration method (Goudriaan, 1986) (see Appendix G). This numerical algorithm integrates a

function by the calculation of a mean value of the function to be integrated. For the three-points Gaussian Integration this mean value is determined by a weighted sum of three functional evaluations, located on the relative distances 0.113, 0.500 and 0.887 of the domain for integration.

In the case of determination of canopy photosynthesis the function to be integrated is the photosynthetic activity, which, by means of the declining intensity of radiation, depends on the height in canopy. The domain of integration is the total leaf area, which is expressed by the LAI. Thus, calculation of canopy photosynthesis by Gaussian Integration is performed by a weighed sum of photosynthetic activity in three levels of the canopy, multiplied by the LAI.

The photosynthetic activity at a certain level in the canopy is a function of the absorbed radiation on that level. The simplest way to determine the absorbtion is to consider the change of radiation intensity through the canopy to be partly caused by absorbtion, and partly by scattering. The change of radiation intensity at an arbitrary height in the canopy is the derivative of the exponential function describing the radiation profile.

$$dI_{VIS}(x) = -k\ I_{VIS}\ e^{-k \times LAI} \qquad\qquad [Wm^{-2}]\ (I.7)$$

In this equation the extinction coefficient (k) has different values for different types of radiation (diffuse or direct) and LAI (see Appendix D). I_{VIS} is the intensity of radiation at the top of the canopy and x is the relative depth of the considered canopy level, counted from the top. As shown in Appendix D, I_{VIS} can be even larger than the radiation flux in the visible wave band entering the greenhouse (see the discussion on Fig. D.5).

The rate of change of the intensity of radiation originates from absorbtion and reflection of radiation by the canopy. Thus, multiplication of the derivative of the radiation profile with an absorbtion coefficient yields the absorbed radiation flux. This flux is defined in Eqn. I.8.

$$VIS_{abs,dif}(x) = a_{dif}\,k_{dif}\,I_{VIS,dif}\ exp(-k_{dif} \times LAI) \qquad\qquad [Wm^{-2}]\ (I.8)$$

The '$-$' sign from Eqn. I.7 has disappeared because the absorbtion of radiation has a sign opposite to the decrement of light intensity. The absorbtion coefficient for diffuse radiation (a_{dif}) can be deduced from the work of Goudriaan (1977) as being defined by:

$$a_{dif} = 1 - \frac{1 - \sqrt{(1-sc)}}{1 + \sqrt{(1-sc)}} \qquad\qquad [-]\ (I.9)$$

With a scattering coefficient (*sc*) 0.15, which is a common value for a canopy stand (Goudriaan, 1977), Eqn. I.9 yields $a_{dif} = 0.71$.

The computation of the absorbtion of direct radiation is more complicated. In the first place the extinction of direct light is strongly dependent on the angle of solar

elevation. These dependencies are discussed in Appendix D. In the second place the scattering of direct radiation after interception by a leaf surface induces diffuse radiation. Thus the decrement of light intensity from direct radiation is less than the decrement of direct irradiated leaves. To compute the amount of secondary diffuse radiation, the profile of pure direct radiation is subtracted from the profile describing the total radiation intensity from direct radiation. Calling the extinction coefficient of the full direct profile $k_{dir}(\beta)$, the diffuse radiation flux induced by scattering of direct radiation is expressed as:

$$VIS_{abs,dir \rightarrow dif}(x,\beta) = I_{VIS,dir}(k_{dir}(\beta)exp(-k_{dir}(\beta) \times LAI) \qquad [Wm^{-2}] \quad (I.10)$$
$$- k_{sunlit}(\beta)exp(-k_{sunlit}(\beta) \times LAI))$$

Again x denotes the depth of the canopy layer under consideration. The radiation flux $VIS_{abs,dir \rightarrow dif}$ acts the same as the previously defined $VIS_{abs,dif}$. Thus the total amount of absorbed diffuse radiation is described by:

$$VIS_{abs,dif,tot}(x) = VIS_{abs,dir \rightarrow dif}(x) + VIS_{abs,dif}(x) \qquad [Wm^{-2}] \quad (I.11)$$

A third complicating factor of the absorbtion of direct radiation is that throughout the canopy depth, the sunlit surfaces are all irradiated at the same intensity. Thus, the profile of pure direct radiation is rather a description of the fraction of sunlit leaves than a representation of the intensity of the direct radiation. In a formula:

$$fr_{sunlit}(x,\beta) = exp(-k_{sunlit}(\beta) \times LAI) \qquad [-] \quad (I.12)$$

The complement of the sunlit leaves are leaves in the shade. These leaves intercept diffuse radiation only. Thus the assimilation rate of leaves in the shade at arbitrary height in the canopy is described by:

$$MC_{shade}(x) = (1-fr_{sunlit}(x)) \; assim(VIS_{abs,dif,tot}(x)) \qquad [mgs^{-1}m^{-2}] \quad (I.13)$$

As far as the sunlit leaves are concerned a fourth and final complicating factor with respect to direct radiation must be solved, namely the large unevenness of the angle between the beam of direct radiation and the normal of sunlit leaf surfaces. This angle ω determines the 'dilution' of the beam of radiation at the canopy surface. When the angle is zero, the leaf surface is positioned perpendicular at the solar beam, which results in intensities of irradiation up to about 500 Wm^{-2}. When the angle is large, the beam of radiation is spread out over a large leaf surface. Thus this radiation is 'diluted'. Depending on the solar elevation and the geometry of the canopy, a fractional division can be made amongst the leaf surfaces irradiated with a certain dilution factor. In Table I.1 the relative frequency of these dilution factors for a number of solar elevations is presented.

Table I.1 Relative frequency of dilution factors (rounded to one decimal) for direct radiation on a canopy with a planophile leaf angle distribution for a number of solar elevation angles.

β	dilution factor ($\cos(\omega)$)									
	0.1	0.2	0.3	0.4	0.5	0.6	0.7	0.8	0.9	1.0
5	0.368	0.174	0.133	0.097	0.074	0.064	0.045	0.029	0.015	0.003
15	0.206	0.183	0.192	0.127	0.096	0.071	0.053	0.039	0.025	0.008
25	0.138	0.098	0.123	0.208	0.137	0.100	0.079	0.057	0.044	0.017
35	0.090	0.067	0.080	0.097	0.136	0.213	0.113	0.101	0.065	0.036
45	0.060	0.044	0.053	0.064	0.086	0.128	0.235	0.156	0.117	0.058
55	0.035	0.028	0.034	0.046	0.061	0.089	0.134	0.276	0.202	0.095
65	0.018	0.016	0.025	0.032	0.048	0.070	0.108	0.171	0.357	0.155

In the table, the frequency of dilution factors smaller than 0.05 are added to the first column, which is a good approach since the first part of the photosynthetic response-curve is practically linear.

With data from Table 5.1, the carbon dioxide fixation by sunlit leaves can be expressed as

$$MC_{sunlit}(x) = fr_{sunlit}(x) \sum_{i=1}^{10} \{f(\beta,i) \, assim(VIS_{abs,dir}(i))\} \qquad [mgm^{-2}s^{-1}] \quad (I.14)$$

with

$$VIS_{abs,dir}(i) = a_{dir} \, VIS_{dir\perp} \, i/10 + I_{abs,dif,tot}$$

where MC_{sunlit} denotes the assimilation rate of sunlit leaves, fr_{sunlit} the fraction of sunlit leaves, $f(\beta,i)$ the fraction of the sunlit leaves intercepting direct radiation with an intensity which is a factor $i/10$ of the radiation perpendicular on the direct beam, a_{dir} the absorbtion coefficient of leaves and $VIS_{dir\perp}$ the intensity of radiation perpendicular to the direct beam. The factor $i/10$ dilutes $VIS_{dir\perp}$ and $VIS_{abs,dif,tot}$ adds the diffuse radiation to the total amount of radiation on the sunlit canopy leaf. From the work of Goudriaan can be deduced that a_{dir} equals 0.82 for radiation in the visible range of wavelengths.

Using the Gaussian integration method, the canopy assimilation rate can now be found from

$$MC_{AirCan} = \{ 0.278 \, (MC_{shade}(0.11) + MC_{sunlit}(0.11)) \qquad [kgm^{-2}s^{-1}] \quad (I.15)$$
$$+ 0.444 \, (MC_{shade}(0.50) + MC_{sunlit}(0.50))$$
$$+ 0.278 \, (MC_{shade}(0.88) + MC_{sunlit}(0.88)) \} \, 1 \cdot 10^{-6} \, LAI$$

In this equation 0.278, 0.444 and 0.278 are the weighing factors of the contribution of the photosynthesis at 0.11, 0.50 and 0.88 of the canopy depth to compute the mean photosynthetic activity per m^2 leaf area. Multiplication with the LAI yields the canopy photosynthesis. The term $1 \cdot 10^{-6}$ converts mg to kg.

APPENDIX J: SOLAR ELEVATION AND AZIMUTH

The position of the sun in the sky vault is defined by its azimuth and elevation. The azimuth is the angle between the sun and the geographical south, measured on a horizontal plane. The angle between the sun and that plane is the elevation. If the orbit of the sun was a perfect circle, the azimuth could be computed from the time of day as a fraction of 24 hours. However, because the orbit of the earth around the sun is an ellipse, the time at which the sun reaches its highest point, corresponding with an azimuth 180, is either somewhat advanced or retarded. This advance or retard is called the equation of time. An empirical formula to compute the equation of time reads (France and Thornly, 1984):

$$\Delta t = -7.13 \cos(\gamma) - 1.84 \sin(\gamma) - 0.69 \cos(2\gamma) + 9.92 \sin(2\gamma) \qquad [min] \quad (J.1)$$

with γ the year angle. The year angle is zero at the vernal equinox on 21 March. Thus the year angle can be expressed as a function of day number by:

$$\gamma = 360 \ (daynr\text{-}80)/365 \qquad\qquad\qquad [°] \ (J.2)$$

with *daynr* the sequential day of year, counted from January 1st. With Eqn. J.1, the azimuth as a function of time can be expressed by:

$$az = 360 \ (hr+\Delta t/60\text{-}12)/24 \qquad\qquad\qquad [°] \ (J.3)$$

with *hr* the local solar time. During winter time, the local solar time of a place at a specific longitude is a factor 24·*longitude*/360 hr less than the local middle European time. During summer time the local time is another hour less.

The solar elevation can be expressed as a function of the latitude, the actual azimuth and the solar declination (δ). The solar declination is the angle between the line joining the centres of the sun and the earth, and the equatorial plane. The declination angle depends on the day of year (expressed with the year angle γ) according to (France and Thornly, 1984):

$$\delta = 0.38 - 0.77 \cos(\gamma) + 23.27 \cos(\gamma) \qquad\qquad [°] \ (J.4)$$

When ϕ denotes the latitude, the sine of the elevation angle (ζ) is expressed by (France and Thornly, 1984):

$$\sin(\zeta) = \sin(\phi)\sin(\delta) + \cos(\phi)\cos(\delta)\cos(az) \qquad\qquad [-] \ (J.5)$$

from which the elevation follows from the arcsine of Eqn. J.5.

APPENDIX K: NOTATION

A   surface (m^2)

A_0 surface of a window (m^2) (see Figure 5.4)

I   radiation intensity (Wm^{-2})

LAI   leaf area index [-]

l   length of a heating pipe per m^2 floor surface (m^{-1})

ℓ characteristic dimension of a canopy leaf (the width) (m) (Eqn. 5.56)

d   diameter of a heating pipe (m)

r   resistance (sm^{-1})

T   temperature

t   time (s)

t_s step size in a numerical integration procedure (s)

CO2   partial carbon dioxide pressure (Pa)

C   forced carbon dioxide flux $(kgs^{-1}m^{-2})$

HEC   heat exchange coefficient $(Wm^{-2}K^{-1})$

k   extinction coefficient

MTC   mass transfer coefficient $(kgs^{-1}m^{-2}Pa^{-1})$

N   number of cells in the shift register representing the storage tank (-)

P   forced heat flux (Wm^{-2})

r   resistance sm^{-1}

REC   radiative heat exchange coefficient $(Wm^{-2}K^{-4})$

SC   screen closure fraction (-)

SO   absolute screen opening (m) (see Figure 5.5)

u wind speed (ms^{-1})

v velocity of water through a heat distribution loop (ms^{-1})

VP   partial vapour pressure (Pa)

W   gutter to gutter distance (m) (see Figure 5.5)

x   moisture content (gkg^{-1})

Greek symbols

α   heat exchange coefficient ($Wm^{-2}K^{-1}$); absorbtion coefficient (-, Appendix E)

β   thermal expansion coefficient (K^{-1}), solar elevation angle

γ   psychometric constant (65.8 Pa K^{-1}).

ΔH heat of evaporation ($2.45 \cdot 10^6$ Jkg^{-1}).

ε   long-wave emission coefficient (-)

θ   window-opening angle, relative to the roof (degrees) (see Figure 5.4)

λ   air factor (-, Chapter 4); thermal conductivity (WmK^{-1}, Chapter 5)

μ   partial mass fraction of constituents of exhaust gases of combustion devices kg per m^3 combusted gas)

ν   wavelength (m)

ρ   density (kgm^{-3}); reflection coefficient (-, Section 5.5.2.3, Appendix E)

σ   Stefan Boltzman constant ($5.67 \cdot 10^{-8}$ $Wm^{-2}K^{-4}$)

Φ   combustion rate of natural gas (m^3 natrural gas per second)

$\Phi^\bullet$ combustion rate of natural gas normalized to the greenhouse floor surface (m^3 natrural gas per second per m^2).

φ   air flux (m^3s^{-1})

φ"   flux per m^2 floor surface ($m^3m^{-2}s^{-1}$) or (Wm^{-2})

ψ   roof slope of the saw-tooth greenhouse cover (degrees) (see Figure 5.4)

ω   angle (radians)

φ   mass flux of water through heating pipes, normalized per m^2 greenhouse surface ($kgm^{-2}s^{-1}$)

Dimensionless numbers

Le   lewis number

Nu   nusselt number

Gr   grashoff number

Ra   raleigh number

LAI   leaf area index

Pe   Peclet number

Subscripts

air	greenhouse air compartment. When the thermal screen is opened the greenhouse air compartment represents all the air in the enclosure. If the thermal screen is closed the air compartment represents the air below the screen only.
alu	artificial illumination
b	boundary layer
can	canopy
cov	greenhouse cover
d	downward
do	lower side
flr	greenhouse floor
H	heat
i	internal
i,j	indices
low	lower heating pipe
NIR	short-wave radiation in near infra red waveband
out	outside
pip	heating pipe
scr	thermal screen
sti	i^{the} storage tank compartment
so1..so6	first up to the sixth soil layer
so7	boundary condition in the soil
top	air compartment above the screen.
u	upward
up	upper side
upp	upper heating pipe
V	vapour
VIS	short-wave radiation in the visible waveband

SUMMARY

During the past two decades, the production per m^2 floor surface of glasshouse horticulture in the Netherlands has almost doubled. Besides improvements of the greenhouse construction, the genetic properties of the plant and its nutrition, an important factor contributing to this increment is the improved control of greenhouse indoor climate. CO_2 supply and artificial illumination have become particularly widespread and the growth season has been lengthened.

Coupled to the intensification of the production process, the mean energy consumption per m^2 greenhouse surface shows a steady increment of (0.05 $GJm^{-2}year^{-1}$ per year during the last 5 years). For the current glass covered area of almost $11 \cdot 10^3$ hectare, this means a yearly extra energy consumption of 5 PJ^a. Together with the growth rate of the glass covered area of som 175 hectare per year, the total primary energy consumption of horticulture in the Netherlands increases with some 7 PJ per year.

In 1993, the primary energy consumption of horticulture was 138 PJ, which is 5% of the domestic energy consumption.

Because of the growing concern about the effect of the increasing carbon dioxide concentration in the atmosphere, which is strongly related to the combustion of fossil fuels, the government of the Netherlands aims to diminish primary fuel consumption. In order to reach that goal, agreements have been made with all energy intensive sectors of economy. Representatives of horticulture in the Netherlands have formulated a target with respect to energy conservation. This target is to cut the primary energy consumption per unit of production value by half by the end of the century compared to its value in 1980. The official agreement, henceforth referred to as the MJA (Meerjarenafspraak), also included the definition of a measuring unit that enables this target to be monitored. This measuring unit is referred to as ENSEC (Economically Normalized Specific Energy Consumption). By an economic normalization of the production, the course of the ENSEC can be computed for any mix of horticultural products.

In Chapter 2 the definition of ENSEC is presented and the course of ENSEC during the period 1980 to 1993 is shown. It appears that ENSEC's tendency, after a rapid fall in the period 1980 to 1985, is to remain constant at around 65. This level is quite far from the stated objective (an ENSEC=50 in the year 2000). Moreover, when extrapolating the tendencies of the last 5 for the primary energy consumption and production value per m^2 greenhouse, ENSEC can be expected to grow to 72 in the year 2000. Thus, in order to reach the target, the current tendencies have to change direction.

---

[a] 1 PJ = $1 \cdot 10^{15}$ J which is equivalent to about $32 \cdot 10^6$ m^3 of natural gas.

Principally, the decrement of the ENSEC can be achieved by a decrement of primary energy consumption or by an increment of production. However, it has been shown for the second case that the general governmental objective to decrease the absolute level of CO_2-exhaust[a] , will be severely violated, providing that the current tendency of increment of the glass covered area persists. Therefore, measures proposed in the MJA to achieve the agreed target are focused on the other factor that determines the ENSEC; the decrement of primary energy consumption.

From the 25 measures that are proposed, nine subjects to be evaluated on their energy saving prospective are selected. These subjects are arranged into three groups. The first group concerns simple measures with respect to the engineering of the heating system that can be readily applied. The second group involves the improvement of the greenhouse building by the decrement of leakage and by improving the degree of insulation of the covering structure. The third group includes energy conserving heating devices. In this group the potentials of a condenser, a short- term heat storage facility and a combined heat and power engine are evaluated.

The energy saving effects of the selected measures are difficult and time consuming to study in a working greenhouse. Difficult because it is very hard to exclude effects from other factors than the measures to be studied and time consuming since the experiments should span at least one year. Therefore, a method is needed that judges energy-saving techniques for modern horticultural practice in an unambiguous and reconstructible way. To serve this need, in this study a deterministic simulation model is developed that describes the energy consumption of a modern greenhouse, accounting for the typical characteristics of the indoor greenhouse climate, the greenhouse climate controller and the heating system.

In Chapter 3 the requests on such a simulation model are presented. From these requests it is deduced that the primary state variables to be described concern the heating pipe temperatures, the indoor air conditions with respect to temperature, humidity and CO_2 concentration and the temperature at the top and bottom side of the heat storage tank. To describe the dynamics of these entities, a number of other state variables are defined. Also the boundary variables on the model are presented.

In order to be able to keep up with the dynamics of modern greenhouse climate controllers, it is argued that the simulation model requires a resolution in time of

---

[a]The general governmental objective to decrease the CO_2-exhaust aims to have decreased the exhaust at the end of the century to 96% of its value in 1990 for all energy intensive sectors of economy.

up to one minute. In order to create easy interpretable parameters and to ensure that the model can be applied in numerous variations, it was decided to develop a deterministic model. As an introduction to the detailed description of the model developed, the essentials of the selected model type are presented.

The presentation of the developed model is divided over two chapters. Chapter 4 describes the components of the heating system simulation, the connection of these components to each other and the connection of the heating system simulation to the greenhouse climate simulation model. For each of the components in the heating system a sub-model that describes the characteristic behaviour of the device is presented. In Chapter 5 the greenhouse climate simulation model is presented briefly but integrally. Unlike the greenhouse heating system simulation (Chapter 4), the greenhouse climate simulation model proceeds from the current state-of-the-art.

The connection between the heating system (model) and the greenhouse climate (model) can be seen as being performed by the greenhouse climate controller. Therefore, Chapter 4 begins with a description of the functionality of a customary greenhouse climate controller. The controller attempts to achieve a setpoint with respect to air temperature, humidity and CO_2 concentration. The realization of the temperature setpoint is performed by heating or ventilation. Ventilation is also applied when the humidity exceeds a certain threshold. In that case, if temperature of the outside air is below the greenhouse air temperature, this results in a heat demand as well. The realization of a CO_2-concentration is performed by exhaust gases supply. Thus, temperature control and, indirectly, humidity control induce a heat demand. Eventually the heat demand causes combustion of primary energy (natural gas) by the boiler or CHP engine. CO_2 supply also forces the combustion of primary energy.

In the heating system simulation model six components are distinguished namely the heating circuit, the boiler, the condenser, the CHP-engine, the heat storage tank and the expansion vessel. From the point of view of the model concept, the simulation of the expansion vessel could be omitted. However, this device is still discussed here because one of the energy-saving measures mentioned in MJA concerns the expansion vessel.

In order to describe the dynamics a horticultural heating circuit, which from horticultural point of view is the major component of the heating system, a model has been developed that takes account of its special characteristics. The model is compared to detailed measurements in a semi-practical research facility. The results of the model show a good resemblance with the measured values.

It was argued that a description of the dynamics of a boiler is not required for the present purpose of the model. However, since the insulation of the boiler is one

of the energy-saving measures proposed in the MJA, the relation between heat loss and insulation thickness is determined, on the basis of general theory on heat exchange.

With respect to the condenser it is known that the energy saving achieved depends on the temperature of the water fed to the device, the volume flux of the exhaust gases passing the condenser and the combustion characteristics of the boiler. On behalf of the present heating system model these relations are quantified.

The CHP-engine is discussed briefly because, as argued in this work, the heating system model considers its reject heat as an on/off heating power.

The energy-saving prospectives of the heat storage tank is one of the major items of the energy saving measures to be evaluated. Therefore, with respect to the present study, an extensive model describing its dynamics has been developed. The model results are compared to measurements. The comparison shows that both charging and discharging of the storage tank are well described.

Finally, in Chapter 4 the devices in the heating system are connected to each other. The dynamic behaviour of this entire heating system is shown in some graphs.

In Chapter 5 the greenhouse climate simulation, which is the second component of the model, is presented. The simulation model includes the application of thermal screens and artificial illumination.

The greenhouse climate simulation model is divided into three parts. The first part concerns the description of the CO_2 concentrations in the greenhouse. The second part describes the modelling of humidity of the greenhouse air. The third part of the model comprises the thermal part of greenhouse climate simulation. The relations described in Chapter 5 are derived from the recent literature on greenhouse climate modelling.

In Chapter 6 the results of the aggregated simulation model are compared to detailed measurements made in a research facility, which serves as a semi-practical greenhouse. A rose canopy was grown in the research facility. From August to April artificial illumination was applied, subject to a customary illumination control. First, comparisons on a small time scale are made for a short period. This means that ten minute mean values of greenhouse air conditions with respect to temperature, humidity and CO_2-concentration, heating power and pipe temperatures were compared with measured values, gathered on three successive days.

The values and dynamics of the modelled quantities were very much the same as the measured values, although sometimes distinct differences could be noticed. Also the climate controller actions with respect to window aperture, the closure of the thermal screen and illumination control were almost equal to the registered control actions. The control of CO_2 supply showed some differences with the

control in the research facility.

On a year round time scale, the daily mean greenhouse air temperature was well simulated, except during very warm periods. During those periods the modelled temperature was higher than the measured value. Also the modelled daily water consumption was compared with the registered water consumption. In spring and summer the model over-estimated the daily evaporation, but in autumn and winter the daily water consumption was simulated well. The year round result with respect to heat demand of the greenhouse was modelled with an accuracy of 98%.

After the model quality is shown by comparing its results with results from the small research facility, the simulation model is applied to the study of energy saving potentials of the measures selected from the options proposed in the MJA (Chapter 2). To do so, the model is re-parametrized so that it represents a modern greenhouse of 1 hectare growing tomatoes in the Netherlands. Its heating system is supposed to be equipped with a condenser and a heat storage tank of 80 m^3. For this reference greenhouse, a set of customary greenhouse climate controller settings is defined. The controller settings are suitable for a tomato crop, planted on 1 December and removed on 15 November. Furthermore, with respect to the models boundary variables a set of weather data is chosen that can be considered representative of typical weather in the Netherlands.

The first group of energy saving measures to be studied consisted of relatively simple improvements to the boiler house, involving the increment of the insulation thickness of the boiler, the insulation of transport pipes and the replacement of the place of connection of the expansion vessel. With respect to the computation of the effect of the insulation of transport pipes, six pipe types are defined. These have been distinguished according to their function in the heating system. The savings achieved by replacing the attachment of the expansion vessel are computed for the reference greenhouse (including a heat storage tank) and a greenhouse without a storage tank.

It appears that the energy savings achieved by these simple measures are small. However, since the proposed measures are easy, and therefore relatively cheap to implement they can still be advantageous.

The second item of energy-saving measures studied with the simulation model concerned the decrement of energy losses from the greenhouse cover by the decrement of leakage through windows, the application of a thermal screen and the application of alternative cladding materials (coated glass panes and double glazing).

Under the circumstances created to study the effect of the prevention of leakage through windows the decrement of heat demand was small (1.6%). The other measures show energy savings ranging from 18% (a tin-oxide coating) to up to 47% (an option using double glass where each glass is coated with a tin-oxide

coating and a particular polymer coating). However, the thermal screen and most of the alternative cladding materials result in a decreased transparency of the greenhouse. This results in a decrement of photosynthesis. To combine the energy-saving effect with the loss of production, the qualities of the thermal screen and the alternative cover materials are rated according to their impact on the decrement of specific energy consumption. The specific energy consumption is defined as the yearly amount of primary energy required per unit of yearly photosynthesis. With respect to the specific energy consumption the achieved savings range from 10% (a tin-oxide coated cover) to 39% (double coated double glass).

An interesting aspect of increasing insulation properties of the greenhouse cover is its effect on the increase of the (absolute and relative) portion of energy demand related to dehumidification of the greenhouse. This effect is quantified for each of the options discussed with respect to measures in the second item. The results show that the portion is about doubled for the greenhouse with the best insulated cover, compared to the reference greenhouse.

The third item of energy saving measures concerns the application of a condenser, a short-term heat storage facility and a combined heat and power engine. The condenser is studied for two configurations. It appears that it is advantageous to be able to feed the condenser with return water from both heating circuits instead of a connection solely to the low temperature heating circuit.

The effects of a heat storage tank is studied for a greenhouse with and without a CHP engine. As far as a greenhouse without a CHP engine is concerned, the storage tank is used to carry reject heat from CO_2 supply from the day to the night. Depending on the CO_2 supply strategy, the storage tank appears either mainly to affect the primary energy consumption or mainly the yearly photosynthesis. Energy is saved if the CO_2 is generated by the combustion of natural gas irrespective of the heat demand. For this strategy the storage tank diminishes the occasions that heat surpluses have to be carried off by extra ventilation. If the supply strategy prevents heat surpluses having to be carried off, the implementation of a storage tank does not save primary energy, but enhances the yearly photosynthesis. Again, to combine both effects the prospects of a heat storage tank are judged on its impact on the decrement of specific energy consumption. For both supply strategies, the specific energy consumption as a function of storage tank dimension was computed for three CO_2 supply rates.

In a greenhouse with a CHP engine for electricity demand for its artificial illumination, a storage tank affects both the primary energy consumption and the yearly photosynthesis (assuming a CO_2 supply strategy that avoids extra ventilation). It is shown that the second effect dominates the first.

In the situation where the CHP engine serves the electricity production of the public grid, the major factor that determines the primary energy saving is the

thermal power of the device. Here the energy savings emanate from the decrement of electricity to be produced in public power plants as a part of the public electricity demand is produced by CHP engines in horticulture. It is shown that large energy savings of up to 32% can be achieved. If exhaust gases of the CHP engine can be cleaned to such an extent that they can serve the CO_2 demand of a greenhouse the prospects are even more promising.

In Chapter 7 the conclusions of this study are presented and discussed.

SAMENVATTING

In de afgelopen twee decennia is de produktie per eenheid kas-oppervlak in de Nederlandse glastuinbouw ongeveer verdubbeld. Deze grote toename is naast ver-beteringen aan de kasconstructie, de genetische eigenschappen van het plant-mate-riaal en een verbeterde voeding, voor een belangrijk deel toe te schrijven aan de conditionering van het kasklimaat. CO_2-dosering en assimilatiebelichting worden op uitgebreide schaal toegepast en de gemiddelde teeltperiode is verlengd.

Gerelateerd aan deze intensivering van het produktieproces is het gemiddeld ener-gieverbruik gestaag toegenomen (0.05 $GJm^{-2}jaar^{-1}$ per jaar over de laatste 5 jaren). Bij het huidige glastuinbouwareaal van ruim $10 \cdot 10^3$ hectare betekent dit een jaar-lijks extra energieverbruik van 5 PJ[a] Samen met een areaal-groei van ongeveer 175 hectare per jaar neemt het primaire energieverbruik (fossiele brandstoffen) jaarlijks met ongeveer 7 PJ toe.

In 1993 bedroeg het totale energieverbruik in de Nederlandse glastuinbouw 138 PJ, waarmee de sector verantwoordelijk is voor ongeveer 5% van het jaarlijks nationaal energieverbruik.

Vanwege de groeiende zorg om het effect van een stijgende CO_2-concentratie in de atmosfeer, wat sterk gekoppeld is aan de verbranding van fossiele brandstoffen, heeft de Nederlandse overheid het doel gesteld het gebruik van deze brandstoffen te doen verminderen. Met alle energie-intensieve economische sectoren heeft zij daartoe convenanten afgesloten. In de glastuinbouw heeft zo'n convenant gestalte gekregen in de Meerjarenafspraak-Energie voor de Nederlandse Glastuinbouw (in het vervolg aangeduid met MJA). De concrete doelstelling met betrekking tot het gebruik van fossiele brandstoffen is een halvering van het primair energieverbruik per eenheid produkt in het jaar 2000 ten opzichte van 1980. Om de realisatie van deze doelstelling te kunnen beoordelen is in de MJA een meet-eenheid overeenge-komen. Deze meet-eenheid, die in dit proefschrift met ENSEC[b] wordt aangeduid geeft het percentage van de waarde van het actuele primair energieverbruik per eenheid produkt ten opzichte van de waarde van deze breuk in 1980. De doelstelling van de MJA is dus een ENSEC=50 aan het eind van de eeuw. De weeg-factor van de verschillende glastuinbouwprodukten in de ENSEC is gebaseerd op hun onderlinge waarde-verhouding.

In hoofdstuk 2 wordt de definitie van de ENSEC in detail besproken en wordt het verloop van de ENSEC over de periode 1980 tot en met 1993 gepresenteerd. Het blijkt dat, na een aanvankelijk sterke daling in de periode '80-'85, de ENSEC ge-

---

[a]1 PJ = $1 \cdot 10^{15}$ J en komt overeen met de vebrandingswaarde van ongeveer $32 \cdot 10^6$ m^3 aardgas.

[b]Economisch genormaliseerd specifiek energieverbruik

durende de laatste jaren constant rond de 65 is gebleven. Bovendien, wanneer de tendensen met betrekking tot energieverbruik en produktie van de afgelopen 5 jaren worden doorgetrokken, komt de ENSEC in 2000 uit op 72. Om de doelstelling van de MJA te halen zullen de huidige trends dus moeten worden omgebogen.

In principe kan een verkleining van de ENSEC zowel worden bereikt door een vermindering van het primair energieverbruik als door een vergroting van de produktie. Echter, bij een vermindering van de ENSEC middels produktie-verhoging zal, bij voortzetting van de huidige groeivoet van het glastuinbouwareaal, de algemene CO_2-doelstelling die de overheid heeft gesteld[a] bij lange na niet worden gehaald. Daarom is alle aandacht in de MJA gericht op een vermindering van het primair energieverbruik.

Van de 25 energie-besparende opties die in de MJA genoemd worden, zijn er negen in het kader van dit proefschrift bestudeerd. Deze negen opties zijn in drie clusters gegroepeerd. Het eerste cluster omvat maatregelen rond het verwarmingssysteem die eenvoudig kunnen worden toegepast. Het tweede cluster heeft betrekking op maatregelen die de warmteverliezen van de kasconstructie verminderen. Het derde cluster betreft energie-besparende installaties zoals een condensor, een warmte-opslag tank en een warmtekracht installatie (WKK-installatie).

De bestudering van de effecten van de geselecteerde energie-besparende opties kan moeilijk in een praktijkexperiment worden uitgevoerd, omdat andere invloedsfactoren dan de bestudeerde optie haast niet uit te sluiten zijn. Bovendien zou zo'n praktijkexperiment tijdrovend zijn omdat voor veel maatregelen een goed oordeel pas kan worden gegeven na bestudering van een jaarrondsituatie. Daarom is er behoefte aan een methode waarmee de effecten van voorgestelde energie-besparende maatregelen in de tuinbouwkundige context eenduidig kunnen worden ingeschat. Teneinde in deze behoefte te voorzien is er in het kader van dit proefschrift een deterministisch simulatiemodel ontwikkeld dat het energieverbruik van een moderne kas berekent in afhankelijkheid van de specifieke eisen aan het kasklimaat, de werking van de kasklimaatregelaar en de bedrijfsuitrusting met betrekking tot het verwarmingssysteem.

In hoofdstuk 3 worden de eisen die aan zo'n model moeten worden gesteld geformuleerd. Uit deze eisen wordt afgeleid dat het simulatiemodel in eerste instantie een beschrijving vereist van de pijptemperaturen in de verwarmingsnetten, de kasluchtcondities met betrekking tot temperatuur, vochtgehalte en CO_2-concentratie

---

[a]In het Nationaal milieubeleidsplan-plus (1989) heeft de overheid zich ten doel gesteld de CO_2-uitstoot in het jaar 2000 voor elk van de energie-intensieve economische sectoren terug te hebben gebracht naar 96% van de uitstoot van de betreffende sectoren in 1990.

en de watertemperatuur boven- en onderin de warmte-opslag tank.

Om het dynamisch gedrag van deze grootheden te kunnen beschrijven, worden een groot aantal andere toestandsgrootheden gedefinieerd. Ook worden de variabelen die aan de systeemgrenzen op het model worden gelegd toegelicht. Tenslotte worden, als aanzet tot de gedetailleerde beschrijving van het simulatiemodel, de essenties van het gebruikte modeltype besproken.

Het ontwikkelde simulatiemodel wordt beschreven in hoofdstuk 4 en 5. Hoofdstuk 4 beschrijft de componenten die in het kasverwarmingssysteem zijn onderscheiden, de onderlinge koppeling van deze componenten en de koppeling tussen het verwarmingssysteem simulatiemodel en het kasklimaat simulatiemodel. Voor elke component van het verwarmingssysteem wordt een sub-model geformuleerd dat het specifieke gedrag van die component beschrijft. In hoofdstuk 5 wordt het kasklimaatsimulatiemodel kort doch integraal beschreven. De beschrijving is kort omdat dit deel van het model, in tegenstelling tot het verwarmingssysteem model, gebaseerd is op kasklimaatmodelbeschrijvingen in de literatuur.

In het modelconcept wordt de koppeling tussen het verwarmingssysteem(model) en het kasklimaat(model) verondersteld te worden gerealiseerd door de kasklimaatregelaar. Daarom begint hoofdstuk 4 met een beschrijving van de essentie van gangbare kasklimaatregelaars.

De kasklimaatregelaar tracht een temperatuur, vochtigheid en CO_2-setpoint te realiseren middels verwarming, ventilatie en CO_2-dosering. Ventilatie vindt plaats op grond van temperatuur- of vochtcriteria. CO_2-dosering wordt verondersteld te worden gerealiseerd middels ketelrookgassen.

De regeling van het kasklimaat zal dus resulteren in een warmtevraag die op een of andere manier ingevuld zal worden door de verbranding van primaire brandstoffen (in de tuinbouw vrijwel uitsluitend aardgas) in een ketel of een WKK-installatie.

Ten behoeve van de beschrijving van de relatie tussen warmtebehoefte van de kas en de verbranding van primaire brandstoffen zijn in het verwarmingssysteem simulatiemodel zes componenten onderscheiden. Dit zijn het verwarmingscircuit, de ketel, de condensor, de WKK-installatie, de warmte-opslag tank en het expansievat. Vanuit het modelconcept is de beschrijving van expansievat niet vereist maar deze is aan het hoofdstuk toegevoegd omdat één van de energie besparende opties betrekking heeft op het expansievat.

Het verwarmingscircuit is vanuit tuinbouwkundig oogpunt het belangrijkste onderdeel van het verwarmingssysteem. Om het dynamisch gedrag van dit onderdeel goed te kunnen beschrijven is een model ontwikkeld waarin de karakteristieke aspecten van zo'n circuit zijn opgenomen. De resultaten van dit model zijn vergeleken met gedetailleerde metingen aan het verwarmingscircuit in een afdeling van een proefkas. De overeenkomst was erg goed.

Met betrekking tot de ketel is beargumenteerd dat voor dit onderdeel van het verwarmingssysteem een statisch model volstaat. De ketel wordt als onbeperkt regelbare vermogensbron beschouwd. Omdat vergroting van de ketelisolatiedikte één van de maatregelen is die in de MJA worden voorgesteld is de beschrijving van warmte-verliezen aan de wand van de ketel als functie van de isolatiedikte in het model opgenomen.

Van de condensor is bekend dat het energie besparend effect afhangt van de ingaande watertemperatuur, de doorstroomsnelheid van de rookgassen en de branderafstelling van de ketel. Deze invloedsfactoren zijn gekwantificeerd en in een statisch condensor-model ondergebracht.

De WKK-installatie is, net als de ketel, beschouwd als warmtebron waarin geen rekening hoeft te worden met de dynamica van het systeem.

Het laatste belangrijke onderdeel van het verwarmingssysteem is de warmte-opslag tank. De toepassing van zo'n tank krijgt ruime aandacht in de uitwerking van de voorstellen in het kader van de MJA. Daarom wordt in dit werk een uitgebreid dynamisch model voor de beschrijving van het dynamisch gedrag van dit onderdeel van het verwarmingssysteem gepresenteerd. Dit model is vergeleken met metingen aan een proef-opstelling. Het model bleek het gedrag van de tank goed te beschrijven.

Tenslotte wordt in hoofdstuk 4 een rekenschema opgesteld waarmee de verschillende onderdelen op elkaar worden aangesloten.

In hoofdstuk 5 wordt het gebruikte kasklimaatmodel gepresenteerd. Het kasklimaat is de tweede hoofdcomponent van het simulatiemodel. In het model is expliciete aandacht besteed aan assimilatiebelichting en energieschermen.

Het kasklimaatmodel is opgedeeld in een CO_2-model, een vocht-model en een thermisch model.

In hoofdstuk 6 worden de resultaten van het complete simulatiemodel vergeleken met gedetailleerde en lange termijn metingen in een proefkas met belichte rozen. De gedetailleerde vergelijking is uitgevoerd aan de hand van 10 minuten gemiddelde meetwaarden over een periode van drie dagen in januari 1995. De vergelijkingen betreffen de kasluchtcondities met betrekking tot temperatuur, vochtdeficit en CO_2-concentratie, pijptemperaturen en warmtevraag. De gesimuleerde waarden en dynamiek kwamen erg goed overeen met de metingen, hoewel er ook enkele opmerkelijke verschillen konden worden waargenomen.

Ook zijn de gesimuleerde kasklimaatregelaar-akties vergeleken met de akties van de regelaar in de proefkas. Raamopening, schermregeling en assimilatiebelichting werden goed gesimuleerd. De regeling van de CO_2-dosering gaf verschillen te zien.

De modelresultaten over een lange periode zijn bestudeerd aan de hand van jaar-rondmetingen van de kasluchttemperatuur, het energieverbruik en de gewasver-damping. De kasluchttemperatuur werd goed beschreven, met uitzondering van zeer warme perioden. Gedurende die perioden berekende het model te hoge temperaturen. Het gesimuleerde waterverbruik van het gewas kwam goed overeen met het gemeten verbruik in het najaar en in de winter. In het voorjaar en zomer berekende het model te hoge waterverbruiken.

Het energieverbruik werd goed beschreven. Het gesimuleerde jaarverbruik was slechts 2% lager dan het gemeten verbruik.

Nadat de kwaliteit van het simulatiemodel is gedemonstreerd aan de hand van de metingen in de proefkas is het model toegepast ten behoeve van de beoordeling van energie besparende maatregelen. Daartoe werden de parameters van het model gebaseerd op de bedrijfsuitrusting van een tomatenteelt in een moderne Neder-landse Venlo-kas van één hectare. Het verwarmingssysteem werd verondersteld te zijn uitgerust met een condensor en een warmte-opslagtank van 80 m^3. De kas-klimaatregelaar werd ingesteld volgens gangbare inzichten. De teelt bestreek een periode van 1 december tot 15 november. Er werd gebruikt gemaakt van typisch Nederlands weer.

De eerste categorie energiebesparende maatregelen die met het model zijn bestu-deerd betreft eenvoudige maatregelen in het ketelhuis. Hieronder vielen ketel- en pijpisolatie en de aansluiting van het expansievat. Ten behoeve van de berekening van de effecten van pijpisolatie werden zes pijp-typen onderscheiden naar hun functie in het verwarmingssysteem. De berekening van energie-verliezen aan het expansievat zijn uitgevoerd voor de referentiekas (met een warmte-opslagtank) en voor een kas zonder opslagtank.

Het blijkt dat de energie-besparing die met deze eenvoudige maatregelen kan worden gerealiseerd klein is. Echter, omdat het om relatief goedkope maatregelen gaat kunnen ze toch voordel opleveren.

De tweede cluster van energiebesparende maatregelen die bestudeerd is, betreft de vermindering van energieverliezen aan het kasdek middels verminderde lekverlie-zen door ramen, de toepassing van een energieschermen, de verhoging van de isolatiewaarde van het kasbedekkingsmateriaal.

Het effect van verminderde lekverliezen door de ramen is bepaald door het ener-gieverbruik van een kas waarvan 20% van de ramen altijd minimaal 1 cm open bleven staan te vergelijken met dat van de referentiekas. Het verschil in energie-verbruik bleek klein (1.6%).

Het gebruik van een energiescherm leverde een energiebesparing op van 23%. Echter, doordat het scherm-pakket in opgevouwen toestand 4% licht onderschep-ping geeft, resulteert een energiescherm ook in een verminderde gewasopbrengst.

Om beide effecten in één kental samen te vatten zijn de energiebesparings-effecten van maatregelen die invloed hebben op de gewasproduktie beoordeeld op grond van hun effect op het specifiek energieverbruik. Het specifiek energieverbruik is gedefinieerd als jaarlijks primair energieverbruik per eenheid jaarphotosynthese. Het specifiek energieverbruik wordt uitgedrukt in $MJkg^{-1}$. Uitgedrukt in specifiek energieverbruik leverde een energiescherm een besparing van 20%.

Met betrekking tot de bestudering van de effecten van hoog-isolerende kasbedek-kings-materialen is het model geschikt gemaakt voor de beschrijving van een dubbel glas kasdek en voor verschillende typen coatings op enkel en dubbel glas. De energie-besparingen die hierdoor werden behaald varieerden van 18% (een tin-oxide coating) tot 47% (een optie waarin een kasdek van dubbel-gecoat dubbel glas werd verondersteld). De meeste van de alternatieve kasbedekkingsmaterialen resulteren echter ook in een verminderde lichtdoorlatendheid. Wordt dit effect meegenomen, door het effect van deze materialen op het specifiek verbruik te berekenen, dan varieerden de besparingspercentages van 10% (een tin-oxide coating) tot 39% (dubbel-gecoat dubbel glas).

Een neven-effect van de toepassing van kasbedekkingsmaterialen met een ver-hoogde isolatiegraad is de (absolute en relatieve) toename van de hoeveelheid energie die wordt gebruikt voor de vochtbeheersing in de kas. Dit effect is voor elk van de opties gekwantificeerd. De berekeningen lieten zien dat het absolute energiegebruik ten behoeve van de vochtbeheersing in de zwaarst geïsoleerde kas bijna twee maal zo groot was als voor de referentie-kas.

De derde cluster van energiebesparende maatregelen betreft het gebruik van een condensor, een warmte-opslagtank en een warmtekracht-installatie (WKK-instal-latie). Het effect van de condensor werd berekend voor twee wijzen van inpassing in het verwarmingssysteem. Het bleek dat het een voordeel oplevert, indien de condensor niet alleen op het secundair verwarmingscircuit, maar ook op het pri-maire verwarmingscircuit kan worden aangesloten.

Het effect van de toepassing van een warmte-oplagtank is bestudeerd voor een kas zonder een kas mét een WKK-installatie. In het laatste geval werd de WKK-instal-latie gebruikt voor de elektriciteitsvoorziening van de assimilatiebelichting.

Voor kassen zonder WKK-installatie wordt de warmte-opslagtank gebruikt om warmte die vrijkomt bij de CO_2-dosering met ketelrookgassen op te slaan voor ge-bruik tijdens de nacht. Afhankelijk van de CO_2-doserings strategie uit het effect van de opslagtank zich vooral in energiebesparing of in produktieverhoging.

Warmte-opslag vermindert het energieverbruik als de CO_2-dosering onafhankelijk is van de actuele warmtevraag. In dat geval worden warmte-overschotten in de tank opgeslagen in plaats van door vergrootte ventilatie te worden vernietigd. Is de CO_2-dosering strategie zodanig dat warmtevernietiging wordt voorkomen, dan zal een warmte-opslagtank leiden tot een verhoogde CO_2-gift, en daarmee tot een

verhoogde produktie. Ook hier kunnen beide effecten onder één noemer worden gebracht door de energiegebruikseffecten uit te drukken in termen van specifiek energieverbruik. Deze berekeningen zijn gemaakt voor beide doseer-strategieën en voor drie doseersnelheden.

Voor een bedrijfssituatie waarin een WKK-installatie de elektriciteitsvoorziening van de assimilatiebelichting verzorgt, beïnvloedt een warmte-opslagtank zowel het energieverbruik als het produktieniveau, aangenomen dat CO_2 wordt gedoseerd zolang de afvalwarmte niet vernietigd hoeft te worden. De berekeningen toonden aan dat het produktie-effect groter is dan het energiebesparings-effect.

Wanneer een WKK-installatie elektriciteit produceert voor het openbaar net, dan levert dit een energiebesparing op omdat het totaal-rendement van de conversie van aardgas naar warmte en kracht (elektriciteit) van een dergelijke installatie hoger is dan wanneer aardgas in centrales wordt omgezet in elektriciteit en op het tuinbouwbedrijf in warmte. Het energiebesparings-effect wordt echter alleen zichtbaar als de vermindering van het gasverbruik van centrales (door elektriciteitsproduktie bij kassen) in de beschouwing wordt meegenomen. Het gasverbruik op het tuinbouwbedrijf stijgt bij de toepassing van WKK namelijk aanzienlijk.

De energiebesparing die voortvloeit uit de toepassing van WKK hangt voor het grootste geheel af van de capaciteit van de WKK-installatie (het elektrisch vermogen per m^2 kasoppervlak). De berekeningen laten zien dat door de toepassing van WKK besparingspercentages tot 32% kunnen worden behaald. Indien de rookgassen van WKK-installaties voldoende zuiver zouden zijn om toegepast te kunnen worden als CO_2-bron in plaats van ketelrookgassen kunnen de besparingspercentages nog verder toenemen.

In hoofdstuk 7 worden de conclusies getrokken uit de analyses die in het kader van dit proefschrift hebben plaatsgevonden. Enkele punten daaruit worden nader bediscussieerd.

CURRICULUM VITAE

Hendrik Feije de Zwart werd op 29 januari 1965 te Bennebroek geboren. Van 1967 tot 1971 en van 1972 tot 1976 woonde hij in Indonesië. Het grootste deel van zijn lagere school-tijd viel in de tweede periode van vier jaar. In die jaren is hij, samen met zijn één jaar jongere broer, door zijn moeder onderwezen. Terug in Nederland vond hij een goede aansluiting met de zesde klas van de lagere school.

Na de lagere school doorliep hij het Atheneum van de 'scholengemeenschap Leiden Zuid-West', waarvan de naam in 1978 veranderde in 'De Vlietschans'. Het VWO-diploma behaalde hij in 1983.

In datzelfde jaar begon hij zijn wetenschappelijke opleiding aan de Landbouwhogeschool te Wageningen, waarvan de naam in zijn studieperiode overging naar Landbouwuniversiteit Wageningen. In januari 1989 behaalde hij aldaar het doctoraalexamen in de studierichting Landbouwtechniek (vrije oriëntatie). Zijn afstudeervakken betroffen modelvorming en simulatie (6 maanden) en regeltechniek (eveneens 6 maanden).

Na een korte periode als prakticumleider bij de vakgroep Natuur- en Weerkunde van de Landbouwuniversiteit Wageningen te hebben gewerkt, begon hij in december 1989 bij IMAG-DLO aan het onderzoek dat uiteindelijk tot dit proefschrift heeft geleid. Sinds begin 1996 werkt hij daar in een dienstverband voor onbepaalde tijd binnen de afdeling Energietechniek.

DANKWOORD

Op de middelbare school leerde ik dat er drie vereisten zijn voor de totstandkoming van een produkt, namelijk kapitaal, arbeid en ondernemingszin. Wat betreft het eerste is de totstandkoming van dit proefschrift te danken aan de financiële bijdrage van NOVEM (Nederlandse Onderneming Voor Energie en Milieu bv) en de middelen die door IMAG-DLO beschikbaar zijn gesteld.

De twee andere doorslaggevende factoren kunnen vrij worden vertaald met transpiratie en inspiratie. Inspiratie zou ik daarbij voorop willen stellen omdat dat een voorwaarde is om je niet door transpiratie te laten weerhouden.

Voor wat betreft die inspiratie ben ik veel dank verschuldigd aan de mensen die de afgelopen jaren bij het onderzoek rond dit proefschrift betrokken zijn geweest. Het moet voor mijn naaste collega, Jo Huijs, en mijn begeleiders Gerard Bot en Bert Speelman niet gemakkelijk geweest zijn om als gesprekspartner op te treden en mij feed-back te geven, gezien mijn zwalkende ideeën over aanpak, richting en inhoud van dit onderzoek. Vele malen ging de zaak op de schop en werden ideeën die eerst zinvol leken om uitgewerkt te worden bij de volgende bijeenkomst weer als irrelevant of oninteressant door mij van de hand gewezen. De flexibiliteit die zij daarin opbrachten is bewonderenswaardig en ik ben blij dat zij telkens toch weer hun vertrouwen in mijn werk hebben getoond.

De drie genoemde meest betrokkenen hebben allen op hun eigen wijze hun bijdrage doen gelden. Heel praktisch heeft Jo me gezond gehouden met een dagelijks stukje fruit. Ook de paar stressige dagen, voorafgaand aan de dead-line waarop het proefschrift naar de drukker moest, heeft hij enorm veel werk verzet in het opmaken en inplakken van de grafieken en figuren. Zonder zijn inzet was het niet op tijd klaar geweest. Inhoudelijk was Jo, door zijn globalistische kijk op mijn onderzoek, een prettige en kritische gesprekspartner. Heel wat inconsistenties, modellerings- en rekenfouten kwamen aan het licht door zijn vragen en opmerkingen. Daarnaast heeft hij in de eerste jaren van het onderzoek, als leider van het project waar mijn werk een onderdeel van vormde, alle management-activiteiten een effectieve wijze gestalte gegeven. We waren een sterk team en ik hoop dat dat nog een aantal jaren kan worden voortgezet.

Gerard Bot wil ik met name bedanken voor zijn grondige bestudering van alle concept-hoofdstukken die in de loop der jaren door mij werden ge- of herschreven. Het moet je veel tijd gekost hebben. Daarnaast is mij door hem veel vakinhoudelijke kennis bijgebracht.

Bert Speelman wil ik bedanken voor de tijd en aandacht die hij ondanks zijn volle agenda aan mij heeft besteed. De begeleidingsgesprekken met jou en Gerard waren altijd opbouwend en stimulerend. Na zo'n begeleidingsbijeenkomst vervolgde ik telkens met hernieuwd elan mijn werk.

Graag wil ik op deze plek ook mijn collega's van de gang bedanken voor de

plezierige werksfeer die door hen gestalte krijgt. Rinus Telle, vanwege zijn schier onuitputtelijke bron van citaten en anekdotes, Jo Huijs, op deze plaats nogmaals genoemd vanwege zijn positieve invloed op de werksfeer, Nico van de Braak, vanwege zijn welgemeende belangstelling en nuchtere relativeringen, Peter Knies vanwege zijn praktische en pragmatische instelling (hij bedacht het handelsmerk - KASPRO - voor het simulatieprogramma dat in dit proefschrift beschreven staat), Jo Breuer vanwege zijn uitgebreid archief en Frank Kempkes vanwege zijn vocabulaire kunstzinnigheden.

Steef van Aggelen en Ferry Corver wil ik bedanken voor hun teeltkundige bijdrage aan de metingen in kassen. Rein Bijkerk en Hans Jansen ben ik dankbaar om hun alerte bewaking van de continuïteit in de verzameling van meetgegevens en Henny van Dorland en Appie Baadilla voor de ondersteuning in het aanbrengen van aanpassingen in de kas en het meet-systeem.

Tenslotte noem ik Jan Selten en Harry Oldenhof vanwege de tips en trucs die zij mij op software-gebied aanreikten.

Niet vanwege hun bijdrage aan de inhoudelijke kant van het werk, maar vanwege de morele steun en interesse die ik van hen ondervond wil ik graag mijn dank betuigen aan vrienden en familie. Ik was altijd een beetje vaag over wat ik nou precies aan het doen was, maar dat heeft jullie er niet van weerhouden toch regelmatig te informeren naar de stand van zaken, maar vooral naar mijn subjectieve beleving daarin. Hierin wil ik speciaal Mariette noemen omdat zij mij telkens weer over momenten van twijfel heeft heengeholpen.

Tenslotte wil ik Mariette nogmaals noemen omdat zij mijn leven in het algemeen gelukkig maakt.